2

AVAL POSTGRADUATE SCHOOL
Monterey, California

THESIS

**AUTOMATIC PULSE SHAPING WITH THE
AN/FPN-42 AND AN/FPN-44A
LORAN-C TRANSMITTERS**

by

Dean C. Bruckner

December 1992

Thesis Advisor:	Murali Tummala
Second Reader:	Roberto Cristi

REPORT DOCUMENTATION PAGE

1a. REPORT SECURITY CLASSIFICATION UNCLASSIFIED	1b. RESTRICTIVE MARKINGS
2a SECURITY CLASSIFICATION AUTHORITY	3. DISTRIBUTION/AVAILABILITY OF REPORT Approved for public release; distribution is unlimited
2b. DECLASSIFICATION/DOWNGRADING SCHEDULE	
4. PERFORMING ORGANIZATION REPORT NUMBER(S)	5. MONITORING ORGANIZATION REPORT NUMBER(S)
6a. NAME OF PERFORMING ORGANIZATION Naval Postgraduate School 6b. OFFICE SYMBOL *(if applicable)* EC	7a. NAME OF MONITORING ORGANIZATION Naval Postgraduate School
6c. ADDRESS *(City, State, and ZIP Code)* Monterey, CA 93943-5000	7b. ADDRESS *(City, State, and ZIP Code)* Monterey, CA 93943-5000
8a. NAME OF FUNDING/SPONSORING ORGANIZATION 8b. OFFICE SYMBOL *(if applicable)*	9. PROCUREMENT INSTRUMENT IDENTIFICATION NUMBER
8c. ADDRESS *(City, State, and ZIP Code)*	10. SOURCE OF FUNDING NUMBERS PROGRAM ELEMENT NO. | PROJECT NO. | TASK NO. | WORK UNIT ACCESSION NO.

11. TITLE *(Include Security Classification)*
AUTOMATIC PULSE SHAPING WITH THE AN/FPN-42 AND AN/FPN-44A LORAN-C TRANSMITTERS (U)

12. PERSONAL AUTHOR(S)
Bruckner, Dean C.

13a. TYPE OF REPORT Master's Thesis	13b. TIME COVERED FROM 07/90 TO 10/92	14. DATE OF REPORT *(Year, Month, Day)* October 1992	15. PAGE COUNT 199

16. SUPPLEMENTARY NOTATION The views expressed in this thesis are those of the author and do not reflect the official policy or position of the Department of Defense or the United States Government.

17. COSATI CODES			18. SUBJECT TERMS *(Continue on reverse if necessary and identify by block number)*
FIELD	GROUP	SUB-GROUP	Loran, pole-zero modeling, ARMA modeling, steepest-descent, Yule-Walker, Shank's, VXIbus

19. ABSTRACT *(Continue on reverse if necessary and identify by block number)*

Automatic pulse shape control is simulated for the AN/FPN-42 and AN/FPN-44A tube type transmitters. A linear, time invariant (LTI) pole-zero model is developed for each transmitter at a typical operating point using the least squares modified Yule- Walker method and Shank's method. LTI models for a range of operating points are catenated to represent observed nonlinear behavior, and observed time variations are added. After these combined models are tested, a linear controller based on the method of steepest descent is implemented. These models, the control algorithm and transmitter system details such as power supply droop, dual rating and noise are then incorporated into a MATLAB simulation program.

In a variety of realistic tests the control algorithm successfully shaped the Loran-C pulse, except that zero-crossing times were not always in tolerance and the algorithm showed a sensitivity to noise. The algorithm controlled Envelope-to-Cycle Difference, produced an entire Phase Code Interval of pulses while compensating for droop and phase code bounce, and produced a near- optimal transmitter drive waveform for the transmitter/antenna system using the dummy load.

20. DISTRIBUTION/AVAILABILITY OF ABSTRACT ☒ UNCLASSIFIED/UNLIMITED □ SAME AS RPT. □ DTIC USERS	21. ABSTRACT SECURITY CLASSIFICATION UNCLASSIFIED	
22a. NAME OF RESPONSIBLE INDIVIDUAL Murali Tummala	22b. TELEPHONE *(Include Area Code)* (408) 646-2645	22c. OFFICE SYMBOL EC/TU

Automatic Pulse Shaping with the AN/FPN-42 and AN/FPN-44A Loran-C Transmitters

by

Dean C. Bruckner
Lieutenant, United States Coast Guard
B. S., United States Coast Guard Academy, 1985

Submitted in partial fulfillment of the
requirements for the degree of

MASTER OF SCIENCE IN ELECTRICAL ENGINEERING

from the

NAVAL POSTGRADUATE SCHOOL
December 1992

Author: Dean C. Bruckner
Dean C. Bruckner

Approved by: Murali Tummala
Murali Tummala, Thesis Advisor

Roberto Cristi
Roberto Cristi, Second Reader

for Michael A. Morgan, Chairman, Department of Electrical
and Computer Engineering

ABSTRACT

Automatic pulse shape control is simulated for the AN/FPN-42 and AN/FPN-44A tube type transmitters. A linear, time invariant (LTI) pole-zero model is developed for each transmitter at a typical operating point using the least squares modified Yule-Walker method and Shank's method. LTI models for a range of operating points are catenated to represent observed nonlinear behavior, and observed time variations are added. After these combined models are tested, a linear controller based on the method of steepest descent is implemented. These models, the control algorithm and transmitter system details such as power supply droop, dual rating and noise are then incorporated into a MATLAB simulation program.

In a variety of realistic tests the control algorithm successfully shaped the Loran-C pulse, except that zero-crossing times were not always in tolerance and the algorithm showed a sensitivity to noise. The algorithm controlled Envelope-to-Cycle Difference, produced an entire Phase Code Interval of pulses while compensating for droop and phase code bounce, and produced a near-optimal transmitter drive waveform for the transmitter/antenna system using the dummy load.

TABLE OF CONTENTS

LIST OF TABLES

LIST OF FIGURES

ACKNOWLEDGMENT

I would like to thank Professors Tummala, Cristi, Therrien, and Chen at the Naval Postgraduate School for their assistance and advice. LT Tom Johnson, USN, and LT Chuck Schue, USCG, students at NPS, helped significantly too. Thanks are also in order to LCDR Greg Kmiecik and all the personnel at the Loran Branch at the Coast Guard Electronics Engineering Center for the great support during this project. CAPT Ben Peterson at the Coast Guard Academy, CDR Doug Taggart at Coast Guard Headquarters (Navigation Systems Branch), and personnel at the Coast Guard Pacific Area Headquarters and Maintenance and Logistics Command, Coast Guard Training Center Petaluma, and Coast Guard Loran Station Middletown were also helpful. Finally, thanks to my family and friends for their support and patience.

I. INTRODUCTION

Modernizing old electronic systems has always presented a challenge to design engineers, and the U.S. Coast Guard's effort to redesign the control system for its Loran-C transmitters is no exception. Coast Guard engineers have identified commercially-available hardware to replace much of the old cont:ol equipment. This new equipment will be easier to maintain and operate and will allow more Loran-C control functions to be automated. To realize this capability, however, new software must be developed to perform each function. This is one of the most challenging aspects of the redesign effort.

One of the most important control functions is shaping the pulse produced by older classes of Loran transmitters. A Loran receiver uses the envelope of the pulse to identify a standard zero-crossing; if the envelope is distorted, the receiver may lock onto the wrong zero-crossing, resulting in a large position error. The software to shape the pulse automatically requires a reliable algorithm. In this thesis, a control algorithm based on the method of steepest descent is adapted to meet this need.

In order to test the algorithm fully and to provide a tool for future study, a detailed MATLAB computer program is developed to simulate two older transmitter classes, the AN/FPN-42 and AN/FPN-44A. With no documentation available on the theory behind the design of these transmitters, this is an exercise in system identification and modeling. With its wealth of linear algebra and signal processing functions, MATLAB is an ideal operating environment for this work.

Many details of the '42 and '44A transmitter systems and of their operation affect the shape of the transmitted pulse. To make the simulation a realistic one, as many of these details as possible are included. Chapter II gives an overview of Loran-C and provides the background needed to understand these details. It explains each of the pulse shape tests found in the Coast Guard's *Specification for the Transmitted Loran-C Signal* [Ref. 1]. In Chapter III, mathematical models for the '42 and '44A transmitters are developed; in Chapter IV, the control algorithm is presented. These models and the control algorithm then form the foundation of the simulation program described in Chapter V. Chapter V also includes results from a variety of tests performed using the simulation program. Finally, conclusions and recommendations for further study are given in Chapter VI.

II. AN OVERVIEW OF LORAN-C

A. LORAN-C IN BRIEF

1. History

LORAN, short for LOng RAnge Navigation, is a radionavigation system developed during World War II by the famous Radiation Laboratory at the Massachusetts Institute of Technology. The first version, called Loran-A, was used during the war to guide Allied military ships and aircraft in the North Atlantic and Pacific Oceans. By war's end, Loran coverage extended over most of the areas in the North Atlantic and Pacific where U.S. forces operated. Loran-A, with its one to two nautical mile (Nm) fix accuracy and its range of 600 to 800 miles, was a significant factor in bringing the war quickly to an end and in preventing the loss of aircraft because of inaccurate navigation [Ref. 2: p. 153].

After the war, while Loran-A continued to operate, research began on a similar system called the Cycle Matching Tactical Bombing (CYTAC) navigation system for the U.S. military. In 1958 the U.S. Coast Guard assumed control of the CYTAC system, which was renamed Loran-C. By using a lower frequency band of 90 to 110 kHz instead of 1.7 to 2.0 MHz as in Loran-A, greater range was possible. Also, other technical improvements brought more accurate geographic positioning [Ref. 3: p. 2–12].

At first, Loran-C was used mainly by the Department of Defense. As the number and size of ships passing through coastal U.S. waters increased and as several new radionavigation systems were developed, it became apparent that the U.S. government should designate one system which it would support. In 1974 the Secretary of Transportation adopted Loran-C as the official radionavigation system for coastal U.S. waters with a minimum accuracy requirement of 0.25 Nm and a minimum reliability of ninety-five percent of the time in the Coastal Confluence Zone (CCZ), essentially the area from the shore out to 50 Nm. By the early 1980s, the Coast Guard had phased out the last of its Loran-A stations and had extended Loran-C coverage over the entire CCZ [Ref. 4: p. 12]. In 1990, at the request of the Federal Aviation Administration, the Coast Guard began a project to extend Loran-C coverage from coast to coast in the continental U.S. Today the Coast Guard operates Loran-C stations in the U.S.; its territories; and in "host nations" such as Italy, Japan and Turkey. In addition, Loran-C stations are operated by other nations, such as Saudi Arabia, China and Russia. Figure 2.1 shows the locations of Loran-C stations now operating in the U.S.

2. How Loran-C Works

Like Loran-A, Loran-C is based on time differences (TDs) between the signals of a master station and one or more secondary stations. Beginning with the master, each of the stations in the "chain" transmits in turn a sequence of short pulses. A receiver located in the chain's area of coverage measures and displays the elapsed time between the signals from each station. The time difference between the master and secondary indicates that the receiver is located at some point on a hyperbolic line of position. A number of time difference lines of position from one baseline (one master and one secondary station) are shown in Fig. 2.2. When more stations are added, their time difference lines overlay these and form a grid of hyperbolic lines. The secondaries, up to four in number, are designated W, X, Y, and Z. Given two or more lines of position, the receiver "fixes" its position at the intersection of these lines.

The chain's master and the secondary stations repeat the sequence of pulses at a fixed rate, according to the Group Repetition Interval (GRI) assigned

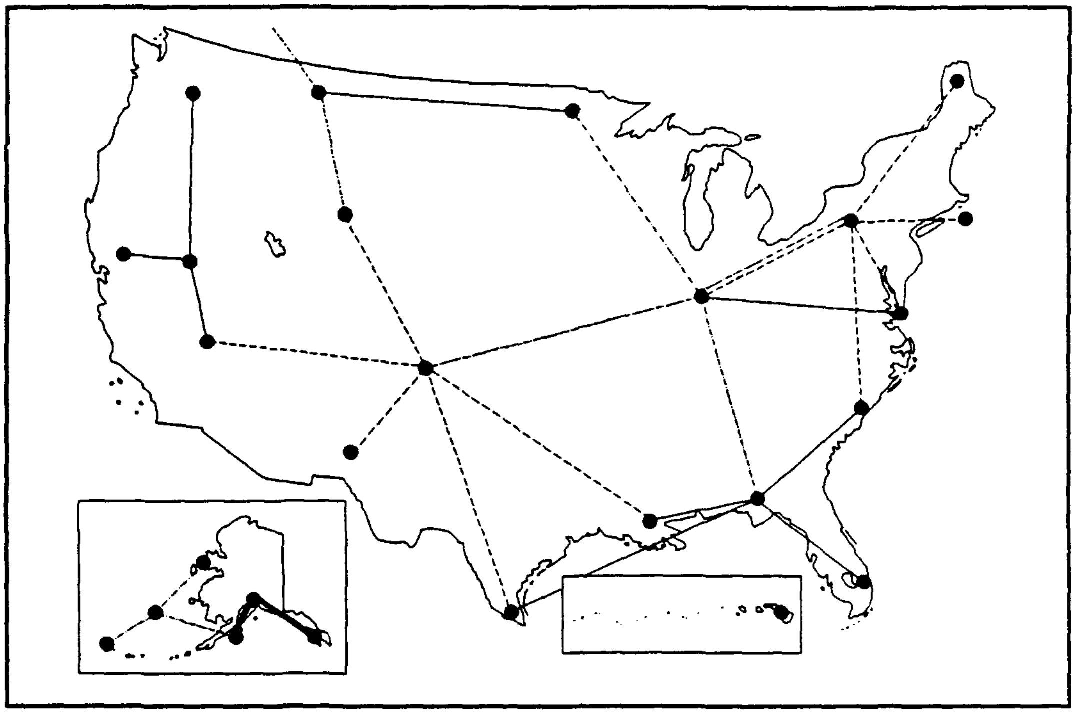

Figure 2.1: Locations of U.S. Loran stations.

to the chain when it was first installed. Assigned GRIs vary from 40,000 to 99,990 microseconds, so the chain's cycle may repeat anywhere from 10 to 20 times each second. By convention in Loran-C, elapsed time is generally described in microseconds or nanoseconds, but not in milliseconds. Each station in a chain transmits its own pulse sequence with the same GRI. Progressively longer emission delays, with reference to the master, are assigned to each secondary so the signals of each secondary arrive in the same order throughout the chain's area of coverage [Ref. 1: p. 2-5]. Emission delays for a chain with three secondaries are diagrammed in Fig. 2.3.

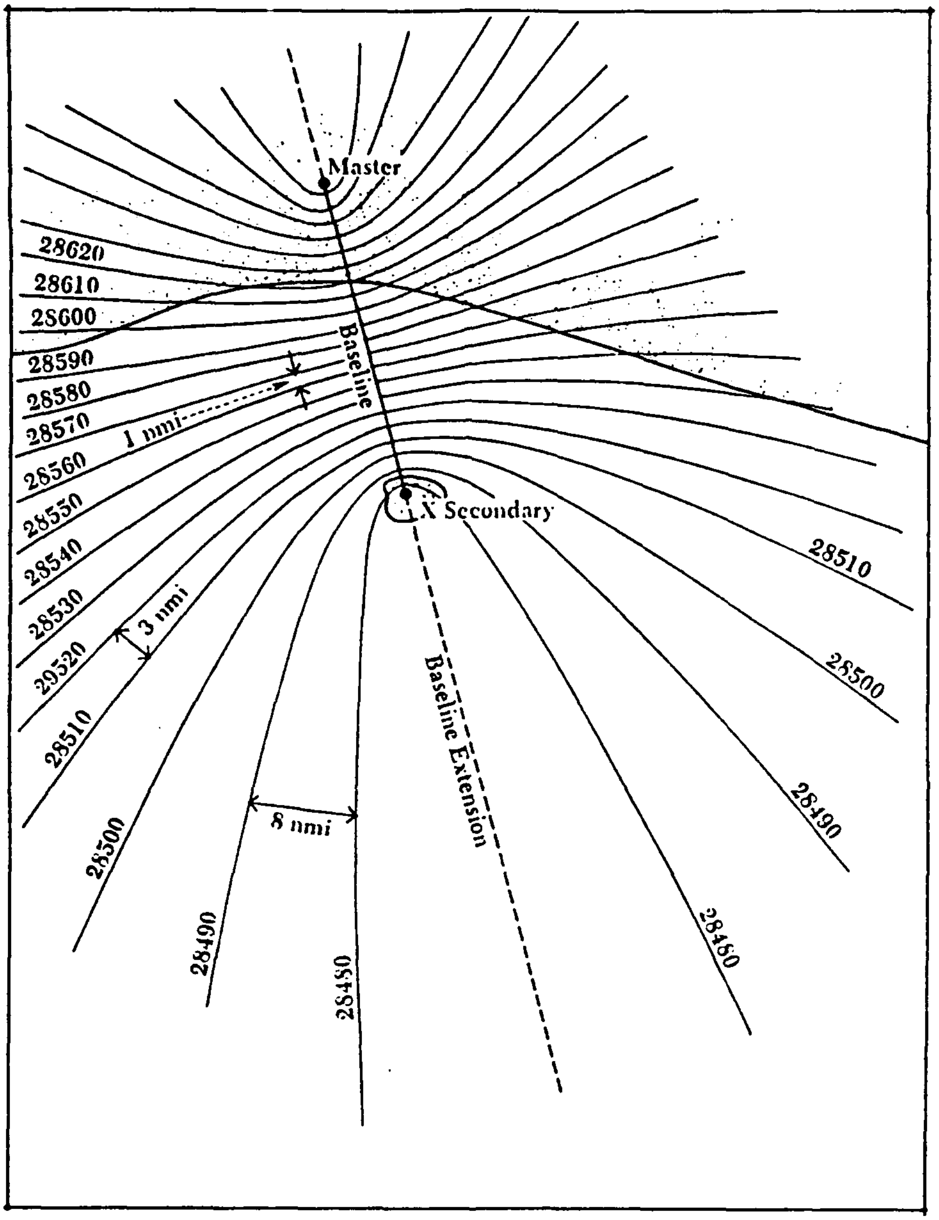

Figure 2.2: Hyperbolic LOPs [Ref. 27].

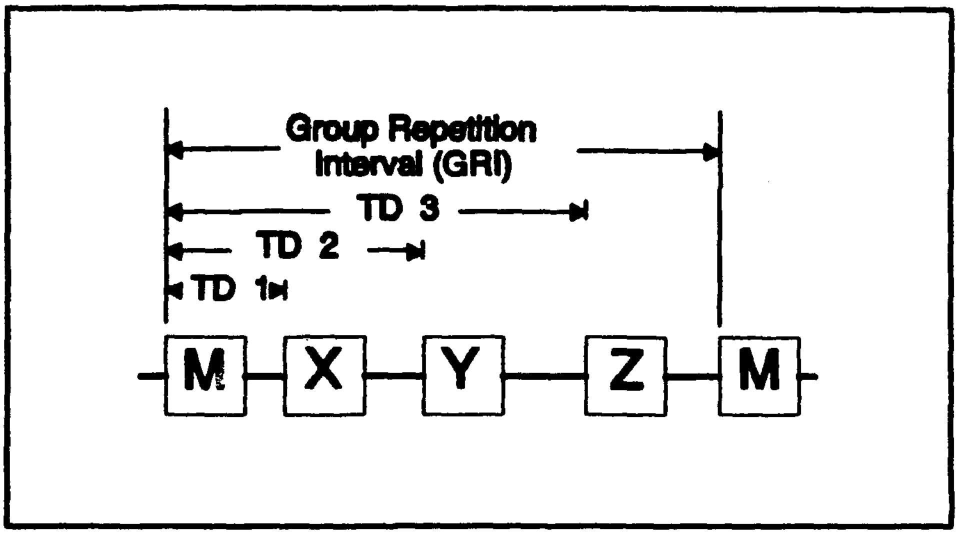

Figure 2.3: Emission delays.

For consistently accurate emission delays, each station's repetition rate (the time in which its pulse sequence repeats) must be exactly equal to the assigned GRI, so that the stations' pulse sequences do not move relative to each other. To ensure this, each station operates three cesium time reference standards (clocks), which are constantly compared to each other to check for drift and whose accuracy is on the order of 10^{-12} seconds. Periodically, the clocks of each station are also compared to the master station's cesium clocks. If the stations' repetition rates are all identical, the control station, with data supplied by two or more monitor stations in the chain's area of coverage, remotely adjusts the emission delay of each secondary station's signal relative to the signal of the master.

3. The Accuracy, Reliability and Availability of Loran-C

Absolute accuracy and repeatable accuracy are two measures of the accuracy of geographic positions obtained by Loran-C. Absolute accuracy is a measure of the error between a charted and an observed time difference. Different radio propagation speeds over land and water, inclement weather and other factors change the geometry of the grid of hyperbolic lines of position and produce errors. Nevertheless, Loran-C meets the minimum accuracy requirement of 0.25 Nm ninety-five percent of the time throughout the CCZ. In many areas Loran-C places the receiver within 0.1 Nm (200 yards) from its true position [Ref. 4: p. 167]. Repeatable accuracy, on the other hand, is a measure of Loran-C's consistency. If a receiver is placed at a known position, repeatable accuracy measures the error between two or more Loran readings taken at different times. This type of accuracy would be useful when returning to a favorite fishing spot or finding one's home channel entrance in the fog. Loran-C's repeatable accuracy is one of its greatest strengths and is often within 50 feet [Ref. 5: p. 44].

Another strength of Loran-C is its reliability, the percentage of the time the master and at least two secondary stations in the chain covering a given area are operating correctly. The Coast Guard's published reliability goal is 99.7%, which it has met consistently [Ref. 6].

Signal availability, the percentage of the time a single station operates within established tolerances, is the cornerstone of Loran-C's reliability. The Coast Guard's goal for availability is 99.9%, and it has achieved 99.95% over the years [Ref. 7]. This corresponds to a little more than four hours per year when the average Loran-C station is not providing a reliable radionavigation signal.

4. Loran-C's Future

Loran-C will continue as a vital radionavigation system in the U.S. in the near future for several reasons. Loran-C receivers are inexpensive (they start at about $450), Loran-C coverage (in the U.S. and in many areas overseas) is extensive and reliable, domestic Loran-C users number over one million, and the U.S. federal government's commitment to support it remains firm. According to the Federal Radionavigation Plan, the satellite-based Global Positioning System (GPS) and the Coast Guard's Differential GPS program will eventually replace Loran-C, but only after several years of reliable operation [Ref. 5: p. 44]. Accordingly, the Coast Guard will continue to operate Loran-C in the United States for at least ten to twenty more years.

Currently, the Coast Guard is not involved in any type of Loran other than Loran-C. Therefore, throughout the rest of this thesis, general references to Loran refer to Loran-C.

B. THE LORAN-C SIGNAL

1. The Individual Loran Pulse

a. General Description

The Loran pulse is the basic component of the Loran signal. The designers of Loran chose to use pulses instead of a continuous wave signal to achieve desired range and performance characteristics with less power supplied to the transmitter [Ref. 8: p. 33]. The first $65\mu s$ of the Loran pulse, called the leading edge, is the only part the Loran receiver uses. This part is specified completely by: [Ref. 1: p. 21]

$$i(t) = (t-\tau)^2 e^{-2(t-\tau)/65} \sin(0.2\pi t + \pi C_p) \quad \tau < t < 65 + \tau \tag{2.1}$$

where

A is a normalization constant related to the magnitude of the peak antenna current in amperes,
t is time in microseconds,
τ is the Envelope-to-Cycle Difference (ECD) in μs, and
C_p is the phase code parameter: 0 for positive, 1 for negative.

The first $90\mu s$ of the pulse are shown in Fig. 2.4.

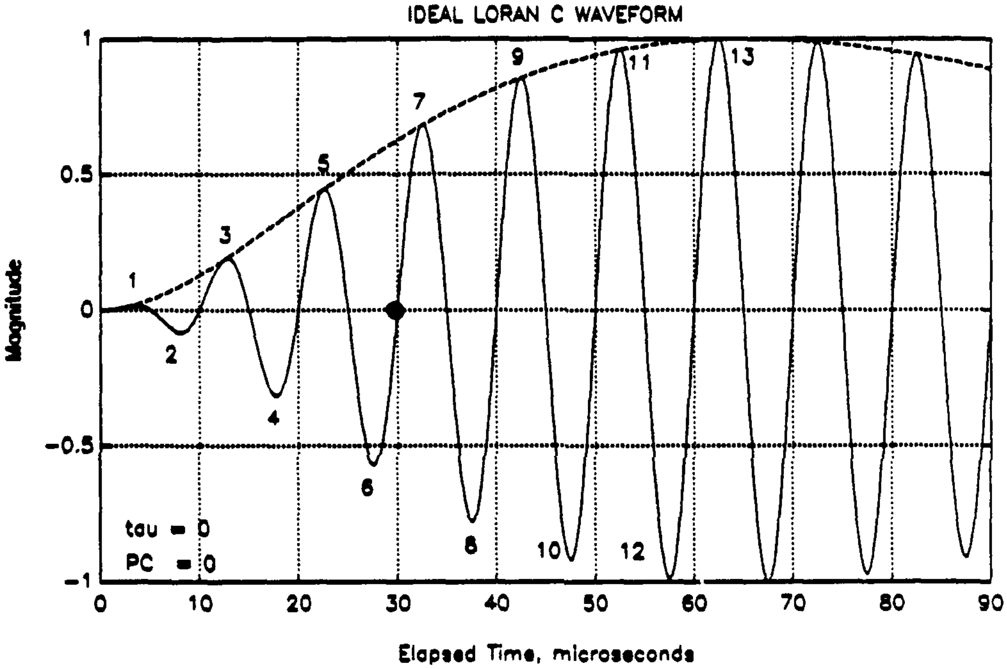

Figure 2.4: Ideal loran pulse.

The "tail" of the pulse, also called the trailing edge, is not shown in Fig. 2.4. The dynamics of the particular type of Loran transmitter shape this part. There are two requirements for the tail of the pulse: it must not generate significant frequency components outside the 90 to 110 kHz band, and its amplitude after $t = 500\mu s$ must not exceed a threshold level established for the particular transmitter. In other words, one pulse must decay essentially to zero well before the beginning of the next pulse in the sequence, and it must be well-behaved as it decays.

The important part of the Loran-C pulse is the third negative-to-positive zero-crossing, marked in Fig. 2.4. The receiver uses this "standard" zero-*crossing*, also called the 30 microsecond point, to find the elapsed times between the master station's signal and the secondary stations' signals. The receiver can measure these time differences accurately and consistently once it acquires, or locks onto, this zero-crossing. In this lock-on process, the receiver first tries to find coherent energy at 100 kHz. When it locates a Loran pulse, it measures the amplitudes of adjacent pulse peaks. Because the fifth and seventh positive peak amplitudes have a unique ratio, the receiver is able to locate the standard zero-crossing which lies between them. The receiver sets up a strobed window over the zero-crossing and keeps measuring it, thus maintaining "lock" on the signal. If the pulse is distorted in some way, the receiver may have *trouble maintaining* a lock on the pulse and in some cases may not be able to lock cnto it at all.

b. Specification: Individual Pulse (Four Tests)

To minimize the problem caused by distorted pulses, the Coast Guard has established a strict specification for the individual transmitted Loran pulse [Ref. 1]. This specification defines four measures of Loran-C pulse shape and establishes tolerances for them. These four tests compare the measured Envelope-to-Cycle Difference (ECD), the half-cycle peak amplitudes (ensemble tolerance), the half-cycle peak amplitudes (individual tolerance) and the zero-crossings against these established tolerances. This Subsection describes each in detail.

These four tests use a parameterization of the Loran-C antenna current pulse, measured in amperes using a current transformer at the transmitter ground return. The parameters consist of the first 13 half-cycle peak amplitudes (normalized so the largest positive value of the pulse equals one) and the first 12 zero-crossings (in μs, relative to the standard zero-crossing). This parameter choice highlights those parts of the pulse most important to the receiver and reflects the limitations of signal processing hardware available in the 1950s and 1960s.

The first three tests apply only to half-cycles one through eight where the standard zero-crossing is located. The term "transmitted" pulse refers to the current pulse measured at the transmitter ground return, *not to the pulse in the far field.* The terms "assigned" and "ideal" are used interchangeably to indicate standard or theoretical values as listed in the signal specification. Similarly, the terms "actual" and "measured" are used interchangeably to describe the characteristics of the real-world Loran signal.

Test 1: Envelope-to-Cycle Difference (ECD). The Envelope-to-Cycle Difference is an indication of the position in time of the envelope of the Loran pulse relative to the position of the zero-crossings. Figure 2.5 shows the first few half-cycles of three Loran pulses with ECD values of -5, 0, and $+5\mu s$, respectively. A negative ECD indicates that the envelope has been shifted left (or appeared earlier in time) relative to the zero-crossings. A positive ECD indicates the opposite. The ECD of the Loran pulse may be controlled arbitrarily, within specified limits, at the transmitter to obtain a desired pulse shape.

One problem with ECD is that it changes as the pulse propagates. First, when the Loran-C pulse is transmitted, a 90° carrier phase shift occurs by the time the pulse has reached the far E-field [Ref. 1: p. 21], resulting in a change in the ECD of $+2.5\mu s$. Second, depending on ground or ocean conductivity, ECD continues to change as the pulse propagates over the earth's surface. One model predicts that for every 100 Nm the pulse travels over the ocean ECD changes by $-0.25\mu s$ These

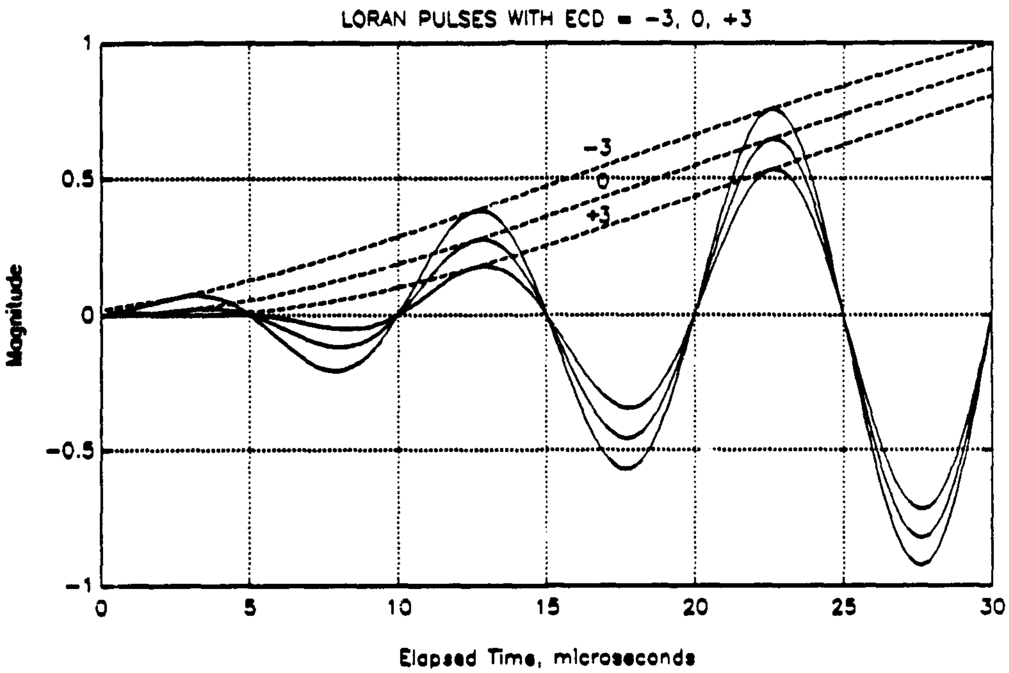

Figure 2.5: Loran pulses with three ECDs.

changes are the result of different propagation speeds of the envelope and of the zero-crossings [Ref. 9].

A large ECD can wreak havoc on a Loran receiver. It may cause the receiver to misidentify the $20\mu s$ or the $40\mu s$ zero-crossing as the standard $30\mu s$ zero-crossing. This results in a large time difference error which could translate to a position error of a mile or more. Fortunately, changes in ECD because of propagation are predictable with some accuracy, and Loran receivers can be designed to compensate [Ref. 9].

A receiver cannot, however, compensate for unpredictable changes in ECD at the point of transmission. Therefore, the ECD of the transmitted pulse is con:rolled carefully. Each station is assigned a local, or transmitted, ECD value, usually zero. The station's *actual* transmitted ECD must differ by more than $\pm 0.5\mu s$ from the *assigned* transmitted ECD. This tolerance is just one sixth of the largest ECD difference shown in Fig. 2.5.

Estimating the ECD of a Loran pulse is a complicated process, but it can be done iteratively using the values of the first eight half-cycle peak amplitudes. Appendix A outlines this procedure. Once the ECD of the transmitted pulse is estimated, an ideal pulse with the same ECD may be generated according to Eq. (2.1). The half-cycle peak amplitudes of this ideal pulse are used in the next two tests, which apply only for transmitted ECD values of -2.5 to $+2.5\mu s$.

Test 2: Half-cycle Peak Amplitudes (Ensemble Tolerance). The root-mean-square (rms) error between the first eight actual half-cycle peak amplitudes and first eight ideal half-cycle peak amplitudes must not be more than one percent of the peak amplitude of the pulse. Specifically, let S_p, $p = 1, 2, \cdots, 8$, represent the "ensemble" of the first eight half-cycle peak amplitudes of the actual antenna current waveform, in amperes, normalized so the largest positive value of the entire pulse (usually at, or near, half-cycle number 13) equals one. Let I_p, $p = 1, 2, \cdots, 8$, represent the ensemble of the first eight half-cycle peak amplitudes of the ideal antenna current waveform, in amperes, normalized in the same way. Then,

$$\sqrt{\frac{\sum_{p=1}^{8}(I_p - S_p)^2}{8}} \leq .01 \qquad (2.2)$$

Test 3: Half-cycle Peak Amplitudes (Individual Tolerances). In the first eight half-cycles of the pulse, the largest difference between the ideal and actual half-cycle peak amplitudes must not exceed three percent of the peak amplitude of the pulse. In half-cycles 9 through 13, this requirement is relaxed to ten percent:

$$|I_p - S_p| \leq .03 \qquad 1 \leq p \leq 8 \tag{2.3}$$

$$|I_p - S_p| \leq .10 \qquad 9 \leq p \leq 13 \tag{2.4}$$

Test 4: Zero-crossings. Loran transmitters are extremely narrowband amplifiers designed to resonate at exactly 100.00 kHz. They are usually well tuned to this frequency, but instantaneous frequency distortions may exist in the Loran pulse, especially in the first two half-cycles. Since a Loran receiver depends heavily on the time-domain behavior of the Loran pulse when sampling zero-crossings and half-cycle peak amplitudes, any instantaneous frequency distortions in the pulse can affect the performance of the receiver. A simple frequency domain spectrum analysis of the entire Loran pulse may not adequately detect instantaneous frequency distortions in the pulse. Therefore, a time domain analysis of instantaneous frequency *covering the first 13 half-cycles of the pulse is used instead.*

The zero-crossing times and tolerances in Table 2.4 have been established for the Loran-C pulse [Ref. 1]. Category 1 tolerances are the most stringent and are generally applied to the newer generations of transmitters. Category 2 tolerances are more lenient and are usually applied to the older transmitters. Reference 1 lists exactly which category applies in each test for every station in the Coast Guard.

2. The Loran-C Pulse Group

a. Format of the Pulse Group

The Loran signal consists of a group of eight individual pulses transmitted in rapid succession. This increases the average signal power available to the receiver [Ref. 8: p. 33]. In addition to these eight pulses, the master station also

TABLE 2.1: ZERO-CROSSING TIMES AND TOLERANCES

Zero-crossing (μs)	Time (μs)	Tolerance (ns)	
		Category 1	Category 2
5	−25	±1000	±2000
10	−20	100	1500
15	−15	75	1000
20	−10	50	500
25	− 5	50	250
30	standard zero-crossing	(time reference)	
35	5	50	100
40	10	50	100
45	15	50	100
50	20	50	100
55	25	50	100
60	30	50	100

transmits a ninth pulse, which helps the receiver to identify the master. The ninth pulse, when "blinked" ON and OFF according to a preset code, allows the master station to notify a secondary station in the chain that the secondary is transmitting a signal outside of specified tolerances. The Loran pulse decays essentially to zero in $500\mu s$; the pulses in the group are $1000\mu s$ apart, except that the master's ninth pulse is transmitted $2000\mu s$ after its eighth pulse.

b. Multipulse Trigger

From the receiver's point of view, the standard zero-crossing provides the time reference for each pulse in the group and from group to group. From the transmitter's point of view, the time reference is the Multipulse Trigger (MPT). When it is time for a station to transmit a pulse group, the Loran timer equipment sends 8 trigger signals, spaced $1000\mu s$ apart, to the pulse generator (PGEN) (and one more trigger 2000μs later in the case of the master station). When the PGEN receives a trigger signal, it sends a transmitter drive waveform (TDW) to the transmitter and a Loran pulse is produced and is radiated from the antenna. When controlling the transmitted Loran signal, then, the MPT is used as the main time reference point for the Loran signal. In this thesis, the standard zero crossing is used only to perform the zero crossing test on an individual pulse.

c. Pulse Group Phase Coding

Another reason for the Loran-C pulse group is to distinguish the Loran groundwave from Loran skywaves. As in other low-frequency systems, radio waves may take multiple paths to reach a receiver. The groundwave follows the surface of the earth while skywaves are refracted and reflected by the ionosphere to return to the earth's surface. Generally the groundwave is used to calculate Loran time differences. Therefore a skywave, which has traveled a longer path and is thus delayed significantly, represents a spurious signal and may cause a large time difference error if interpreted accidentally as the groundwave. To distinguish the groundwave from skywaves, pulse group phase coding is used.

Phase coding is based on the fact that only the skywave undergoes a change in phase when traveling from the transmitter to receiver. The ionosphere refracts and reflects the pulses in the group and changes their phases by an arbitrary amount. The groundwave's pulse group, on the other hand, arrives at the receiver without a phase change (except for the 90° carrier phase shift from the near to the far field, which affects all the pulses about equally). Phase coding shifts the phases of certain pulses in the group by exactly 180° at transmission, according to a standard pattern shown in Table 2.2.

TABLE 2.2: LORAN-C PHASE CODES

Pulse Group	Station	
	Master	Secondary
A	+ + − − + − + − +	+ + + + + − − +
B	+ − − + + + + + −	+ − + − + + − −

A "+" indicates no phase change, and a "−" indicates a 180° phase change. Equipped with this expected pattern, the receiver successfully distinguishes the groundwave from skywaves. Two successive pulse groups, A and B, are required to implement this scheme. This two-GRI transmission sequence, called a Phase Code Interval (PCI), repeats constantly.

d. Transmitter Power Supply Droop

When eight or nine pulses are transmitted in rapid succession, the transmitter's power supply may not recover fully from pulse to pulse. This problem, most prevalent in older transmitters, causes the amplitude of each successive pulse in the group to decrease. In general, the first pulse in the group is the largest and the last pulse is the smallest. The decrease in amplitude of the smallest pulse relative to the largest pulse is called the "droop" and is defined in percent. The Coast Guard has established droop tolerances, which are included in the pulse group uniformity tests described later in this subsection.

The practice of dual-rating, explained more fully in Subsection B.4., accentuates the droop. A dual-rated station, located between two contiguous Loran chains, transmits pulse groups for two chains. Since the power supply of a dual-rated station often has less time to recover than that of a single-rated station, dual-rated stations are given larger tolerances for droop.

e. Specification: Uniformity of Pulses Within a Group (Three Tests)

Of the four tests applied to the individual Loran pulse, and explained earlier in Subsection B.1.(b), the tests of the half-cycle peak amplitudes (ensemble tolerance), the half-cycle peak amplitudes (individual tolerance) and the zero-crossings are applied only to pulse one. To measure uniformity of the pulses within the group, the test of ECD (as described in Subsection B.1.) is applied to each pulse. Two more tests, which examine pulse-to-pulse amplitude differences and pulse-to-pulse timing differences, are also applied.

Test 1: Pulse-to-Pulse ECD Differences. This test reflects in a general way how the shape of one pulse differs from the shapes of the others in the group. The ECD of any single pulse must not differ from the average ECD of all the pulses in the group by more than the tolerances in Table 2.3.

TABLE 2.3: PULSE-TO-PULSE ECD TOLERANCES

	Category 1	**Category 2**
Single-rate	$0.5\mu s$	$1.0\mu s$
Dual-rate	$0.7\mu s$	$1.5\mu s$

Test 2: Pulse-to-Pulse Amplitude Differences. The amplitude of the smallest pulse in a group must not differ from the amplitude of the largest pulse in that group by more than the limits in Table 2.4, calculated as follows:

TABLE 2.4: PULSE-TO-PULSE AMPLITUDE TOLERANCES, OR PERCENT DROOP (D)

	Category 1	Category 2
Single-rate	5%	10%
Dual-rate	10%	20%

$$D = \frac{I_{pk}\max - I_{pk}\min}{I_{pk}\max} \times 100 \qquad (2.5)$$

where

$I_{pk}\max$ is the value of $i(t)$ at the peak of the largest pulse
$I_{pk}\min$ is the value of $i(t)$ at the peak of the smallest pulse

Test 3: Pulse-to-Pulse Timing Differences. Pulses two through eight are transmitted at consecutive integer multiples of 1000μs after pulse one. Relative to the standard zero-crossings of pulse one, the standard zero-crossings of pulses two through eight must meet the tolerances listed in Table 2.5.

Pulse nine, which follows pulse 8 by 2000μs in the master pulse group only, is used mainly to identify the master signal and is not used for navigation [Ref. 1: p. 2–9]. Thus a tolerance is not assigned to its position in time.

3. Blink and "Out-of-tolerance"

Whenever a baseline is not useable for navigation, the first two pulses of that secondary station's pulse group are "blinked" ON and OFF repeatedly (0.25 seconds on, 3.75 seconds off). The Loran receiver passes along this warning to the user, often actually blinking ON and OFF the time difference reading on its display

TABLE 2.5: PULSE-TO-PULSE TIMING TOLERANCES

	Category 1	Category 2
Single-rate	$(p-1)1000\mu s \pm 25ns$	$(p-1)1000\mu s \pm 50ns + C$
Dual-:ate	$(p-1)1000\mu s \pm 50ns$	$(p-1)1000\mu s \pm 100ns + C$

Note: p is the pulse number (2 through 8) of the pulses which follow the first pulse within each group. C is 0 for positively phase coded pulses; $|C| \leq 150ns$ for negatively phase coded pulses. The standard zero-crossing of pulse one is the time reference within each group.

panel. The transmitter station or the control station initiates blink for any of the following reasons [Ref. 1: p. 2–8]:

- Time difference out of tolerance,
- ECD out of tolerance,
- Improper phase code or GRI, or
- Master or secondary station operating at less than one half of specified output power, or master station off air (not transmitting a signal at all).

Automatic alarms at the transmitter station and the control station sound when these quantities are out of tolerance.

In the definition of blink, the four tests of pulse number one and the three tests of the entire pulse group explained above are conspicuously absent. There are at least two reasons for this. The first is that the control station, with its Loran receivers, is monitoring the most important aspects of the Loran signal as far as the user is concerned: it ensures that a receiver can maintain lock and that the time difference is correct. In this sense, the fine details of the pulse which are the subject of these seven tests go beyond the minimum requirements of the Loran system to keep a useable baseline. The second reason is that most of the Loran control equipment suite was designed and built before modern signal processing equipment was available, and consequently these demanding tests are not conducted continuously either at the transmitting station or control station.

Instead, during a one-hour period each day designated for "system sample," an operator at each transmitter station manually tests ECD, the half-cycle peak amplitudes (ensemble tolerance), and the half-cycle peak amplitudes (individual tolerance), using an oscilloscope to measure the pulse peaks. He or she then enters the values by hand into a computer, which performs the tests and records the results. If a failed test is not accompanied by one of the conditions requiring blink, station personnel usually do not initiate blink, but instead interpret the test as an indication that transmitter maintenance is needed. From time to time, station personnel perform all seven tests and several more as well using a portable Loran Data Acquisition (LORDAC) unit. They use these results to keep the transmitter operating properly, but generally do not initiate blink if a test fails.

These seven tests thus represent a stricter standard than the conditions requiring blink and serve as an early warning of possible transmitter system problems which may later require blink. Therefore, a pulse out of tolerance in one of these seven tests may still be useable for navigation, but this is not a desired condition.

4. Dual-rating and Dual-rate Blanking

As mentioned briefly before, a dual-rated station, located between two contiguous chains, transmits pulse groups for two chains. These chains always have different GRIs, or rates. Since each chain is independently controlled, dual-rated stations are subject to competing, and sometimes conflicting, requirements as the pulse groups from the two GRIs periodically overlap in time. Since it is undesirable to transmit part of one pulse group and part of another, the conflict is solved by transmitting one and suppressing, or "blanking," the other. Blanking, which relates to the synchronization of two rates, should not be confused with blink, an indication of an out-of-tolerance condition.

Implementing dual-rate blanking is straightforward. A dual-rated tube transmitting station's timing equipment sets up a blanking interval over each pulse group, beginning $500\mu s$ before the first pulse is triggered and ending $1400\mu s$ after the last pulse is triggered. The timing equipment tracks the two blanking intervals as they move in time. When they overlap, the timer sends MPTs for only one of the two rates to the PGEN.

Two methods are used to decide which rate is blanked when an overlap occurs. In priority blanking, the same rate is always blanked, generally the shorter one. In alternate blanking, the priority role is passed back and forth between the rates at a time interval equal to the length of four times the longer GRI [Ref. 1: p. 2-9].

5. Frequency Spectrum Requirements

The energy that a station transmits outside the assigned 90 to 110 kHz band must not exceed one percent of total radiated energy. Furthermore, neither the energy below 90 kHz nor the energy above 110 kHz may exceed 0.5% of total radiated energy.

C. PRODUCING THE SIGNAL

1. The Loran Transmitter

a. Types of Transmitters

As mentioned previously, Loran-C transmitters are extremely narrowband amplifiers designed to resonate at exactly 100.00 kHz. The Coast Guard currently operates four types of transmitters, as listed in Table 2.6. The three types of transmitters with vacuum-tube power amplifier stages represent three generations of tube transmitter technology. The fourth generation, the solid-state transmitter, is now the state-of-the-art in Loran-C.

The solid-state transmitter is superior to the vacuum tube transmitter: it has a cleaner output signal, it has a higher ratio of output power to supplied line power, it is more robust, and it requires less maintenance than any other transmitter type. It also has an automatic pulse generating and control system. Many of the stations equipped with this transmitter are unmanned and remotely operated.

For all these reasons, the Coast Guard has considered replacing all of its older transmitters with the solid-state transmitter. However, the relatively high replacement cost ($2 million to $4 million per station) and the impending closure of some tube stations have kept the tube transmitters in operation for the foreseeable future. When the last AN/FPN-39 transmitters are removed from service in the next year or two, the only tube transmitter classes remaining will be the AN/FPN-42 and the AN/FPN-44/44A/44B/45. The '44 variants and the '45 are essentially the same transmitter with progressively more power amplifier stages and consequently greater output power. The '42 and the '44A, the subjects of this report, adequately represent the remaining tube transmitters.

b. Transmitter Loads

Each station has two different transmitter loads: the antenna and the resistive dummy load. Several types of antennas are in service, and they vary in radiated power and range. The two most common types are the 625-ft and the 700-ft top-loaded monopoles. The radiating part of these antennas consists of a single steel tower and an umbrella-like cap of guy wires leading from the top of

TABLE 2.6: TYPES OF LORAN TRANSMITTERS

Transmitter Designation	When Designed	Shape Control	Amplifier Type	Peak Power (KW)
AN/FPN-39	1950s	Manual	tube	250
AN/FPN-42	1950s	Manual	tube	300
AN/FPN-44A/45	1960s	Manual	tube	400/2000
AN/FPN-64	1970s	Auto	solid-state	400/800

the antenna down to anchors arranged on the ground in a circle around the antenna. A ground plane consisting of underground copper wires radiating outward from the base of the antenna every three degrees forms an electrical mirror image of the antenna. The antenna is connected to the transmitter through an impedance-matching tuning coil. The dummy load, a bank of large resistors, is used to perform various tests and maintenance procedures at varying power levels.

At two of the Coast Guard's research and training sites an antenna simulator is available. Essentially a high-power RLC circuit, the simulator mimics the function of a Loran antenna and allows Coast Guard personnel to conduct research and testing without interfering with Loran chains operating in the area.

c. Normal Loran Operating Procedures

There are two transmitters at each station. One transmitter at a time continually radiates a Loran signal using the antenna. This is designated the "operate" transmitter. Except during maintenance procedures, the second transmitter is kept in a "standby" status, ready to come on-line should a problem occur in the operate transmitter. Periodically the standby and operate designations are switched, allowing technicians to perform maintenance on the formerly operate transmitter. The standby transmitter may send pulses into the dummy load at any time without disturbing the operate transmitter and its signals. When transmitter switches interrupt Loran-C service for less than one minute, the Coast Guard considers the station to be transmitting continuously for availability recording purposes.

d. Nonlinear and Time-Varying Behavior of Tube Transmitters

This thesis incorporates two important assumptions. First, Loran tube transmitters are nonlinear devices, but behave linearly at a given operating point. This assumption is examined and supported in detail in the next chapter. Second, the transfer functions of the tube transmitters also vary with time. As transmitter components, particularly the vacuum tubes in the amplifier sections, age over days and weeks, their amplifying characteristics change. When components are replaced, small step changes occur to the transmitter's transfer function. When the operate and standby transmitters are switched, the pulse shape control system encounters a larger step change in the plant's transfer function. Loran technicians minimize these effects by a great deal of hard work, but the effects still exist to some degree. In addition to these internal factors, weather conditions, such as ice forming on the antenna and high winds (which distort the shape of the antenna slightly) introduce other time variations as well. Thus, from the point of view of a Loran-C control system, the transfer function of this plant exhibits both slow changes and periodic step changes over hours, days and weeks. In the absence of severe weather conditions or component failure, the transmitter may be considered time invariant for a period of several hours. This assumption is used also in the next chapter.

e. Transmitter Phase Code Balance

Tube transmitters use a push-pull amplification system, where the positive and negative parts of each pulse are amplified by separate banks of tube amplifiers. If the transmitter is not balanced properly, the positive half of the signal will be amplified more than the negative half, or vice versa. Most often this is detected when examining pulses whose phase code is different in GRIs A and B. When the pulse flips back and forth, it appears to "bounce." Phase code balance is an adjustment built into the PGEN which increases the magnitude of the TDW for negatively phase coded pulses (those pulses which have been inverted by a 180° phase change). In this way the phase code "bounce" is removed.

2. Transmitter Drive Waveforms and Typical Outputs

A cosine pulse input is used to excite the highly resonant Loran transmitter. A typical TDW and radio frequency (RF) antenna current waveform are shown for both the '42 and the '44A. The *terms input* and *input waveform refer* to the TDW, and the terms output and output waveform refer to the RF pulse captured at the transmitter ground return. Actually both input and output are at the same radio frequency.

In both TDWs, the cosine pulse includes eight full periods or, by Loran convention, sixteen half-cycles. To meet spectrum requirements on the '44A, a "tail drive" circuit adds a damped sinusoid to the end of the input cosine pulse to slow the decay of the RF output pulse. This prevents unwanted frequency components from appearing in the output. When input half-cycle 16 equals zero, as in Fig. 2.7, the tail drive is suppressed.

3. Controlling the Pulse Shape

In Figs. 2.6 and 2.7, each input half-cycle has a different peak amplitude. This is the result of the manual control scheme designed for the vacuum tube transmitters in the 1950s and 1960s and the pulse generator (PGEN) which implements it. By turning one of the 16 dials on the face of the pulse generator, the peak amplitude of any of the 16 input half-cycles may be adjusted in ten discrete steps. The controls of the two PGENs are shown in Fig. 2.8.

By observing the full-wave rectified RF pulse overlaid with the envelope of the ideal pulse, the dials of the PGEN may be adjusted to match the actual RF pulse shape to the ideal. The manual control system used for pulse shaping in the tube transmitters is diagrammed in Fig. 2.9.

The manual process of "pulse building" on a tube transmitter is one of the most difficult tasks in Loran-C system operation. Adjusting one half-cycle of the input affects not just one half-cycle of the output but all of the pulse which follows it in time. Also, the discrete steps available on the PGEN may result in large jumps in the amplitudes of the output pulse's half-cycle peaks. Added to this are the nonlinearities of the tube transmitters. Even with skilled and experienced operators this process can take several hours. Fortunately, time variations in the transmitter's operating characteristics ordinarily change even more slowly, so when pulse building, time variations may be ignored. However, because of these slow time variations, on each occasion when pulse-building is attempted, the transmitter's operating characteristics are slightly different. From one point of view, this amounts to manually controlling in a sixteen-dimensional space a nonlinear device which behaves slightly differently each time the control procedure is attempted.

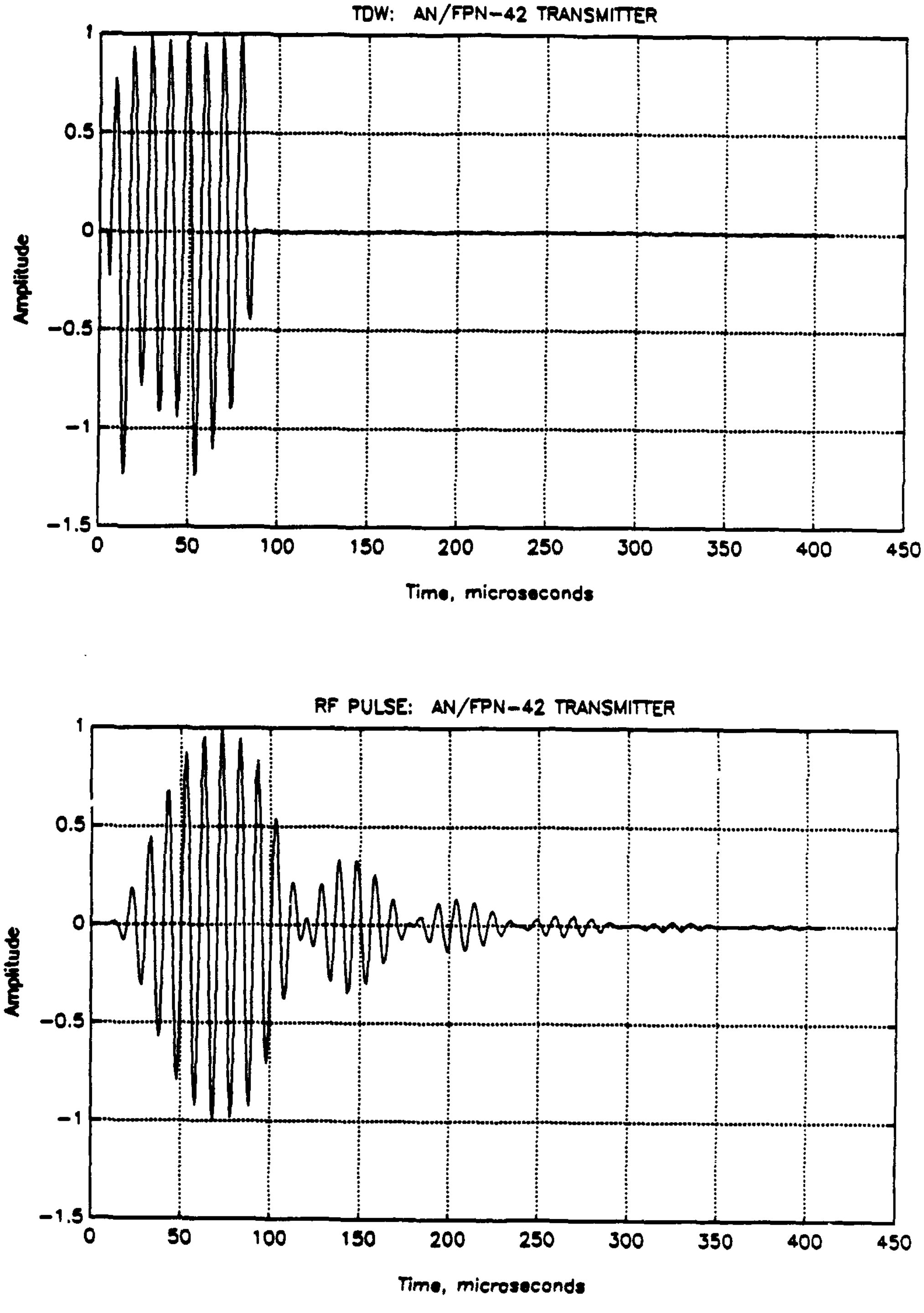

Figure 2.6: '42 input and output, antenna simulator, pair 30.

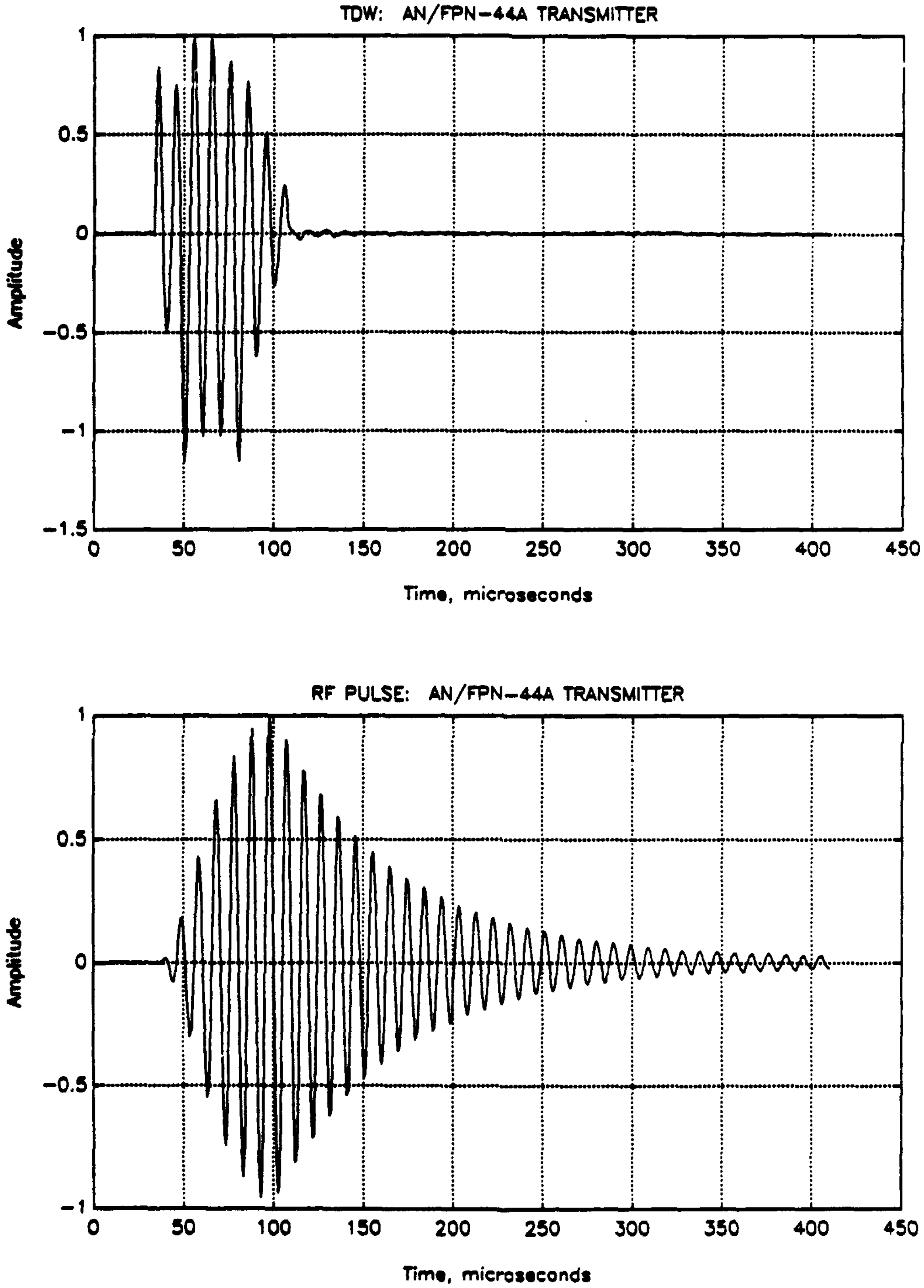

Figure 2.7: '44A input and output, antenna simulator, pair 72.

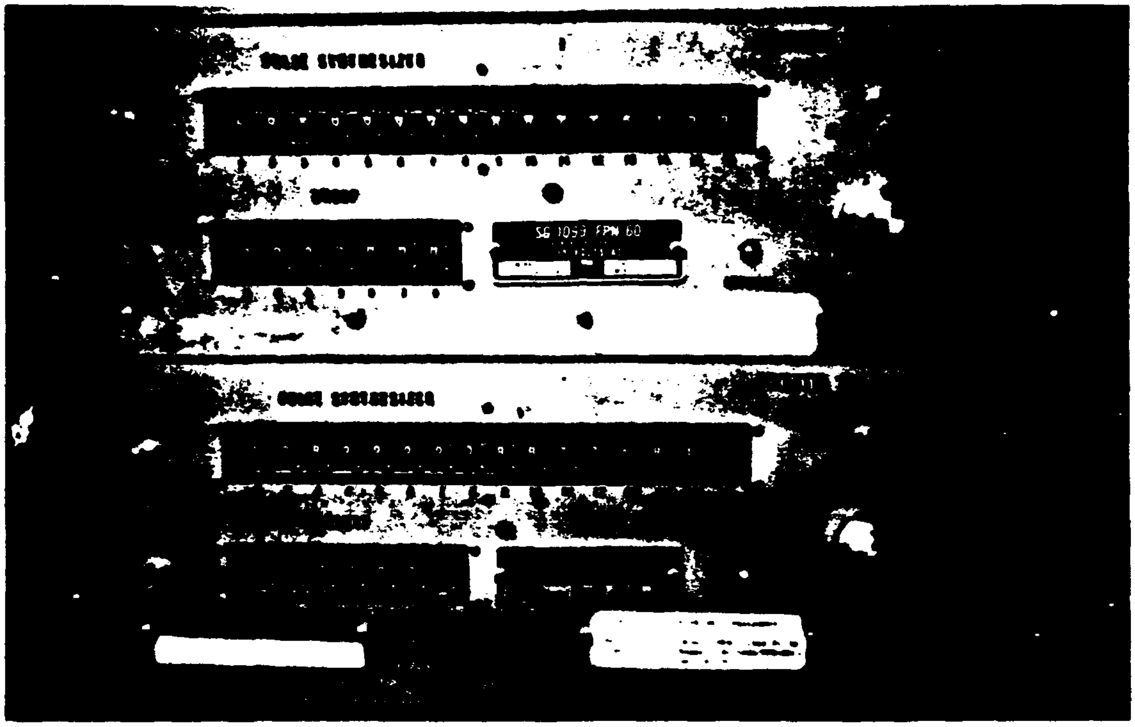

Figure 2.8: Two pulse generators.

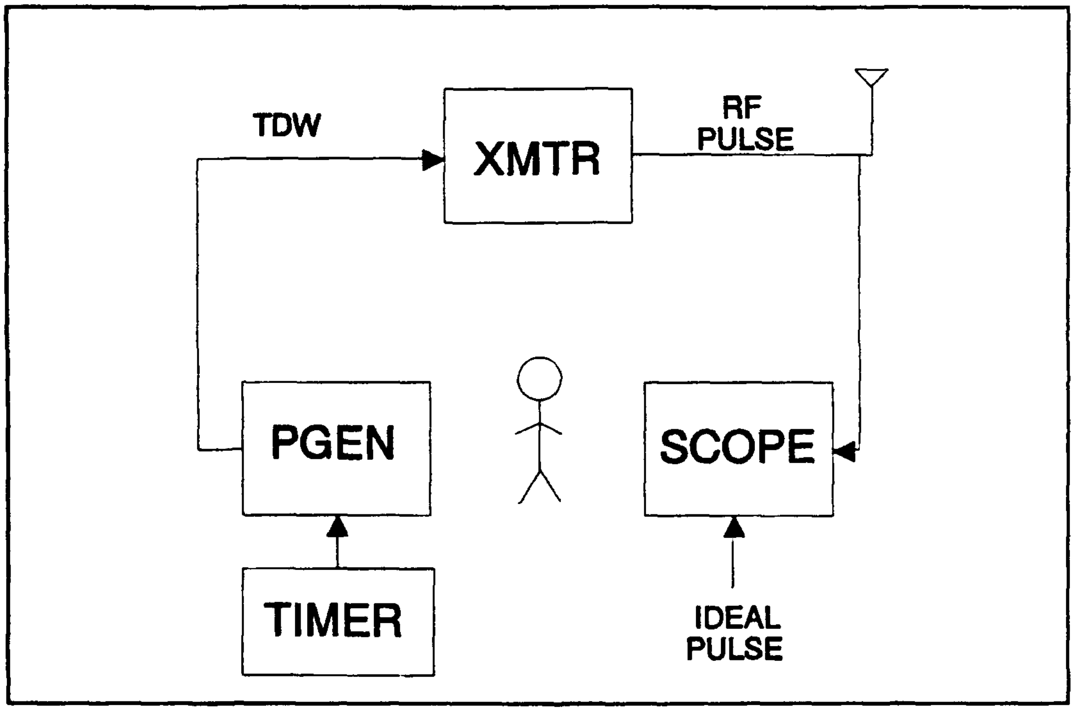

Figure 2.9: Manual control diagram.

Understandably, many technicians have opted to control the pulse from the "back end" by keeping the transmitter tuned identically at all times instead of attempting to compensate for time variations in the transmitter using the PGEN. While the results are often more predictable, this approach is certainly time intensive. Although an automatic pulse generation and control system was designed for the solid-state transmitter, none has yet been implemented for the tube transmitters.

D. THE ELECTRONIC EQUIPMENT REPLACEMENT PROJECT (EERP) AND THE PURPOSE OF THIS RESEARCH

1. The EERP and its Plan 1

In answer to the difficulties of manually controlling a tube transmitter and in response to many other considerations beyond the scope of this paper, in 1990 the Commandant of the U.S. Coast Guard assigned to the Coast Guard Electronics Engineering Center (EECEN) a multi-year project titled the *Electronics Equipment Replacement Project* [Ref. 7]. In identifying portions of the Loran-C system requiring a redesign effort, EECEN considered the following:

- The supportability of current and future equipment,
- The desire to enhance and expand automation,
- The need to respond to new system requirements, and
- The desire to remain in close step with technology.

This process resulted in five major plans. Plan One, titled "EPA/PGEN/-LORDAC Redesign," calls for a redesign of the entire tube transmitter's monitor and control equipment suite, including the Electrical Pulse Analyzer (EPA) and the Loran Data Acquisition (LORDAC) equipment. The new control system should be able to monitor and analyze the Loran pulse continuously, or nearly continuously; generate and control a Loran-C pulse in tolerance automatically; and record the results necessary to build a database of operational history [Ref. 7].

2. The VXIbus Based Loran-C Transmitter and Control System

In 1990 EECEN began to implement Plan One of the EERP by starting project W1180, originally titled "EPA/DPA Redesign" and subsequently renamed "Timing and Control Equipment (TCE) Redesign." In a 1991 report titled "The VXIbus Based Loran-C Transmitter and Control System," Taggart and Turban describe a prototype control system constructed at EECEN which, it is hoped, will perform these functions [Ref. 10]. A simplified diagram of this control system is shown in Fig. 2.10.

The system works as follows: The computer loads an initial TDW into an arbitrary function generator (AFG), which sends the TDW to the transmitter at each timer trigger. A digital storage oscilloscope (DSO) samples the RF pulse and stores it in the computer's memory. In a closed-loop fashion, the controller then computes a new TDW in an attempt to reduce the error between the actual and ideal RF pulses.

Based on the new generation of Automatic Test Equipment known as VMEbus Extensions for Instrumentation (VXIbus), this system will be much smaller and will have fewer components than the equipment used today. It will give the operator new control capabilities over each pulse in the pulse group. This system will thus produce a more consistent Loran signal while reducing maintenance.

Even though the '42 transmitter is not included in the EERP (it will be phased out in the next few years), it is simpler to operate than the '44A and will be valuable when developing this VXIbus system. In the end, the VXIbus control

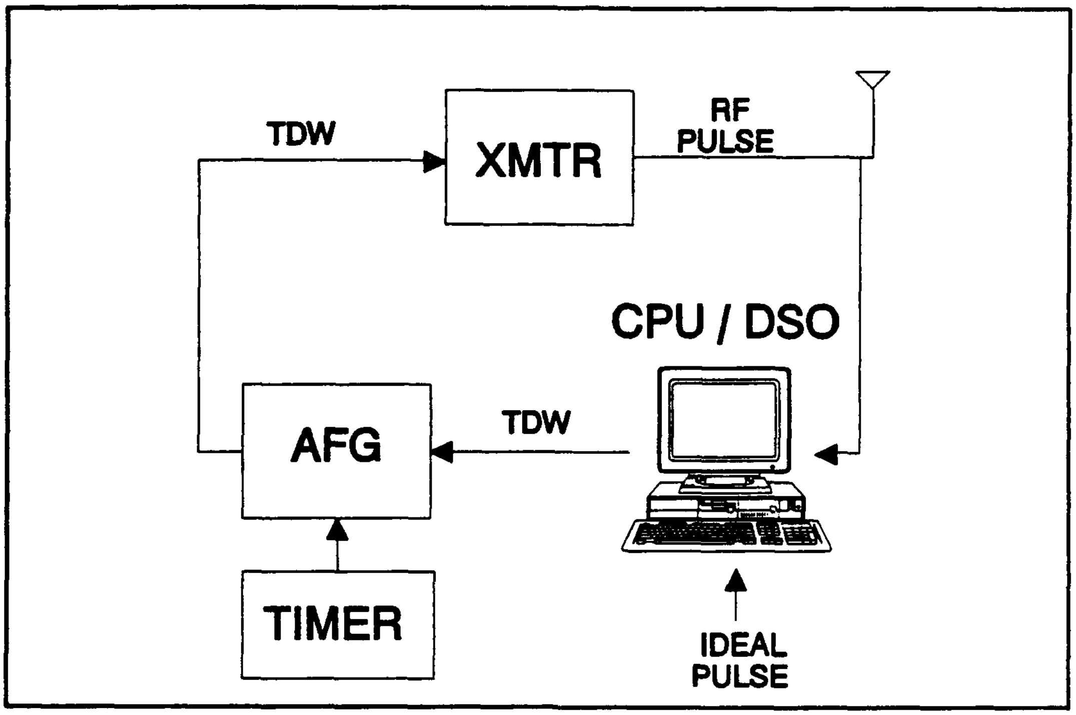

Figure 2.10: Diagram of the VXIbus based control system.

system will operate with the '44A but not with the '42 [Ref. 7, 10]. For these reasons, both the '42 and the '44A are included in this research.

3. Purpose of This Research

a. Primary goal: A Control Algorithm

One of the missing pieces in this VXIbus system is a proven algorithm to generate and control the Loran-C pulse shape automatically. Finding, developing and testing such an algorithm is the primary goal of this research. This paper contributes directly to Phase II of project W1180, *Pulse Generator Redesign* [Ref. 11]. The other phases of Project W1180 are specifically excluded from this paper except where they overlap with Phase II. Furthermore, within Phase II, only the pulse-shaping aspects of the PGEN redesign are considered. Precision timing between pulses and pulse groups is excluded.

b. Necessary Tool: A Computer Simulation Program

Achieving this goal requires a detailed computer program to simulate the operation of the '42 and '44A tube transmitters and those parts of the VXIbus control system involved in pulse shaping. There are at least three reasons for this. First, testing new types of transmitter drive waveforms, especially in closed loop control, is safer on a computer than on a 400 kilowatt transmitter. Second, working with a computer simulation is much faster, much easier and much more convenient both for the researchers in Monterey, California and for the EECEN technicians in Wildwood, New Jersey. Third, in this simulation the researcher controls the transmitter completely and can isolate the effects of different transmitter and control system factors on an algorithm. In this way control algorithms may be tested more thoroughly in simulation than with an actual transmitter. In the next chapter, mathematical models for the '42 and '44A are developed to use in the simulation program.

[THIS PAGE INTENTIONALLY LEFT BLANK]

III. MODELING THE AN/FPN-42 AND 44A LORAN-C TRANSMITTERS

A. INTRODUCTION

Simulating a dynamic physical system requires a dynamic model, a mathematical representation which transforms an input signal into an output signal just as the real system does, under the normal range of operating conditions. In this chapter, explicit mathematical models for the AN/FPN-42 and AN/FPN-44A transmitters are developed and tested. First, the modeling approach and data are described. Second, the unit sample response of the '42 transmitter is identified. Third, a linear, time invariant (LTI) pole-zero model is developed for the '42; next, observed nonlinearities and time variations are added to the model. After the performance of this model is tested, the entire process is repeated for the '44A.

B. THE MODELING APPROACH

1. Discrete-Time Representation

A discrete-time model represents the transmitters in this research, for several reasons. First, the VXIbus is a discrete-time system, and discrete-time techniques are most easily transferable to it. Second, this field is well-developed in the signal processing literature. Third, working with a discrete-time model is most convenient. The data is in discrete-time form already and many useful discrete signal processing algorithms and computer programs are available.

2. Data from the '42 and '44A transmitters

a. Data Collection

EECEN provided eighty-six discrete-time input and output data sequence pairs for this project, sixty-seven pairs for the '42 and nineteen for the '44A. For twenty-seven of these the dummy load was connected to the transmitter instead of the antenna or the antenna simulator. Sampled at 10 MHz by a LeCroix 9410 digital oscilloscope with eight bits of resolution, each sequence is 4096 points in length and covers a time period of 409.6 μs. The input sequence, which is the TDW, and the output sequence, which is the RF pulse, were sampled simultaneously on channels A and B of the oscilloscope. The two signals are synchronized to within 100 ns, the length of time between adjacent samples.

The RF pulses were measured at the ground return line to the transmitter using a Pearson current transformer. Both the TDW and the RF data sequences were measured in volts, with the input impedance of the oscilloscope set to infinity. Accordingly, this simulation uses volts for both TDW and RF pulse. Although the RF pulse is customarily measured in amperes, this difference is only a scaling factor and does not affect the validity of the simulation.

These data sequences are essentially the same as those available on the VXIbus system, which uses an eight-bit Tektronix digital storage oscilloscope. This similarity strengthens the usefulness of this simulation since a control algorithm has nearly identical data to work with in this program as well as in the VXIbus system.

b. Effects of Noise and Quantization

Figures 3.1a and 3.1b show the power spectra of the above two sequences. Figure 3.1c is a closeup of this plot. These are the periodogram estimates

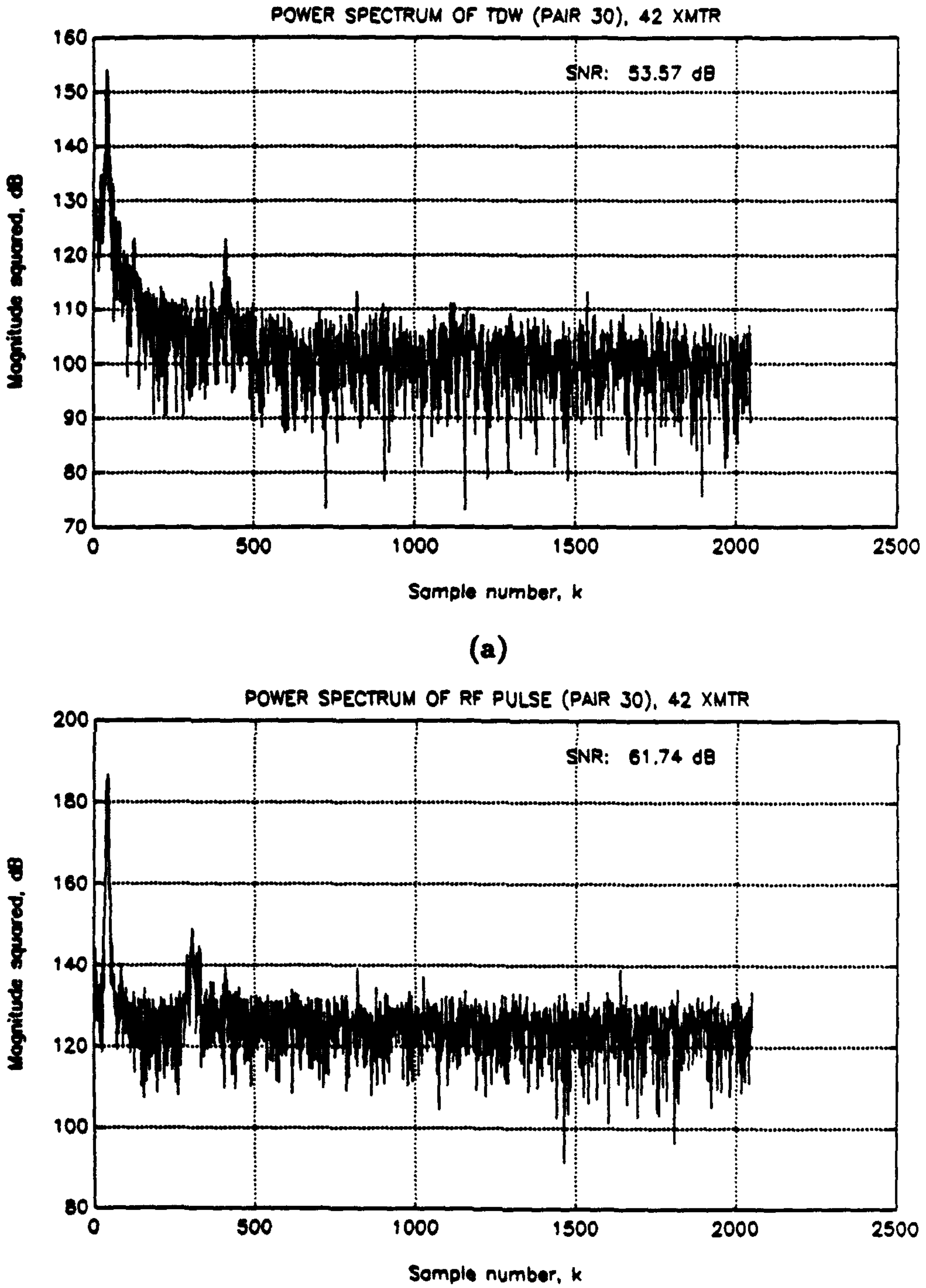
POWER SPECTRUM OF TDW (PAIR 30), 42 XMTR

(a)

POWER SPECTRUM OF RF PULSE (PAIR 30), 42 XMTR

(b)

Figure 3.1: Power spectrum of '42 with antenna simulator, pair 30. (a) TDW and (b) RF pulse.

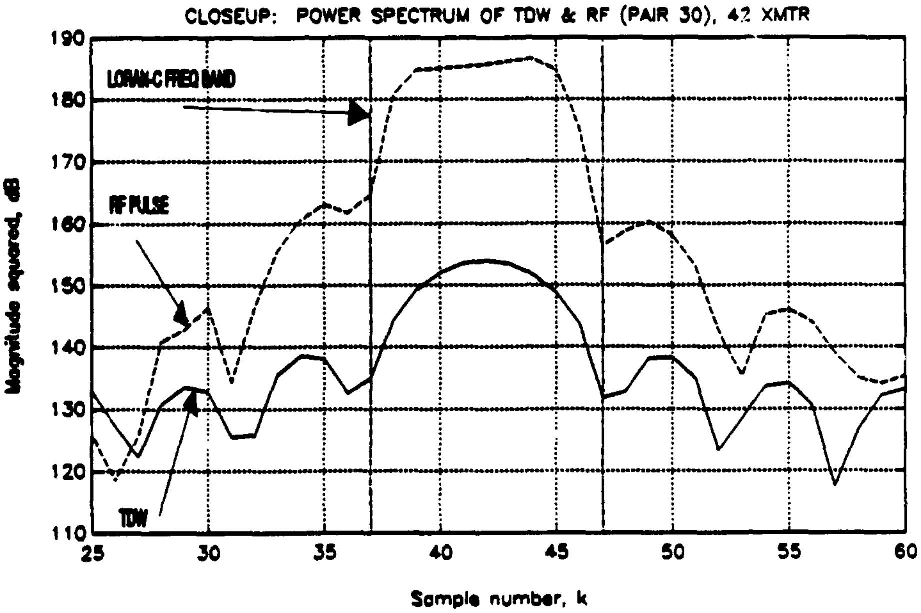

Figure 3.1c: Closeup of power spectrum, '42, pair 30.

expressed in decibels [Ref. 12, p. 448]. Sample 41 corresponds to 100 kHz and sample 2049 corresponds to 5.00 MHz, one half the sample frequency. Figure 3.1c also marks the 90–110 kHz frequency band of Loran-C.

The transmitter's behavior as a highly narrowband amplifier is apparent in these figures. In this data pair the signal-to-noise ratio (SNR) increases from 51 dB to 61 dB from input to output. Here the SNR is defined in decibels as the peak signal value minus the average value of the noise found in the highest twenty percent of the frequency range of the power spectrum. Underlying this definition are the assumptions that the Loran signal power present in this upper frequency band is negligible compared to the noise power and that the noise is white or approximately white. Some of the noise that appears in the output is inherent in the transmitter system itself, and some is quantization noise added by the sampling oscilloscope. Chapter V includes comparison results when each is varied.

3. Linearity and Time Invariance

a. Initial Assumption: Linear, Time Invariant (LTI) Within Each Pulse

In this work, a fundamental assumption was made that the tube transmitters behave as linear, time invariant (LTI) systems at a given operating point, within a limited time interval [Ref. 13, 14].

b. Verifying the Assumption

Testing a system for linearity and time invariance with all possible input sequences would be impossible. However, if the assumption is made that a system is LTI under certain operating conditions, its behavior may be completely represented by a unit sample response sequence, $h(n)$, the discrete version of the impulse response. Then the system output can be represented as a linear convolution,

$$y(n) = \sum_{m=-\infty}^{\infty} x(m)h(n-m) = x(n) * h(n)\,, \tag{3.1}$$

where $x(n)$ is the input sequence. With its shifting, multiplying and summing operations, linear convolution tests the crucial properties of LTI systems [Ref. 12, pp. 24-25, 103]. A good match between a "synthetic" output sequence $y_s(n)$ (produced by convolving actual input $x(n)$ with the proposed $h(n)$) and ıhe actual output sequence $y(n)$ strongly implies that the assumption of LTI behavior is valid. From this point, an analysis of the system may proceed using mathematical techniques applicable only to LTI systems, subject to further validations as more data becomes available or the operating point changes.

From an analysis of the data pairs available, the operating point is assumed to be a function of the shape of the TDW. If this remains unchanged from pulse to pulse, the operating point and the unit sample response also stay the same. As explained in the last chapter, the limited time interval in which this assumption is considered valid is a period of several hours.

The '42 model is developed first for a typical operating point before examining other operating points. The TDW and RF pulse shown in Fig. 2.6 define this typical operating point. The shape of this TDW, including the 80 μs length of the significant part, is representative of the TDWs used in operating the '42 transmitters in the Coast Guard.

Analysis revealed that the '42 transmitter no longer behaves linearly when TDWs are applied which excite the transmitter longer than 90 μs. This is apparent in the frequency domain. By linear theory, the bandwidth of an RF pulse should be no wider than the bandwidth of the input. However, the RF pulse bandwidth remained the same when the input signal bandwidth narrowed, and a linear model could not be constructed. Therefore, for TDWs in this category, this modeling approach is inaccurate and should not be used.

c. Adapting the Assumption to Nonlinear and Time-Varying Behavior

Implicit in the assumption above is the idea that when the shape of the TDW changes, a different unit sample response may be required to represent the transmitter accurately. Catenating a number of LTI models to cover a range of operating points implements this idea. If the transmitter's operating points can be identified with sufficient precision, and if a unit sample response sequence can be identified for each one, then a system which is non-LTI overall may still be treated as LTI.

4. Time-Domain Pole-Zero Modeling

a. Single LTI System

Each unit sample response sequence is by itself a useful mathematical model of the transmitter. Because each has a finite length, they may be classified as finite impulse response (FIR) systems. Modeling an FIR system as an infinite impulse response (IIR) system is often more efficient, because there are less parameters,. It is also more useful, because the roots of the IIR parameters have physical significance. This is the approach used here.

An IIR system may be represented by a constant-coefficient difference equation of the form

$$y(n)+a_1y(n-1)+\cdots+a_Py(n-P)=b_0x(n)+b_1x(n-1)+\cdots+b_Qx(n-Q)\,, \tag{3.2}$$

or

$$\mathbf{a}^T\mathbf{y}=\mathbf{b}^T\mathbf{x}\,, \tag{3.3}$$

where $y(n)$ represents the output sequence and $x(n)$ represents the input sequence. Coefficients $a_1,\cdots,a_P$ and $b_1,\cdots,b_Q$ are real and constant. Taking the z-transform of Eq. (3.2) yields the transfer function

$$H(z)=\frac{b_0+b_1z^{-1}+\cdots+b_Qz^{-Q}}{1+a_1z^{-1}+\cdots+a_Pz^{-P}}\,. \tag{3.4}$$

Factoring the numerator and denominator of this rational polynomial produces the alternate form

$$H(z)=b_0z^{P-Q}\frac{(z-f_1)(z-f_2)\cdots(z-f_Q)}{(z-g_1)(z-g_2)\cdots(z-g_P)}\,, \tag{3.5}$$

where numerator roots $f_1,\cdots,f_Q$ are the zeros of the transfer function and denominator roots $g_1,\cdots,g_P$ are the poles of the transfer function. Complex pole pairs represent the natural or resonant frequencies of the system while zeros represent the system's delays, gains, losses and initial conditions [Ref. 15, p. 3].

Pole-zero modeling in the time domain, as used in this thesis, is the process of estimating the poles and zeros of an IIR system based on the least squares criterion. The **a** coefficients are also known as the Autoregressive (AR) parameters, and the **b** coefficients are also called the Moving Average (MA) parameters. Thus, ARMA modeling is another term for pole-zero modeling, which uses both **a** and **b**.

Pole-zero modeling is characteristically applied to random processes [Ref. 16]. Most of these sequences represent systems with underlying dynamics of a relatively low order, overlaid by random noise. As Section C of this chapter describes, the random noise is expressly filtered out to isolate the system dynamics of the transmitter. These dynamics, not the random noise, are what the pole-zero model is intended to capture.

b. Catenated LTI Models

Each model in the catenation may have a slightly different unit sample response sequence, but each is still an LTI model. Therefore, the catenated model may be expressed as a linear difference equation with non-constant coefficients, of the form

$$y(n) + a_1(t, E_n)y(n-1) + \cdots + a_P(t, E_n)y(n-P)$$

$$= b_0(t, E_n)x(n) + b_1(t, E_n)x(n-1) + \cdots + b_Q(t, E_n)x(n-Q)\,, \qquad (3.6)$$

where each coefficient is a function of time, t, and of parameter E_n, which accounts for the nonlinear behavior of the transmitter at different operating points and is defined in Section E of this chapter. Both n and t are integer indices of discrete time, but they are used differently. Index n, a multiple of the uniform 100 ns sampling interval (for $N = 1$), appears in equations which represent transmitter dynamics within a period of 409.6 μs. This period is too short to experience the time variations described in the last chapter. Index t, on the other hand, represents the non-uniform time taken by one iteration of the Loran-C pulse shape controller. This sampling interval of t is set to four seconds in the simulation program and is lengthened slightly whenever the controller skips a blanked GRI. The time variations of the transmitter are also indexed along t. Every t_d iterations of t, coefficients $\mathbf{a}(t, E_n)$ and $\mathbf{b}(t, E_n)$ are incrementally changed. Using a realistic value of $t_d = 300$, the parameters change incrementally every 15 minutes; after a few hours these changes may become noticeable. For analysis and testing, the rate of the time variations may be increased by lowering t_d. In effect this compresses time scale t. These time variations are incorporated into the pole-zero model in Section E of this chapter. The process of calculating the non-constant coefficients to produce a nonlinear, time-varying model of the '42 transmitter is also described there.

The following section of this chapter is devoted to estimating the unit sample response of the transmitter, $h(n)$, at the typical operating point. Section D contains the algorithms which estimate the poles and zeros for this sequence in the time domain.

C. IDENTIFYING THE SYSTEM UNIT SAMPLE RESPONSE ('42 WITH ANTENNA SIMULATOR)

1. Frequency-Domain Deconvolution and its Numerical Problem

Building on the assumption of LTI behavior within each pulse, an idea used previously in pulse-shaping research on the VXIbus system is adapted to estimate the unit sample response: frequency-domain linear deconvolution using the discrete Fourier transform (DFT). In this operation, the DFT of the output sequence is divided, sample by sample, by the DFT of the input sequence. The resulting complex sequence $H(k)$ in the frequency domain may be interpreted as the DFT of the time-domain unit sample response $h(n)$. This sequence $h(n)$ is real and is obtained directly from $H(k)$ using the inverse DFT (IDFT). The fast Fourier transform (FFT) speeds the computation of the DFT greatly.

One significant problem exists with this approach: spurious peaks in the frequency domain, caused when output DFT samples are divided by input DFT samples close to zero. An ideal filter eliminates most of this numerical noise by setting equal to zero the elements of $H(k)$ corresponding to frequencies less than 50 kHz (sample 40) and greater than 150 kHz (sample 123). Because the sequences have been zero-padded to twice their original lengths, sample 82 now represents 100 kHz. However, spurious peaks still exist in the 50–150 kHz frequency band, as Fig. 3.2 demonstrates. These spurious peaks distort $h(n)$ significantly; unfortunately, zeroing frequencies in this range also distorts $h(n)$. A more sophisticated filter is required here.

2. Removing Spurious Peaks with Median Smoothing

A nonlinear smoothing technique consisting of running medians and a lowpass linear filter can remove the spurious peaks in $H(k)$ [Ref. 17]. First, the signal is considered to be the sum of rough and smooth parts R[H(k)] and S[H(k)]:

$$H(k) = R[H(k)] + S[H(k)]. \tag{3.7}$$

The running median $M_U[H(k)]$, simply the median of the U-point sequence $H(k - M + 1), \cdots, H(k-1), H(k), H(k+1), \cdots, H(k + M - 1)$, replaces sample $H(k)$. Here U is an odd integer and $M = (U+1)/2$. This smoother separates the rough and smooth parts of the signal by removing single samples with large errors. The smoother's output effectively follows a low-order polynomial curve without distorting the surrounding samples as a linear filter would [Ref. 17, p. 158]. This smoother preserves sharp discontinuities, a property useful in many applications.

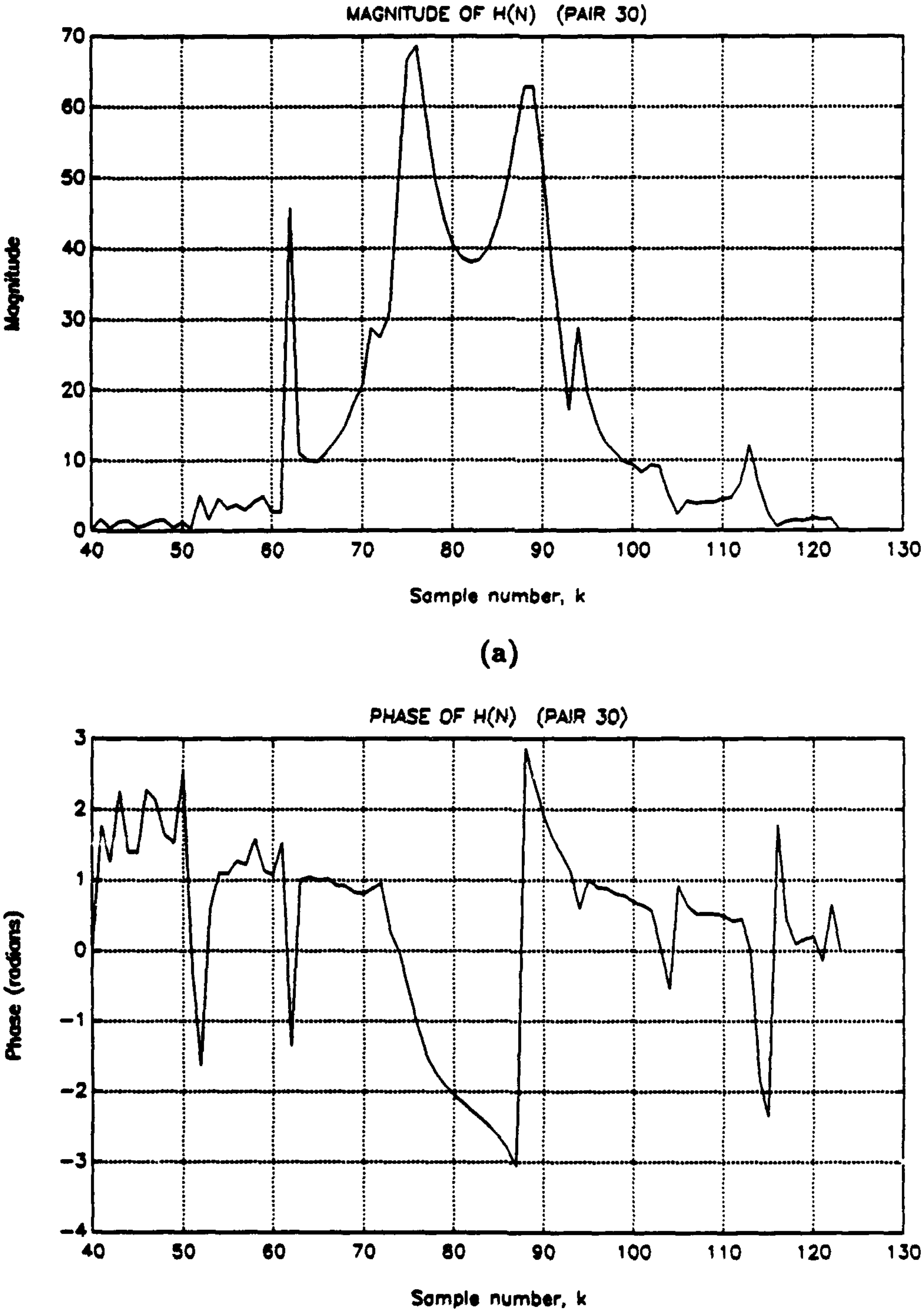

(a)

(b)

Figure 3.2: $H(n)$ for '42 with antenna, pair 30, with antenna simulator. (a) Magnitude and (b) phase.

Often, however, a linear filter is used in combination with the median smoother to soften these discontinuities. Here a succession of a five-point median smoother, a three-point median smoother and a three-point lowpass hanning filter is used. The hanning filter has unit sample response

$$\begin{aligned} h(n) &= 1/4, \qquad n = 0 \\ &\ 1/2, \qquad n = 1 \\ &\ 1/4, \qquad n = 2. \end{aligned} \tag{3.8}$$

This combination smoother is applied twice each to the parts of $H(k)$ corresponding to frequencies 50-90 kHz (samples 41–74) and 110-150 kHz (samples 91–122). The smoother is not used in the Loran frequency band, 90-110 kHz, since no spurious peaks were observed in this band.

This approach proved to be quite effective, as Fig. 3.3 demonstrates. The presence of more than one sharp discontinuity within U points can reduce the effectiveness of this technique, as samples 114–118 of the phase plots demonstrate. The estimated unit sample response, which appears in Fig. 3.4a, represents the relatively low-order system dynamics virtually free of random noise and of the numerical errors inherent in the frequency-domain deconvolution technique. This $h(n)$ is tested using linear convolution as before, with another similar input and output data sequence pair. Figure 3.4b shows that the estimated sequence correctly represents not only the resonances of the transmitter but also the amplitude and phase.

Simulation tests using $h(n)$ from both filtered and unfiltered $H(k)$ show that in the absence of spurious peaks in the 50–150 kHz band, the entire filtering operation increases the mean squared error (MSE) between the synthetic pulse and the

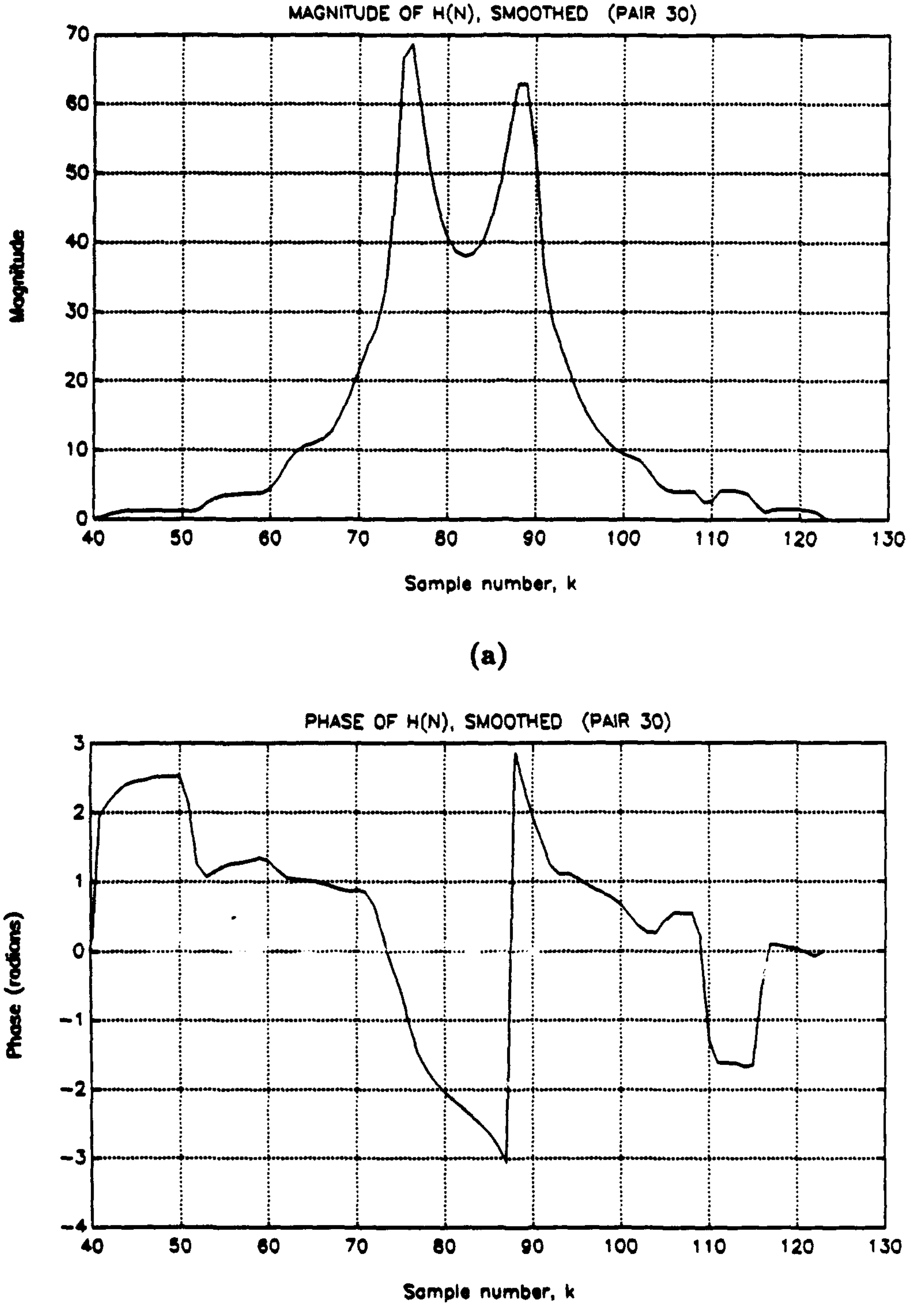

(a)

(b)

Figure 3.3: Smoothed $H(n)$ for '42 with antenna, pair 30, with antenna simulator. (a) Magnitude and (b) phase.

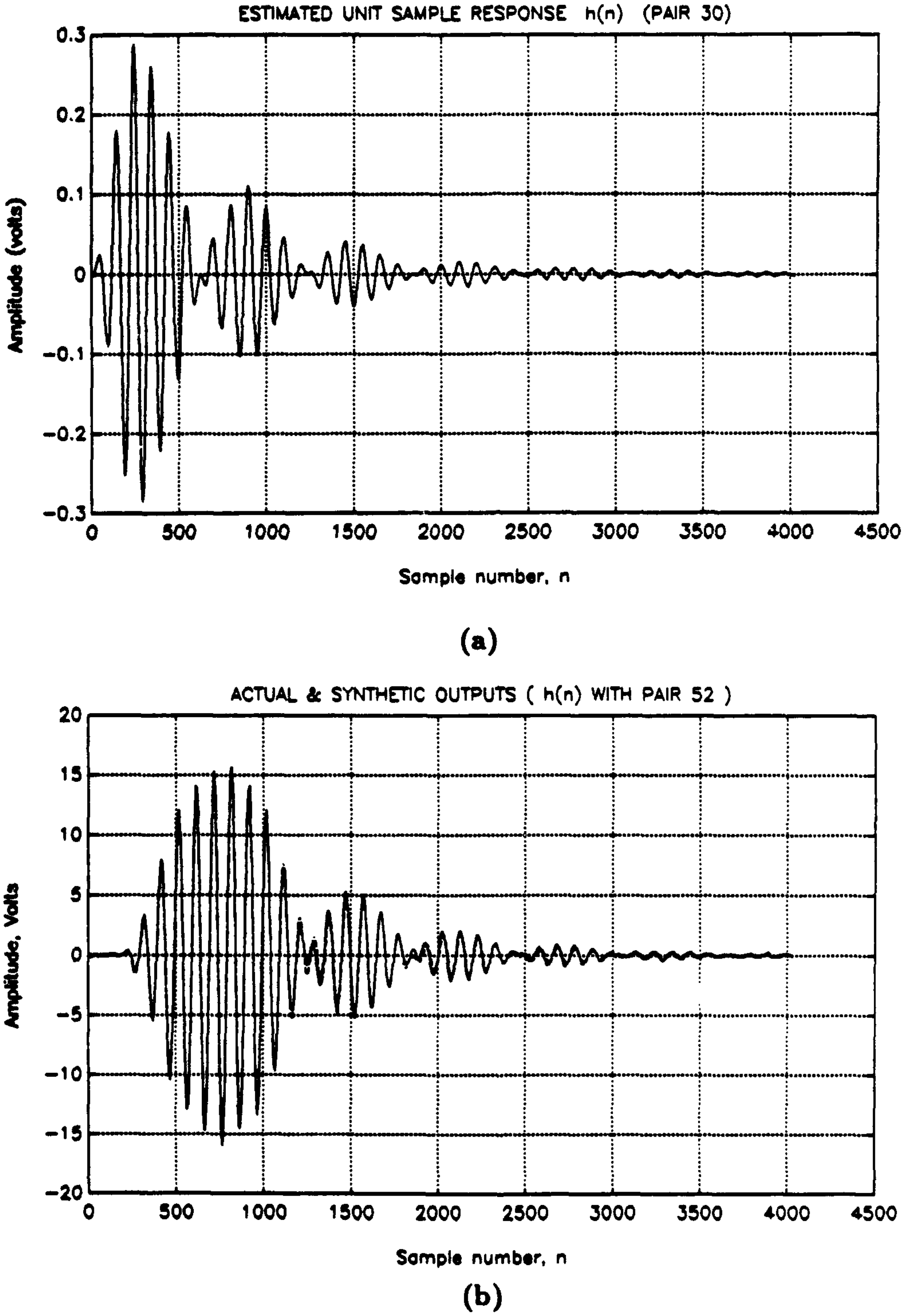

Figure 3.4: (a) Estimated unit sample response $h(n)$, pair 30, with antenna simulator, and (b) actual and synthetic RF pulses, $y(n)$ and $y_s(n)$, LTI model, with pair 52.

actual pulse by a maximum of two percent. The mean-squared error between two arbitrary sequences $w_1(n)$ and $w_2(n)$, each of length L, is defined as

$$e_{ms} = \frac{1}{L}\sum_{n=0}^{L-1}[w_1(n) - w_2(n)]^2. \tag{3.9}$$

When spurious peaks are present in this band, the filtering operation reduces greatly the mean squared error and makes an unusable $h(n)$ into a usable one.

This technique provides a quick and accurate way to estimate the unit sample response of the transmitter for any RF pulse, if the TDW is also provided. Now a pole-zero model may be constructed for this sequence.

D. A POLE-ZERO MODEL OF THE SYSTEM UNIT SAMPLE RESPONSE ('42 WITH ANTENNA SIMULATOR)

1. Sampling Frequency Considerations

As mentioned previously, the data sampling frequency f_s = 10 MHz is quite high relative to the Loran-C frequency band, 90–110 kHz. Ideally, a lowpass filter with cutoff frequency f_c = 110 kHz could be applied and the data could be sampled at f_s = 220 kHz without losing any significant Loran-C information. Thus, from one point of view, the data has been oversampled by a factor of 45.

EECEN personnel sampled the data at f_s = 10 MHz to provide the most information possible for this research. In particular, the high f_s selected allows a more thorough analysis of the system noise and provides accurate zero crossing times. The push-pull amplification of the tube transmitters may cause zero-crossing distortion from time to time, so this extra information is valuable.

If desired, a lowpass filter may be applied to these data vectors and they may be resampled at a lower rate (i.e., decimated) for analysis and simulation. In fact, many advantages exist in this approach: the data vectors are shorter and require less storage; the speed of the modeling and simulation programs increases; the poles and zeros are not as close to the real axis and to the unit circle in the z-plane, yielding a more stable system; and the modeling algorithm performs better when the frequencies of the roots are farther apart from each other.

Disadvantages also exist in decimating these vectors, however. In the presence of quantization and other noise, a great deal of resolution in the zero-crossing times is lost. For example, at $f_s = 1.25$ MHz (corresponding to a decimation factor of $N = 8$), the maximum error allowed for the '44A pulse's 40 μs zero-crossing is 50 ns, *one-sixteenth* the sampling interval. Zero-crossing times estimated by interpolation at this f_s are not as accurate as when interpolated at $f_s = 10$ MHz. Also, for sampling frequencies less than 10 MHz, interpolation is necessary when estimating the half-cycle peak amplitudes. This is because the samples do not fall at exactly the peak of each half cycle in general. This interpolation introduces noise which may cause problems in closed-loop control. At $f_s = 10$ MHz the peak estimation error is less than 0.1 percent of the peak value and may be safely ignored.

To reflect these two competing criteria, the data was analyzed at four different sampling frequencies: 1.25 MHz, 2.5 MHz, 5 MHz, and 10 MHz, corresponding to decimation factors $N = 8$, 4, 2, and 1, respectively. The best overall performance occurred at 10 MHz, and so the following sections on pole-zero modeling are presented at this sampling frequency.

2. Technique for Estimating the AR Parameters: The Least Squares Modified Yule-Walker Method

A number of techniques for linear modeling are based on the statistical characteristics of the signal being modeled. In this section, the least squares modified Yule-Walker method is used to find the $\mathbf{a}$ parameters of the IIR model of $h(n)$.

The autocorrelation function of $h(n)$ is defined as

$$R_h(i) = \sum_{m=-\infty}^{\infty} h(m)h(i+m), \qquad -\infty < i < \infty. \tag{3.10}$$

From Eq. (3.2), $R_h(i)$ can be expressed in the difference equation form

$$\begin{aligned} &R_h(i) + a_1 R_h(i-1) + \cdots + a_P R_h(i-P) \\ &= b_0 h(i) + b_1 h(i-1) + \cdots + b_Q h(i-Q), \end{aligned} \tag{3.11}$$

which can be written in matrix form [Ref. 16, p. 565]:

$$\begin{bmatrix} \mathbf{R}_B \\ \mathbf{R}_E \end{bmatrix} a = \begin{bmatrix} \gamma \\ 0 \end{bmatrix}. \tag{3.12}$$

Here $\mathbf{R}_B$ has dimensions $(Q+1) \times (P+1)$

$$\mathbf{R}_B = \begin{bmatrix} R_h(0) & R_h(-1) & \cdots & R_h(-P) \\ R_h(1) & R_h(0) & \cdots & R_h(1-P) \\ \vdots & \vdots & & \vdots \\ R_h(Q) & R_h(Q-1) & & R_h(Q-P) \end{bmatrix}, \tag{3.13}$$

and $\mathbf{R}_E$ is $(L-Q) \times (P+1)$

$$\mathbf{R}_E = \begin{bmatrix} R_h(Q+1) & R_h(Q) & \cdots & R_h(Q-P+1) \\ \vdots & \vdots & & \vdots \\ R_h(L) & R_h(L-1) & \cdots & R_h(L-P) \end{bmatrix}, \tag{3.14}$$

with $L > P + Q$. The components of vector $\boldsymbol{\gamma}$ are given by

$$\gamma(j) = \sum_{m=-\infty}^{\infty} b(j)h^*(m-j), \tag{3.15}$$

with $b(j)$ defined as

$$b(j) = \begin{cases} b_j\,; & 0 \le j \le Q \\ 0\,; & \text{otherwise} \end{cases}. \tag{3.16}$$

The lower partition of Eq. (3.12) is solved first to yield an estimate of **a**. If the correlation function and the model order P, Q were known exactly, only P equations would be required to find **a**, and $\mathbf{R}_E$ would need only P rows. The remaining

$L-(P+Q)$ rows of $\mathbf{R}_E$ would be redundant. However, because these quantities are not known exactly, the overdetermined set of equations is more appropriately solved for $\mathbf{a}$ in the least squares sense. Let $\boldsymbol{\epsilon}$ be the error vector that results from an arbitrary choice of $\mathbf{a}$:

$$\mathbf{R}_E\mathbf{a} = \boldsymbol{\epsilon}\,. \tag{3.17}$$

The solution of the following equation minimizes $\boldsymbol{\epsilon}$:

$$(\mathbf{R}_E^{*T}\mathbf{R}_E)\mathbf{a} = \begin{bmatrix} \boldsymbol{\epsilon}^{*T}\boldsymbol{\epsilon} \\ \mathbf{0} \end{bmatrix}\,. \tag{3.18}$$

This equation is solved by partitioning $\mathbf{R}_E$ as

$$\mathbf{R}_E = \begin{bmatrix} | & \\ \mathbf{r}_0 & \mathbf{R}'_E \\ | & \end{bmatrix} \tag{3.19}$$

and estimating $\mathbf{a}$ using the pseudoinverse:

$$\mathbf{a} = -\mathbf{R}_E'^{+}\mathbf{r}_0\,. \tag{3.20}$$

The MATLAB left division command ("\") provides a method for computing the pseudoinverse of a rectangular matrix with a high degree of numerical precision. This algorithm is based on the QR decomposition [Ref. 18]. The Singular Value Decomposition (SVD) could not be used here because of the large size of $\mathbf{R}_E$ (with 4093 rows in $\mathbf{R}_E$, the SVD unitary matrix $\mathbf{U}$ is (4093 × 4093) and requires 134 MB of computer memory). Results obtained with the SVD using smaller portions of $\mathbf{R}_E$ proved to be less accurate than those obtained with the MATLAB *left division* command when using all of $\mathbf{R}_E$.

3. Technique for Estimating the MA Parameters: Shank's Method

If the above statistical approach was continued, vector $\mathbf{b}$ could now be solved by first calculating $\boldsymbol{\gamma}$, using

$$\boldsymbol{\gamma} = \mathbf{R}_B\mathbf{a} \tag{3.21}$$

and then applying spectral factorization techniques. However, a better time-domain match is obtained using the deterministic approach of Shank's method [Ref. 17, pp. 510–512, 558–560].

Shank's method begins with the estimate of **a** found by one of the least squares methods, as in the previous Subsection. This all-pole model may be expressed by the transfer function

$$H_A(z) = \frac{1}{A(z)}, \tag{3.22}$$

where $A(z)$ is the denominator of Eq. (3.4). The desired IIR model transfer function is then

$$H(z) = B(z)H_A(z). \tag{3.23}$$

Using the all-pole model's unit sample response $h_A(n)$, which is derived from $H_A(z)$, the time-domain modeling error of the pole-zero model is

$$e_B(n) = h(n) - h_A(n) * b(n). \tag{3.24}$$

Figure 3.5 is a schematic representation of Eq. (2.4). $B(z)$ is chosen so that the sum of squared errors is minimized:

$$\mathcal{S}_B = \sum_{n=0}^{L-1} |\mathrm{e}_B(n)|^2. \tag{3.25}$$

Then vector **b** satisfies

$$\mathbf{H}_A\mathbf{b} = \mathbf{h} \tag{3.26}$$

in the least squares sense, where

$$\mathbf{H}_A = \begin{bmatrix} h_A(0) & 0 & \cdots & 0 \\ h_A(1) & h_A(0) & \cdots & 0 \\ \vdots & \vdots & & \vdots \\ h_A(Q) & h_A(Q-1) & \cdots & h_A(0) \\ \vdots & \vdots & & \vdots \\ h_A(L-1) & h_A(L-2) & \cdots & h_A(L-Q-1) \end{bmatrix} \tag{3.27}$$

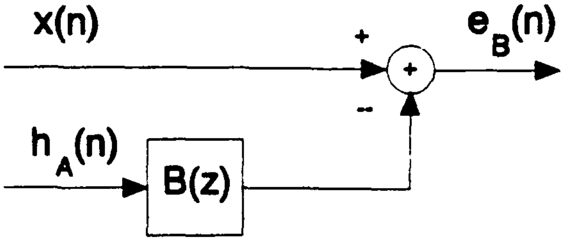

Figure 3.5: Diagram of Shank's method.

and

$$\mathbf{h} = \begin{bmatrix} h(0) \\ h(1) \\ \vdots \\ h(Q) \\ \vdots \\ h(L-1) \end{bmatrix} . \tag{3.28}$$

Vector **b** is estimated using the pseudoinverse, as before:

$$\mathbf{b} = \mathbf{H}_A^{+}\mathbf{h} . \tag{3.29}$$

4. The Pole-Zero Model

By trial and error, model order $P = 4$, $Q = 3$ was chosen. Vectors

$$\mathbf{a} = \begin{bmatrix} 1.0000 \\ -3.9856 \\ 5.9645 \\ -3.9723 \\ 0.9934 \end{bmatrix} \tag{3.30}$$

and

$$\mathbf{b} = \begin{bmatrix} 0.0513 \\ -0.1508 \\ 0.1640 \\ -0.5650 \end{bmatrix} \tag{3.31}$$

model $h(n)$ of Fig. 3.4a with the minimum mean squared error. Here **a** has the form $[1, a_1, a_2, \cdots, a_P]'$ and **b** has the form $[b_0, b_1, b_2, \cdots, b_Q]'$. The process of selecting the model order is examined in detail later in this section.

The poles and zeros of this model are calculated from **a** and **b**:

$$\text{poles} = \begin{bmatrix} 0.9983\, e^{+j0.0675} \\ 0.9983\, e^{-j0.0675} \\ 0.9984\, e^{+j0.0569} \\ 0.9984\, e^{-j0.0569} \end{bmatrix} \qquad \text{zeros} = \begin{bmatrix} 1.0361\, e^{+j0.0677} \\ 1.0361\, e^{-j0.0677} \\ 1.0260\, e^{j0} \end{bmatrix} . \qquad (3.32)$$

When the elements of **a** and **b** of are substituted into Eq. (3.2), a unit sample input yields the model sequence $h_{AB}(n)$. Figure 3.6a contains a z-plane plot of these poles and zeros while Fig. 3.6b is a time-domain plot of $h(n)$ and $h_{AB}(n)$.

Overall, the time-domain match is excellent, indicating that the pole-zero modeling algorithm has performed well. This is a non-minimum phase system and therefore cannot be inverted because that would result in an unstable system. Controlling this system using certain algorithms is now potentially more difficult.

5. Two Criteria for Selecting Model Order

The competing criteria of accuracy and simplicity are used to select the IIR model order. The criterion of accuracy is expressed by two time-domain measurements. The first is the mean-squared error between $h(n)$ and $h_{AB}(n)$. The second is the mean squared error between actual and synthetic RF pulses $y(n)$ and $y_s(n) = x(n) * h(n)$, where $x(n)$ is the actual TDW sequence corresponding to $y(n)$. This is the same simulation test described previously. In this case, however, both $y(n)$ and $y_s(n)$ are normalized so that the maximum positive amplitude of each equals one. This quantity, called the normalized mean squared error (NMSE), measures the effectiveness of the modeling algorithm by comparing shape and phase information while ignoring any difference in the maximum pulse peak amplitudes of $y(n)$ and $y_s(n)$. The reason for ignoring the amplitude difference lies in the data. The overall transmitter gain for data pairs obtained weeks and months apart was not generally the same, perhaps because of the components periodically replaced over

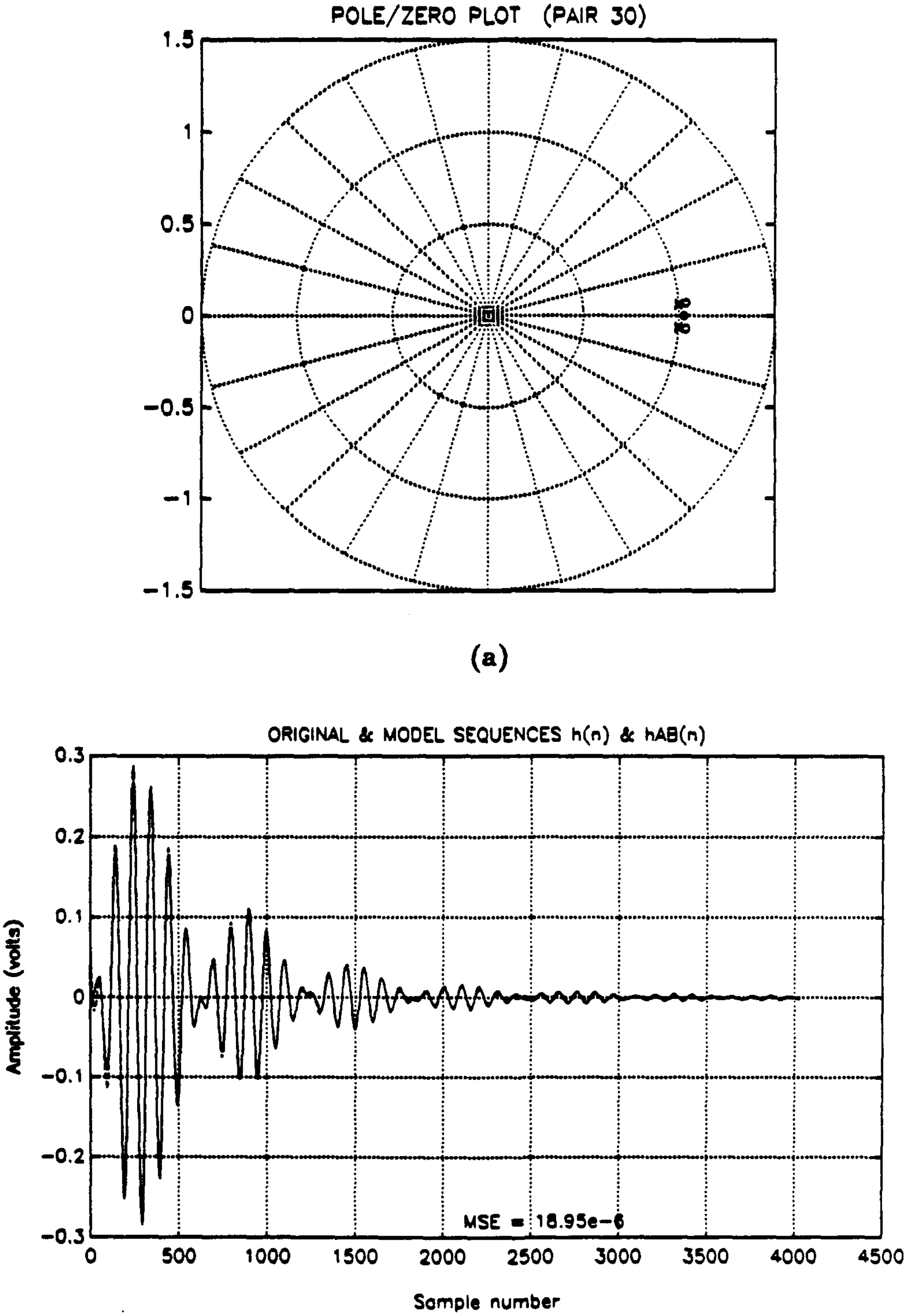

(a)

(b)

Figure 3.6: (a) Pole-zero plot of '42 LTI model, pair 30, with antenna simulator, and (b) original and model sequences, $h(n)$ and $h_{AB}(n)$.

that time period. Therefore, differences in the amplitudes of the $h(n)$ sequences for these pairs may be excused. Special data pairs were obtained to map the relationship between input and output maximum positive amplitudes, and the simulation program uses these to scale the output. Thus this problem is not a serious one.

The criterion of simplicity indicates that a lower model order is better. In the simulation program, assigning more poles and zeros takes more time. Therefore, increasing the model order without obtaining a corresponding increase in accuracy is undesirable. Also, when the model order is unnecessarily high two negative effects may occur. The first is that the poles and zeros may not be consistent from one $h(n)$ sequence to the next. For example, one $h(n)$ may have a complex zero pair and a real zero, while the next may have three real zeros. This hampers the implementation of the nonlinear model described in the next section. The second is that the effective rank of $\mathbf{R}_E$ may be less than P, or the effective rank of $\mathbf{H}_A$ may be less than Q. This may cause numerical problems in the modeling algorithm when computing the pseudoinverse. Other indications that the order is too high are pole-zero cancellations (when poles and zeros migrate to the same locations and, in the transfer function, cancel each other out) and large negative real zeros.

Selecting model order, then, is necessarily a somewhat subjective process. Table 3.1 lists the two criteria and associated remarks for a range of model orders for the '42 transmitter. Pair 30 provides the sequence $h(n)$, as before; pair 52 provides the test TDW and RF pulse. Orders below $P = 4$, $Q = 1$ were wholly inadequate. Model order $P = 4$, $Q = 3$ was chosen according to these criteria. AR models obtained by the least squares modified Yule-Walker method are not effective at this sampling frequency, but at lower sampling frequencies their accuracy approaches that of the ARMA models. However, they still require nearly double the number of parameters. Perhaps a more deterministic AR modeling algorithm such as Prony's

TABLE 3.1: BASIS FOR SELECTING MODEL ORDER, AN/FPN-42 TRANSMITTER

P	Q	Measure 1 MSE	Measure 2 NMSE	Remarks
4	1	2.1069×10^{-4}	1.2325×10^{-3}	
4	2	7.6821×10^{-5}	1.2633×10^{-3}	
4	3	1.8948×10^{-5}	9.0733×10^{-4}	Best overall *******
4	4	1.8314×10^{-5}	9.1274×10^{-4}	4th zero: at $z = -350 + j0$
5	3	3.2620×10^{-5}	8.8762×10^{-4}	
5	4	1.8585×10^{-5}	8.9258×10^{-4}	
5	5	1.9309×10^{-5}	7.4982×10^{-4}	Mtx close to singular
6	3	5.5609×10^{-5}	9.7328×10^{-4}	
6	4	1.8415×10^{-5}	9.1727×10^{-4}	
6	5	4.6451×10^{-5}	7.3653×10^{-4}	Mtx close to singular
6	6	1.1680×10^{-4}	1.3550×10^{-3}	
10	0	2.9922×10^{-3}	9.7445×10^{-2}	AR models
18	0	1.2797×10^{-3}	4.5499×10^{-2}	
24	0	2.3607×10^{-3}	7.3931×10^{-2}	

Method would produce better AR models [Ref. 15, pp. 88–89; Ref. 16, p. 550]. However, that is not the subject of this thesis. Completely deterministic ARMA modeling (for example, using Prony's Method to find **a** and Shank's method to find **b**) is not quite as effective here as the statistical/deterministic combination of the least-squares modified Yule-Walker method and Shank's method.

E. NONLINEAR, TIME-VARYING MODEL OF THE AN/FPN-42 TRANSMITTER

1. Representing Nonlinearities by Moving Poles and Zeros

a. Changes in the Positions of Poles and Zeros Caused by Changes in TDW Shape

The transmitter's unit sample response changes slightly as the shape of the TDW changes. The pole-zero models of these sequences are correspondingly different also. The pole-zero scatter plot of five data sequence pairs in Fig. 3.7 illustrates this. All five were obtained within a period of three hours, avoiding time variations in the transmitter. The length of time each TDW excited the transmitter ranged from 5 μs to 80 μs, which provides a range of differently shaped TDWs. The average MSE between $h(n)$ and $h_{AB}(n)$ for these five pairs is 3.4641×10^{-6}, indicating an excellent match. This validates the assumption of LTI behavior at operating points other than the typical one described previously.

b. Assigning Poles and Zeros by Parameter E_n

The apparent trajectories of the poles and zeros in Fig. 3.7 imply that the transmitter may be simulated effectively by assigning the poles and zeros of the model based on the shape of the TDW. In forming this catenated model a reliable way is needed to relate the changes in TDW shape to the trajectories of each pole and zero.

The energy of the normalized TDW (with the TDW's maximum positive amplitude equal to one) can be used to assign poles and zeros according to TDW shape. This energy, in units of watt-seconds, is defined as

$$E_n = \frac{x(n)^T x(n) T}{\{\max[x(n)]\}^2 R}, \tag{3.33}$$

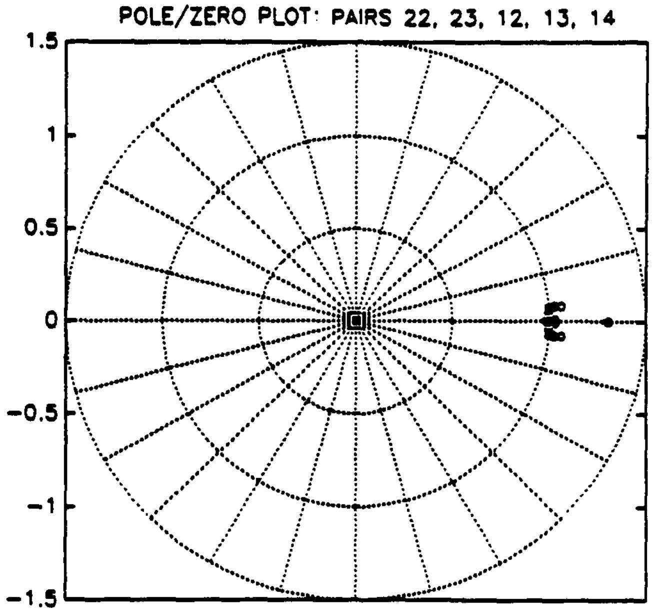

Figure 3.7: Pole-zero scatter plot for '42 with antenna simulator for five LTI models.

where sampling interval T is in seconds and load resistance R is normalized to one. The choice of parameter E_n reflects an assumption that the most important characteristic of the TDW shape is the length of time the TDW provides a significant level of excitation to the transmitter. As observed before, transmitter behavior changes significantly for TDWs that excite the transmitter longer than 100 μs, and the transmitter no longer behaves linearly for TDWs that excite the transmitter longer than 90 μs. It seems reasonable, then, to assume that the length of time the TDW excites the transmitter is an important indication of transmitter behavior also when this length is less than 90 μs. If the pole and zero locations are consistent from one $h(n)$ to another, if the poles and zeros form a fairly predictable trajectory as they move with respect to E_n, and if the synthetic RF pulse $y_s(n)$ matches the actual RF pulse $y(n)$, the approach using E_n may be considered valid.

Poles and zeros are assigned using E_n as follows. First, the trajectory of each pole and zero is assumed to be smooth and continuous, rather than a series of discrete steps. The magnitude and phase of the kth root from each data pair are plotted, so that there as many data points on the magnitude plot and the phase plot of the kth root as the number of data pairs. A polynomial curve is fitted to the points on both plots, and the process is repeated for each root.

A special MATLAB function MOD2 was written to fit these curves. The user selects the order of the polynomial curve and may even add points at his or her discretion to stabilize or bend the curve. The original points are denoted "o" and any added points are denoted "*". When the user is satisfied with the curve, he or she selects the minimum and maximum values of E_n and so defines the range over which the curve is valid. The program stores these endpoints and the polynomial values at the endpoints. These are used when assigning poles and zeros if E_n falls outside the endpoints. The coefficients $c_\ell, c_{\ell-1}, \cdots, c_1, c_0$ of the polynomial

$$c_\ell(E_n)^\ell + c_{\ell-1}(E_n)^{\ell-1} + \cdots + c_1 E_n + c_0 \tag{3.34}$$

are stored as well. The curves fit by this program for the magnitude and phase of the inner pole appear in Fig. 3.8. If the pole and zero locations in one $h(n)$ sequence are not consistent with those of other $h(n)$ sequences, then that $h(n)$ may create a spike in one or more of the parameter curves. These outlier $h(n)$ sequences may be discarded to fit the curve more accurately.

When a TDW is presented to the MATLAB function XMTR, which simulates the transmitter, the function first computes E_n for the TDW. The function recalls in turn the stored coefficients of each polynomial, evaluates them at this

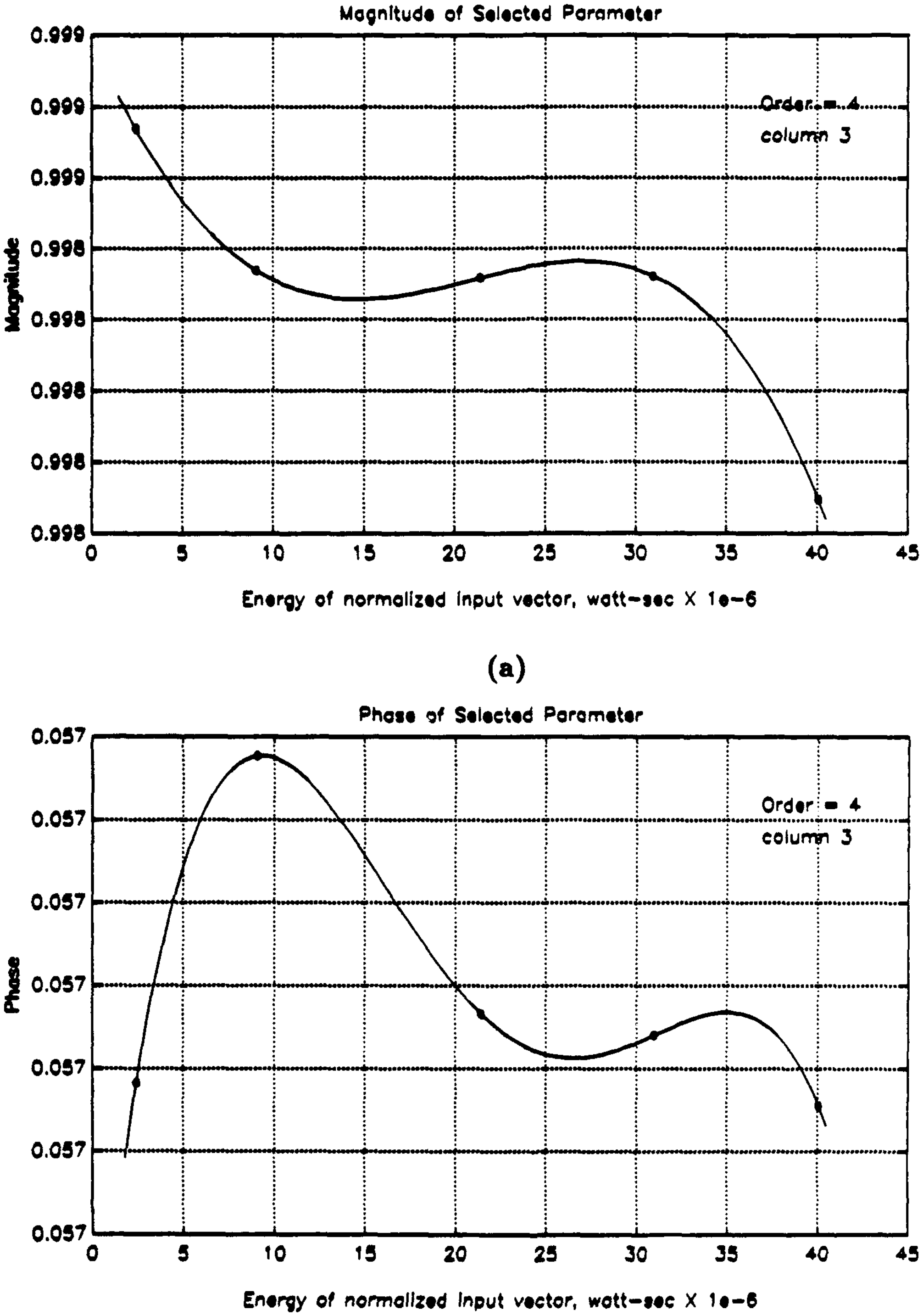

(a)

(b)

Figure 3.8: Fitted curves for inner pole pair, '42 with antenna simulator (5 pairs). (a) Magnitude, and (b) phase.

E_n, and combines these magnitudes and phases into poles and zeros. Vectors **a** and **b** are then formed from these roots. Next, a unit sample and Eq. (3.2) produce $h_{AB}(n)$, which is then convolved with $x(n)$ to yield $y_s(n)$. Finally, the amplitude of $y_s(n)$ is scaled appropriately, according to the input/output energy relationship from special data pairs obtained for this purpose.

c. Performance of the Catenated Model

The catenated model, as implemented in the function XMTR, was tested using the five data pairs described previously. As an example, the normalized actual and synthetic RF pulses $y(n)$ and $y_s(n)$ for pair 14 appears in Fig. 3.9. The sequences are normalized because of the overall transmitter gain difference discussed previously. The match is an excellent one; the plots of the other four pairs of $y(n)$ and $y_s(n)$ show about the same level of performance. The NMSE values between $y(n)$ and $y_s(n)$ for all five pairs appear in Table 3.2. As a basis for comparison, the same tests are performed using the linear model of pair 30 developed earlier in this chapter instead of the catenated nonlinear model. Table 3.2 also includes these results. The simulation error of the nonlinear model is about an order of magnitude smaller in these tests than the simulation error of a simple linear model, for an average reduction of 93.4 percent. For data pair 14 the performance of both models is about the same. These results validate this method of representing the transmitter's nonlinearities and demonstrate that the model accurately reflects the transmitter's behavior over a wide range of operating points. This extra degree of accuracy could make the difference between developing an algorithm that works on the nonlinear transmitter and VXIbus control system and developing an algorithm that does not. Next, the time variations of the transmitter are added to this model.

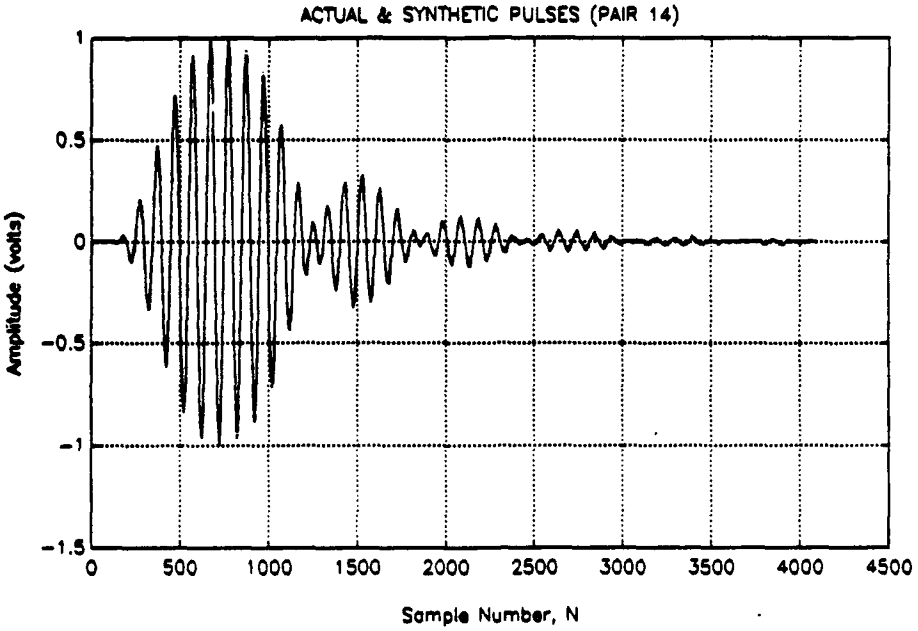

Figure 3.9: Actual and synthetic RF pulses, $y(n)$ and $y_s(n)$, catenated model of '42 with antenna simulator.

Table 3.2: PERFORMANCE IMPROVEMENT IN SIMULATION FOR NONLINEAR MODEL VERSUS LINEAR MODEL

Data Pair	NMSE (Linear model)	NMSE (Nonlinear model)
22	1.2698×10^{-2}	5.7835×10^{-4}
23	3.2698×10^{-3}	2.3224×10^{-4}
12	4.6052×10^{-3}	1.3439×10^{-4}
13	5.6114×10^{-4}	8.6276×10^{-5}
14	3.9731×10^{-4}	3.9176×10^{-4}
Mean Values	4.3062×10^{-3}	2.8460×10^{-4}

2. Representing Time Variations by Changing Polynomial Coefficient c_0

a. Changes in the Positions of Poles and Zeros Caused by Time Variations

Pole-zero models were produced for three data sequence pairs with nearly identical TDWs, obtained over a period of nine months. Figure 3.10a shows the first 1000 samples of the TDWs and Fig. 3.10b displays the pole-zero scatter plot of the three pole-zero models. From Fig. 2.10b, it is apparent that time variations in the transmitter's transfer function manifest themselves in the same way as nonlinearities: by movements in the pole and zero locations of the IIR model. These variations are about one-fourth the size of the variations due to changes in TDW shape. From what is known about the transmitter's time variations, the poles and zeros can be expected to drift slowly over hours, days and weeks. When a different transmitter is switched on line, the pulse shape controller sees a step change in pole-zero *locations.*

b. Moving Poles and Zeros Using Coefficient c_0

Changing coefficient c_0 slightly in each polynomial as a function of time t (every t_d iterations) is an effective way to model slow time variations in the transmitter. As a result, each polynomial curve drifts up and down independently of the others with respect to time t. This causes the poles and zeros to drift also with respect to t. Introducing a larger random change in the c_0 of each polynomial implements a transmitter switch; the curves, and the poles and zeros, jump to a new location. The size of the change to c_0 is different for each curve, characteristically small for the poles and larger for the zeros. Initially the maximum allowable change of c_0 can be set to approximately one fourth the difference between the maximum and minimum values of the polynomial curve in the valid range of E_n.

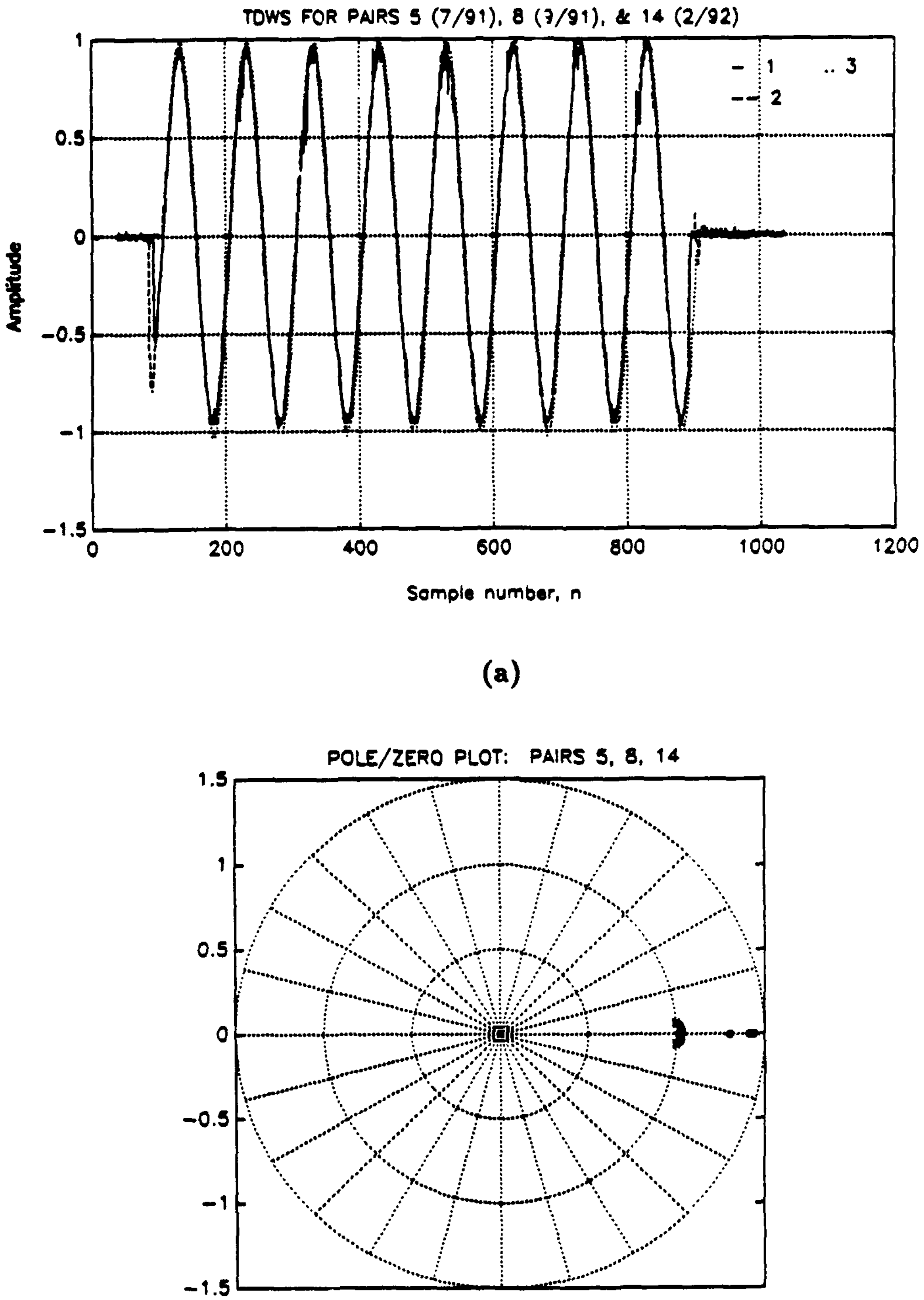

(a)

(b)

Figure 3.10: (a) Three TDWs (from pairs obtained over a 9-month period) for '42 with antenna simulator, and (b) pole-zero scatter plot.

c. Simulating Slow Drifts Using an AR2 Random Process

The following AR2 random process driven by white noise produces slow drifts generally in the range $(-1, 1)$:

$$d(t) - 2(0.996)d(t-1) + (0.996)^2 d(t-2) = w(t)\,. \tag{3.35}$$

Here $d(t)$ is the output and $w(t)$ is a white noise input with variance 6.25×10^{-8}. The system's double pole at 0.996 filters the noise and produces the slow drifts. The exact value of these parameters were chosen by trial and error. An example output $d(t)$ over 1000 iterations appears in Fig. 3.11. Chapter V contains details on how parameter drift is implemented in the simulation program.

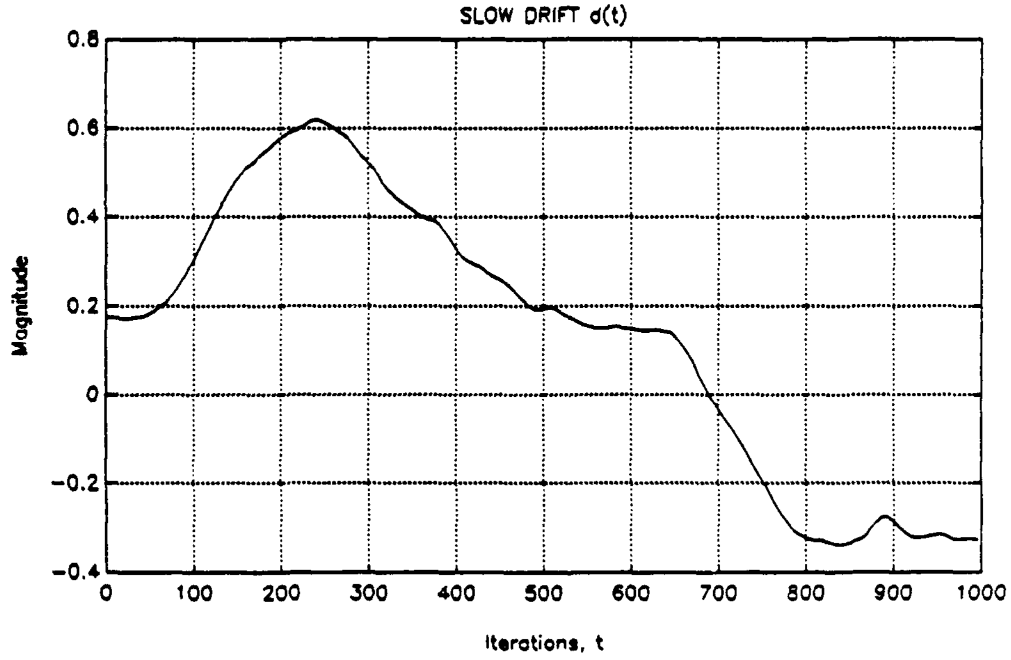

Figure 3.11: Slow drift produced by AR2 process.

3. The Combined Nonlinear, Time Varying Model

The catenated model from Subsection E. 1. and the time variations described in E. 2. combine to form an accurate nonlinear, time-varying model of the '42 transmitter. Only one more modification is necessary: the inclusion of all the data pairs available. Figure 3.12 shows the magnitude and phase of the inner pole (positive phase) using nineteen data pairs for the '42 transmitter. Appendix C contains a complete set of these curves. As mentioned before, on occasion the user may elect to remove one or more outliers; therefore all the points in the five-point curves of Fig. 3.8 may not necessarily appear in these final curves.

From these curves, new maximum values of c_0 may be determined simply by estimating a standard deviation of the data points by eye from the curve. Granted, some of the deviation may be from nonlinearities as well as time variations. If, however, the curve is allowed to drift to cover most of the points (it will drift approximately one standard deviation from its normal position), the combined model effectively duplicates nearly all the behavior observed in the data, both nonlinearities and time variations.

The combined model thus meets the need for which it was designed: it simulates all the observed nonlinear and time-varying behaviors of the transmitter *during the convergence of a pulse-shape control algorithm.* As the control algorithm changes the TDW shape, the model's transfer function changes also, just as the real transmitter's transfer function does. This dynamic feature is essential for testing control algorithms. One of its disadvantages, however, is that the simulation errors of the combined model are now higher than those of the linear model. Tested with all nineteen data pairs, the linear model's average NMSE is 2.8531×10^{-3} while the combined model's average NMSE (without drift) is 1.0943×10^{-2}, 284 percent higher. Visually, however, $y(n)$ and $y_s(n)$ for the combined model still match well. Therefore, the value of the dynamic feature of the combined model outweighs the disadvantage of the increased simulation error, and the combined model may still be used with reasonable confidence despite this increased error.

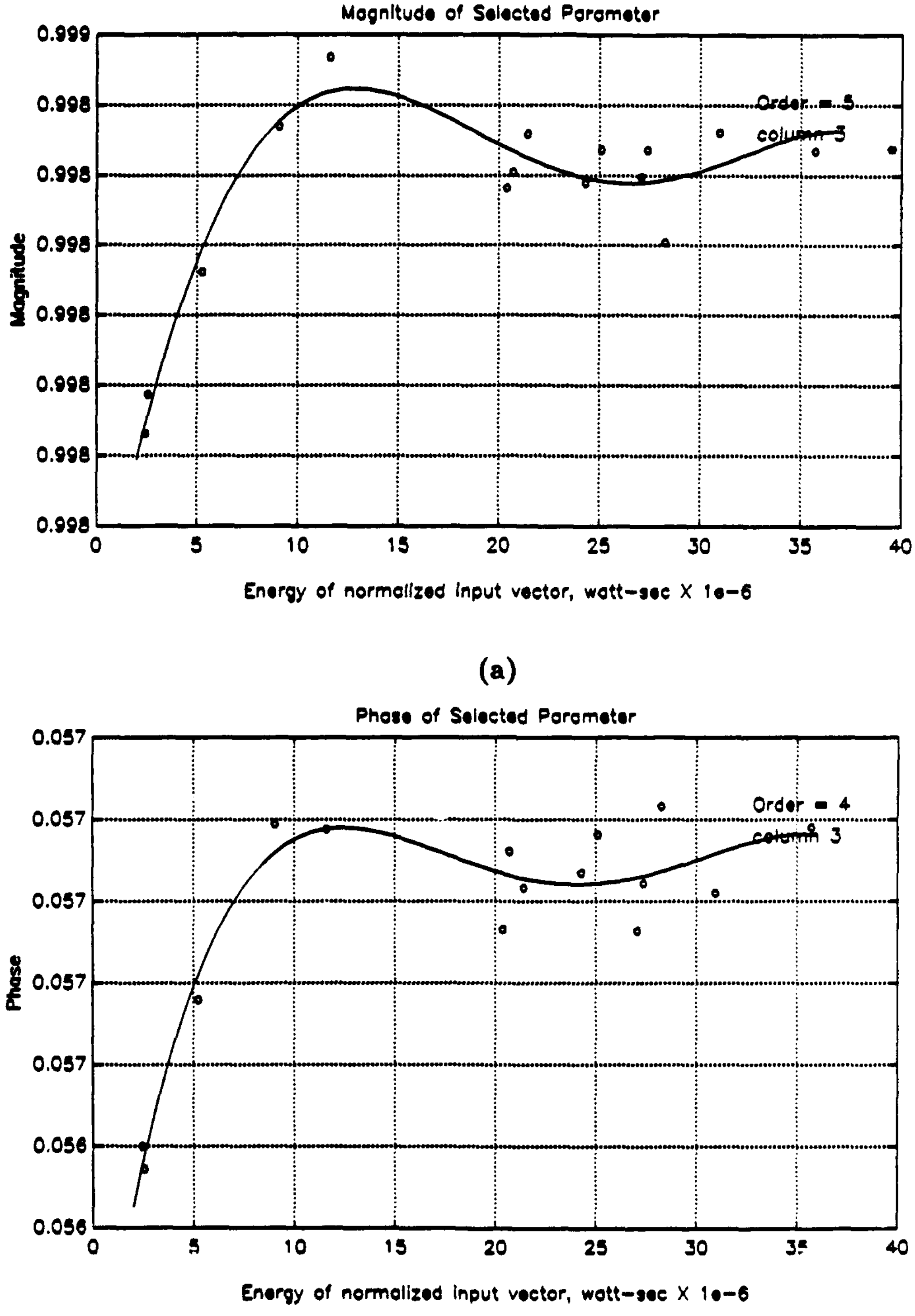

(a)

(b)

Figure 3.12: Fitted curves for inner pole pair, '42 with antenna simulator (19 pairs). (a) Magnitude, and (b) phase.

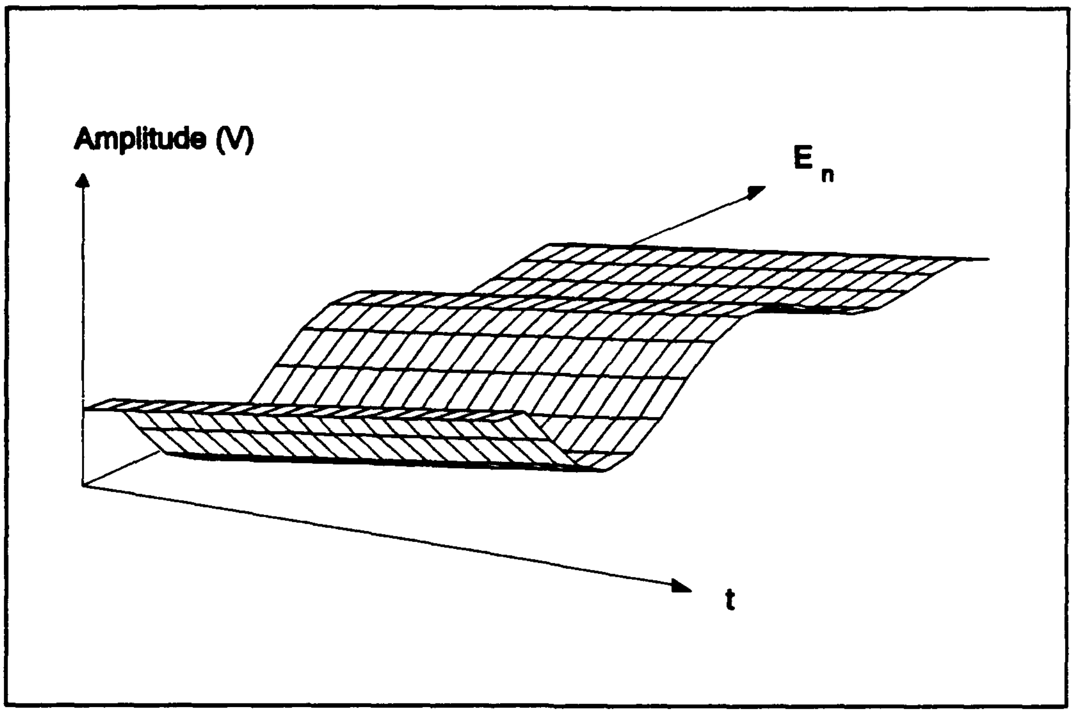

Figure 3.13: Second AR coefficient a_2 as a function of t and E_n.

Finally, the combined model can be related to the linear difference equation with non-constant coefficients in Eq. 3.6. The simulation program stores only the roots of $\mathbf{a}(t, E_n)$ and $\mathbf{b}(t, E_n)$, not the coefficients themselves. However, these coefficients may easily be computed. For example, Fig. 3.13 shows $a_2(t, E_n)$ for $0 \leq t \leq 20$ hours, and $2 \times 10^{-6} \leq E_n \leq 40 \times 10^{-6}$ watt-seconds.

4. Adding the Dummy Load to the Combined Model

Figures 3.14a and 3.14b show a data sequence pair for the '42 transmitter connected to the resistive dummy load instead of the antenna simulator. Figures 3.14c and 3.14d present sequences $h(n)$ and $h_{AB}(n)$ and the pole-zero plot corresponding to $h_{AB}(n)$ for model order $P = 2$, $Q = 1$. The time-domain match is

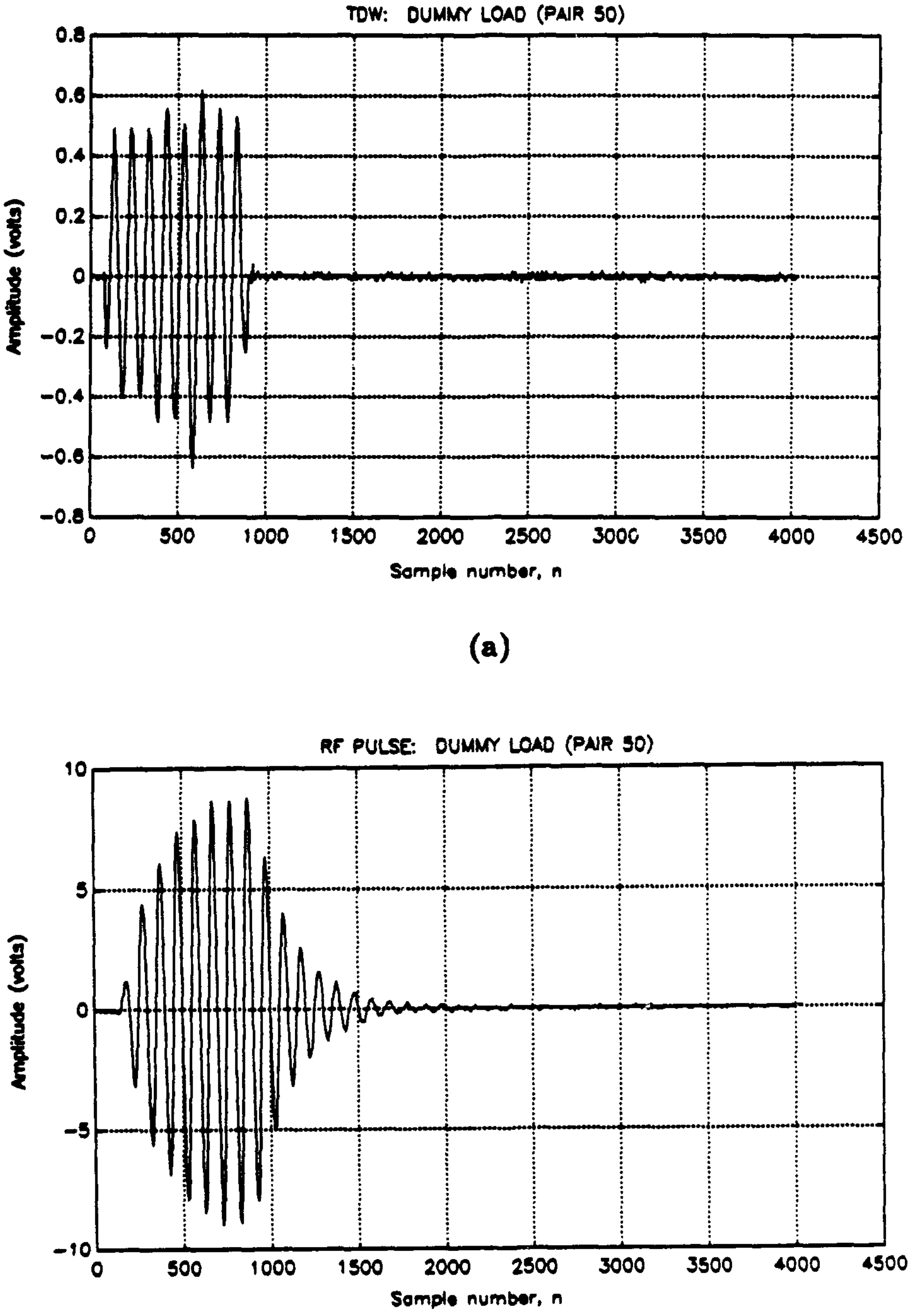

(a)

(b)

Figure 3.14: '42 input and output, dummy load, pair 50. (a) TDW and (b) RF pulse.

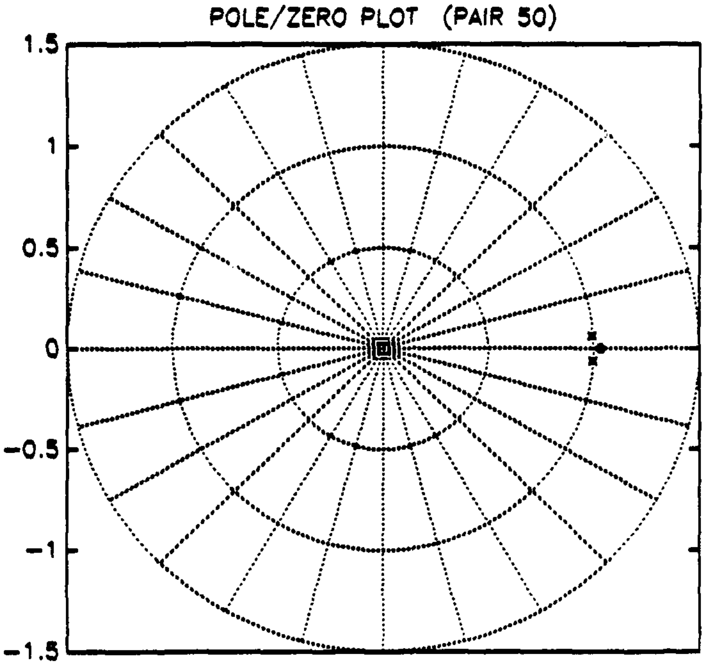

(c)

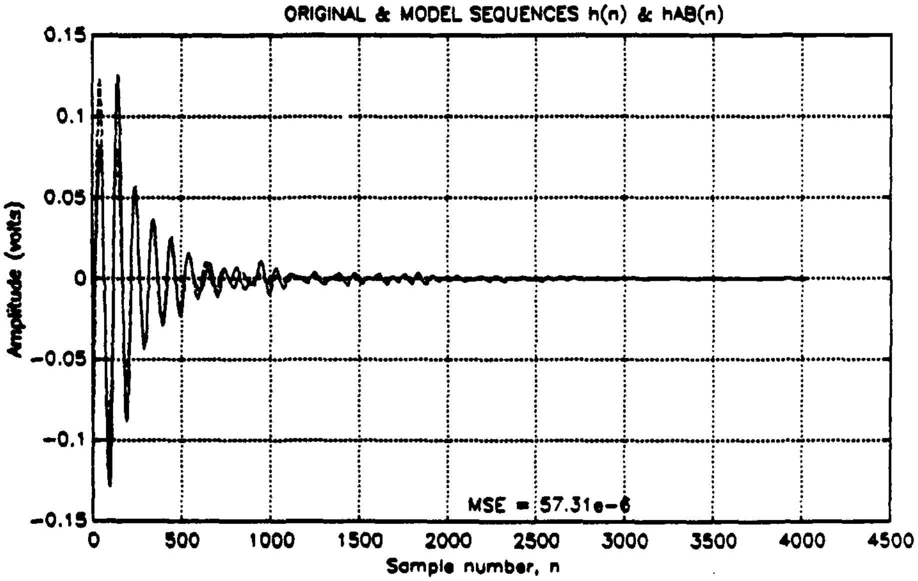

(d)

Figure 3.14: (c) Pole-zero plot of '42 LTI model, pair 50, with dummy load, and (d) original and model sequences, $h(n)$ and $h_{AB}(n)$.

not quite as good as with the antenna simulator sequences because a lower model order was chosen for the dummy load. Slightly higher model orders yield a modest decrease in MSE but the locations of the poles and zeros are no longer consistent and are thus unusable in the catenated model. As a result, order $P = 2$, $Q = 1$ is used and is considered adequate. Appendix C also includes curves for these dummy load poles and zeros.

F. NONLINEAR, TIME-VARYING MODEL OF THE AN/FPN-44A TRANSMITTER

The same procedure produced a combined model for the AN/FPN-44A transmitter, with order $P = 6$, $Q = 5$. A linear model of typical pair 71 has the following **a** and **b**:

$$\mathbf{a} = \begin{bmatrix} 1.0000 \\ -5.9652 \\ 14.8348 \\ -19.6972 \\ 14.7246 \\ -5.8759 \\ 0.9779 \end{bmatrix} \qquad \mathbf{b} = \begin{bmatrix} -0.0100 \\ 0.0504 \\ -0.1013 \\ 0.1019 \\ -0.0514 \\ 0.0104 \end{bmatrix}, \tag{3.36}$$

The poles and zeros are

$$\text{poles} = \begin{bmatrix} 0.9947e^{j\pm 0.0850} \\ 0.9986e^{j\pm 0.6559} \\ 0.9956e^{j\pm 0.4519} \end{bmatrix} \qquad \text{zeros} = \begin{bmatrix} 1.0009e^{j\pm 0.1023} \\ 1.0025e^{j\pm 0.0413} \\ 1.0255e^{j0} \end{bmatrix}. \tag{3.37}$$

All the data vectors for the '44A were obtained on the same day, so typical time variations of this transmitter model were inferred. The combined model was tested with fifteen data pairs against the linear model from pair 71, as before. The linear model's average NMSE is 1.3059×10^{-2}, and the combined model's average NMSE is 5.0988×10^{-3}. The catenated model thus reduces NMSE by 61.0 percent.

Figures 3.15–3.17 are the plots for the '44A modeling process. Appendix C contains the pole-zero curves for the '44A.

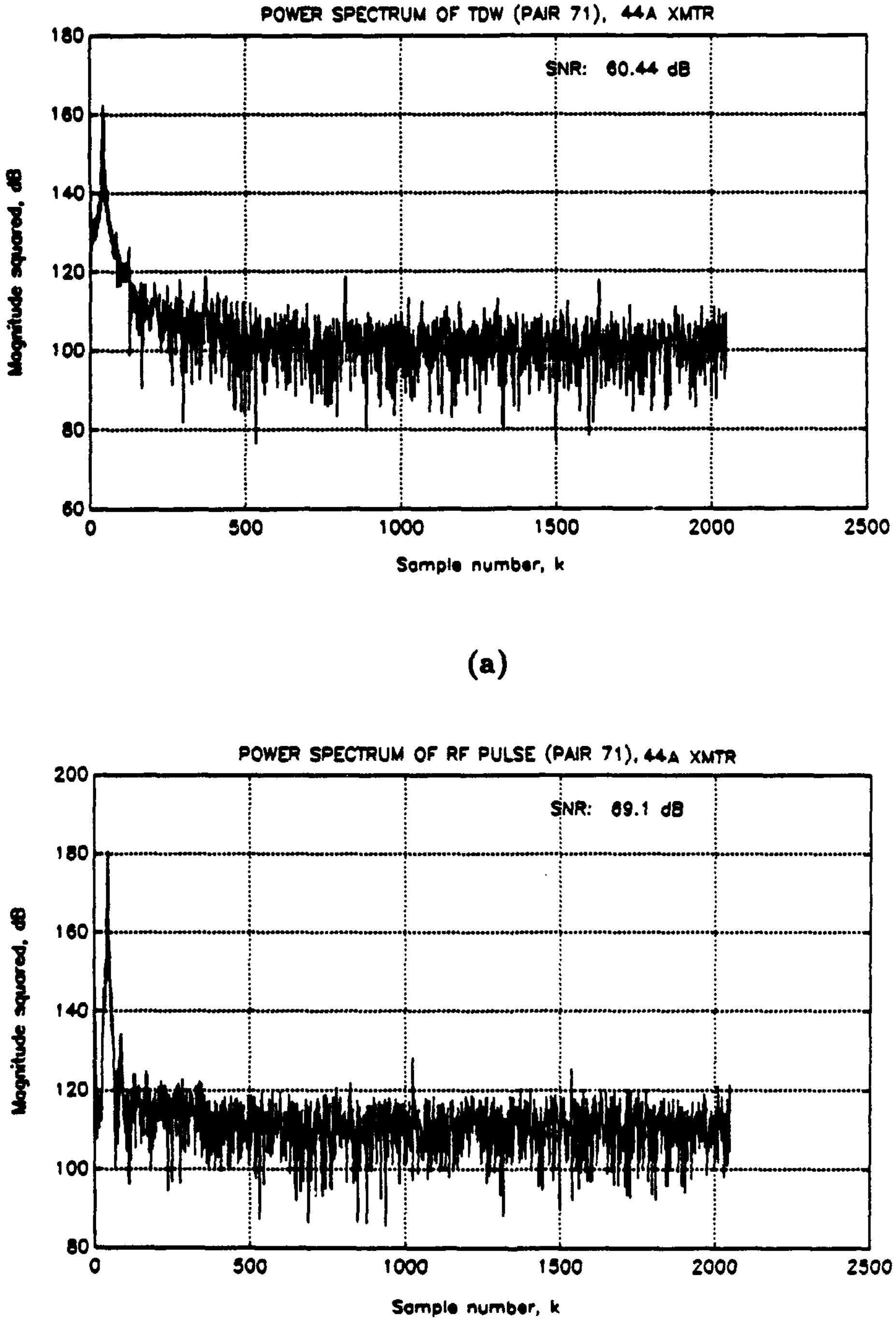

(a)

(b)

Figure 3.15: Power spectrum of '44A with antenna simulator, pair 71. (a) TDW and (b) RF pulse.

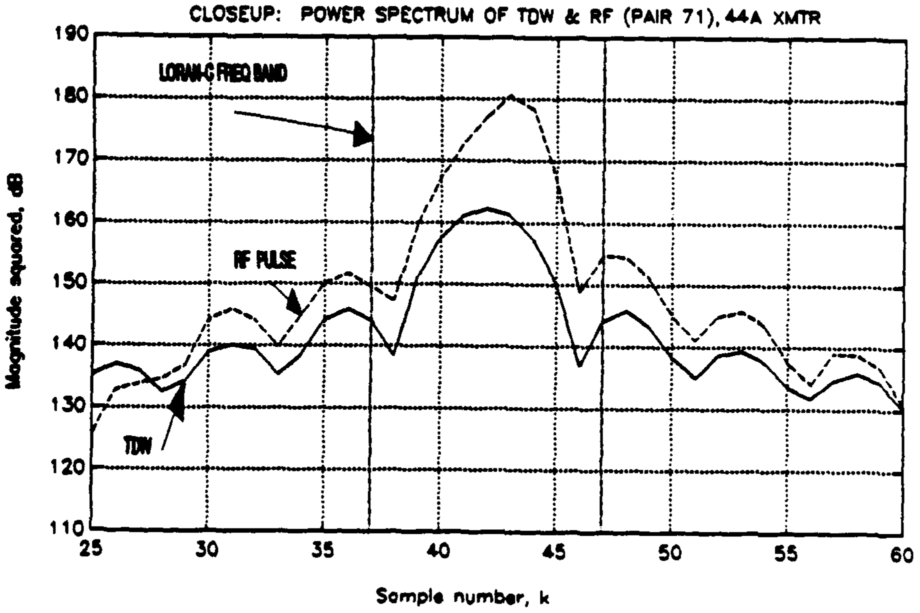

Figure 3.15c: Closeup of power spectrum, '44A, pair 71.

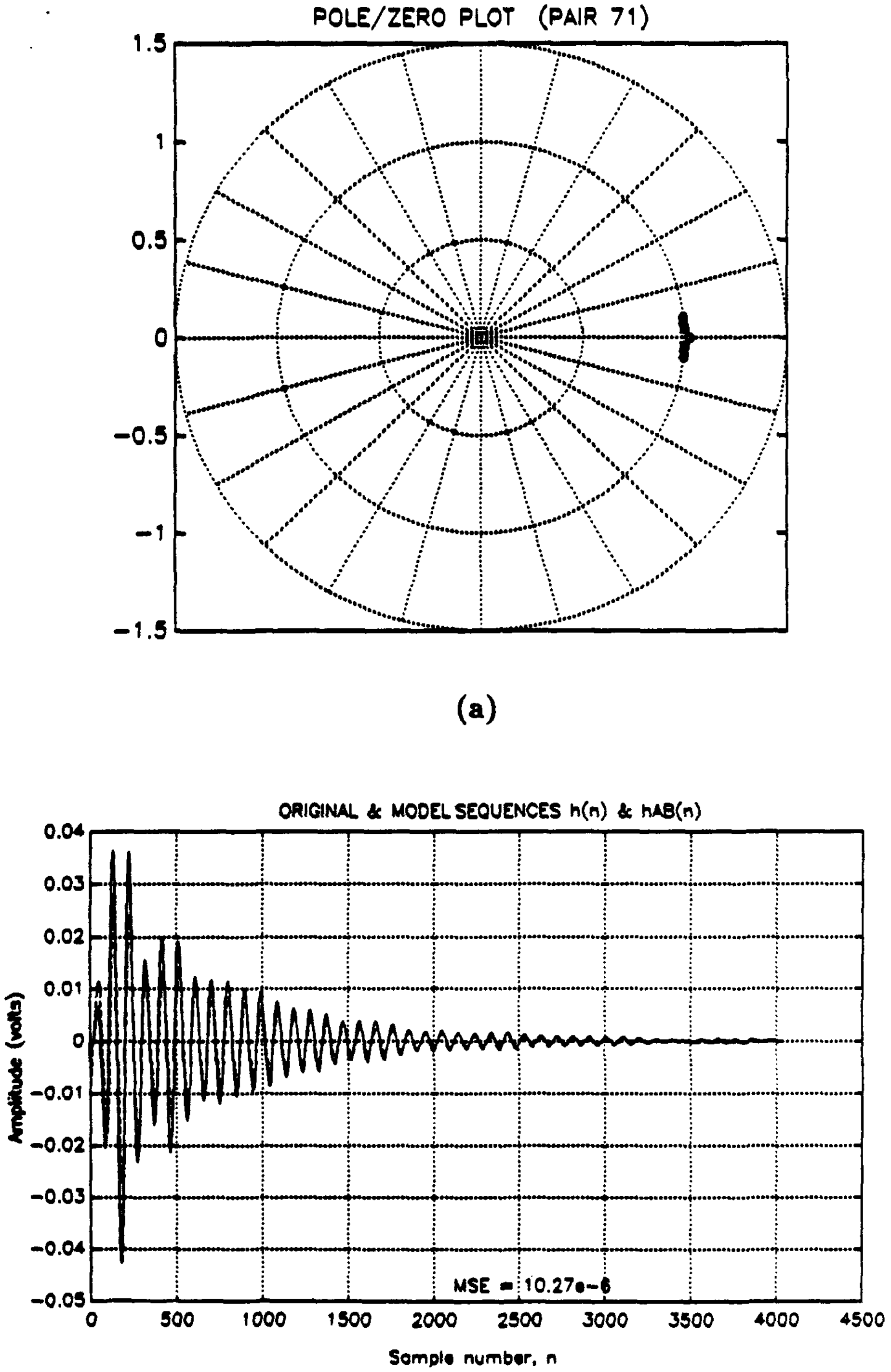

(a)

(b)

Figure 3.16: (a) Pole-zero plot of '44A LTI model, pair 71, with antenna simulator, and (b) original and model sequences, $h(n)$ and $h_{AB}(n)$.

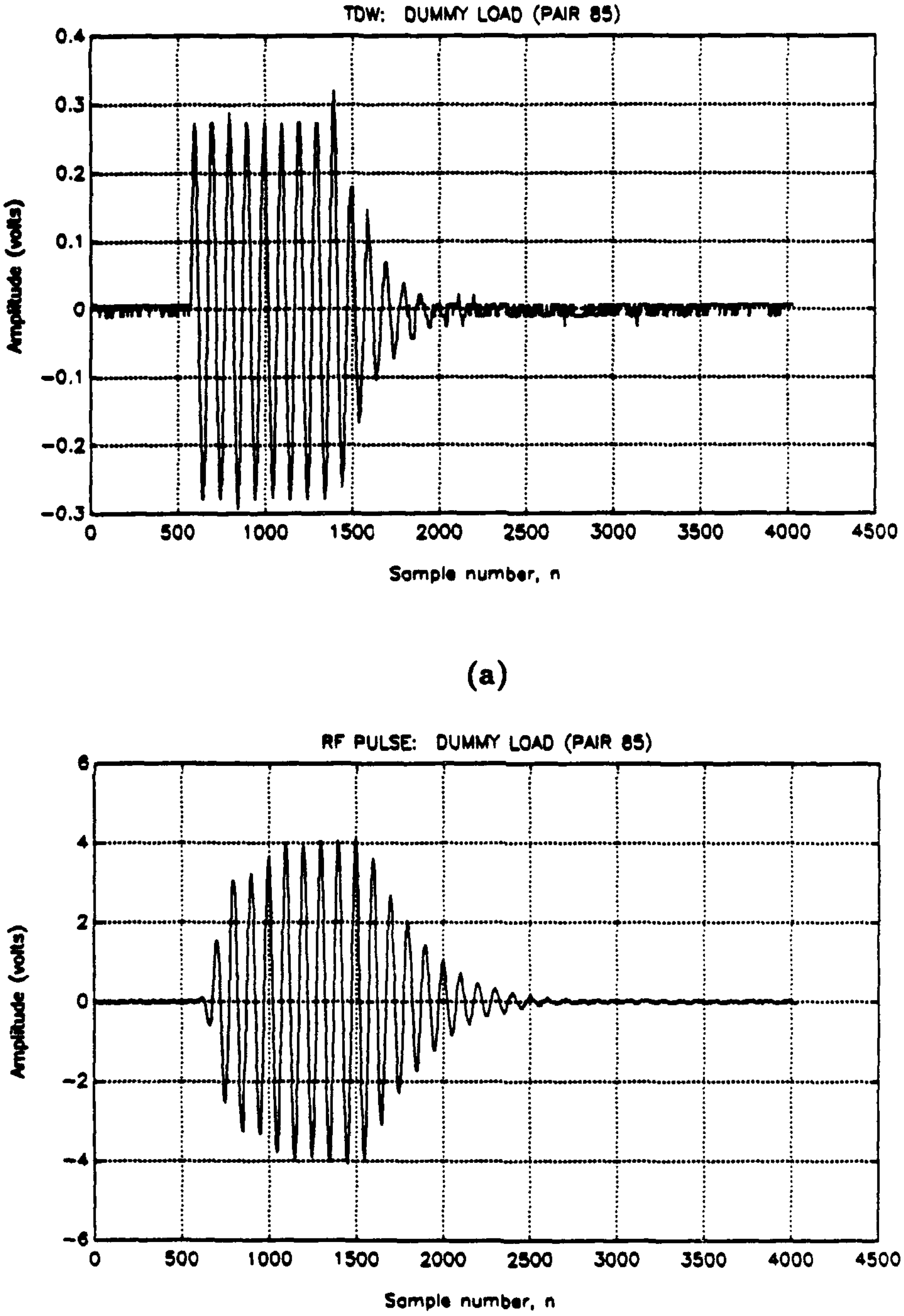

(a)

(b)

Figure 3.17: '44A input and output, dummy load, pair 85. (a) TDW and (b) RF pulse.

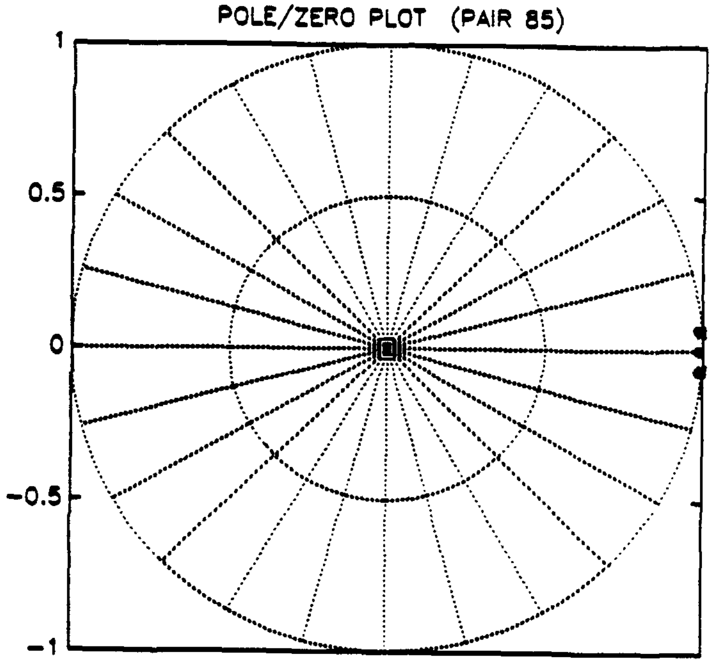

(c)

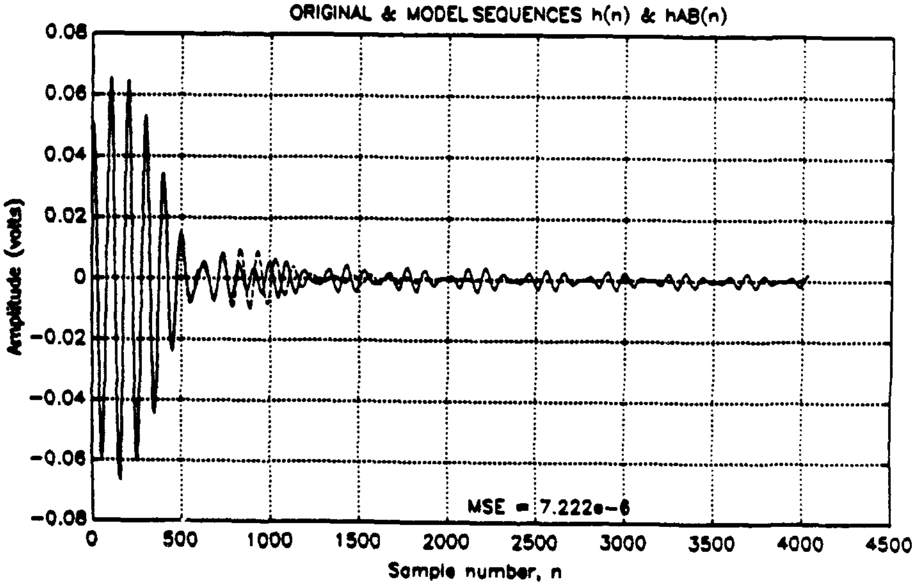

(d)

Figure 3.17: (c) Pole-zero plot of '44A LTI model, pair 85, with dummy load, and (d) original and model sequences $h(n)$ and $h_{AB}(n)$.

IV. THE STEEPEST DESCENT ALGORITHM

A. INTRODUCTION

This chapter presents an algorithm that generates and controls the Loran-C pulse shape automatically. First, the Loran-C control problem is described. Second, the algorithm is derived and its advantages and limitations are discussed. Finally, the algorithm is successfully tested with the combined '42 and '44A transmitter models from Chapter III.

B. PULSE SHAPE CONTROL IN LORAN-C

The VXIbus pulse shape control system (See Fig. 2.10) uses a batch processing approach to monitor and control the Loran-C pulse shape. The oscilloscope captures and stores in memory an entire RF pulse, or possibly an entire GRI or even a PCI. A resident computer program reduces the waveform(s) to parametric form, compares these parameters to the parameters from an ideal pulse, and produces a new TDW in parametric form. In the final step, the program expands these TDW parameters into a digital data vector, which the AFG then converts into an analog TDW. This operation constitutes one iteration of the Loran-C pulse shape controller. The controller shapes the pulse by changing the TDW parameters to minimize the error in the RF pulse parameters.

The simplest form of the controller uses a parametric form consisting of 16 TDW half-cycle peak amplitudes

$$\mathbf{x}_p = [x_p(1), x_p(2), \cdots, x_p(16)]' \tag{4.1}$$

and 16 RF pulse half-cycle peak amplitudes:

$$\mathbf{y}_p = [y_p(1), y_p(2), \cdots, y_p(16)]'. \tag{4.2}$$

These are tracked in successive control iterations; Fig. 4.1 illustrates this for $x_p(3)$ and $y_p(3)$. The half-cycle peak amplitudes of the ideal pulse of Eq. (2.1) are

$$\mathbf{y}_{0p} = [y_{0p}(1), y_{0p}(2), \cdots, y_{0p}(16)]', \tag{4.3}$$

with output error vector

$$\mathbf{e}_y = \mathbf{y}_p - \mathbf{y}_{0p} = [e_y(1), e_y(2), \cdots, e_y(16)]'. \tag{4.4}$$

Thus the Loran-C pulse shape control problem is formulated as a 16-dimensional regulator problem where $\mathbf{y}_p$ is maintained as close as possible to $\mathbf{y}_{0p}$ [Ref. 22].

C. THE STEEPEST DESCENT ALGORITHM

1. Derivation

A linear controller feedback which uses the method of steepest descent effectively shapes the Loran-C pulse by minimizing the quadratic error $\mathbf{e}_y^T\mathbf{W}\mathbf{e}_y$, where $\mathbf{W}$ is a weighting matrix. In the steepest descent method, also used in adaptive filtering, the error gradient is used to find the bottom o^f^ an error performance surface [Ref. 19, p. 197]. The controller presented here is appropriately called the steepest descent algorithm in this thesis. This control algorithm, developed by Peterson and successfully implemented in a hardware simulation by Steinvorth, is derived as follows [Ref. 20, 21].

The transmitter is modeled as a linear system

$$\mathbf{A}_0\mathbf{x}_p = \mathbf{y}_p, \tag{4.5}$$

where $\mathbf{A}_0$ is the matrix of impulse response samples (peak amplitude samples are used in this thesis):

$$\mathbf{A}_0 = \begin{bmatrix} h_p(0) & 0 & 0 & \cdots & 0 \\ h_p(1) & h_p(0) & 0 & \cdots & 0 \\ \vdots & \vdots & \vdots & & \vdots \\ h_p(16) & h_p(15) & h_p(14) & & h_p(0) \end{bmatrix}. \tag{4.6}$$

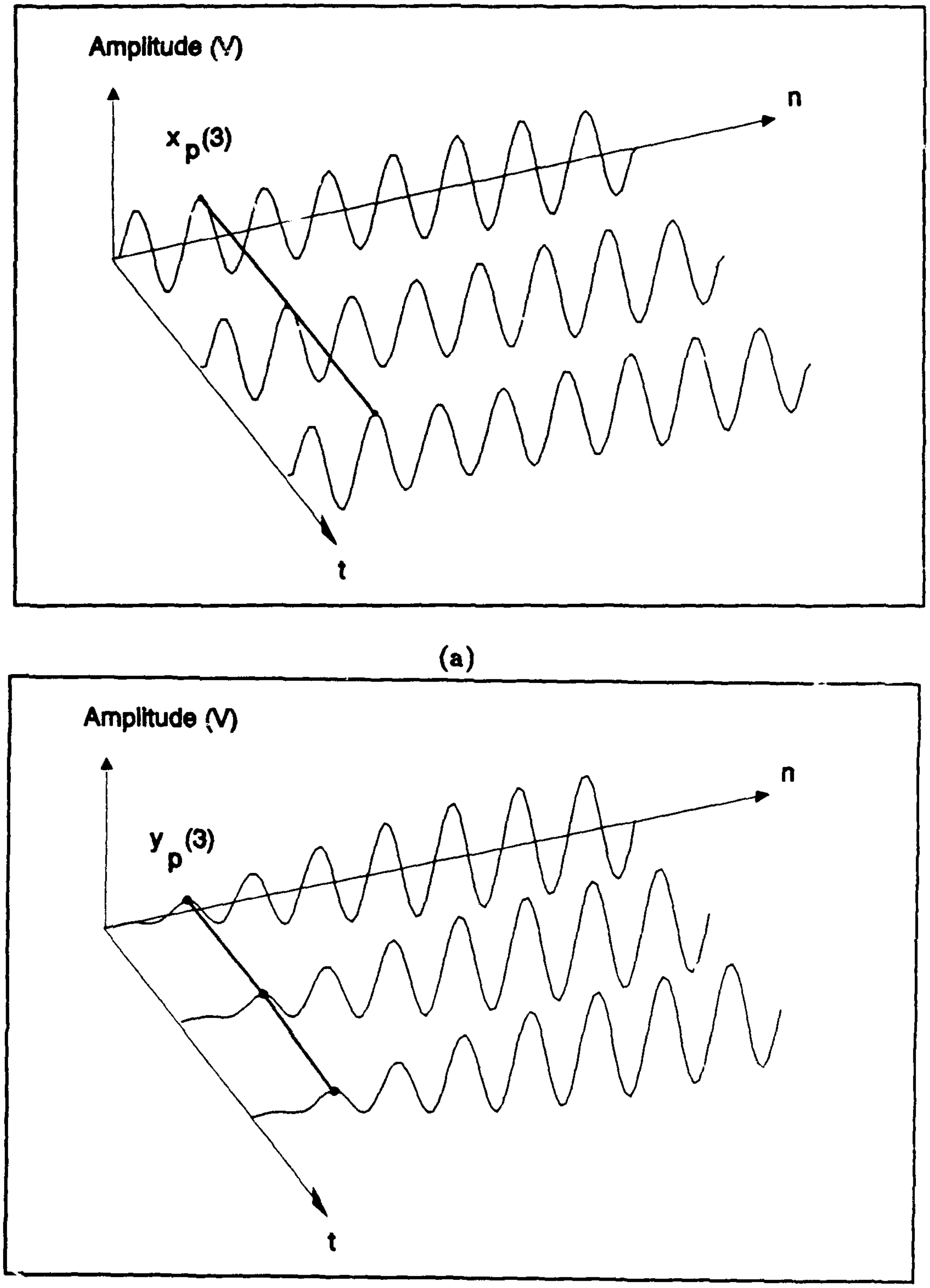

(a)

(b)

Figure 4.1: Loran-C pulse shape control strategy. (a) Input and (b) output.

Let $\mathbf{x}_{0p}$ be the vector of optimum TDW half-cycle peak amplitudes. Multiplying the true (but unknown) system matrix $\mathbf{A}_0$ and optimum TDW half-cycle peak vector $\mathbf{x}_{0p}$ yields the ideal pulse peaks:

$$\mathbf{A}_0\mathbf{x}_{0p} = \mathbf{y}_{0p} \,. \tag{4.7}$$

Let

$$\mathbf{e}_x = \mathbf{x}_p - \mathbf{x}_{0p} \tag{4.8}$$

be the vector of errors in the TDW half-cycle peak amplitudes. Beginning with A, the best estimate of $\mathbf{A}_0$, the first vector of TDW half-cycle peak amplitudes is

$$\mathbf{x}_p\Big|_{t=1} = \mathbf{A}_0^+\mathbf{y}_{0p} \,. \tag{4.9}$$

Vector $\Delta\mathbf{x}_p$ updates $\mathbf{x}_p$ at each iteration t in the direction of steepest descent on the quadratic error surface defined by $\mathbf{e}_y^T\mathbf{W}\mathbf{e}_y$:

$$\Delta\mathbf{x}_p = -\frac{\mu}{2}\nabla_{\mathbf{e}_x}[\mathbf{e}_y^T\mathbf{W}\mathbf{e}_y] \,, \tag{4.10}$$

where μ is a small constant greater than zero and $\nabla\mathbf{e}_x[\kappa]$ is the vector of partial derivatives of scalar κ with respect to the elements of $\mathbf{e}_x$.

Equation (4.10) may be expanded to the form

$$\Delta\mathbf{x}_p = -\frac{\mu}{2}\nabla_{\mathbf{e}_x}[\mathbf{e}_x^T\mathbf{A}_0^T\mathbf{W}\mathbf{A}_0\mathbf{e}_x] \,. \tag{4.11}$$

Diagonal matrix $\mathbf{W}$ weights the elements of $\mathbf{e}_x$ and $\mathbf{e}_y$. $\mathbf{W} = \mathbf{I}$ weights all the errors equally, while a $\mathbf{W}$ whose diagonal elements decrease in size from upper left to lower right implements a tighter tolerance in the first part of the pulse. Equation (4.11) then becomes

$$\Delta\mathbf{x}_p = -\mu\mathbf{A}_0^T\mathbf{W}\mathbf{A}_0\mathbf{e}_x \,, \tag{4.12}$$

then

$$\Delta\mathbf{x}_p = -\mu\mathbf{A}_0^T\mathbf{W}\mathbf{e}_y \,. \tag{4.13}$$

Matrix **A**, which is known, is substituted for unknown $\mathbf{A_0}$, resulting in the steepest descent algorithm

$$\boxed{\Delta \mathbf{x}_p = -\mu \mathbf{A}^T \mathbf{W} \mathbf{e}_y}. \tag{4.14}$$

For negatively phase coded pulses the "−" sign is removed. Finally, if $[\mathbf{A}^T\mathbf{W}\mathbf{A}_0]^{-1}$ is positive definite and

$$\mu < \frac{2}{\text{largest eigenvalue of } [\mathbf{A}^T\mathbf{W}\mathbf{A}_0]}, \tag{4.15}$$

the system is stable.

2. Advantages and Limitations

The algorithm of Eq. (4.14) has two main advantages and two primary limitations. The algorithm's advantages are its effectiveness and its simplicity. As the next section shows, the algorithm works well for the data available. Also, the simple parametric form allows the algorithm to be implemented with only two (16 × 16) matrix multiplications per iteration (with 768 real multiplications and 512 real additions). The algorithm's limitations are its assumption of an overall linear controller system and its inability to control zero-crossing times. By using small values of μ and a standard 16-half-cycle TDW, the controller keeps the transmitter confined to an approximately linear region. If the controller is also "tuned" by updating **A** from time to time to compensate for time variations, the first limitation is not a serious one. The second limitation simply requires the zero-crossing times to be adjusted as they have always been: by keeping the transmitters well-maintained and well-tuned to 100 kHz. This limitation imposes no extra burden on Loran-C operation or maintenance, so likewise it is not a serious one. Admittedly, having an algorithm that adjusts zero-crossing times automatically would be quite advantageous, but this capability is not absolutely necessary in order to implement automatic pulse shaping successfully.

D. CONTROLLING PULSE SHAPE IN THE COMBINED MODEL USING THE STEEPEST DESCENT ALGORITHM

The steepest descent algorithm effectively generates and controls the Loran-C pulse peak amplitudes in the combined models of both the '42 and the '44A. The zero-crossing tolerances were met for the '42 but not the '44A.

Figures 4.2a through 4.2d illustrate the performance of the steepest descent algorithm with the '42 combined model without time variations. Figure 4.2a shows the smooth convergence of the mean squared error $\mathbf{e}_y^T\mathbf{e}_y$ for the first 100 iterations, and Fig. 4.2b presents the convergence of three measures of Loran-C error for the same 100 iterations. These are the half-cycle peak amplitudes (ensemble tolerance) and the half-cycle peak amplitudes (individual tolerance) for half-cycles 1–8 and for half-cycles 9–13. The temporary rise in mean squared error from iteration 10 through 18 in Fig. 4.2a is a result of linearly controlling a nonlinear system. Figures 4.2c and 4.2d show the first 800 samples of the ideal and synthetic RF pulses after 100 iterations. All half-cycle peak amplitudes of the initial TDW (at iteration $t = 1$) were set to 0.4 volts. In these plots, normalized μ

$$\mu_n = \mu \, \frac{\text{largest eigenvalue of } [\mathbf{A}^T\mathbf{W}\mathbf{A}]}{2} \tag{4.16}$$

is set to 0.7. Next, beginning with iteration 101 and ending with iteration 200, time variations are introduced at each iteration. This approximates a 25-hour period. These figures demonstrate the algorithm's ability to compensate for slow time variations in the transmitter's transfer function.

Figures 4.4 and 4.5 illustrate similar success with the '44A except that zero-crossing times are not within tolerance. Half-cycle peak amplitudes 15 and 16 of the final TDW are larger, to fill out the end of the controlled part of the pulse, but

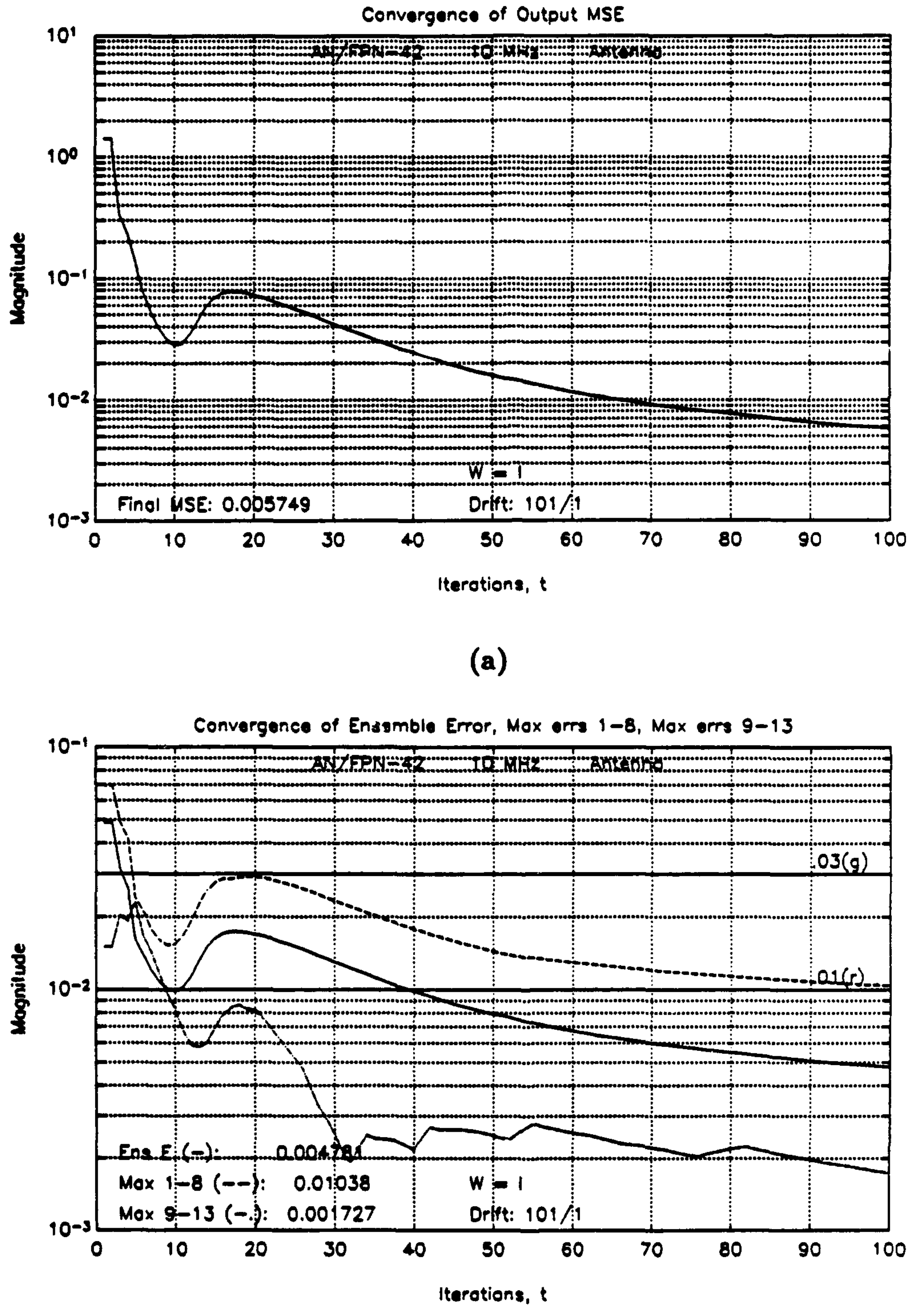

(a)

(b)

Figure 4.2: Testing steepest descent algorithm with '42 and antenna. (a) Convergence of mean-squared error $\mathbf{e}_y^T\mathbf{e}_y$, and (b) convergence of three measures of Loran-C error.

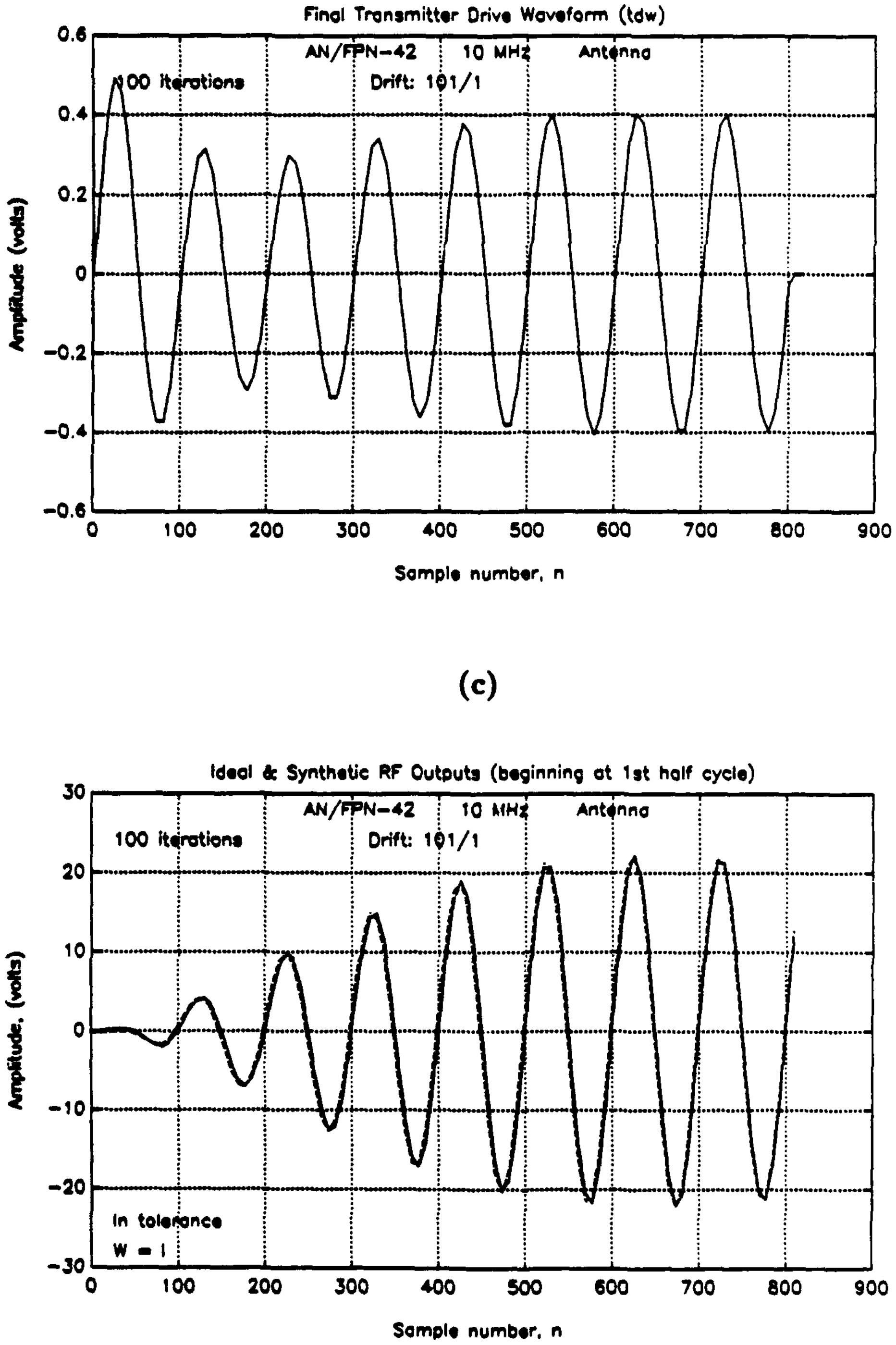

(c)

(d)

Figure 4.2: Testing steepest descent algorithm with '42 and antenna. (c) Final TDW and (d) ideal and synthetic RF pulses.

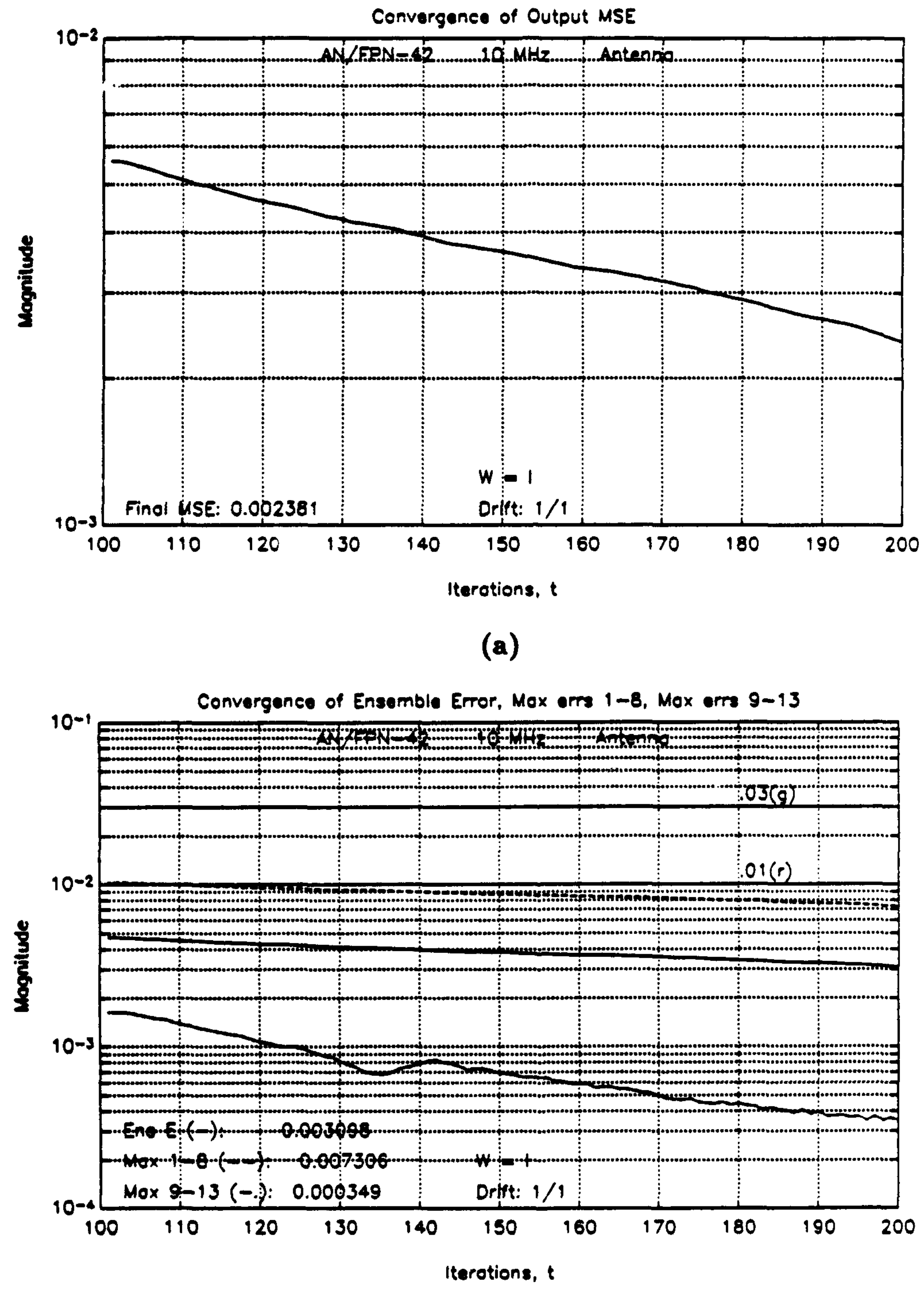

(a)

(b)

Figure 4.3: Testing steepest descent algorithm with time-varying model, '42. (a) Convergence of mean-squared error $e_y^T e_y$, and (b) Convergence of three measures of Loran-C error.

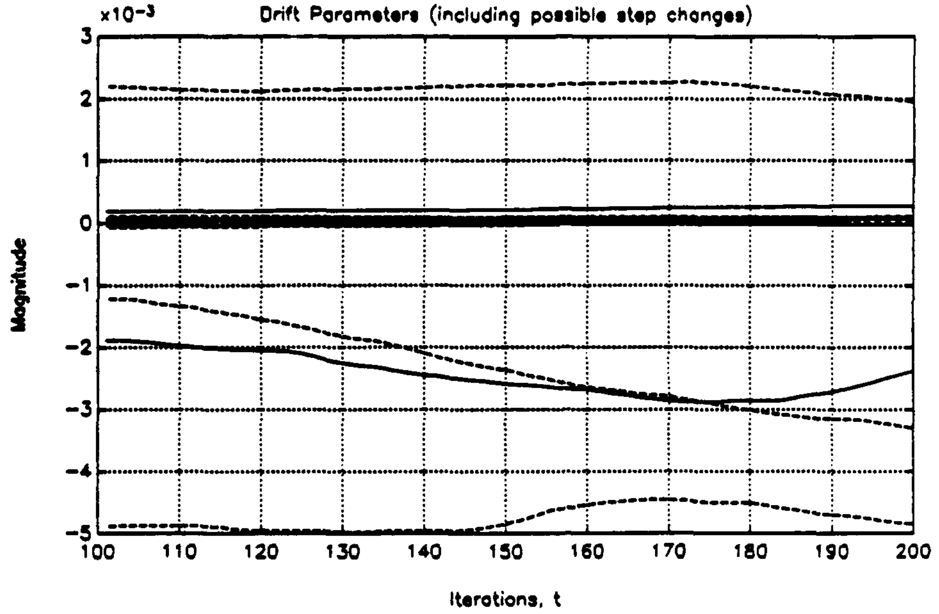

Figure 4.3c: Testing steepest descent algorithm with time-varying model, ‘42, drift parameters (c_0 coefficients).

this has an unintended effect with the ’44A combined model. This is because the tail drive decays exponentially starting from the amplitude of half-cycle 16. With such a large 16th half-cycle, the tail of the TDW contains almost as much energy as half-cycles 1–14. If actually implemented, half-cycles 15 and 16 could be attenuated to compensate for this problem. Also, the phase difference in Fig. 4.4d reflects the change in transmitter delays that may be produced by time variations in the transmitter's transfer function. As stated before, emission delays are not addressed in this simulation.

These figures show that the steepest descent algorithm effectively shapes the Loran-C pulse. However, these tests of the algorithm are unrealistic because complicating factors such as noise, quantization error and power supply droop are not included. Also, only one pulse of the PCI has been controlled. In the next chapter, the combined models of Chapter III and the steepest descent algorithm are incorporated into a comprehensive simulation program which does provide a realistic test. Experimental results from the simulation program are also included.

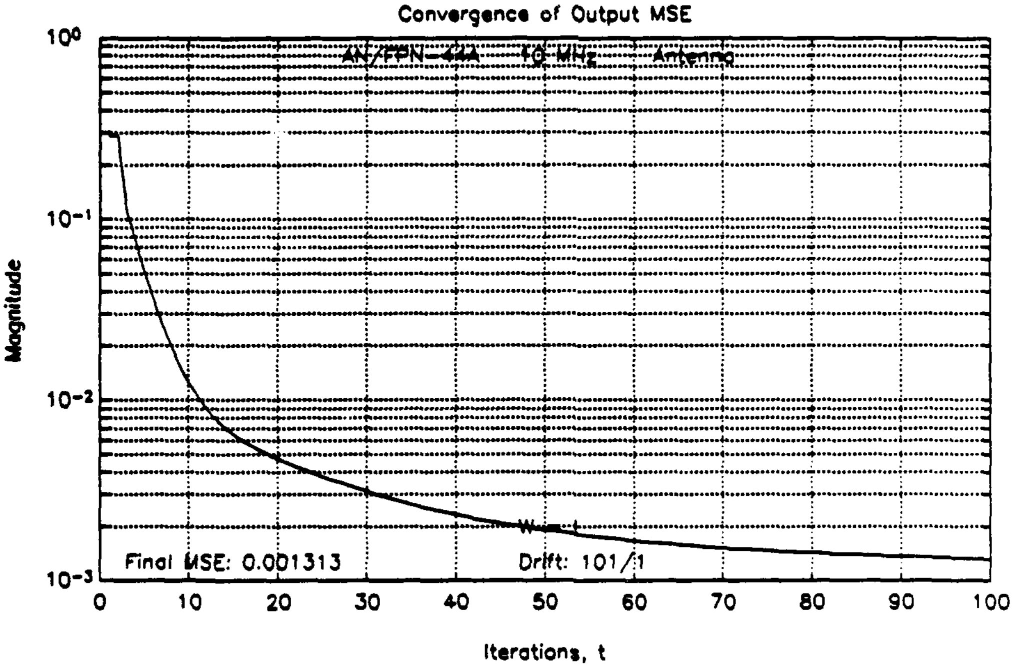

Figure 4.4a: Testing steepest descent algorithm with '44A and antenna. Convergence of mean-squared error $\mathbf{e}_y^T\mathbf{e}_y$.

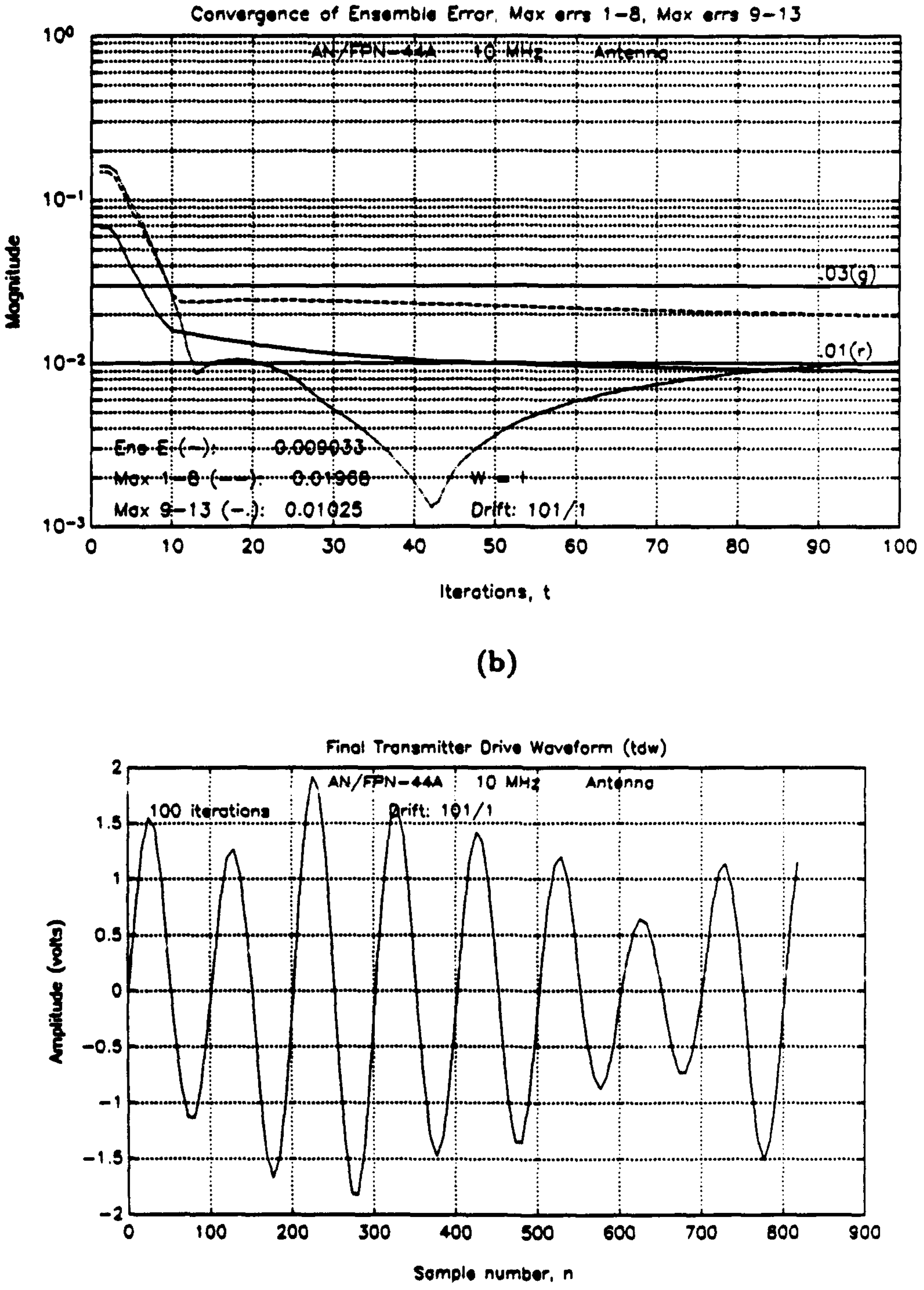

(b)

(c)

Figure 4.4: Testing steepest-descent algorithm with '44A and antenna. (b) Convergence of three measures of Loran-C error and (c) final TDW.

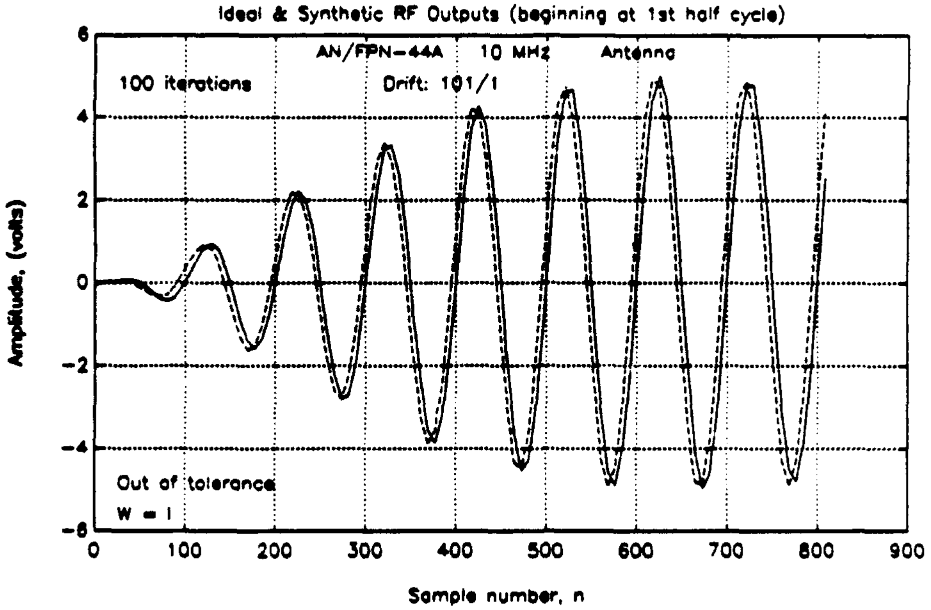

Figure 4.4d: Testing steepest descent algorithm with '44A and antenna. Ideal and synthetic RF pulses.

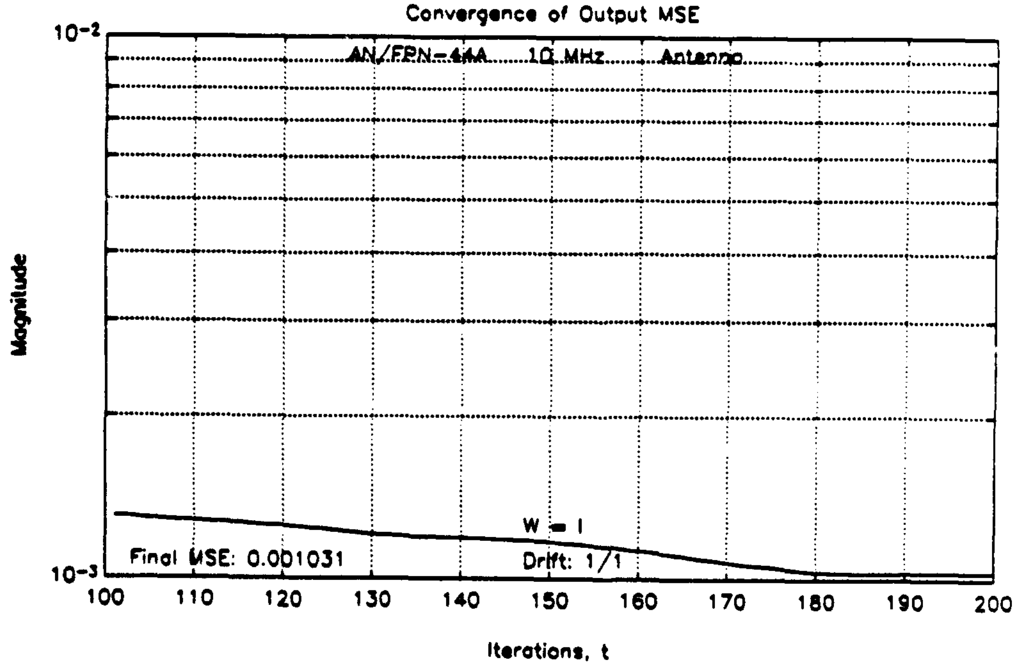

Figure 4.5a: Testing steepest descent algorithm with time-varying model, '44A. Convergence of mean-squared error $e_y^T e_y$.

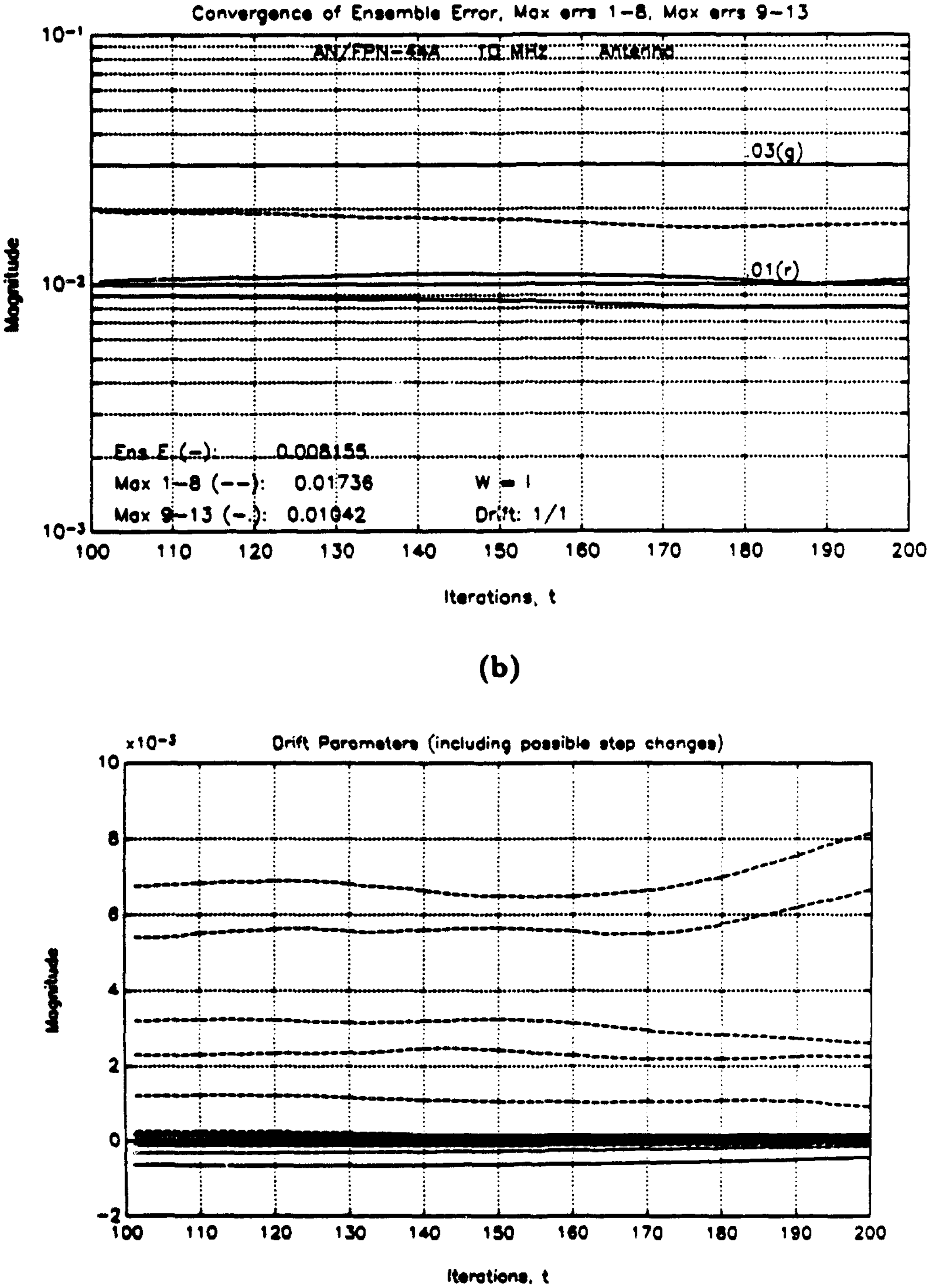

(b)

(c)

Figure 4.5: Testing steepest descent algorithm with time-varying model, '44A. (b) Convergence of three measures of Loran-C error and (c) drift parameters (c_0 coefficients).

V. SIMULATION PROGRAM AND RESULTS

A. INTRODUCTION

In this chapter the models of Chapter III and the control algorithm of Chapter IV are incorporated into a comprehensive MATLAB computer program which simulates the pulse-shaping control process on the AN/FPN-42 and AN/FPN-44A transmitters. Also, key results obtained from this simulation program are featured.

B. THE SIMULATION PROGRAM

1. Structure

The diagram in Fig. 5.1 shows the basic structure of the simulation program. In brief, the user selects the options for the simulation run, including which pulses of the PCI he or she wishes to control. For each of the selected pulses, the program *completes a specified number of control* iterations. A control iteration consists of obtaining the RF pulse, determining the error in the RF pulse parameters, and producing a new TDW. After the iterations are finished, a pulse analysis is performed and the program moves to the next selected pulse. This program simulates controlling the shorter rate of a dual-rated station, and from time to time the rate is blanked. When this occurs, the controller skips an entire control iteration and does not increment the loop counter. Thus the blanking process is simulated but is invisible to the pulse shape controller.

2. Explanation of Features Appearing on Main Menu

a. Main Menu

The user controls the simulation program through a main menu, which appears in Fig. 5.2. Using this menu, the user configures the transmitter and

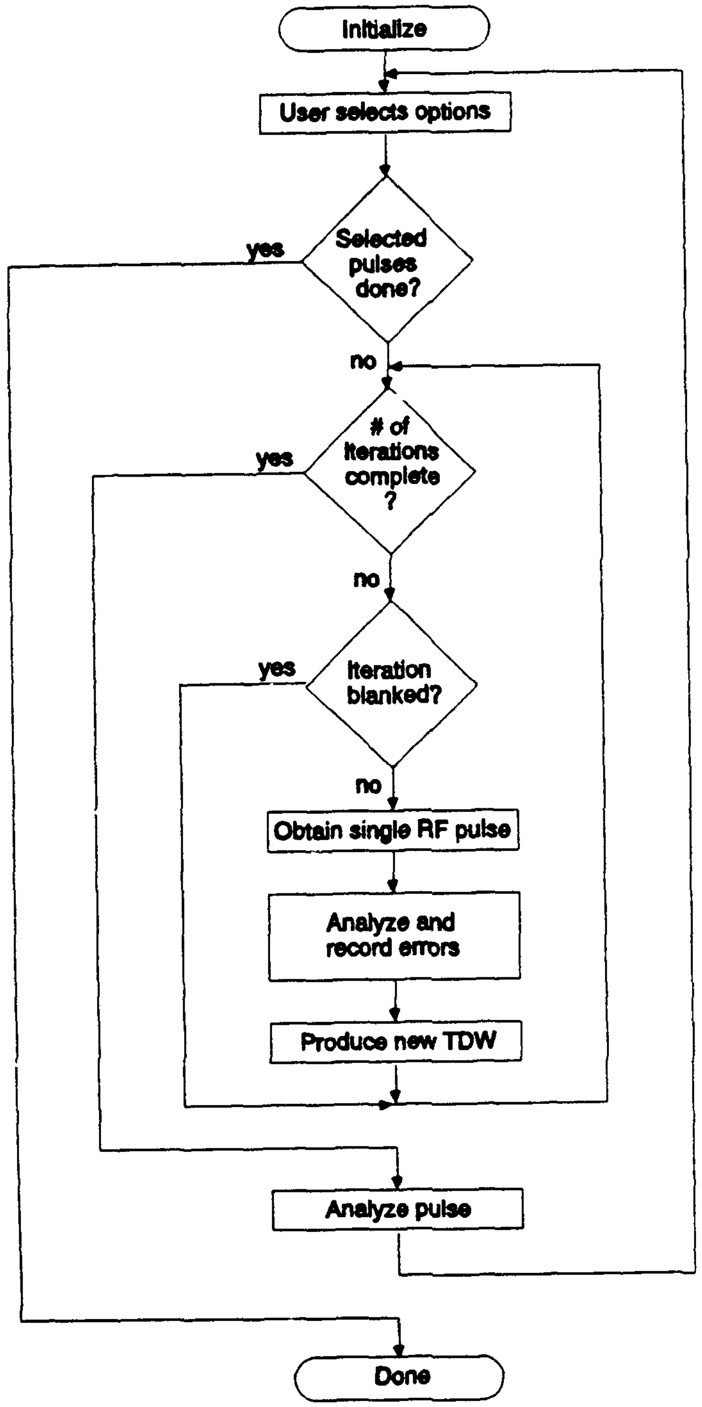

Figure 5.1: Basic structure, simulation program.

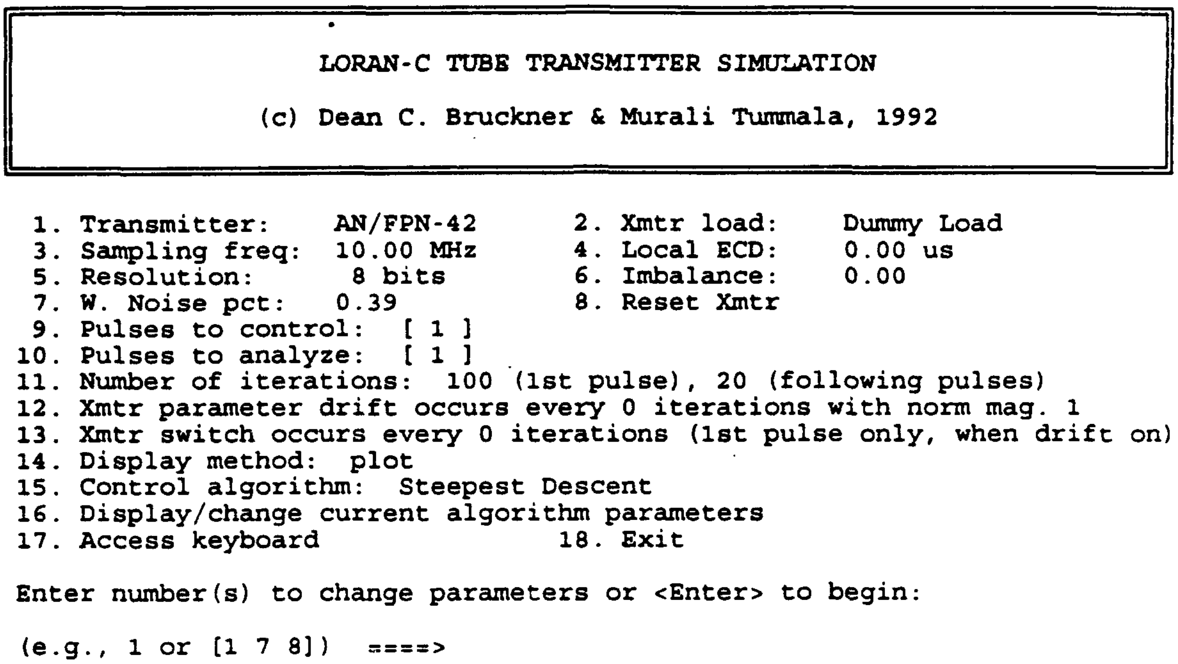

```
                 LORAN-C TUBE TRANSMITTER SIMULATION

            (c) Dean C. Bruckner & Murali Tummala, 1992

 1. Transmitter:     AN/FPN-42        2. Xmtr load:     Dummy Load
 3. Sampling freq:   10.00 MHz        4. Local ECD:     0.00 us
 5. Resolution:       8 bits          6. Imbalance:     0.00
 7. W. Noise pct:    0.39             8. Reset Xmtr
 9. Pulses to control:   [ 1 ]
10. Pulses to analyze:   [ 1 ]
11. Number of iterations:  100 (1st pulse), 20 (following pulses)
12. Xmtr parameter drift occurs every 0 iterations with norm mag. 1
13. Xmtr switch occurs every 0 iterations (1st pulse only, when drift on)
14. Display method:  plot
15. Control algorithm:  Steepest Descent
16. Display/change current algorithm parameters
17. Access keyboard                18. Exit

Enter number(s) to change parameters or <Enter> to begin:

(e.g., 1 or [1 7 8])  ====>
```

Figure 5.2: Main menu, simulation program.

control algorithm and selects the desired display, analysis and recording options. In this section each menu item is briefly explained.

b. Transmitter Selection

The user may select either the AN/FPN-42 or the AN/FPN-44A transmitter. The program loads the polynomial coefficients for the selected transmitter, which have been stored in a single matrix with one polynomial in each row, as in Fig. 5.3. The polynomial coefficients of the *k*th root appear in adjacent rows — the first for magnitude and the second for phase. The program reinitializes variables governing the transmitter's operation and resets the drive waveforms and control algorithm.

c. Transmitter Load

The simulation program operates with either the antenna or the dummy load. The polynomial curves for the dummy load are in the lower partition of the matrix in Fig. 5.3. The program implements a load switch by resetting a row pointer for this matrix to select either the upper or lower partition. In its default mode, the program uses the dummy load to produce a near-optimum TDW for the antenna. The program switches to the antenna when the output errors fall below a threshold. This minimizes the time the pulse is out of tolerance when transmitting on the antenna. The "ideal" dummy load RF pulse used in this process was obtained by allowing the algorithm to converge on the antenna, switching to the dummy load and recording the output of this TDW. After switching to the antenna, usually the RF pulse is in tolerance within an iteration or two. Here the antenna and antenna simulator are used interchangeably.

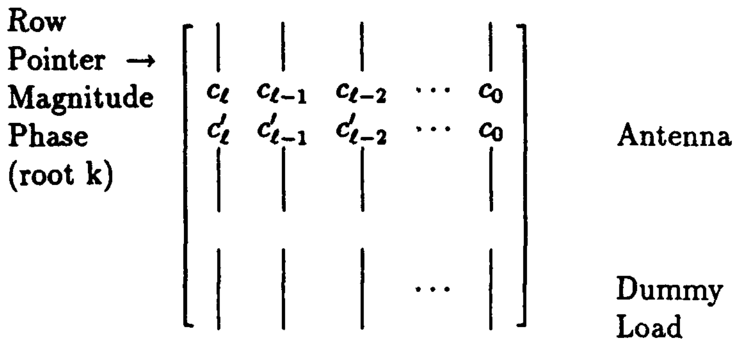
Row
Pointer →
Magnitude
Phase
(root k)
c_ℓ $c_{\ell-1}$ $c_{\ell-2}$ $\cdots$ c_0
c'_ℓ $c'_{\ell-1}$ $c'_{\ell-2}$ $\cdots$ c_0
$\cdots$
Antenna
Dummy
Load

Figure 5.3: Polynomial coefficient matrix.

d. Sampling Frequency

This program runs at four data sampling frequencies: 10 MHz, 5 MHz, 2.5 MHz, and 1.25 MHz, as discussed in Chapter III, Subsection D.1. The best error convergence is at f_s = 10 MHz, but the program runs the fastest and requires the least storage at f_s = 1.25 MHz. The algorithm resets the transmitter and control algorithm when a new sampling frequency is selected.

e. Local ECD

The program controls the local (transmitted) ECD of the RF pulse by generating a new ideal Loran pulse with the desired ECD from Eq. (2.1) and using the new pulse in the control algorithm. Currently in the Coast Guard, ECD is controlled by inserting a phase shift called the Early Timing Adjust (ETA) into the TDW. This program bypasses the ETA altogether and successfully controls ECD to within $0.44\mu s$ in the range $-2.5\mu s \leq \tau \leq 2.5\mu s$ by changing the ideal waveform. The LOIS program, used in the daily Loran-C system sample, is used to measure ECD by hand.

f. Amplitude Resolution and System Noise

The simulation program incorporates the noise model shown in Fig. 5.4. The noise present in the actual data pairs may be duplicated in simulation by selecting eight-bit quantization and adding white noise to the synthetic TDW and

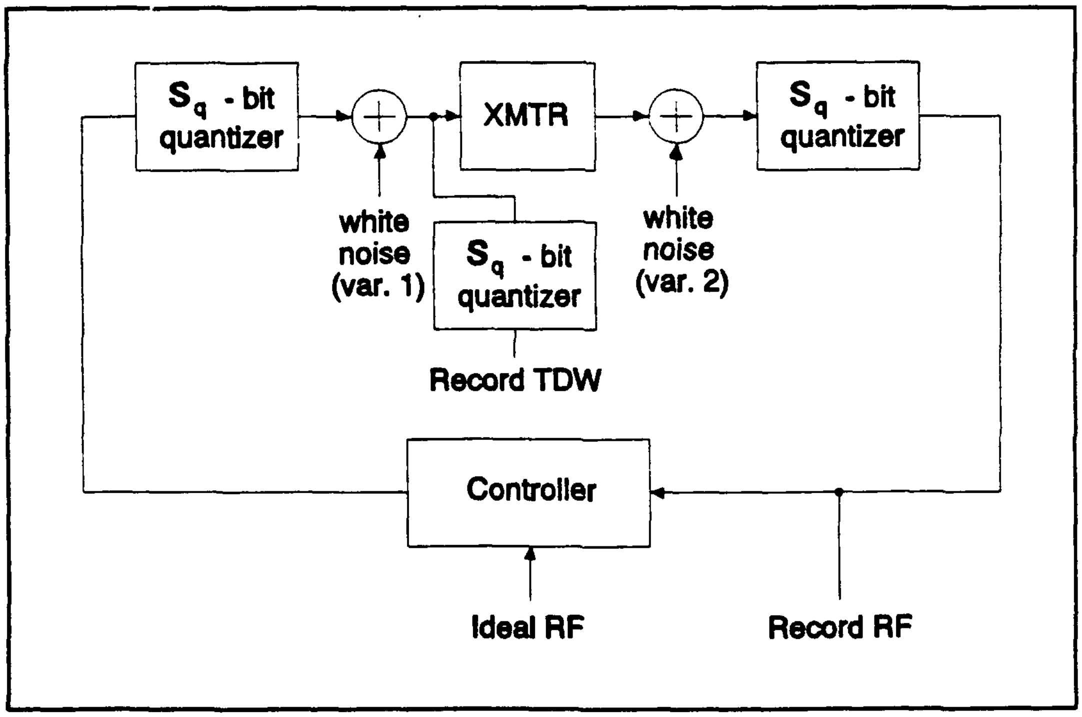

Figure 5.4: Transmitter system noise model.

TABLE 5.1: AVERAGE SNR OF MEASURED DATA PAIRS (ANTENNA)

Transmitter	SNR (dB)	
	TDW	RF Pulse
AN/FPN-42	56.4	62.0
AN/FPN-44A	56.1	66.6

RF pulse until the SNRs of both match the average SNRs of the actual data (as defined in Chapter III, Subsection B.2.b.). These average SNRs are listed in Table 5.1.

Because the relative amplitudes of the '42 and '44A waveforms are different, the standard deviation of the white noise is expressed as a percentage of the maximum positive amplitude of the waveform. The SNRs in Table 5.1 are achieved in simulation using the settings in Table 5.2.

The user specifies the number of bits and the noise percentage of the RF pulse in menu items five and seven, respectively; the program then sets the TDW noise percentage automatically by multiplying the RF pulse noise percentage by 2.7 for the '42 and 1.8 for the '44A. Other quantization settings available are $S_q = 12$ bits, $S_q = 16$ bits and $S_q = \infty$ (maximum resolution, to machine precision). These represent a best-case scenario, because all the quantization levels are used. In the real system, some of the levels at the top and bottom are not usually used to avoid saturation, reducing the effective bit resolution. The capability to reproduce the observed noise level in the transmitter system is extremely important as it allows the simulation to be a realistic one. Results of different quantization settings are presented in Section C of this chapter.

TABLE 5.2: PROGRAM SETTINGS WHICH REPRODUCE SNR OF MEASURED DATA

Transmitter	Number of bits, S_q	Std. Dev. of White Noise (% of peak amplitude) TDW	RF Pulse
AN/FPN-42	8	1.05	0.39
AN/FPN-44A	8	0.97	0.54

g. Transmitter Imbalance

As described in Subsection C.1.e. of Chapter II, an imbalance between the two vacuum-tube amplifier banks in a transmitter reduces the amplitude of the negatively phase coded pulses. The program simulates this imbalance by reducing the amplitudes of these RF pulses by a percentage defined by the user in this menu item. The program automatically compensates for this imbalance by increasing the TDW amplitude by an appropriate amount. As with ETA, the phase code balance adjustment in the PGEN is bypassed entirely.

h. Reset Transmitter

When the program completes controlling and analyzing all the selected pulses in a PCI, the main menu appears again and the user has the option to continue where the program left off. The reset feature allows the user to start the control process from the beginning again without exiting the program. When the user selects this item, the program resets the drive waveforms, the control algorithm and the random transmitter drift settings (if drift is enabled), but it leaves intact the other control and analysis settings in the main menu.

i. Pulses to Control

The program can control any or all of the pulses in a PCI, as specified by the user. The TDWs for all selected pulses of the PCI are stored in successive columns of matrix $\mathbf{D}_c$, which represents a data output buffer to the AFG. The control approach is sequential, beginning with the first selected pulse. The program "drives" the transmitter model by presenting the TDW in column one of $\mathbf{D}_c$ as an input argument to the function XMTR. The resulting RF pulse is in turn presented as an input argument to the control algorithm, which produces the new TDW. This TDW, which is the best estimate of the optimal TDW for each pulse, is loaded into all the columns of $\mathbf{D}_c$ and proper phase-coding is applied. The amplitude of each TDW may also be scaled up exponentially to compensate for power supply droop as explained later in this section. When the specified number of control iterations are completed, the final RF pulse is stored in column one of matrix $\mathbf{R}_c$ and the program moves to the next selected pulse. As the program controls the pth pulse, columns p and following of $\mathbf{D}_c$ are updated every iteration, but columns one through $p-1$ are not. When the entire process is completed, matrix $\mathbf{D}_c$ contains the best estimates of the optimal TDWs for all selected pulses, and $\mathbf{R}_c$ contains the selected output RF pulses. In the VXIbus system, the output data buffer can easily be dumped to the AFG. With an MPT to set the proper time of emission, the desired TDW would be sent to the transmitter.

j. Pulses to Analyze

When the program finishes controlling an RF pulse, it performs an analysis of that pulse and the control process that produced it. The program's default setting is to analyze every selected pulse, but the user may suppress any or all of these analyses. The program then prints the results to a screen and to an ASCII text file, as in Fig. 5.5. Next, the program plots the Loran-C errors and

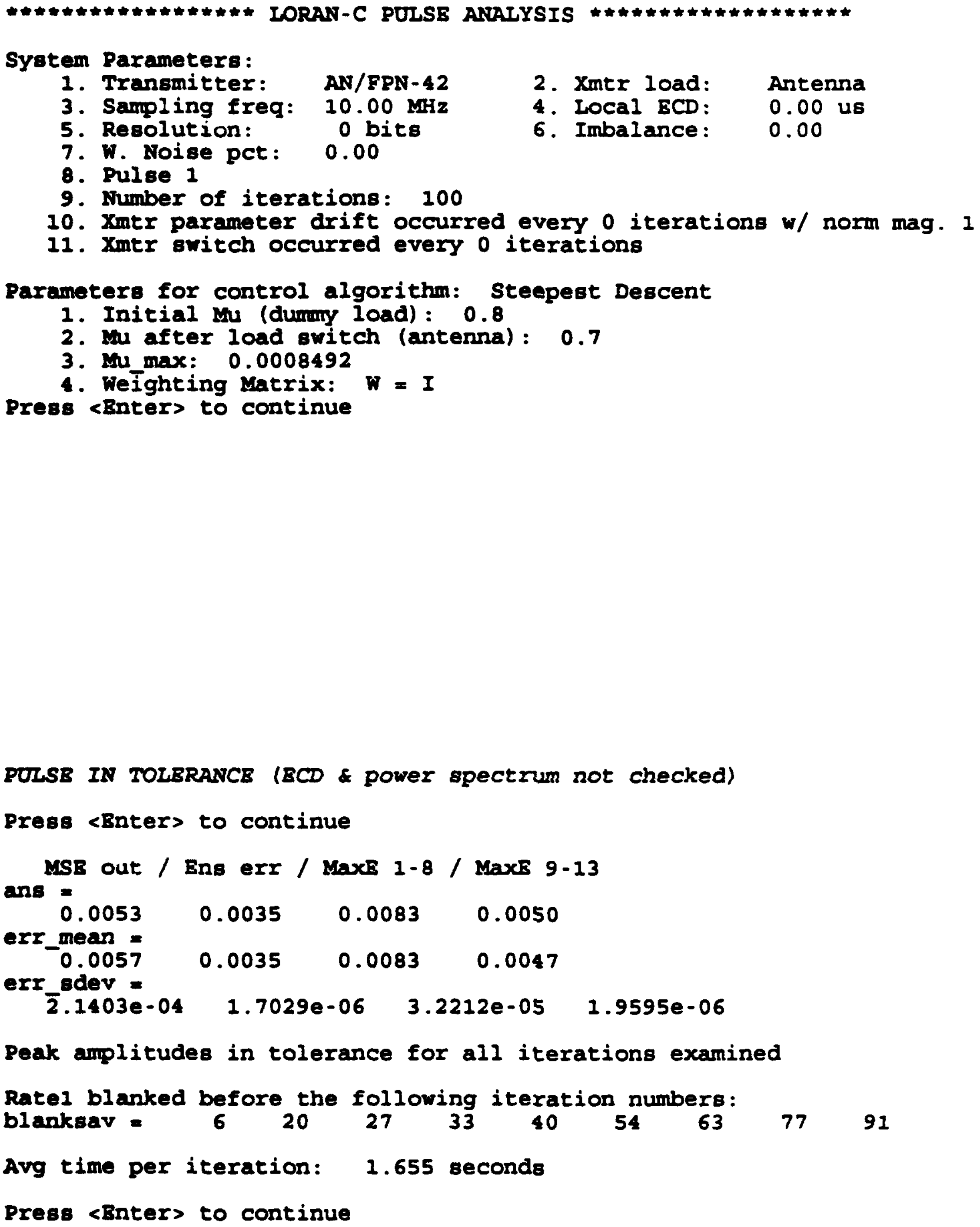

```
****************** LORAN-C PULSE ANALYSIS ******************

System Parameters:
    1. Transmitter:     AN/FPN-42        2. Xmtr load:     Antenna
    3. Sampling freq:  10.00 MHz         4. Local ECD:     0.00 us
    5. Resolution:       0 bits          6. Imbalance:     0.00
    7. W. Noise pct:   0.00
    8. Pulse 1
    9. Number of iterations:  100
   10. Xmtr parameter drift occurred every 0 iterations w/ norm mag. 1
   11. Xmtr switch occurred every 0 iterations

Parameters for control algorithm:  Steepest Descent
    1. Initial Mu (dummy load):  0.8
    2. Mu after load switch (antenna):  0.7
    3. Mu_max:  0.0008492
    4. Weighting Matrix:  W = I
Press <Enter> to continue










PULSE IN TOLERANCE (ECD & power spectrum not checked)

Press <Enter> to continue

   MSE out / Ens err / MaxE 1-8 / MaxE 9-13
ans =
    0.0053     0.0035     0.0083     0.0050
err_mean =
    0.0057     0.0035     0.0083     0.0047
err_sdev =
   2.1403e-04   1.7029e-06   3.2212e-05   1.9595e-06

Peak amplitudes in tolerance for all iterations examined

Rate1 blanked before the following iteration numbers:
blanksav =     6     20     27     33     40     54     63     77     91

Avg time per iteration:   1.655 seconds

Press <Enter> to continue
```

Figure 5.5: Pulse analysis printout.

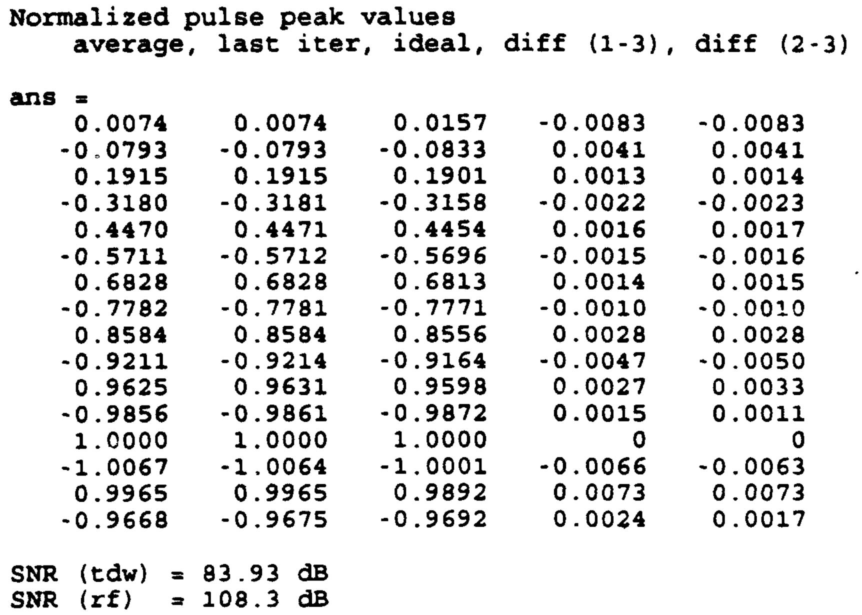

```
Normalized pulse peak values
    average, last iter, ideal, diff (1-3), diff (2-3)

ans =
    0.0074     0.0074     0.0157    -0.0083    -0.0083
   -0.0793    -0.0793    -0.0833     0.0041     0.0041
    0.1915     0.1915     0.1901     0.0013     0.0014
   -0.3180    -0.3181    -0.3158    -0.0022    -0.0023
    0.4470     0.4471     0.4454     0.0016     0.0017
   -0.5711    -0.5712    -0.5696    -0.0015    -0.0016
    0.6828     0.6828     0.6813     0.0014     0.0015
   -0.7782    -0.7781    -0.7771    -0.0010    -0.0010
    0.8584     0.8584     0.8556     0.0028     0.0028
   -0.9211    -0.9214    -0.9164    -0.0047    -0.0050
    0.9625     0.9631     0.9598     0.0027     0.0033
   -0.9856    -0.9861    -0.9872     0.0015     0.0011
    1.0000     1.0000     1.0000          0          0
   -1.0067    -1.0064    -1.0001    -0.0066    -0.0063
    0.9965     0.9965     0.9892     0.0073     0.0073
   -0.9668    -0.9675    -0.9692     0.0024     0.0017

SNR (tdw) = 83.93 dB
SNR (rf)  = 108.3 dB
```

Figure 5.5 (continued): Pulse analysis printout.

output mean squared error, the final TDW and RF pulse, the rest times and estimated power supply voltage (explained later in this section), and the drift parameters. These plots are also recorded in META file format.

k. Number of Iterations

Here the user selects the number of control iterations for the first selected pulse and for all following pulses. The default setting for the first selected pulse is 100, which is usually sufficient time for the algorithm to converge. Because the TDWs of the following pulses are also replaced every iteration during the convergence of the first selected pulse, the pulses are in tolerance or nearly in tolerance at their first control iteration. Bringing these errors into convergence thus requires fewer iterations and so the default setting is twenty iterations.

l. Transmitter Drift

In this item, the user sets both the time scale and the magnitude of the transmitter parameter drift described in Chapter III, Subsections E.2. and E.3. Setting $t_d = 300$ and the normalized magnitude equal to one reasonably approximates the time variations in an actual transmitter. Reducing the value of t_d or increasing the normalized drift magnitude artificially increases these time variations, which is useful in testing and analysis.

m. Transmitter Switch

By introducing a random step change into the c_0 parameters shown in Fig. 5.3, a switch to a different transmitter may be simulated. The program performs transmitter switches at a regular interval, as often as the user desires. In this way, the algorithm may be tested with an infinite number of different '42 and '44A transmitter models as no two random settings of the c_0 parameters are exactly alike. When the number of iterations per transmitter switch is set to zero, however, the identical transmitter model is produced every time. To obtain a random setting and to disable time variations, the user sets the number of iterations per transmitter switch to the number of control iterations (menu item 11) plus one. The load remains the same during a transmitter switch. The performance of the control algorithm following transmitter switches appears in Section C of this chapter.

n. Display Method

To monitor the errors as the algorithm converges, the user may select the text line option of Fig. 5.6a or the plot option of Fig. 5.6b. Or, the

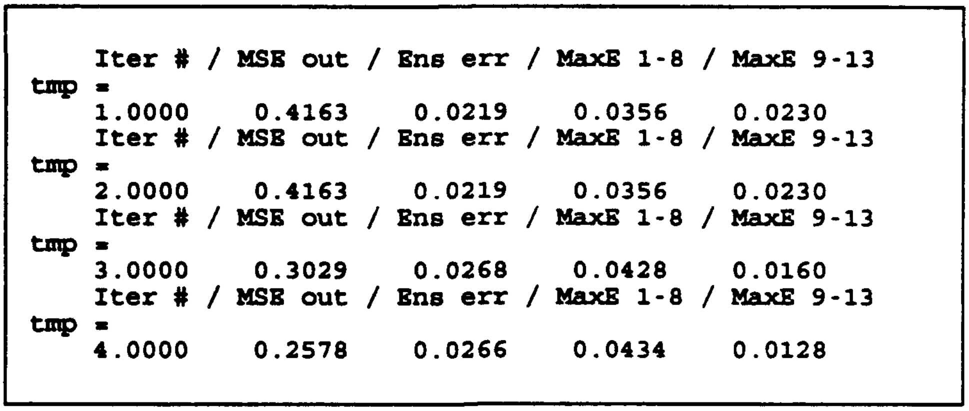

```
    Iter # / MSE out / Ens err / MaxE 1-8 / MaxE 9-13
tmp =
    1.0000    0.4163    0.0219    0.0356    0.0230
    Iter # / MSE out / Ens err / MaxE 1-8 / MaxE 9-13
tmp =
    2.0000    0.4163    0.0219    0.0356    0.0230
    Iter # / MSE out / Ens err / MaxE 1-8 / MaxE 9-13
tmp =
    3.0000    0.3029    0.0268    0.0428    0.0160
    Iter # / MSE out / Ens err / MaxE 1-8 / MaxE 9-13
tmp =
    4.0000    0.2578    0.0266    0.0434    0.0128
```

(a)

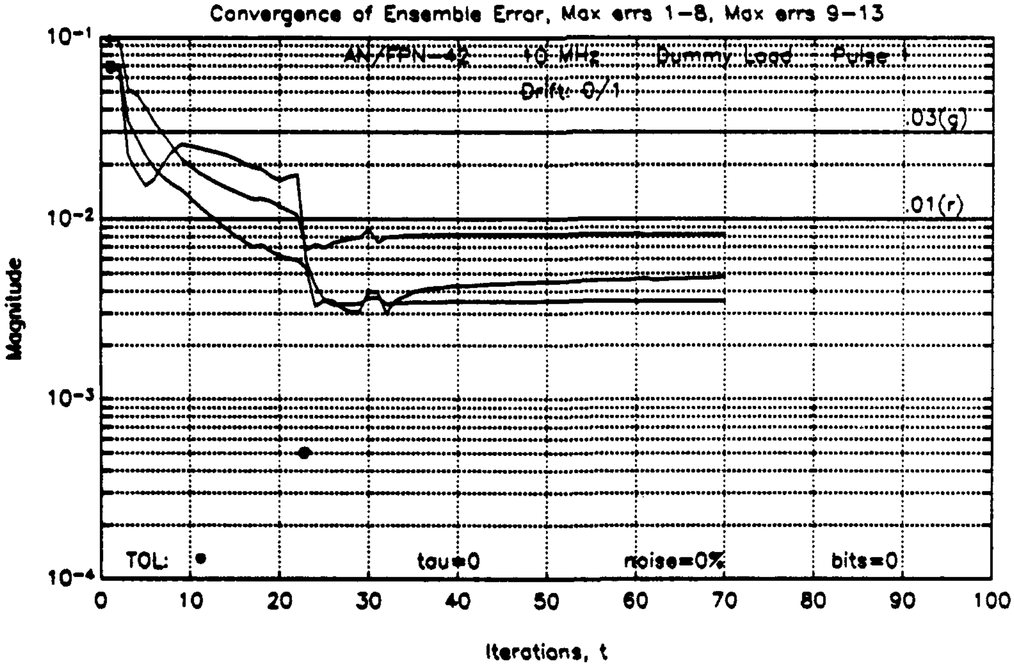

(b)

Figure 5.6: Options for displaying error convergence. (a) Text line, and plot.

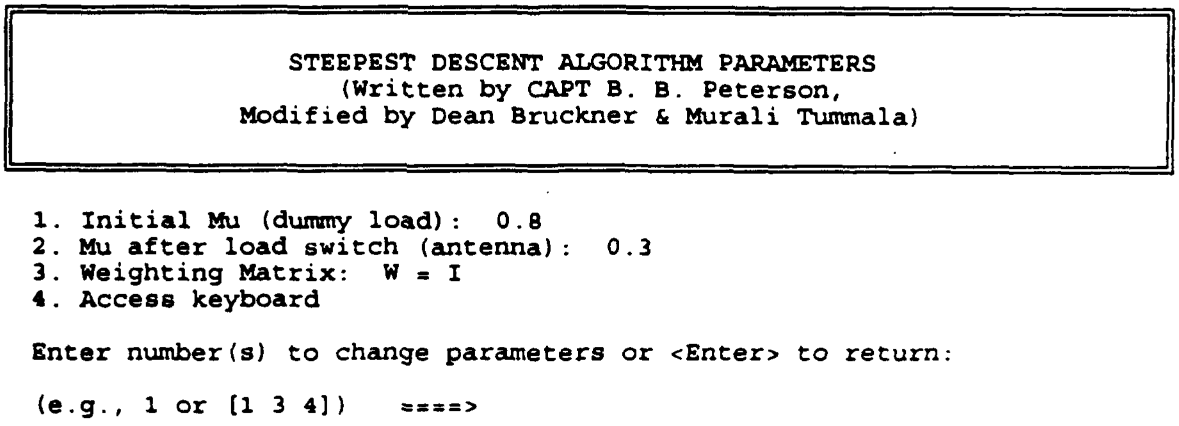

```
                STEEPEST DESCENT ALGORITHM PARAMETERS
                  (Written by CAPT B. B. Peterson,
             Modified by Dean Bruckner & Murali Tummala)

1. Initial Mu (dummy load):  0.8
2. Mu after load switch (antenna):  0.3
3. Weighting Matrix:  W = I
4. Access keyboard

Enter number(s) to change parameters or <Enter> to return:

(e.g., 1 or [1 3 4])    ====>
```

Figure 5.7: Menu for steepest descent algorithm.

user may suppress both of these. The plot is the most comprehensive display method. Load switches are marked by an "$\hat{a}$" and transmitter switches by an "$\hat{x}$".

o. Control Algorithm

Currently only the steepest descent algorithm has been implemented in this simulation program. Because the program is constructed in modular form, other algorithms may easily be added. In this case, the user could select a new algorithm from the main menu.

p. Display/Change Current Parameters

The parameters for each algorithm are changed using a submenu. Figure 5.7 displays this menu for the steepest descent algorithm.

q. Access Keyboard

In this option, the user accesses the MATLAB command line. Here he or she may examine or change parameters not accessible at the menus.

3. Explanation of Features Not Appearing in the Main Menu

a. Simulating Power Supply Droop

The problem of power supply droop has a negative effect on a closed loop Loran-C control system, as described in Subsection B.2.d. of Chapter II. The amplitude of each successive pulse in a GRI is reduced by a small amount, because the power supply of the transmitter does not fully recover within the 1000 μs pulse-to-pulse interval. This program models the power supply voltage v_{ps} as a charging exponential with four parameters:

- The normalized power supply voltage just prior to the last pulse (v_{ℓ}, in the range (0,1]),
- The decrease in power supply voltage due to transmitting the last pulse (Δv_{ℓ}),
- The time the power supply has rested since the last pulse (t_v), and
- The time constant of the charging exponential (τ_v).

These are shown graphically in Fig. 5.8. It was first assumed that the transfer function of the transmitter changed measurably with decreases in the power supply voltage; however, an analysis of an entire GRI revealed no predictable changes in pole and zero locations. Therefore, the effect of droop is modeled solely as a decrease in RF pulse amplitude.

The quantity v_{ps} is estimated before obtaining each RF pulse. In the function XMTR, the RF pulse is multiplied directly by the v_{ps} estimated for that pulse. This simulates the decrease in amplitude due to droop. Quantities Δv_{ℓ}

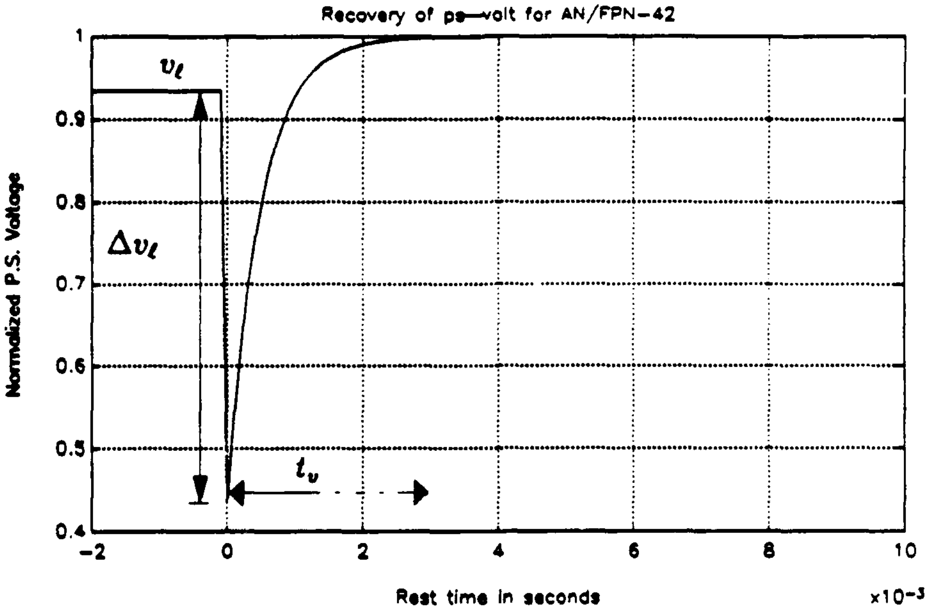

Figure 5.8: Charging Exponential model of power supply voltage.

and τ_v are constant for the entire simulation, but quantities v_ℓ and t_v are not. Here a simplification is made: the power supply voltages of pulses two through eight in each GRI are assumed to decrease exponentially from pulse one, according to the relation

$$v_{ps}\Big|_{\text{pulse } p} = \delta^p v_{ps}\Big|_{\text{pulse } 1}, \qquad p = 2, \cdots, 8, \tag{5.1}$$

where $\delta = 0.992$ for the '42 and $\delta = 0.9988$ for the '44A. Now v_{ps} must be estimated for the first pulse of every control iteration in order to find v_{ps} for any of the other pulses.

Because pulse eight of the last GRI transmitted always precedes pulse one, v_ℓ is held constant in the simulation at 0.935 for the '42 and 0.99 for the '44A. This reflects measured values of droop of 6.5 percent for the '42 and 1.0 percent for the '44A. Realistic values of variable t_v for each control iteration, however, are found only by simulating dual-rated operation.

b. Simulating Dual-Rated Operation

As explained in Chapter II, Subsection B.4., a dual-rated station transmits GRIs for two adjacent chains, and the two GRIs are not synchronized to each other. When the blanking intervals enclosing the GRIs overlap, one of the rates is blanked. When the blanking intervals are very close to each other but do not overlap, however, the droop of the power supply is accentuated. In this case, the transmitter transmits eight pulses spaced 1000 μs apart followed by a rest as short as 1900 μs, which is then followed by eight more pulses spaced at 1000 μs. The interval between the two GRIs is the quantity t_v.

A problem arises when the VXIbus control system happens to sample a pulse in this second GRI. The peak amplitude of the sampled pulse from this GRI will be noticeably smaller than the average peak amplitude of that pulse from other GRIs. This introduces a transient disturbance into the control algorithm. The purpose of including dual-rate operation in this simulation is to study the response of the control algorithm to these transient effects.

The MATLAB function REST was written to produce a vector of consecutive rest times $\mathbf{t}_v$, in seconds, prior to the GRIs of the shorter rate in a dual-rated station. For two secondary rates 99,400 μs and 59,900 μs, 200 samples of this vector are plotted in Fig. 5.9. From this figure, the periodic nature of this function is clear. In this program the pulse shape controller captures a pulse from a GRI every four seconds; with 66 GRIs in a four-second period, realistic values of t_v for pulse one in each GRI are thus obtained by taking every 66th sample from the vector of rest times. Another vector of the same length $\mathbf{b}_v$ indicates the samples

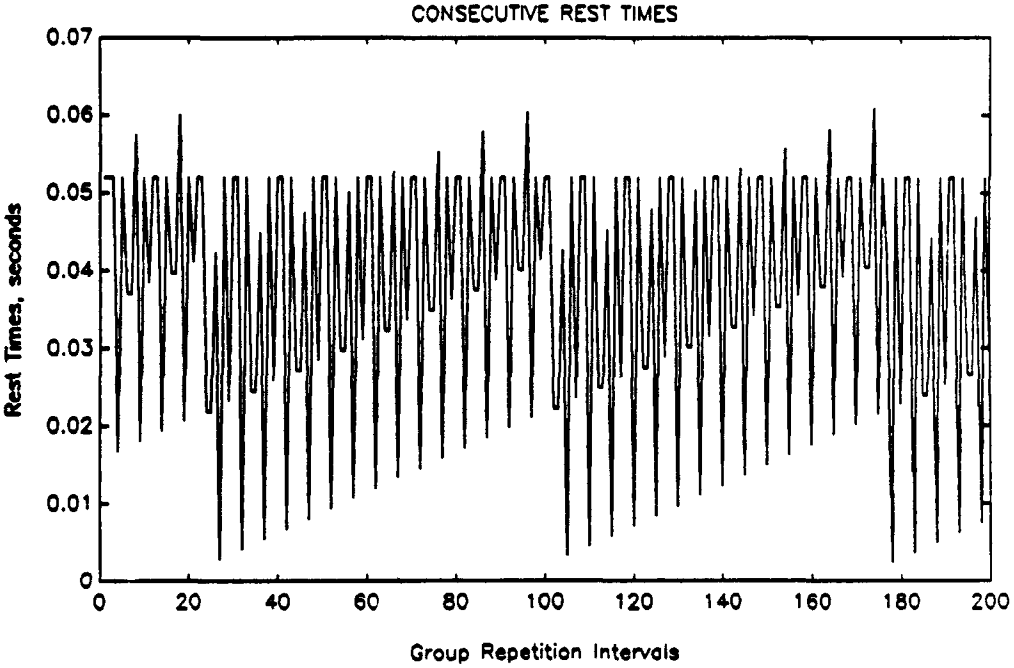

Figure 5.9: Vector of consecutive rest times, 200 samples.

for which the shorter rate was blanked; if the controller encounters one of these, it records the blanked iteration (see Fig. 5.5) and skips that GRI altogether.

Vector $\mathbf{t}_v$ is 503 samples long; when the end of the vector is reached the counter wraps around to the beginning again. Because 503 is a prime number, all of the samples in the vector should eventually be used if the simulation continues long enough. Figures 5.10a and 5.10b show the error convergence plots for a '42 simulation run of 100 samples. The controller switches from the dummy load to the antenna at iteration 24. Figures 5.10c and 5.10d show the estimated values of t_v and v_{ps} for each iteration. The increase in error is clearly visible between iterations 29–32. Fortunately, the algorithm is able to compensate and these errors are transient.

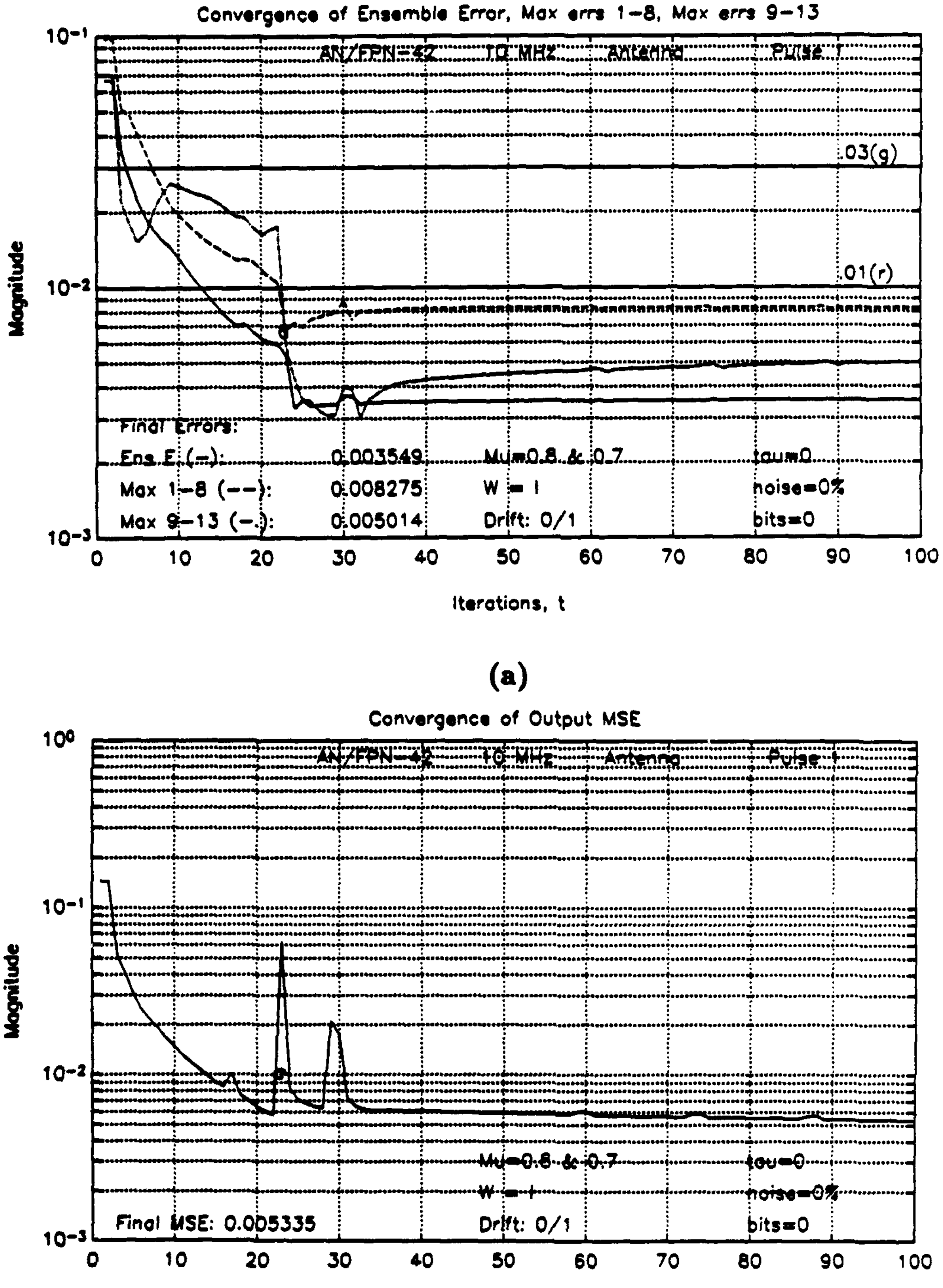

(a)

(b)

Figure 5.10: Effect of transient disturbances. (a) Mean squared error and (b) three measures of Loran error.

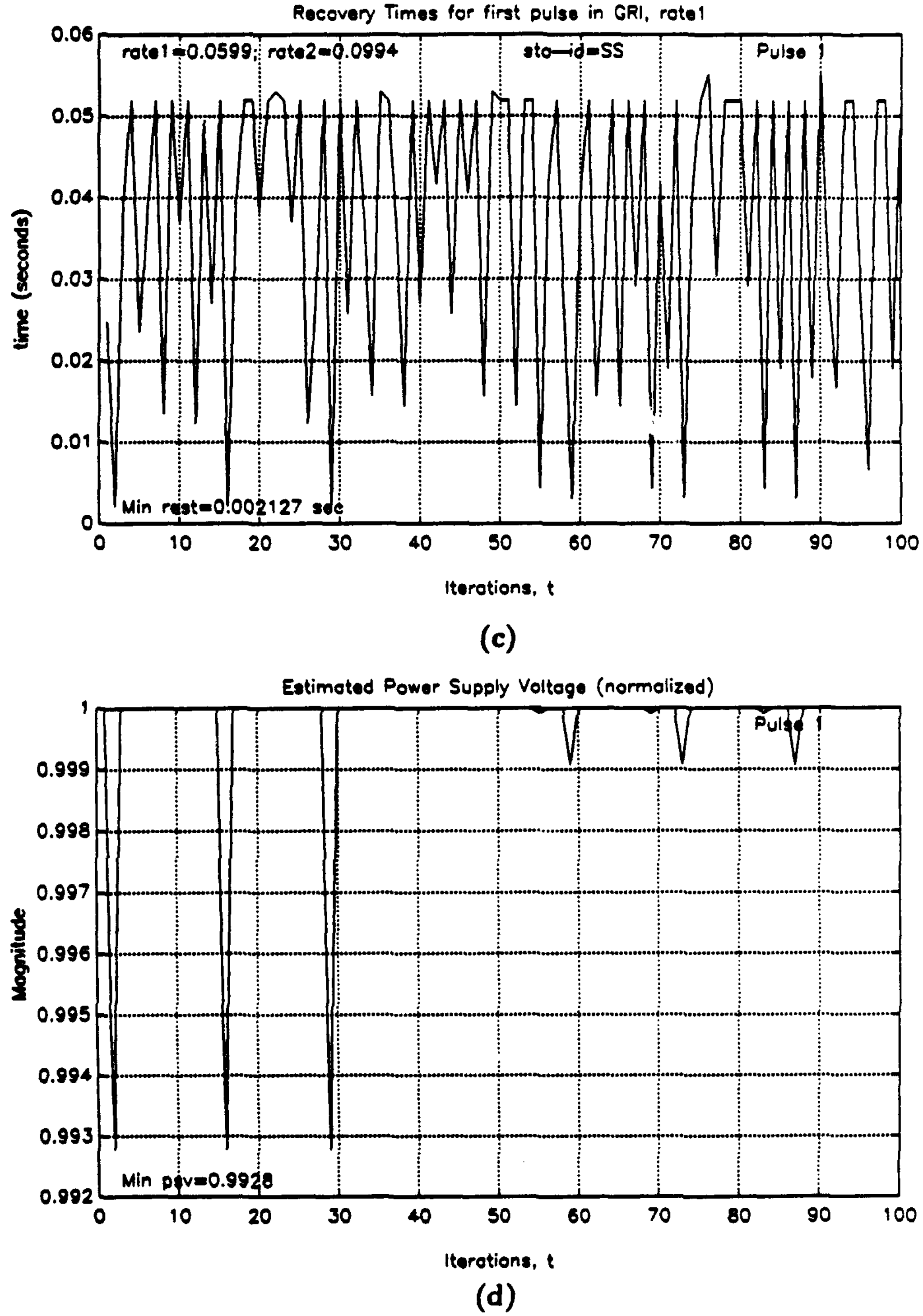

Figure 5.10: Effect of transient disturbances, continued. (c) Rest times and (d) estimated power supply voltage.

c. Exponential Scaling of TDW Amplitudes

In order to speed the convergence of pulses two through eight of the GRI, the program anticipates the droop of the transmitter. It boosts the amplitude of each successive TDW slightly when storing the TDWs in buffer matrix $\mathbf{D}_c$ according to the relation

$$(TDW)\Big|_{\text{pulse } p} = \beta^p (TDW)\Big|_{\text{pulse } 1}, \qquad p = 2, \cdots, 8, \tag{5.2}$$

where $\beta = 1.02$ for the '42 and $\beta = 1.0015$ for the '44A. These values are not exactly the inverses of the δ values given earlier; no specific *a priori* knowledge of droop was assumed, and these values were obtained experimentally. This feature does in fact speed convergence; in most cases, pulses two through eight converge within two to three iterations.

C. RESULTS

1. *Realistic Simulation of the AN/FPN-42*

In a realistic simulation of the '42 with 600 control iterations, the steepest descent algorithr shaped the Loran pulse effectively but maintained the pulse peaks in tolerance for only 78.3 percent of the control iterations in a test interval beginning at interation 101 and ending at iteration 600. The zero-crossings and ECD of the final RF pulse were in tolerance, however. The system noise drove the pulse peaks out of tolerance repeatedly. These out of tolerance cases would not necessarily require blink, but they are undesirable. Whether or not this would be acceptable in actual Loran operation is a policy matter for the Coast Guard to decide. In any case, these fluctuations are an indication that the steepest descent algorithm is sensitive to noise and that it is not as robust as perhaps it should be. Figures 5.11a through 5.11g are the plots for the first 100 iterations of this run; Fig. 5.11h is the printout for the test interval.

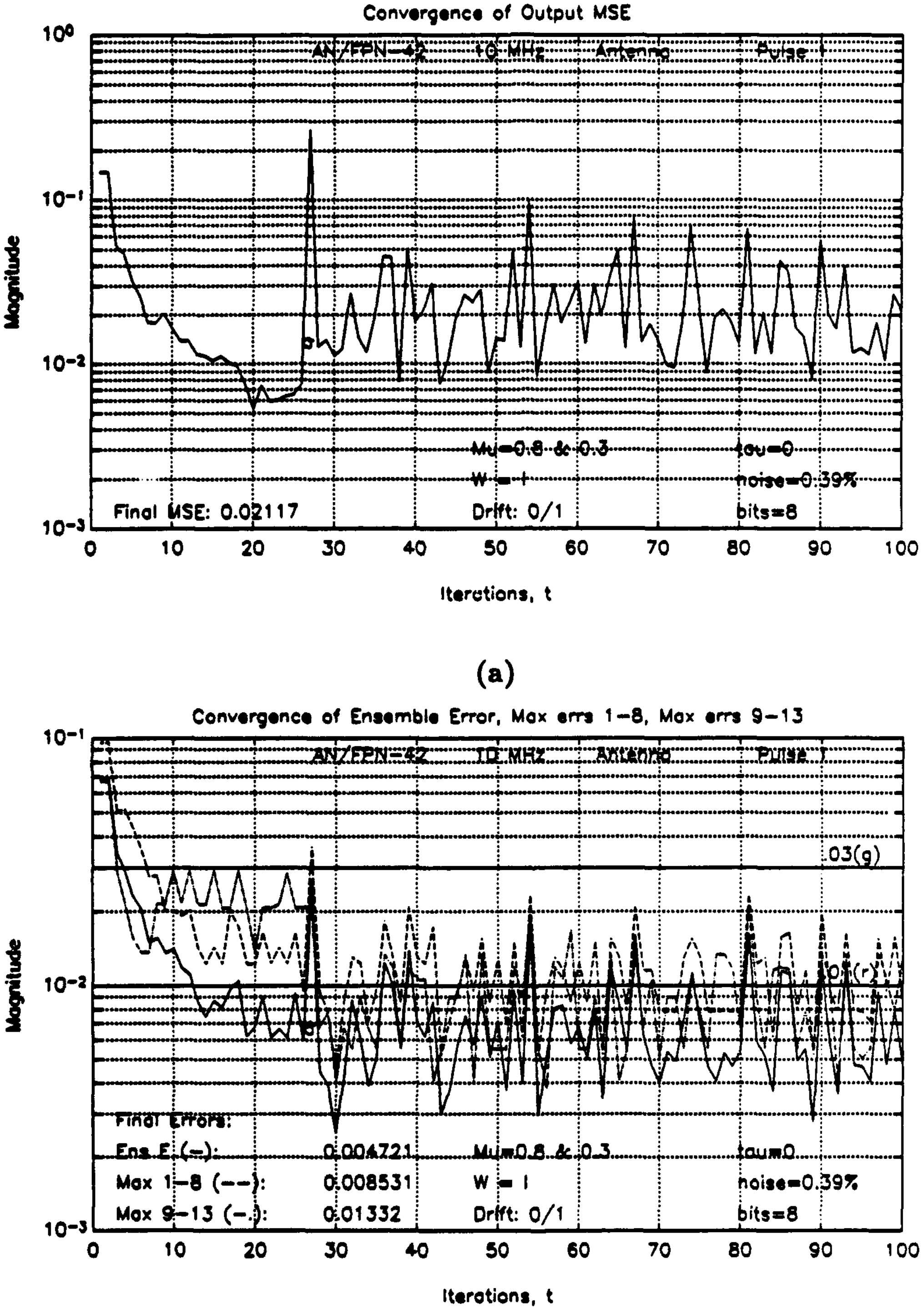

(a)

(b)

Figure 5.11: Realistic simulation results, '42. (a) Mean squared error and (b) three measures of Loran error.

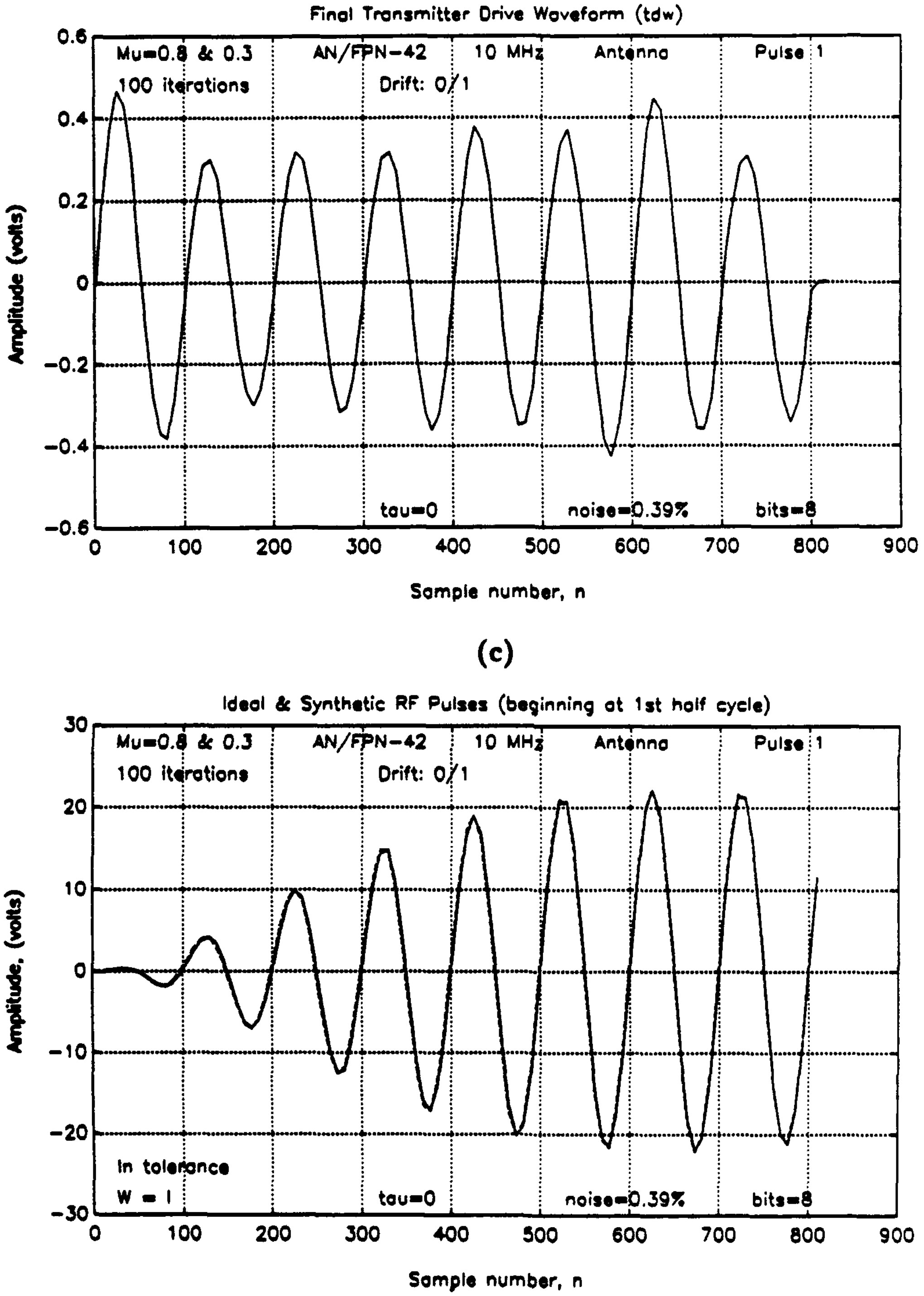

(c)

(d)

Figure 5.11: Realistic simulation results, '42. (c) Final TDW and (d) ideal and final synthetic RF pulses.

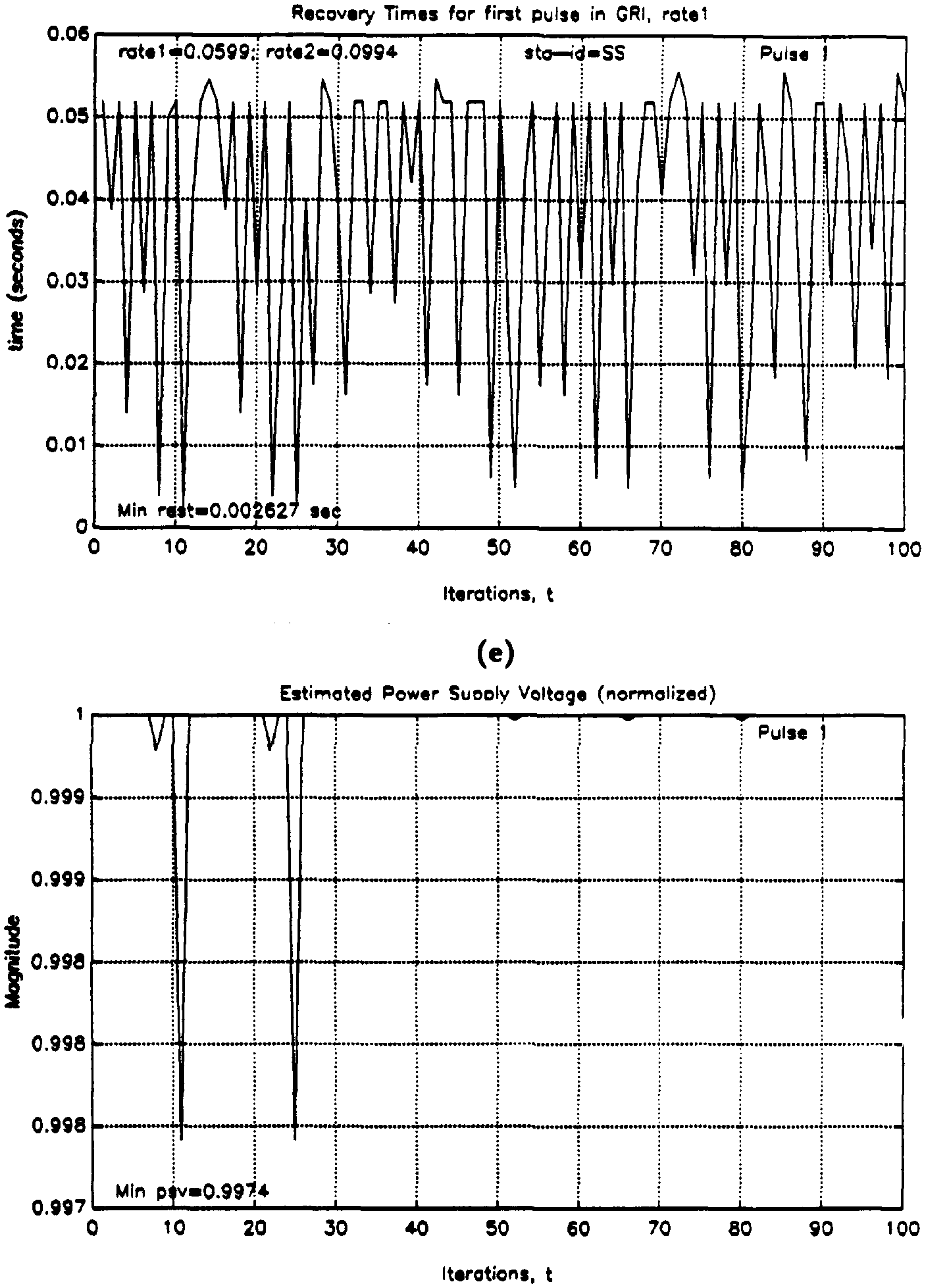

(e)

(f)

Figure 5.11: Realistic simulation results, '42. (e) Rest times and (f) estimated power supply voltages.

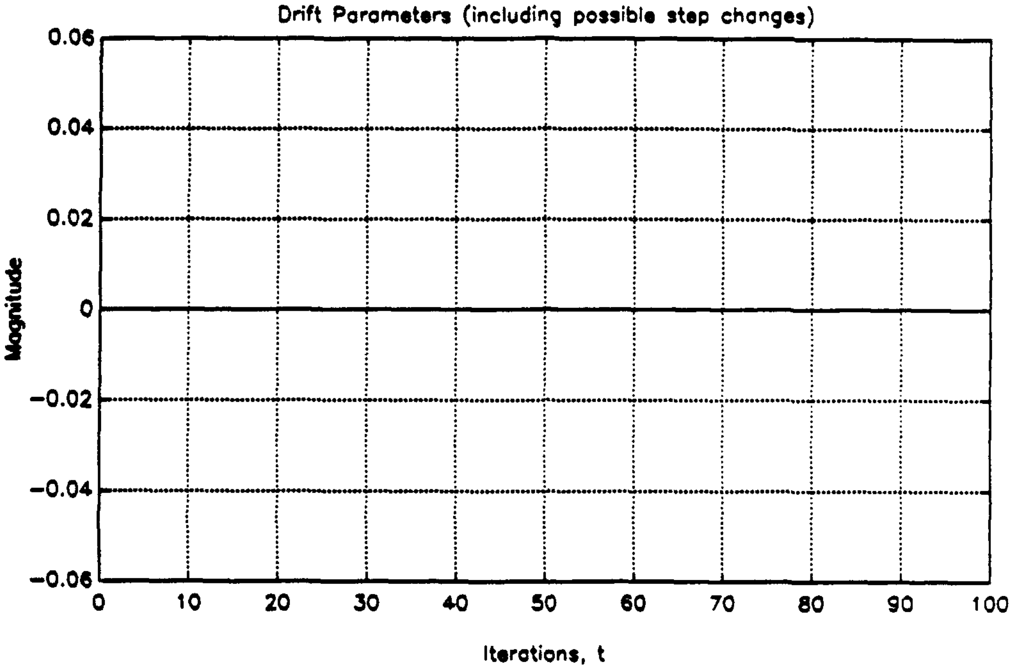

Figure 5.11g: Realistic simulation results, '42, drift parameters.

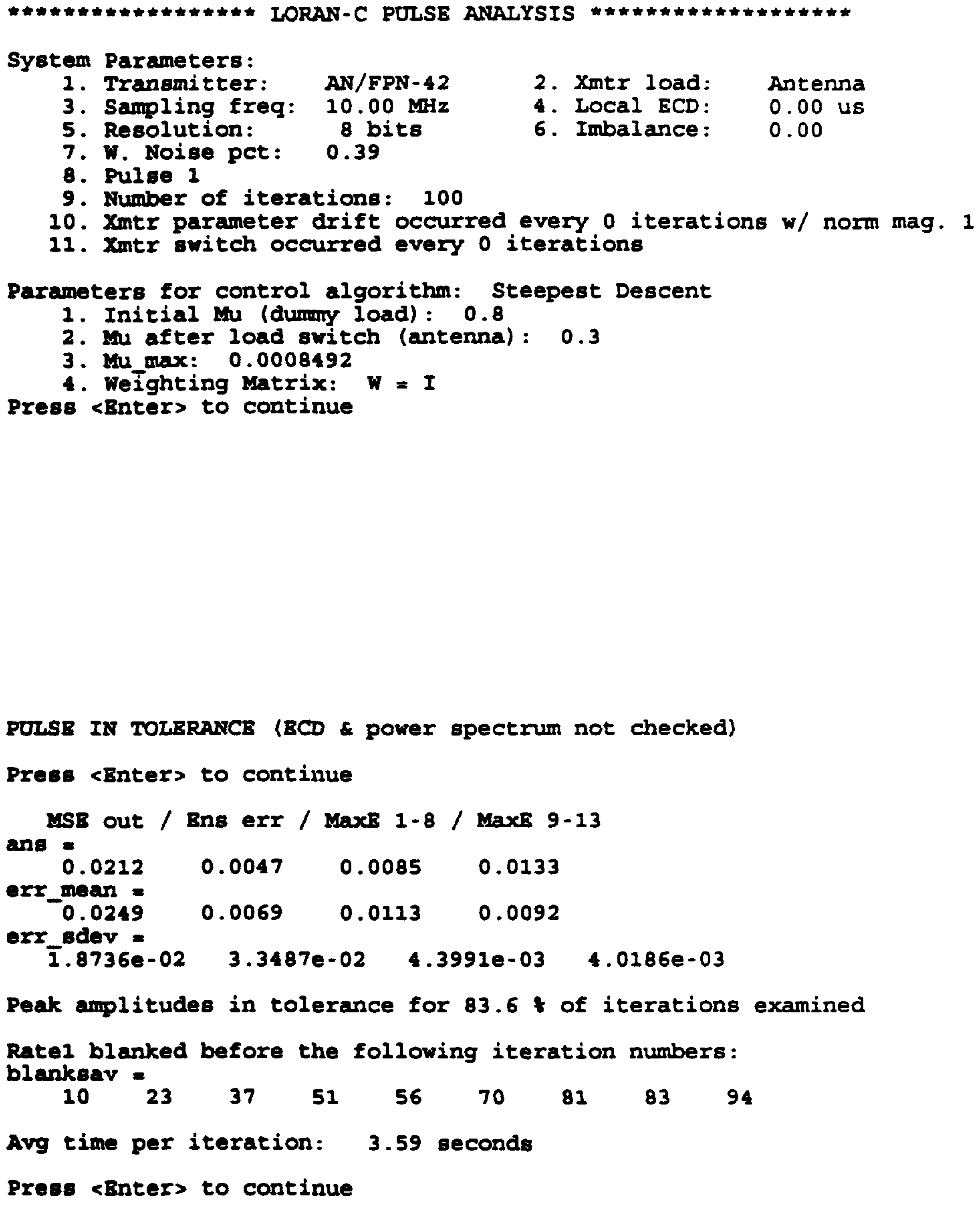

```
****************** LORAN-C PULSE ANALYSIS ******************

System Parameters:
    1. Transmitter:    AN/FPN-42      2. Xmtr load:    Antenna
    3. Sampling freq:  10.00 MHz      4. Local ECD:    0.00 us
    5. Resolution:      8 bits        6. Imbalance:    0.00
    7. W. Noise pct:   0.39
    8. Pulse 1
    9. Number of iterations:  100
   10. Xmtr parameter drift occurred every 0 iterations w/ norm mag. 1
   11. Xmtr switch occurred every 0 iterations

Parameters for control algorithm:  Steepest Descent
    1. Initial Mu (dummy load):  0.8
    2. Mu after load switch (antenna):  0.3
    3. Mu_max:  0.0008492
    4. Weighting Matrix:  W = I
Press <Enter> to continue








PULSE IN TOLERANCE (ECD & power spectrum not checked)

Press <Enter> to continue

   MSE out / Ens err / MaxE 1-8 / MaxE 9-13
ans =
    0.0212     0.0047     0.0085     0.0133
err_mean =
    0.0249     0.0069     0.0113     0.0092
err_sdev =
   1.8736e-02   3.3487e-02   4.3991e-03   4.0186e-03

Peak amplitudes in tolerance for 83.6 % of iterations examined

Rate1 blanked before the following iteration numbers:
blanksav =
    10     23     37     51     56     70     81     83     94

Avg time per iteration:   3.59 seconds

Press <Enter> to continue
```

Figure 5.11h: Realistic simulationresults,'42, pulse analysis printout.

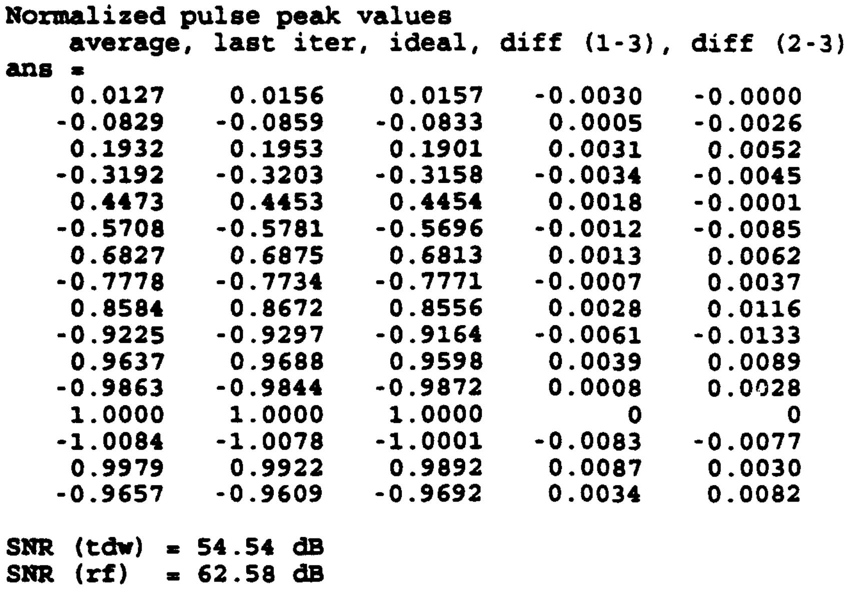

```
Normalized pulse peak values
   average, last iter, ideal, diff (1-3), diff (2-3)
ans =
   0.0127    0.0156    0.0157   -0.0030   -0.0000
  -0.0829   -0.0859   -0.0833    0.0005   -0.0026
   0.1932    0.1953    0.1901    0.0031    0.0052
  -0.3192   -0.3203   -0.3158   -0.0034   -0.0045
   0.4473    0.4453    0.4454    0.0018   -0.0001
  -0.5708   -0.5781   -0.5696   -0.0012   -0.0085
   0.6827    0.6875    0.6813    0.0013    0.0062
  -0.7778   -0.7734   -0.7771   -0.0007    0.0037
   0.8584    0.8672    0.8556    0.0028    0.0116
  -0.9225   -0.9297   -0.9164   -0.0061   -0.0133
   0.9637    0.9688    0.9598    0.0039    0.0089
  -0.9863   -0.9844   -0.9872    0.0008    0.0028
   1.0000    1.0000    1.0000         0         0
  -1.0084   -1.0078   -1.0001   -0.0083   -0.0077
   0.9979    0.9922    0.9892    0.0087    0.0030
  -0.9657   -0.9609   -0.9692    0.0034    0.0082

SNR (tdw) = 54.54 dB
SNR (rf)  = 62.58 dB
```

Figure 5.11h (continued): Pulse analysis printout.

2. Realistic Simulation of the AN/FPN-44A

In a similar realistic simulation of the '44A, the steepest descent algorithm effectively shaped the Loran pulse and maintained the pulse peaks in tolerance for 96.5 percent of the control iterations in the test interval. The ECD of the final RF pulse is in tolerance but the second zero-crossing of this pulse is not in tolerance. Figures 5.12a through 5.12h contain the plots and printout of this simulation run, as before.

3. Controlling ECD

The steepest descent algorithm effectively controlled the ECD of the average half-cycle peak amplitudes to within 0.44 μs, as Table 5.3 shows, during a test interval beginning 20 samples after the antenna switch and ending with sample

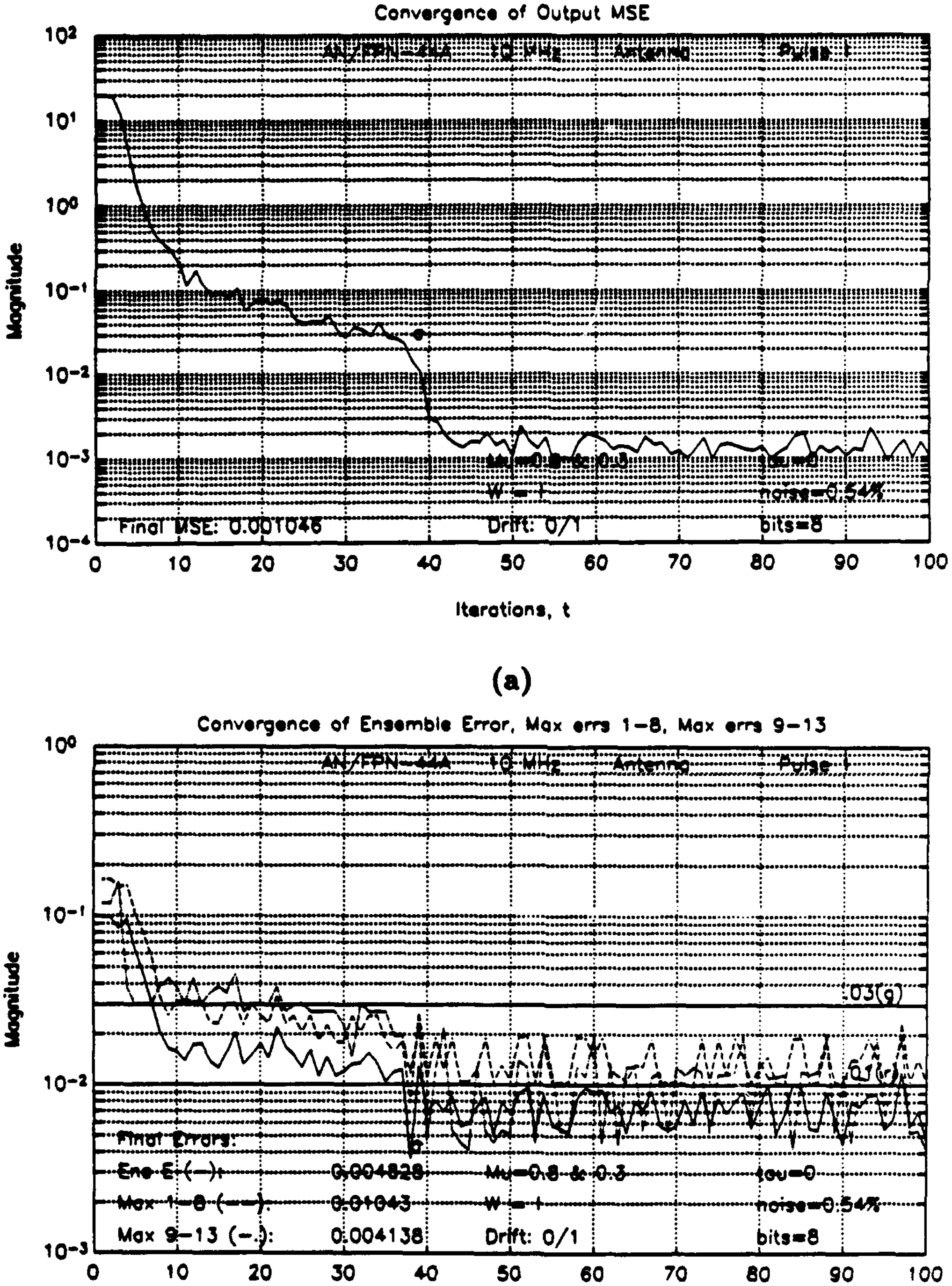

(a)

(b)

Figure 5.12: Realistic simulation results, '44A. (a) Mean squared error and (b) three measures of Loran error.

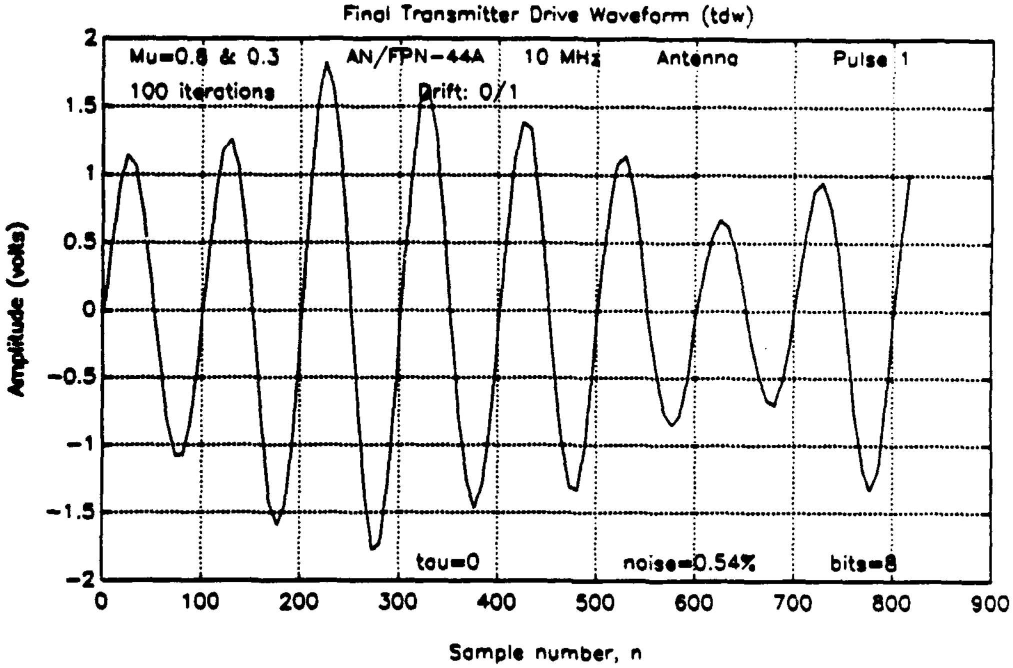

(c)

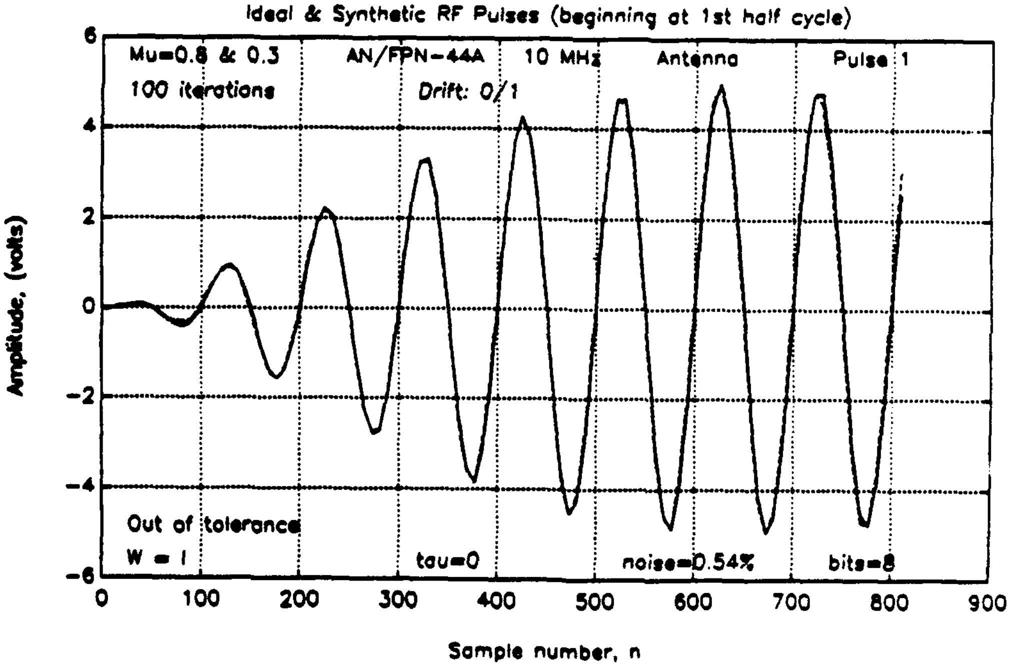

(d)

Figure 5.12: Realistic simulation results, '44A. (c) Final TDW and (d) ideal and final synthetic RF pulses.

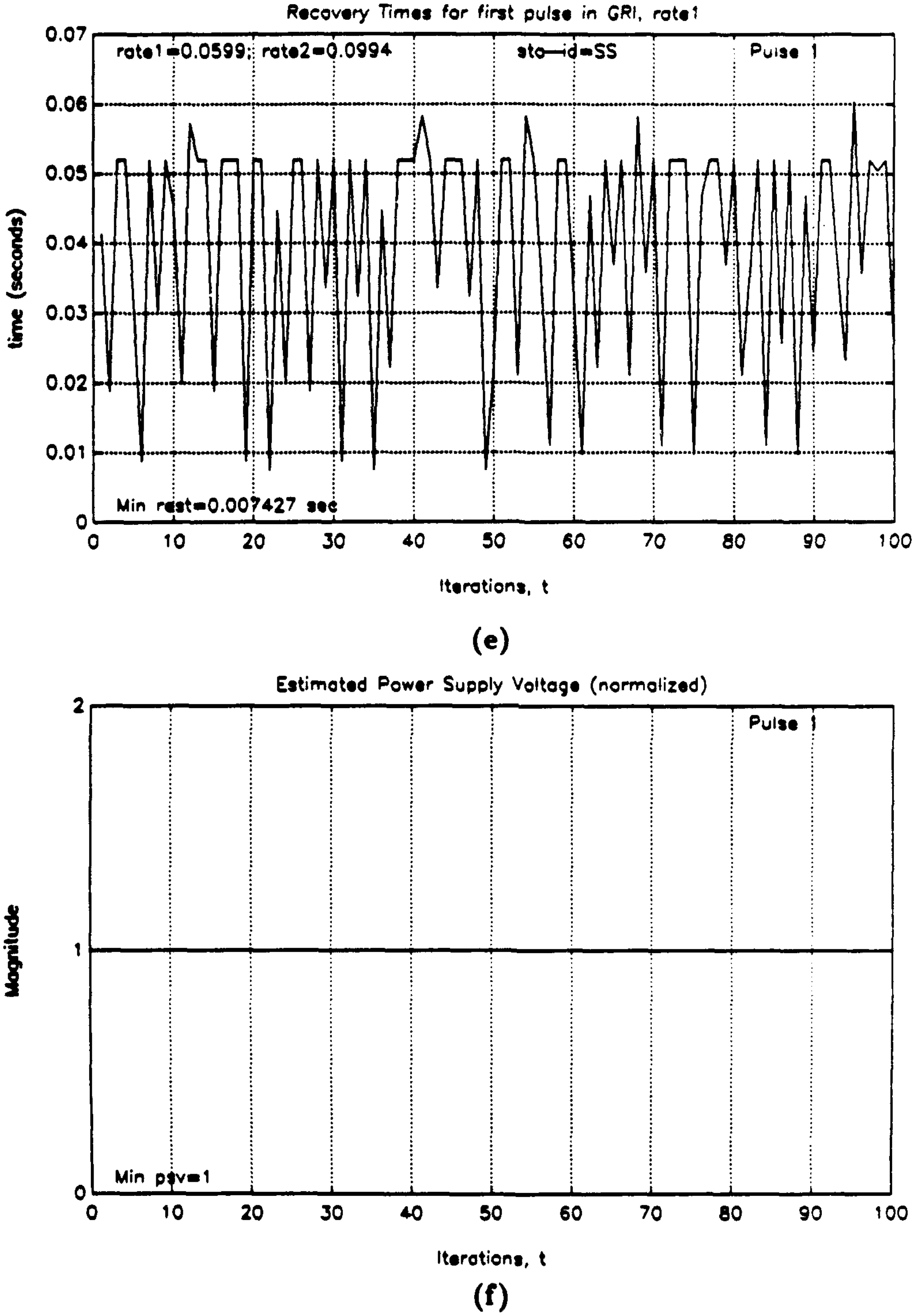

(e)

(f)

Figure 5.12: Realistic simulation results, '44A. (e) Rest times and (f) estimated power supply voltages.

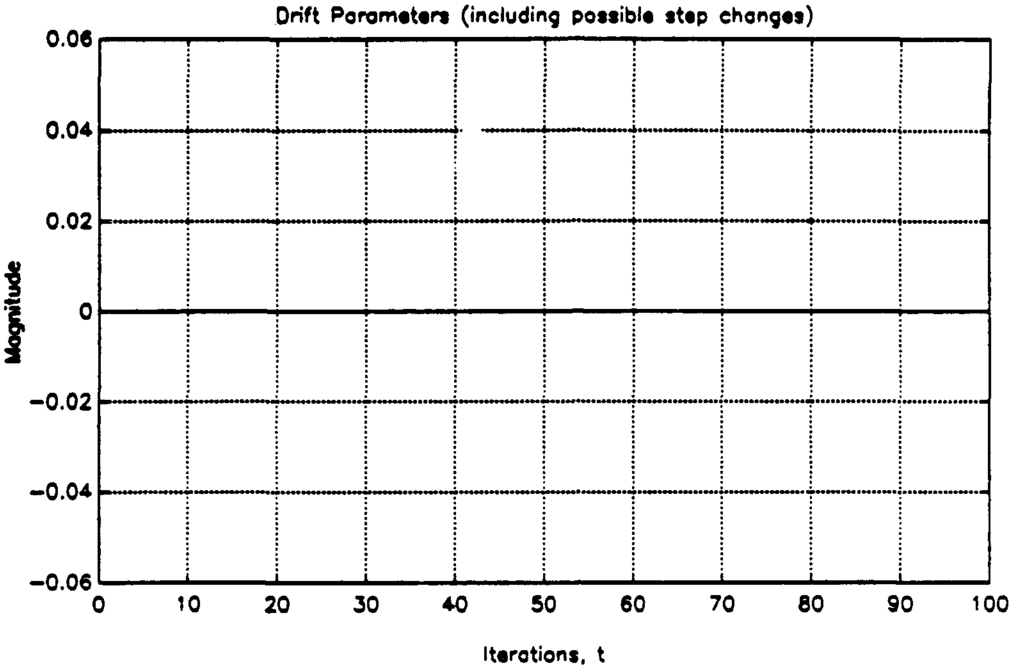

Figure 5.12g: Realistic simulation results, '44A, drift parameters.

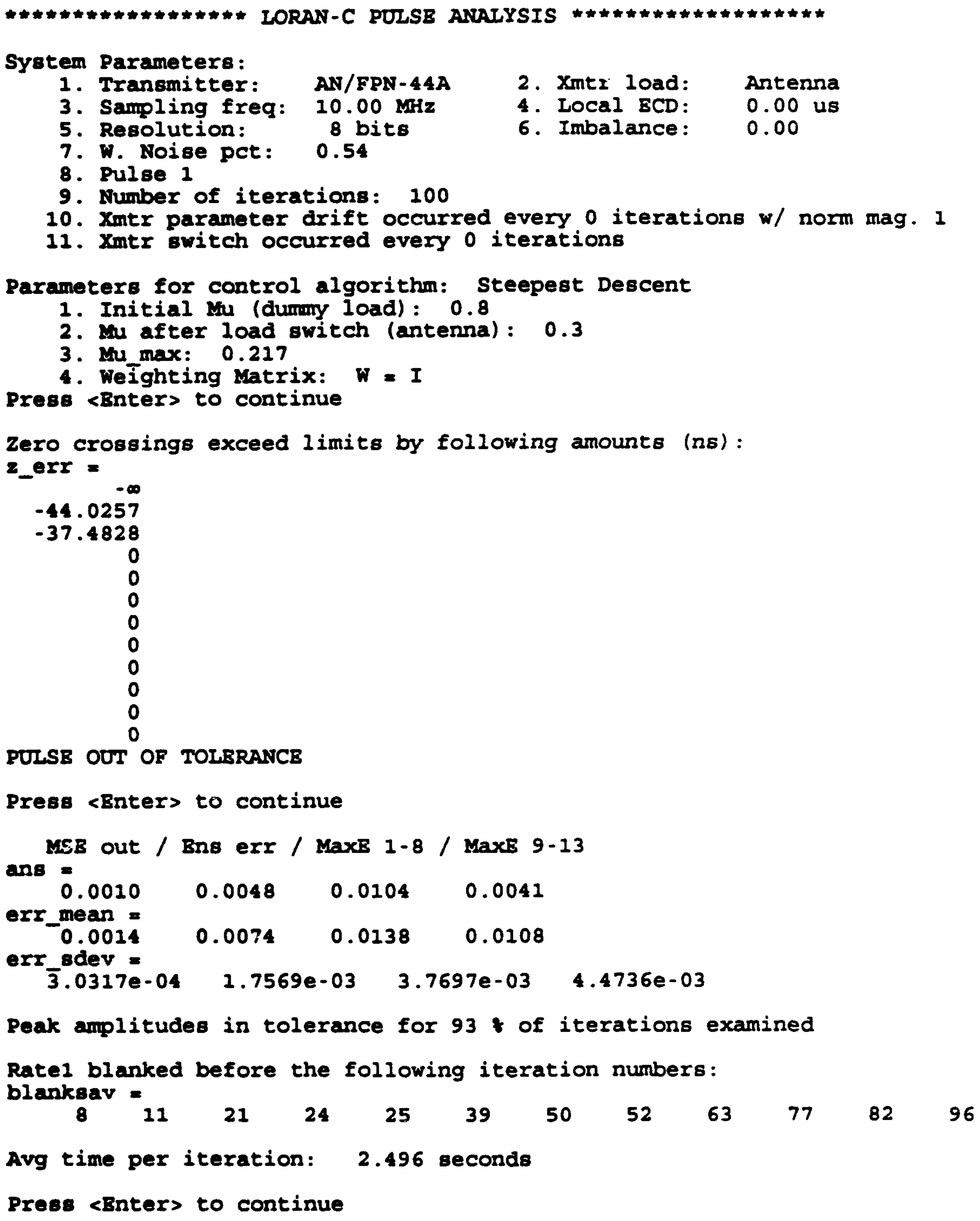

```
****************** LORAN-C PULSE ANALYSIS ******************

System Parameters:
    1. Transmitter:    AN/FPN-44A      2. Xmtr load:     Antenna
    3. Sampling freq:  10.00 MHz       4. Local ECD:     0.00 us
    5. Resolution:      8 bits         6. Imbalance:     0.00
    7. W. Noise pct:   0.54
    8. Pulse 1
    9. Number of iterations:  100
   10. Xmtr parameter drift occurred every 0 iterations w/ norm mag. 1
   11. Xmtr switch occurred every 0 iterations

Parameters for control algorithm:  Steepest Descent
    1. Initial Mu (dummy load):  0.8
    2. Mu after load switch (antenna):  0.3
    3. Mu_max:  0.217
    4. Weighting Matrix:  W = I
Press <Enter> to continue

Zero crossings exceed limits by following amounts (ns):
z_err =
        -∞
  -44.0257
  -37.4828
         0
         0
         0
         0
         0
         0
         0
         0
         0
PULSE OUT OF TOLERANCE

Press <Enter> to continue

   MSE out / Ens err / MaxE 1-8 / MaxE 9-13
ans =
    0.0010    0.0048    0.0104    0.0041
err_mean =
    0.0014    0.0074    0.0138    0.0108
err_sdev =
   3.0317e-04   1.7569e-03   3.7697e-03   4.4736e-03

Peak amplitudes in tolerance for 93 % of iterations examined

Ratel blanked before the following iteration numbers:
blanksav =
     8     11     21     24     25     39     50     52     63     77     82     96

Avg time per iteration:   2.496 seconds

Press <Enter> to continue
```

Figure 5.12h: Realistic simulation results, '44A, pulse analysis printout.

```
Normalized pulse peak values
    average, last iter, ideal, diff (1-3), diff (2-3)
ans =
    0.0280     0.0261     0.0157     0.0123     0.0104
   -0.0781    -0.0783    -0.0833     0.0053     0.0051
    0.1861     0.1913     0.1901    -0.0040     0.0012
   -0.3178    -0.3130    -0.3158    -0.0020     0.0028
    0.4458     0.4435     0.4454     0.0004    -0.0020
   -0.5639    -0.5652    -0.5696     0.0057     0.0044
    0.6761     0.6783     0.6813    -0.0052    -0.0031
   -0.7749    -0.7739    -0.7771     0.0022     0.0032
    0.8534     0.8522     0.8556    -0.0023    -0.0034
   -0.9099    -0.9130    -0.9164     0.0065     0.0033
    0.9533     0.9565     0.9598    -0.0065    -0.0033
   -0.9855    -0.9913    -0.9872     0.0017    -0.0041
    1.0000     1.0000     1.0000          0          0
   -0.9899    -0.9913    -1.0001     0.0101     0.0088
    0.9753     0.9739     0.9892    -0.0139    -0.0153
   -0.9763    -0.9826    -0.9692    -0.0071    -0.0134

SNR (tdw) = 56.76 dB
SNR (rf)  = 66.84 dB
```

Figure 5.12h (continued): Pulse analysis printout.

Table 5.3: CONTROLLING ECD (ALL VALUES IN μs, WITH 8-BIT RESOLUTION AND WHITE NOISE ADDED)

Transmitter	Desired ECD	Measured ECD of Avg. y	ECD Error
AN/FPN-42	–2.50	–2.32	0.18
	0	0.04	0.04
	2.50	2.20	–0.30
AN/FPN-44A	–2.50	–2.06	0.44
	0	0.01	0.01
	2.50	2.42	–0.08

100. The realistic settings of Table 5.2 were used here also, with $\mu_n = 0.7$. ECD values were measured by hand using the LOIS program, which accepts the first eight half-cycle amplitudes as its sole input arguments. The error converged to lower values for positive ECDs than for negative ECDs.

Because ECD was not computed for each iteration, the maximum ECD error and the variance of the ECD errors are not available. Therefore, the precise effects of noise and quantization error on ECD are not known.

4. Performance Improvement With Greater Bit Resolution

Table 5.4 presents the improved performance with the '42 that results from adding more quantization levels to the S_q-bit quantizer in the noise model of Fig. 5.4. A 600-iteration test was conducted as in Section B of this chapter, with the same test interval (iterations 101–600). Bit resolutions $S_q = 7$ and $S_q = 10$ were set manually using the keyboard. Resulution $S_q = 7$ represents a worst case for the VXIbus system, where the waveform's amplitude spans only half the vertical oscilloscope scale and uses only 128 of 256 quantization levels available. Resolution $S_q = 8$ represents the best case where all 256 levels are used. The actual performance of the system should lie in between these two, closer to $S_q = 8$.

Three measures of the algorithm's performance were selected for this comparison: the SNRs of both TDW and RF pulse, averaged over all iterations in the test interval; the percentage of iterations in which the pulse peaks are in tolerance; and the mean and standard deviation of the half-cycle amplitude error (ensemble tolerance). The maximum allowable value for this third measure is 0.01. The ensemble tolerance was chosen because it is usually exceeded first out of all of the pulse peak amplitude tolerances. The variance of the white noise remains the same, from Table 5.2.

Table 5.4: PERFORMANCE IMPROVEMENT WITH GREATER BIT RESOLUTION ('42 TRANSMITTER, WITH WHITE NOISE ADDED AND $\mu_n = 0.3$)

Bits	Average SNR		% of Iter. in Tol.	Half-Cycle Peak Ens. Error	
S_q	TDW	RF	(peaks)	Mean	Std. Dev.
7	54.0	59.9	79.8	0.0085	0.0036
8	54.2	62.1	78.3	0.0077	0.0037
10	54.2	63.3	87.1	0.0065	0.0039
12	54.2	63.4	86.3	0.0065	0.0034
16	54.2	63.4	81.9	0.0070	0.0037
∞*	54.2	63.4	81.2	0.0071	0.0040

* To machine precision.

Although the accuracy of this simulation where $S_q \neq 8$ is not supported by any data (to date, no oscilloscope for the VXIbus exists with more than eight bits), Table 5.4 shows a marginal improvement in all measures with $S_q = 10$, but the performance worsened for higher values of S_q. This is because quantizing into discrete levels removes completely the noise with amplitude less than one-half the bin width. Additional filtering is thus appropriate for all values of S_q. Similar results should be expected for the '44A.

5. Performance Improvement with Less Noise

Reducing the variance of the white noise allowed the steepest descent algorithm to keep the pulse peaks in tolerance consistently with the '42, while still using quantization with 8 bits. Using the same test procedure (used in Chapter IV and in the first part of this chapter) reducing μ_n from 0.7 to 0.3 did reduce the steady-state errors but did not increase the SNRs. The improved performance is apparent in Table 5.5.

TABLE 5.5: PERFORMANCE IMPROVEMENT WITH LESS NOISE (‘42 TRANSMITTER, WITH 8-BIT RESOLUTION AND $\mu_n = 0.3$)

RF Noise (%)	Average SNR		% of Iter. in Tol. (peaks)	Half-Cycle Peak Ens. Error	
	TDW	RF		Mean	Std. Dev.
0.39	54.1	62.1	78.3	0 .0077	0.0037
0.25	57.9	64.7	92.5	0.0060	0.0024
0.20	59.8	65.7	95.2	0.0056	0.0020
0.15	62.1	66.7	98.3	0.0053	0.0014
0.10	65.3	67.9	100	0.0049	0.0009

* To precision of machine

An acceptable solution may not necessarily require the pulse peaks to meet the criteria in the signal specification for 100 percent of control iterations. The minimum acceptable performance level and the method of reducing system noise are thus both subjects for further study. A similar performance improvement may be expected with the '44A.

6. Behavior Following a Transmitter Switch

The steepest descent algorithm converges to the same degree as above after switching to a different '42 transmitter of which it has no specific *a priori* knowledge. In Fig. 5.13, iterations 1-75 show the error convergence for a transmitter with realistic settings whose c_0 coefficients have been randomly displaced as discussed in Subsection D.2. of Chapter III. At iteration 76, the coefficients are changed again, simulating a switch to a different transmitter. The algorithm's quick response shows that it is versatile enough to use with transmitters at other Loran stations in the Coast Guard. Similar performance was seen with the '44A. Again, system noise prevents the error from converging any further.

7. Controlling the Entire PCI

The steepest descent algorithm also performed well in controlling an entire PCI in a realistic simulation with a 3.0 percent transmitter imbalance introduced as well. Here $\mu_n = 0.7$. The pulse-to-pulse ECD and amplitude tolerances from Chapter II, Subsection B.2.e. were easily met. The shortcomings of the control algorithm in dealing with noise appear also in pulses two and following, but the features of the program designed to control these pulses worked successfully. The program controlled ECD without ETA, compensated for droop without a separate droop correction circuit, and corrected phase code bounce without a separate phase code balance adjustment.

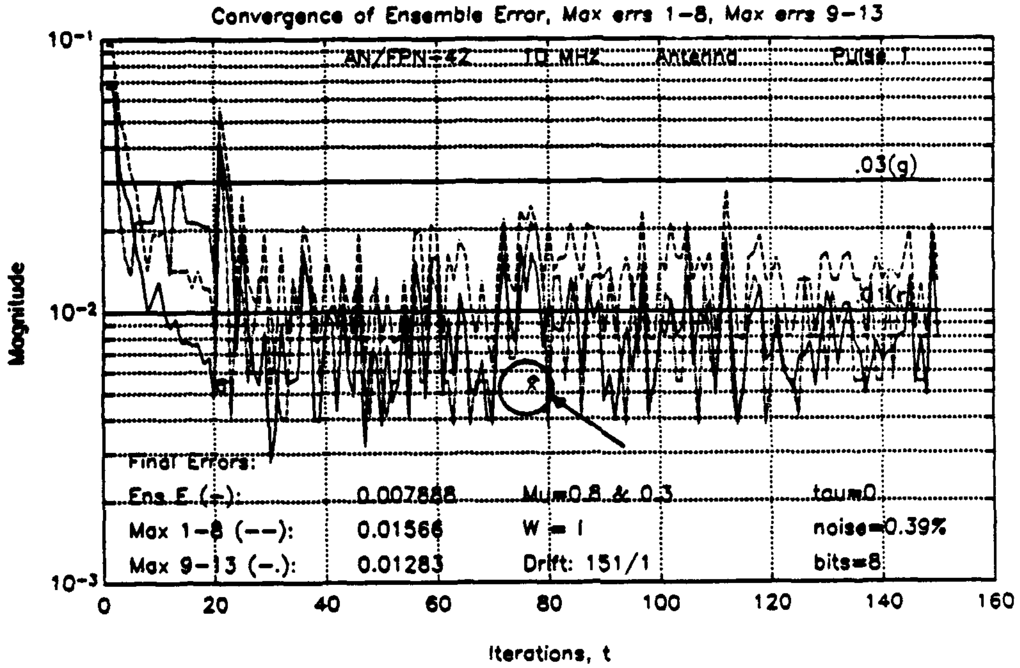

Figure 5.13: Algorithm performance after transmitter switch at iteration 76.

[THIS PAGE INTENTIONALLY LEFT BLANK]

VI. CONCLUSIONS

A. CONCLUSIONS

Modernizing the control systems for Loran-C vacuum-tube transmitters requires a control algorithm to shape the Loran pulse automatically, and in this thesis an algorithm was adapted for this purpose. In order to test the algorithm fully and to provide a tool for future study, a detailed simulation program for two classes of tube transmitters, the AN/FPN-42 and AN/FPN-44A, was developed. This program incorporates discrete-time IIR models of each transmitter.

Based on an initial assumption of LTI behavior at a given operating point, a linear difference equation with non-constant coefficients was chosen to represent the dynamics of the transmitters. Frequency-domain deconvolution, in conjunction with median smoothing, yielded an accurate estimate of the unit sample response at each operating point. Next, the least squares modified Yule-Walker method and Shank's method provided a non-minimum phase pole-zero model of each sequence. These models were catenated to represent the transmitter's nonlinearities, and time variations were added to form a combined model. The non-constant coefficients of the difference equation were defined as functions of time and the energy of the normalized TDW. The accuracy of this model was then demonstrated for both the '42 and the '44A transmitters.

Next, a linear feedback controller which uses the method of steepest descent to minimize the quadratic output error was derived, and its advantages and limitations were discussed. The algorithm successfully shaped the pulse with both the '42 and the '44A by bringing the pulse peaks into tolerance, although zero-crossing tolerances were exceeded in some cases. Then, the models and the control algorithm were incorporated into a simulation program. To this program were added the details of the Loran transmitter system which affect pulse shape. Finally, the algorithm was tested in a variety of transmitter system settings and behaviors. From these tests, four main conclusions can be made.

First, based on all the data available, the MATLAB simulation program and the nonlinear, time-varying models it contains accurately represent the behavior of the '42 and '44A transmitter systems over the range of operating points used. The assumption of LTI behavior at each operating point is a valid one, and the model reproduces it faithfully. The details of Loran operation added to the program make the simulation a realistic one. Therefore the results obtained are directly applicable to the VXIbus system.

Second, the steepest descent algorithm shapes the pulse effectively in realistic simulations of both the '42 and '44A transmitters, with two significant shortcomings: the zero-crossing tolerances are exceeded occasionally with the '42 and always with the '44A, and the algorithm is sensitive to system noise. This noise drives the pulse peaks out of tolerance frequently. Still, under these conditions, the algorithm kept the ECD of pulse one in tolerance and quickly produced an entire PCI which met the pulse group tolerances for amplitude and ECD, even when a transmitter imbalance was added. Further, the algorithm reshaped the pulse effectively after transmitter switches.

Neither of these two shortcomings necessarily disqualify the algorithm *even as presently implemented*, for two reasons. The first reason is that the ability to control zero-crossing times is not an absolute requirement for a pulse-shaping algorithm. The second reason is that the acceptable level of error for the VXIbus control strategy has not yet been defined. Of course, improvements in these two areas will make the algorithm even more useful. With respect to reducing noise, if the SNRs of the TDW and of the RF pulse can be improved by 10 dB and 5 dB, respectively ('42), the algorithm will keep the pulse peaks in tolerance continuously.

Third, power supply droop at dual-rated stations introduces only transient errors into the algorithm's convergence. This causes the controller no significant problem.

Fourth, a near-optimum TDW for the transmitter/antenna system can be obtained successfully off-line using the dummy load. In this way, when switching to the antenna, the newly designated operate transmitter comes on-line in tolerance or nearly in tolerance.

B. RECOMMENDATIONS FOR FURTHER STUDY

Further study is worthwhile in at least five areas. First, a reliable method to improve SNR for different bit resolutions will significantly increase the robustness and effectiveness of the steepest descent algorithm. Simple averaging, lowpass or bandpass filtering, and adaptive equalization are three possibilities. Second, other control algorithms may perform better than the steepest descent algorithm, particularly if they are more robust and can control zero-crossing times automatically. Incorporating adaptive algorithms such as the recursive least squares method or the Kalman filter may work well. Third, a more effective strategy for controlling an entire PCI can possibly be found. For example, a better order in which to control the pulses might be pulse 1 (GRI A), pulse 1 (GRI B), pulse 2 (GRI A), pulse 2 (GRI B), etc. Fourth, defining an acceptable level of error for the control process will be helpful. Keeping the pulse peaks in tolerance as defined by the seven tests in the signal specification for 100 percent of the control iterations may be neither practical nor desirable and may even be impossible. Perhaps an update to the signal specification may become appropriate. Finally, writing a MATLAB function to compute ECD for each iteration will provide statistical information on the effects of white noise and quantization error on ECD.

APPENDIX A

COMPUTATIONAL METHOD OF ESTIMATING ECD

(USCG Academy, New London, Connecticut)

The General Problem

The Loran-C antenna base current waveform can be expiessed as

$$x(t) = 0\ ; \qquad t < \tau\ ,$$

and

$$\begin{aligned} x(t) &= A\left\{\frac{(t-\tau)}{65}\exp\left[1-\frac{(t-\tau)}{65}\right]\right\}^2 \sin\omega_0 t \\ &= Ar(t)\ , \end{aligned}$$

where

t	is time in microseconds
τ	is time origin of envelope (ECD) in microseconds
A	is pulse envelope peak in amperes
ω_0	is angular carrier frequency, 0.2π rad/μ sec

The process of adjusting the TDW to establish an ECD and maintain some desired shape of the output pulse by visual comparison with a reference envelope (i.e., "pulse building") can be thought of as a curve fitting process.

The algorithm that is described accomplishes a MMSE fit that minimizes the squared difference between a set of eight half cycle amplitudes and some reference envelope of amplitude A and ECD τ. The process of visually matching these two data sets when expressed mathematically becomes a cost function, J. This squared error then becomes

$$J = \sum_{i=1}^{8} [s(i) - Ar(i)]^2 ,$$

where $r(i)$ is the model which is a function of ECD. When J is minimized, this constitutes a MMSE fit.

Minimization of the Cost Function, J

In order to minimize J we will use partial derivatives. For well behaved Loran-C pulses and quadratic cost function, there is only one global minimum, and no maxima. Therefore we will set

$$\frac{\partial J}{\partial \tau} = 0 ,$$

and

$$\frac{\partial J}{\partial A} = 0 .$$

Therefore,

$$J = \sum_{i=1}^{8} [s(i) - Ar(i)]^2 ,$$

which implies

$$\frac{\partial J}{\partial A} = \sum_{i=1}^{8} 2[s(i) - Ar(i)][-r(i)] = 0 ,$$

and

$$\frac{\partial J}{\partial \tau} = \sum_{i=1}^{8} 2[s(i) - Ar(i)] \left[-A \frac{r(i)}{\tau} \right] = 0 .$$

The solution for A is straightforward, yielding

$$A = \frac{\sum_{i=1}^{8} s(i) r(i)}{\sum_{i=1}^{8} r^2(i)} .$$

The solution for τ is a bit tougher!

Quadratic Approach

$$J = \sum_{i=1}^{8}[s(i) - Ar(i)]^2$$

is called a quadratic cost function since for linear differences of $[s(i) - Ar(i)]$, J is a second order polynomial. Although $[s(i) - Ar(i)]$ is not a linear difference function of ECD, it becomes approximately linear in the region of minimum J for small differences of ECD. This says

$$J - J_0 = K(\tau - \tau_0)^2 \ ,$$

where

$$J_0 = \text{minimum cost} \ ,$$

and

$$\tau_0 = \text{the associated ECD at that } J_0$$

Now let's choose three points for this function, separated by a common distance, δ. This says

$$\begin{aligned} (J_1 - J_0) &= K(\tau_N - \delta - \tau_0)^2 \ ; \qquad \tau = \tau_N - \delta \\ (J_2 - J_0) &= K(\tau_N - \tau_0)^2 \ ; \qquad \tau = \tau_N \\ (J_3 - J_0) &= K(\tau_N + \delta - \tau_0)^2 \ ; \qquad \tau = \tau_N + \delta \end{aligned}$$

Now we have three equations and three unknowns, so that the solutions are

$$\begin{aligned} K &= \frac{J_1 - 2J_2 + J_3}{2\delta^2} \\ \tau_0 &= \tau + \frac{\delta(J_1 - J_3)}{2(J_1 - 2J_2 + J_3)} \end{aligned}$$

and

$$J_0 = J_2 - K(\tau - \tau_0)^2 \ .$$

However, the τ_0 above does not provide an exact solution to the minimum of J. We'll need an iterative algorithm. This algorithm can be stated as follows:

$$\tau_{k+1} = \tau_k - \frac{\delta_k(J_3 - J_1)}{2(J_1 - 2J_2 + J_3)}$$

a) Let initial ECD = 0, $\delta_1 = 1$, compute J_1, J_2, J_3, τ_2

b) Let $\delta_2 = 0.1$, compute J_1, J_2, J_3, τ_3

c) Let $\delta_3 = 0.01$, compute J_1, J_2, J_3, τ_4

d) Let $\delta_3 = 0.001$, compute J_1, J_2, J_3, τ_5

τ_5 represents the best estimate in the MMSE sense for the ECD.

APPENDIX B

DATA COLLECTION AND FORMATTING

The enclosed MATLAB programs describe how data vectors were collected and formatted for this project. These programs format the original ASCII data vectors and store them as vectors in eight sets in binary MAT-file form. This allows the data to be loaded quickly and easily.

```
% SAV_DAT:  Corrects and formats Loran-C ASCII data files for use in
%   MATLAB & saves them in binary form in sets of manageable size.
%   In each set are several pairs of input and output vectors, labeled
%   xP and yP respectively, where P is the pair number, unique throughout
%   all the sets.  Each set is a single MAT file named datasetS.mat,
%   where S is the data set number.  The variables may be loaded one
%   set at a time or all at once using LORLOAD.
% Calls:  MAX_VOLTS

%   Data pairs available:
%
%     31 July 91:  5 pairs for the 42 xmtr with antenna simulator
%     06 Sept 91:  3 pairs for the 42 xmtr with antenna simulator
%                  3 pairs for the 42 xmtr with dummy load
%     28 Feb 92:   20 pairs for 42 xmtr w/ simulator
%                  20 pairs for 42 xmtr w/ dummy load
%                  (Note:  this data set is subdivided as follows:
%     22 May 92:   16 pairs: an entire GRI, compensated and uncompensated
%                     for droop (42 antenna simulator)
%     30 Jun 92:   19 pairs (20, but pair 80 is actually 2 inputs)
%                     for the '44A xmtr, with dummy load, antenna sim.
%                     & 625' monopole antenna (pairs 81-83 only are
%                        on antenna)

%   This program decimates each data vector to a desired sampling
%   frequency, using a lowpass filter to prevent aliasing.  The zero
%   level of each data vector, estimated by taking the mean of the
%   last 596 sample points, is subtracted so that any DC measurement
%   bias is removed.  Each data vector is normalized to 1 and then
%   then scaled up to the correct voltage.  Although the Loran-C output
%   current is customarily measured, in this engineering model the output
%   voltage is measured, using an infinite input impedance at the
%   oscilloscope.  This is not the same as the voltage read by the
%   Electronic Pulse Analyzer (EPA).  In cases of 6 Sept 91 and following,
%   the transmitter cathode current (TKI) was generally held at about 1.0
%   amp.  All '42 rf vectors were measured from the J6 jack.  The '42
%   rf vectors were measured from the J26 jack.  For the '44A dummy
%   load data a 20 db attenuator was used (model 42, ser # 173-56)
%   since the J26 jack is uncalibrated and unloaded.  If implemented
%   on the '44A this should really be buffered better.

% Dean C. Bruckner, 11/22/91    Rev. 9/4/92

clc;
disp(' Caution: running this program will clear the workspace.');
disp(' Press return to continue or ctrl-C to abort.');disp('');
pause
clear

N1=[1 2 4 8];
N1_indx=menu('Select Decimation factor','1','2','4','8');
N=N1(N1_indx);disp(['N = ',num2str(N),' selected'])
disp('Press <Enter> to continue or ctrl-C to abort'),pause
fs=10e6/N;len=4096/N;

pt=[1  6 12 22 32 42                    % Data pair numbers in each set
    5 11 21 31 41 51];
```

```
[xx,nsets]=size(pt);clear xx;

max_volts                               % Load max volts and dc bias
                                        %   from o-scope measurements

for s=1:nsets;
  S=num2str(s)
  x_str=' ';y_str=' ';
  n=1;                                  % Loop index
  for p=pt(1,s):pt(2,s)
    P=num2str(p)
    eval(['load plot',P,'a.dat; load plot',P,'b.dat;'])
    eval(['x=plot',P,'a(1:4096);'])
    x=x'-mean(x(3501:4096));
    eval(['y=plot',P,'b(1:4096);'])
    y=y'-mean(y(3501:4096));

    X=fft(x,8192);Y=fft(y,8192);        % Apply ideal LP filter
    startf=8192/(2*N)+1;endf=8192-startf+1;
    X(startf:endf)=[];Y(startf:endf)=[];
    x=real(ifft(X));y=real(ifft(Y));
    x(startf:2*(startf-1))=[];
    y(startf:2*(startf-1))=[];

    x=x/max(x)  *  (mv_in(n,s)-dc_in(n,s));
    y=y/max(y)  *  (mv_out(n,s)-dc_out(n,s));

    plot(x);pause(2);plot(y);pause(2);
    eval(['x',P,'=x;'])
    eval(['y',P,'=y;'])
    eval(['clear plot',P,'a plot',P,'b']);

    x_str=[x_str,' x',P];y_str=[y_str,' y',P];
    n=n+1;
  end

  if s==1;
    y4t=y4;                             % correct synch. error
    y4(1:48/N)=y4t(4096/N-48/N+1:4096/N);
    y4(48/N+1:4096/N)=y4t(1:4096/N-48/N);
    disp('y4 adjusted to correct synchronization error');disp('');
  end

  eval(['save dataset',S,'.mat ',x_str,y_str])
  disp(['dataset',S,'.mat:']);
  disp([x_str]);disp([y_str]);

end

% Droop data set for '42 (set 7) & '44 data (set 8)
pt=[52 68
    67 87];
[xx,nsets]=size(pt);clear xx;

for s=1:nsets;

  num_pairs=pt(2,s)-pt(1,s)+1;
  if s==1
    x_scale=4*.2*ones(1,num_pairs);         % .2V/div (.8V 0-pk)
    y_scale=4* 5*ones(1,num_pairs);         %  5V/div (20V 0-pk)
  elseif s==2                       % Here use these to invert also
    x_scale=4*[.5*ones(1,8) 1 1 2 2  127/2  -.5 .5 -1  .5*ones(1,4)];
    y_scale=4*[-2*ones(1,12)         127/2    2 -2  2  -2*ones(1,4)];
  end

  S=num2str(s+6)
  x_str=' ';y_str=' ';
  n=1;                                  % Loop index
  for p=pt(1,s):pt(2,s)

    P=num2str(p)
    eval(['load plot',P,'a.dat; load plot',P,'b.dat;'])
    eval(['x=plot',P,'a(1:4096);'])
    x=x'-mean(x(3501:4096));
    eval(['y=plot',P,'b(1:4096);'])
    y=y'-mean(y(3501:4096));
    mx=max(x);my=max(y);                % Save to restore orig. scaling.

    X=fft(x,8192);Y=fft(y,8192);        % Apply ideal LP filter
    startf=8192/(2*N)+1;endf=8192-startf+1;
    X(startf:endf)=[];Y(startf:endf)=[];
    x=real(ifft(X));y=real(ifft(Y));
    x(startf:2*(startf-1))=[];
    y(startf:2*(startf-1))=[];

    x=x/max(x)*mx/127*x_scale(n);       % Scaled differently than
    y=y/max(y)*my/127*y_scale(n);       %   sets 1-6. 8-bit resolution
                                        %   used in Lecroix o-scope
    if s==1
      if any(find(p==[55 57 67]))
        y=y;
      else
        y= -y;                          % Correct invertion introduced
                                        %   at J6 jack (except for
                                        %   incorrectly sampled vectors,
                                        %   where correction would make
                                        %   phase code incorrect again).
      end
      if any(find(p==65))               % Correct incorrectly sampled
        x= -x;                          %   input data vector (i.e.,
      end                               %   pos phase GRI captured
    end                                 %   instead of negative)

    plot(x);text(.15,.16,P,'sc'),pause;
    plot(y);text(.15,.16,P,'sc'),pause;
    eval(['x',P,'=x;'])
    eval(['y',P,'=y;'])
    eval(['clear plot',P,'a plot',P,'b']);

    x_str=[x_str,' x',P];y_str=[y_str,' y',P];
    n=n+1;
  end

  eval(['save dataset',S,'.mat ',x_str,y_str])
  disp(['dataset',S,'.mat:']);
  disp([x_str]);disp([y_str]);

end
```

```
% MAX_VOLTS:  Measurements from oscilloscope plots for AN/FPN-42
%    Loran-C transmitter.  Each value if the max positive value
%    in volts.  Called from SAV_DAT.  Data sets 7 and 8 were
%    formatted more directly and easily by just using the o-scope scale
%    instead of reading the plots.  But since these were done already
%    they stayed as is.

mv_in=zeros(10,nsets);                      % Max volts of input vectors
mv_out=zeros(10,nsets);                     % Max volts of output vectors
dc_in=zeros(10,nsets);
dc_out=zeros(10,nsets);

mv_in(1:5,1)=     [.72 .74 .28 .28 .48]';     %    (from o-scope plots)
mv_out(1:5,1)=    [17.2 16.2 3.3 1.62 17.2]';
mv_in(1:6,2)=     [.82 .8 .93 .9 .52 .51]';
mv_out(1:6,2)=    [24.5 8.2 27 10 3.0 1.2]';
mv_in(:,3)=      2*[2 .85 .6 .55 .5 .9 3.3 2.3 1.8 1.35]';
mv_out(:,3)= -2*10*[1.55 1.45 1.15 1 .83 .5 .26 .22 .2 .27]';
mv_in(:,4)=      2*[4 4 2.75 .86 .75 .63 .46 .3 .32 .4]';
mv_out(:,4)= -2*10*[1.4 1.37 1.5 1.37 1.29 1.2 .68 -1.3 -1.39 -1.65]';
mv_in(:,5)=      2*[2.4 1.05 .69 .61 .49 1.9 3.75 2.6 1.1 1.09]';
mv_out(:,5)= -2*10*[.49 .47 .39 .265 .22 .46 .14 .12 .135 .141]';
mv_in(:,6)=      2*[3.65 3.95 3.79 1.25 .9 .8 .79 .305 .36 .54]';
mv_out(:,6)= -2*10*[.2 .46 .47 .46 .43 .38 .39 -.4 -.44 -.53]';

% Corrections:
%   -            Outputs accidentally inverted
%   2            Correcting for differences in o-scope input impedance
%                   settings (50 ohm evenly divided voltage with the
%                      load and so its amplitude was only half of those
%                      taken with infinite input impedance.  Thus they need

%                      to be doubled.
%   10           A 10X probe was apparently left out of these meas.

dc_in(1,1)=        .01;          % DC voltage bias in measurements,
dc_out(1:5,1)=    [.1 0 .05 .02 0]';       % from plots
dc_out(1:6,2)=    [.5 .2 .2 .2 .05 0]';
dc_in(:,3)=    .01*[3 zeros(1,8) -1]';
dc_out(:,3)=   .01*[3 zeros(1,5) .5 0 0 0]';
dc_in(:,4)=    .01*[zeros(1,5) .5 0 1 1 1]';
dc_out(:,4)=   .01*[zeros(1,7) 1 2 2]';
dc_in(:,5)=    .01*[3 2 1 1 1 5 5 5 5 2]';
dc_out(:,5)=   .01*[0 0 1 1 1.5 1 .5 .5 .5 .5]';
dc_in(:,6)=    .01*[10 5 5 3 3 3 3 1 1 1]';
dc_out(:,6)=   .01*[.5 1 1 1 1 1 1 2 1 1]';
```

[THIS PAGE INTENTIONALLY LEFT BLANK]

APPENDIX C

FITTED CURVES FOR CATENATED MODELS

This appendix contains fitted curves of magnitude and phase for the catenated models, as follows. For values of E_n outside the endpoints of the curve, the function simply assigns the value of the curve at the nearest endpoint. In the titles "A" indicates the antenna and "D" the dummy load.

Transmitter	Description	Page
AN/FPN-42*	19-point curves for combined model, antenna simulator (4 poles, 3 zeros)	148
AN/FPN-42*	13-point curves for combined model, dummy load (2 poles, 1 zero)	152
AN/FPN-44A*	15-point curves for combined model, antenna simulator (6 poles, 5 zeros)	154
AN/FPN-44A*	4-point curves for combined model, dummy load (4 poles, 3 zeros)	160
AN/FPN-42	5-point curves for first catenated model, antenna simulator only (4 poles, 3 zeros)	164

* 4-part set of curves used in computer simulation program for $N = 1$.

CPLX POLE PAIR 1, '42 (A, N=1)

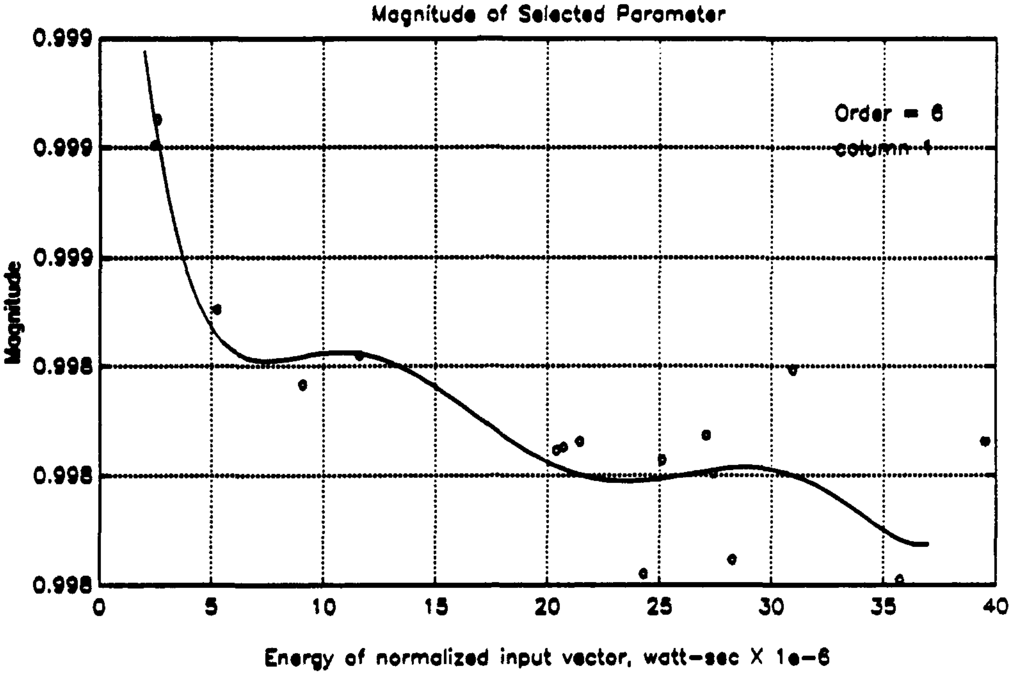

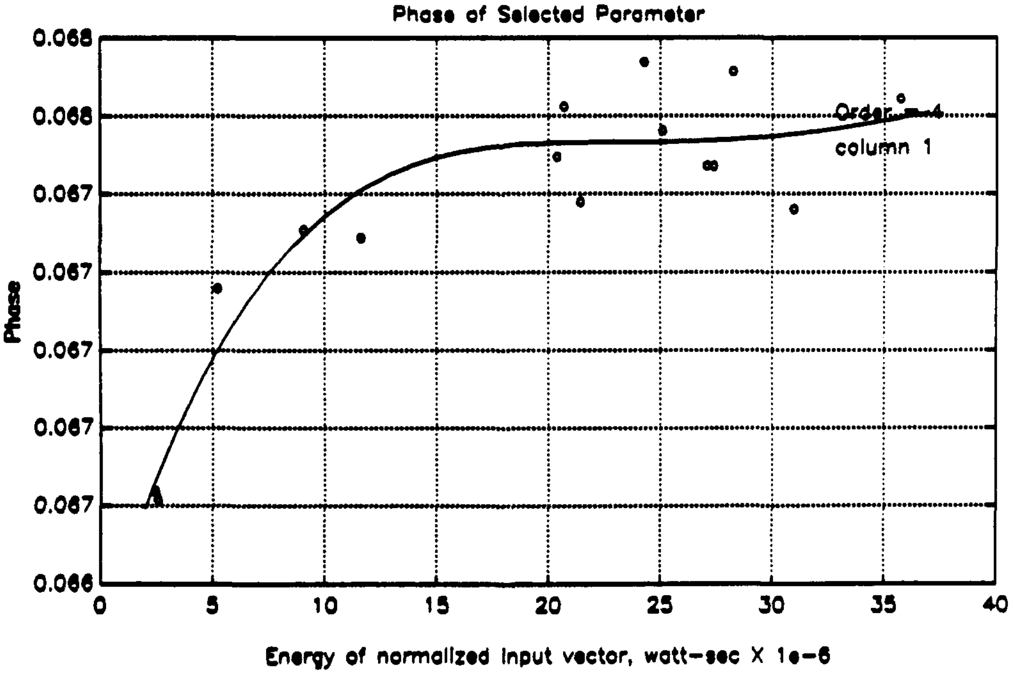

CPLX POLE PAIR 2, '42 (A, N=1)

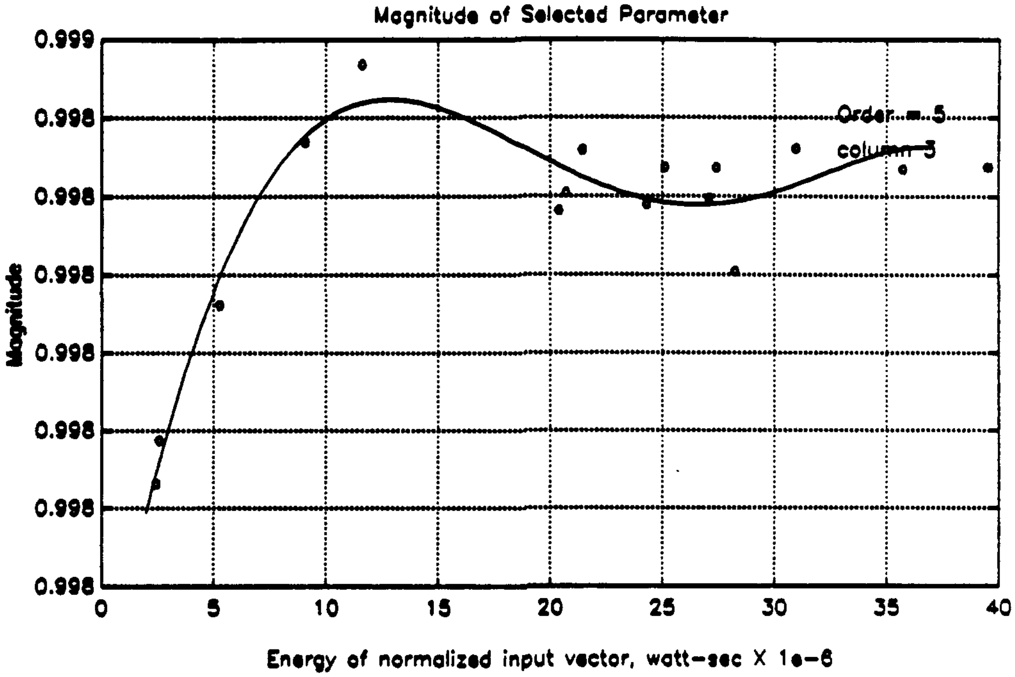

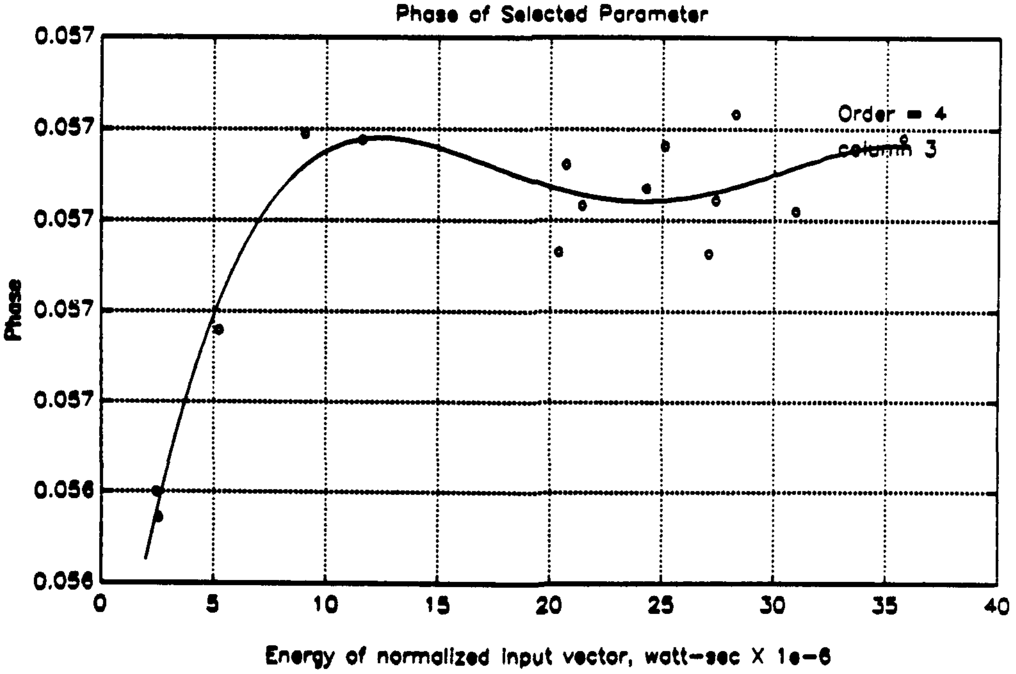

CPLX ZERO PAIR, '42 (A, N=1)

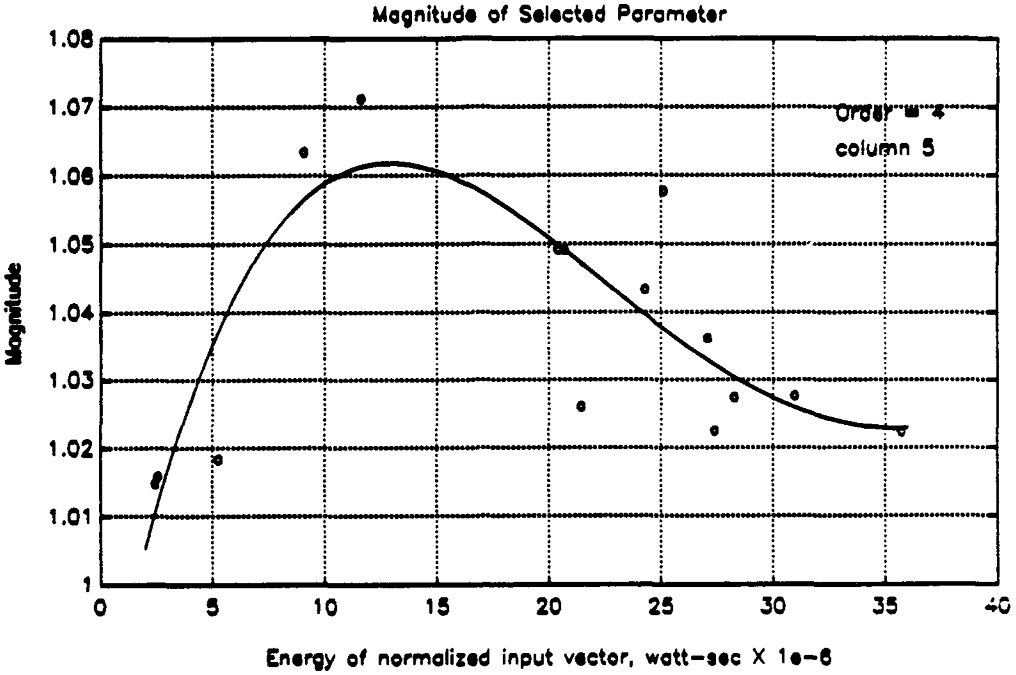

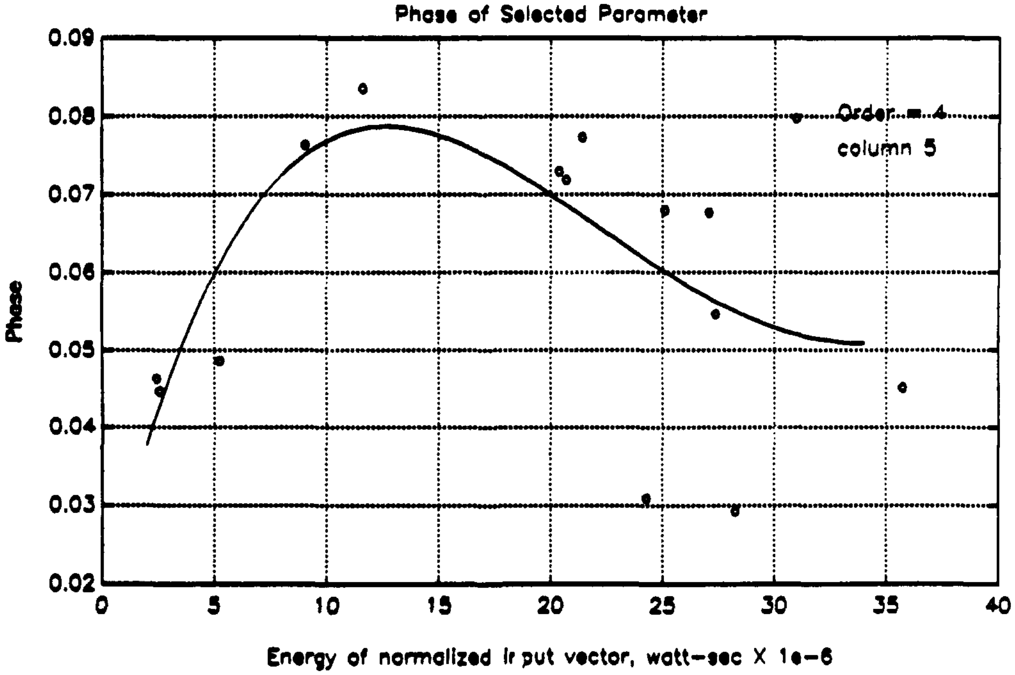

REAL ZERO, '42 (A, N=1)

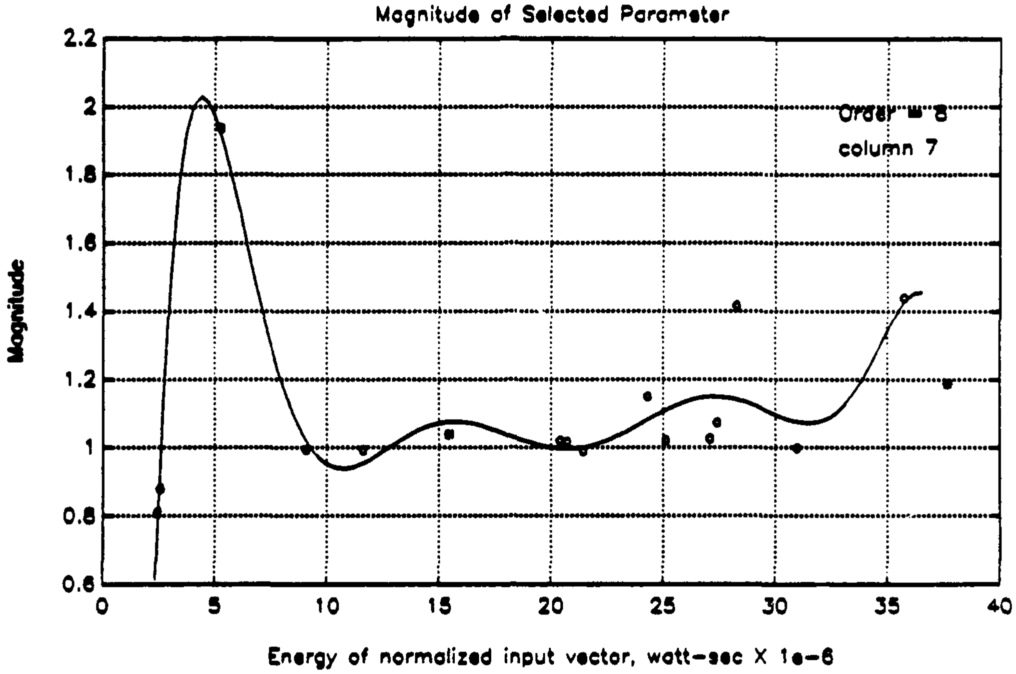

CPLX POLE PAIR, '42 (D, N=1)

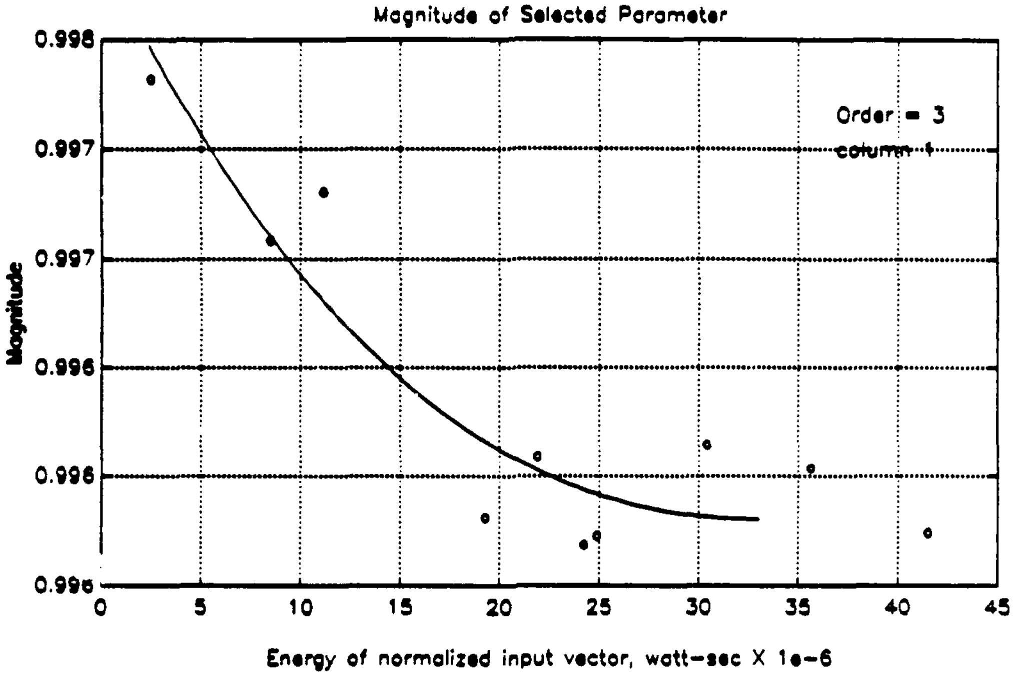

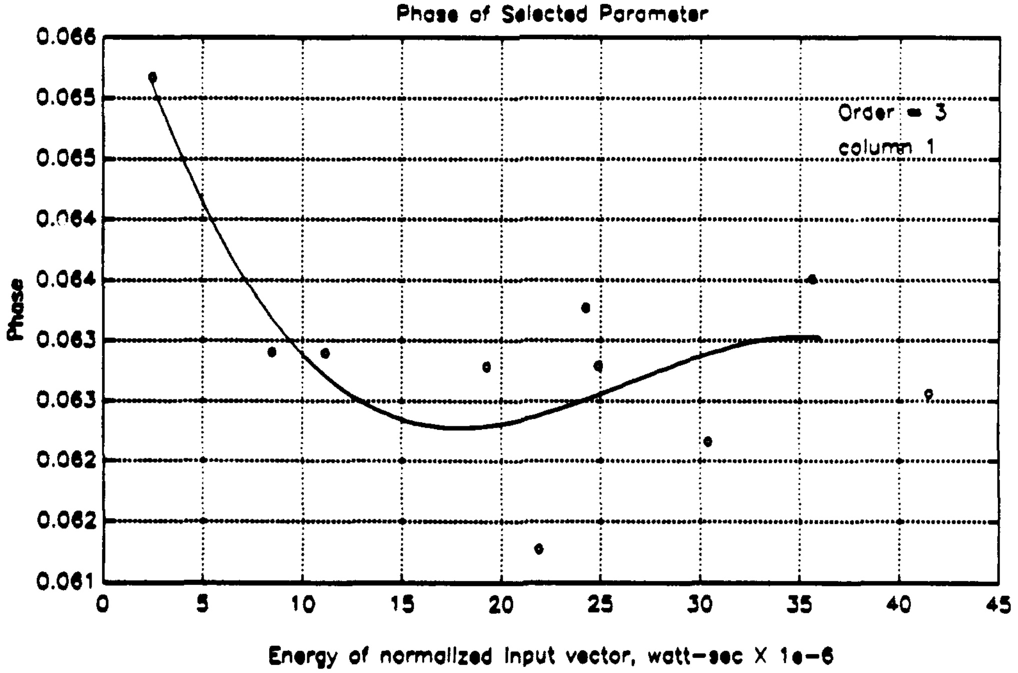

REAL ZERO, '42 (D, N=1)

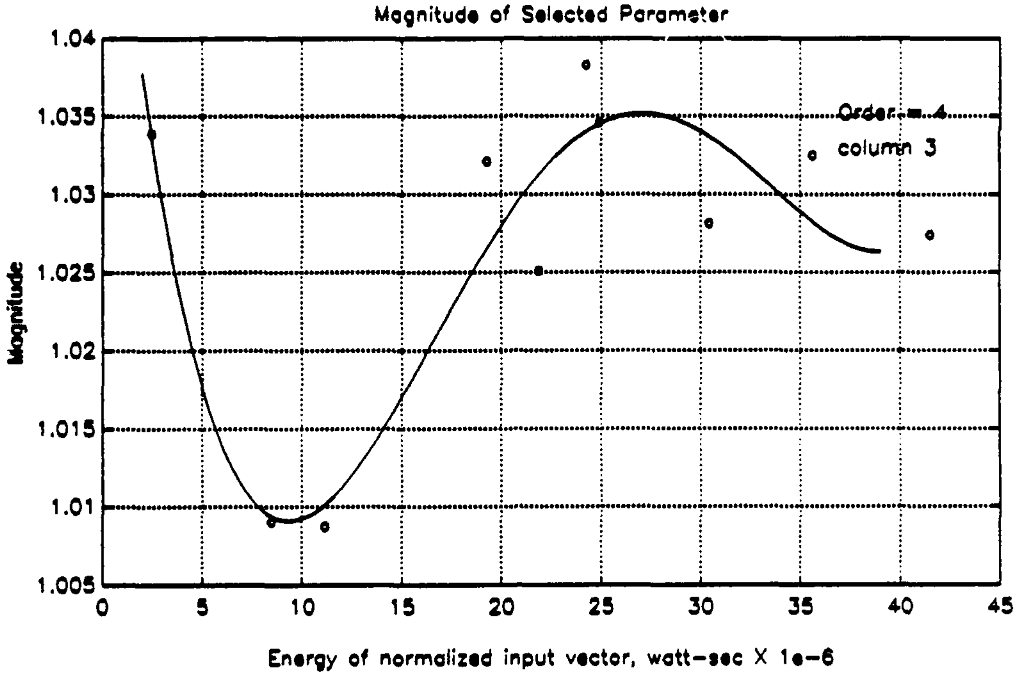

CPLX POLE PAIR 1, '44A (A, N=1)

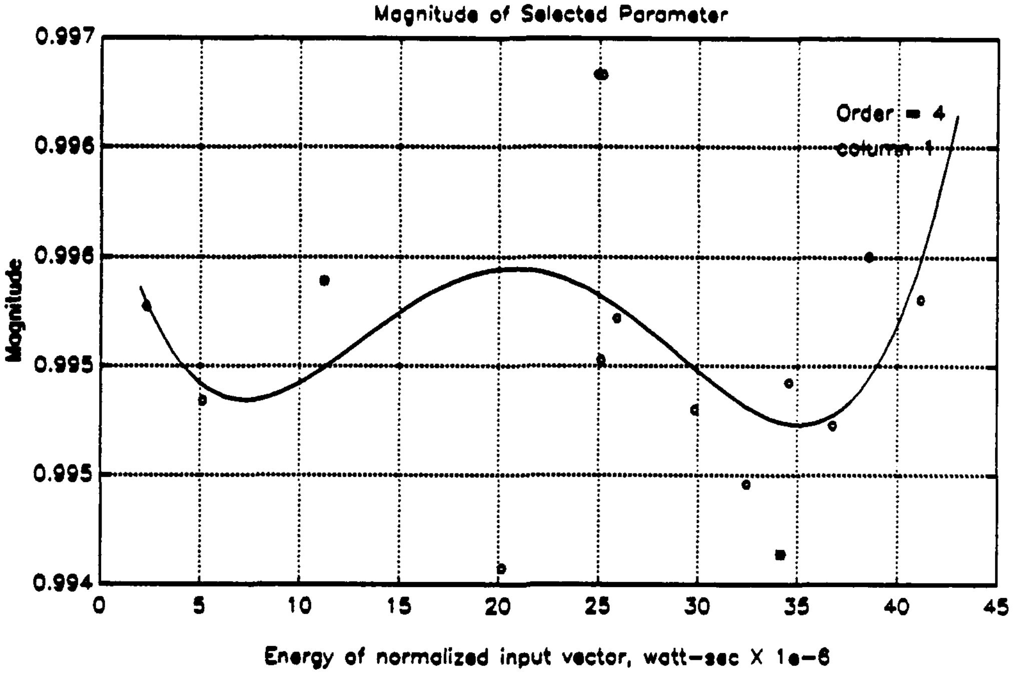

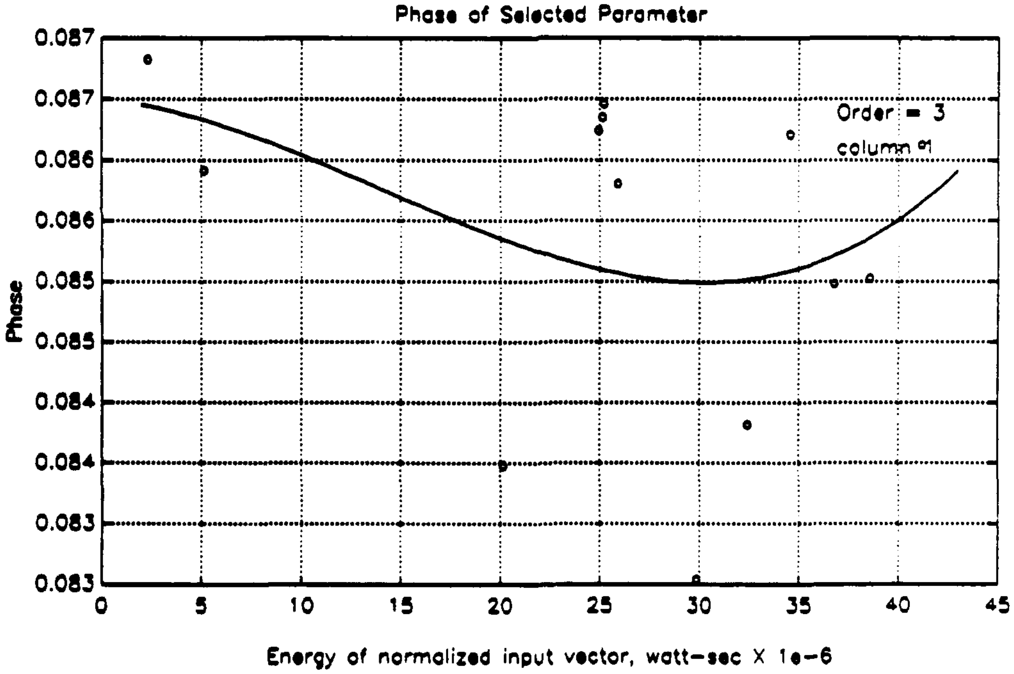

CPLX POLE PAIR 2, '44A (A, N=1)

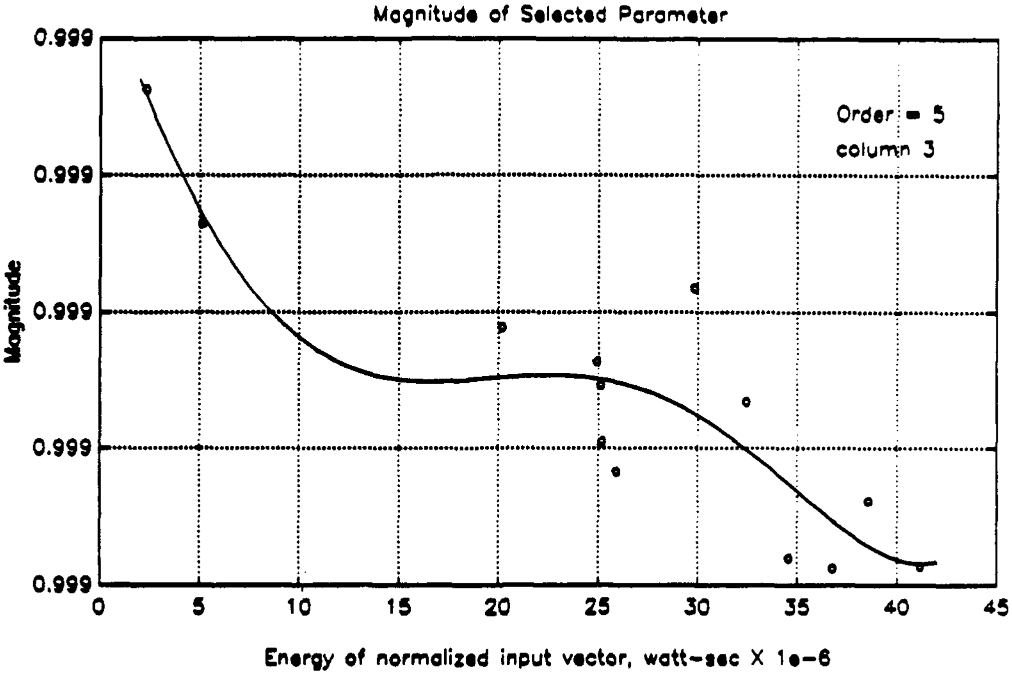

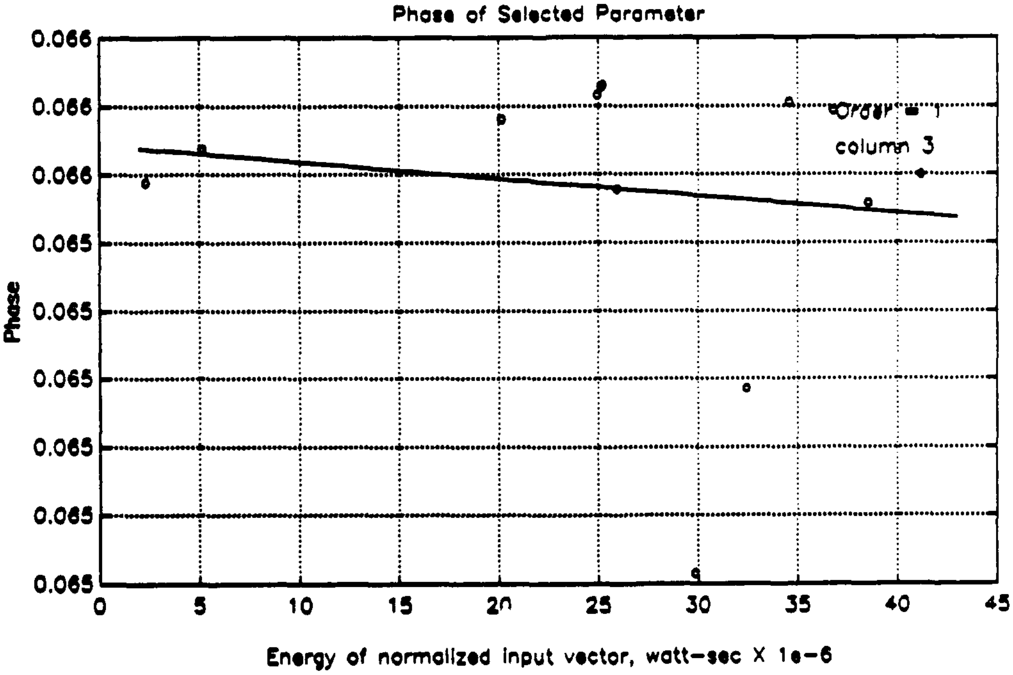

CPLX POLE PAIR 3, '44A (A, N=1)

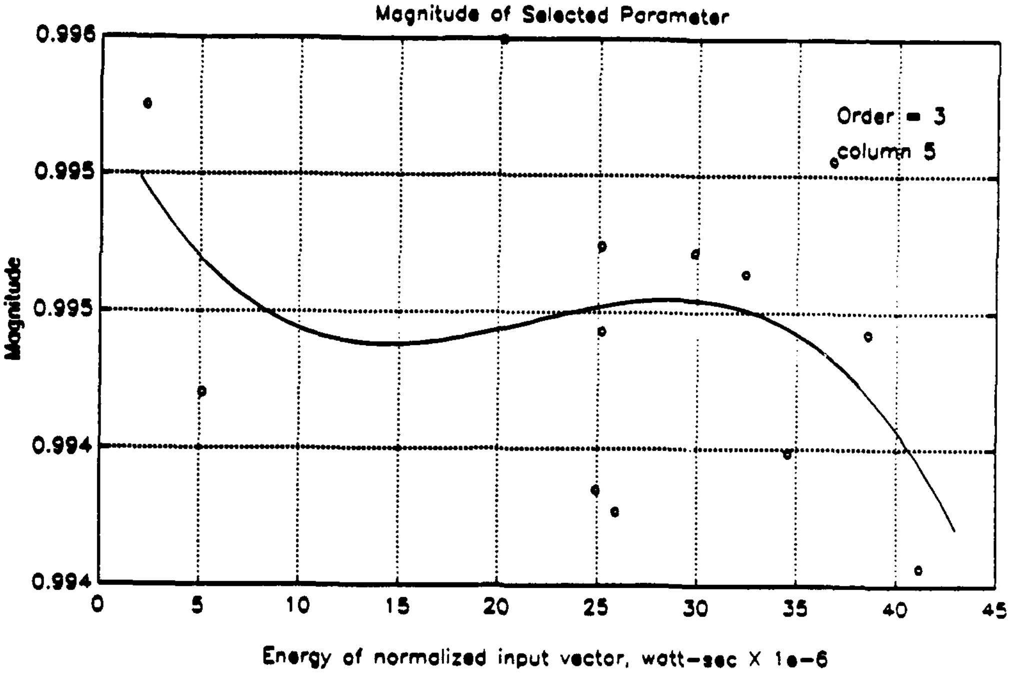

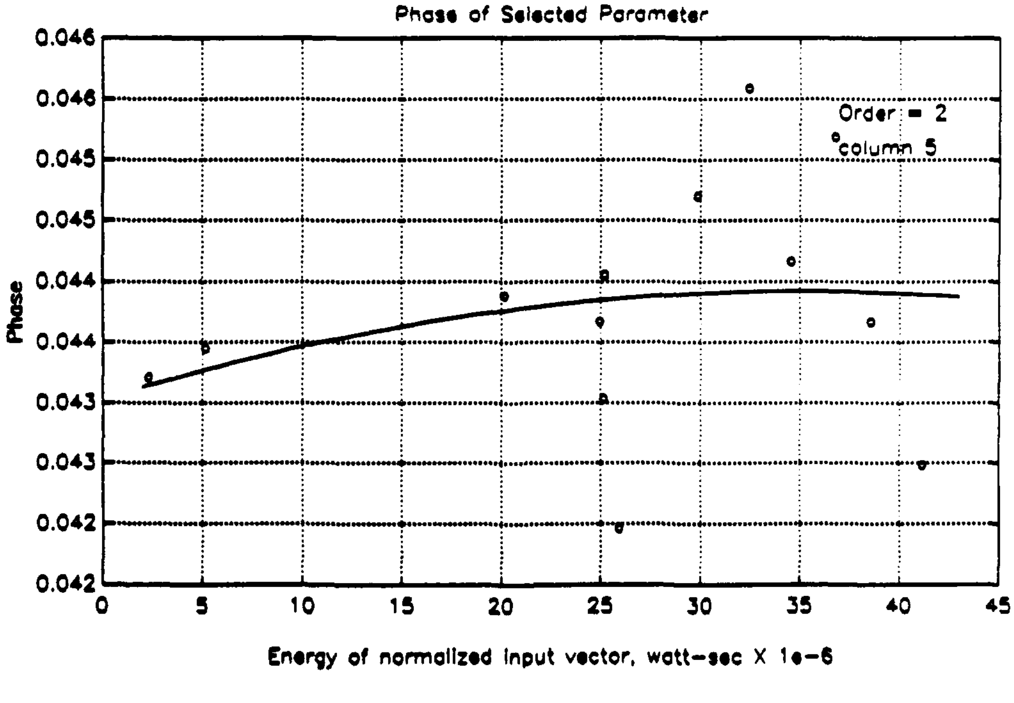

CPLX ZERO PAIR 1, '44A (A, N=1)

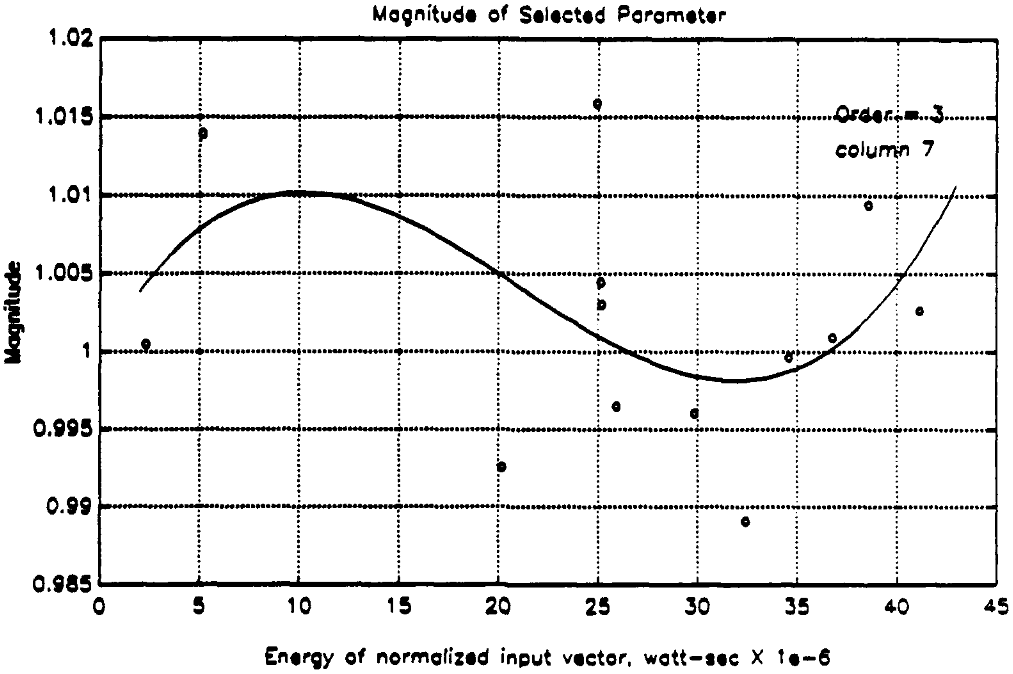

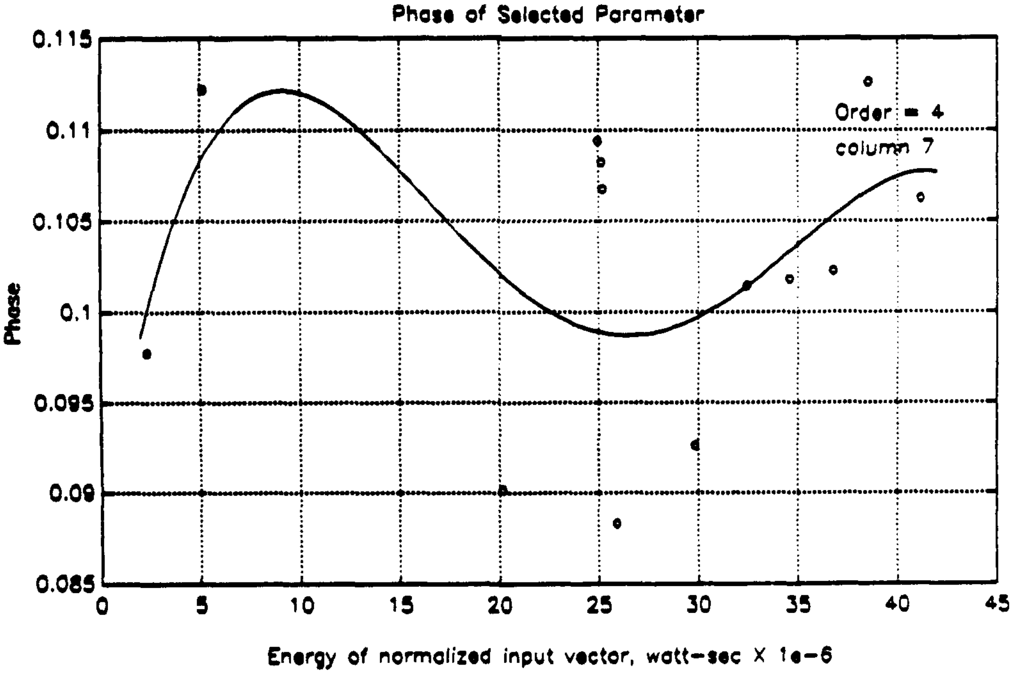

CPLX ZERO PAIR 2, '44A (A, N=1)

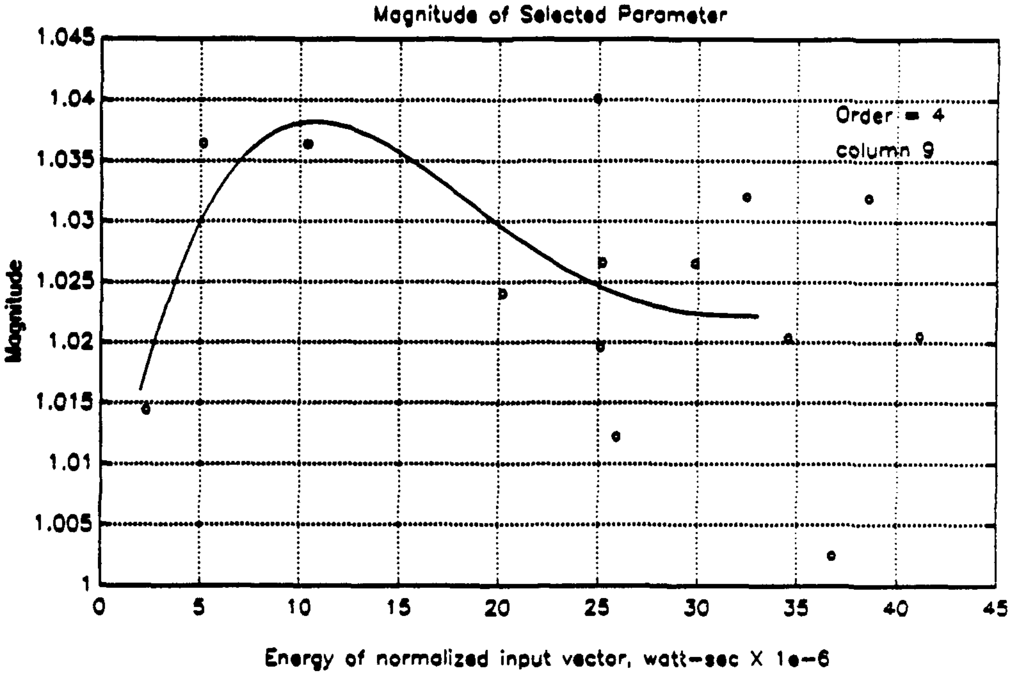

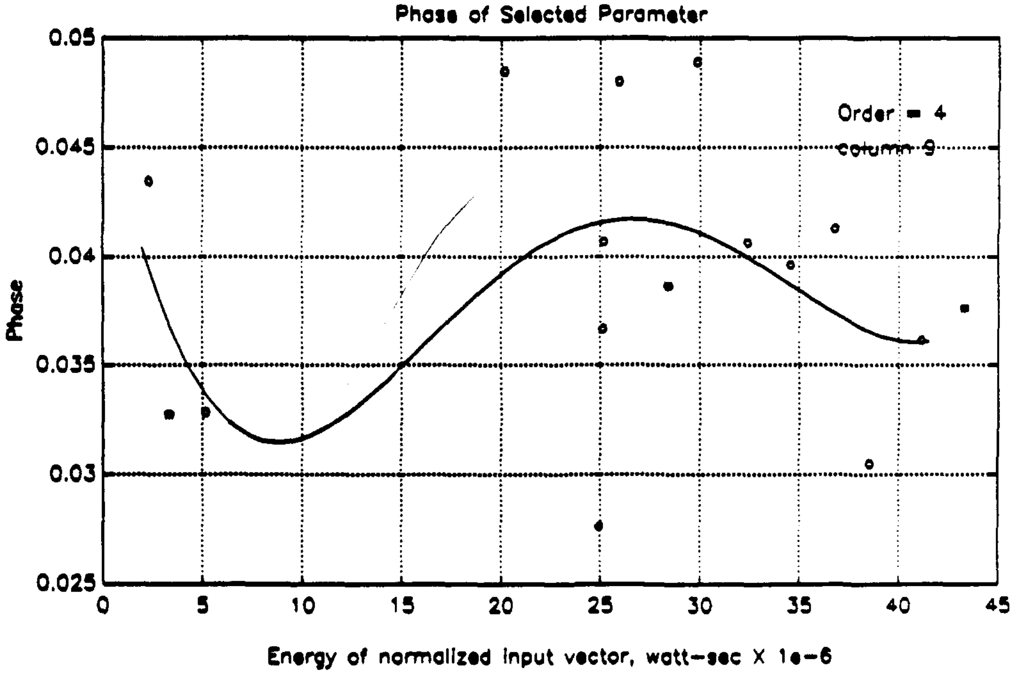

REAL ZERO, '44A (A, N=1)

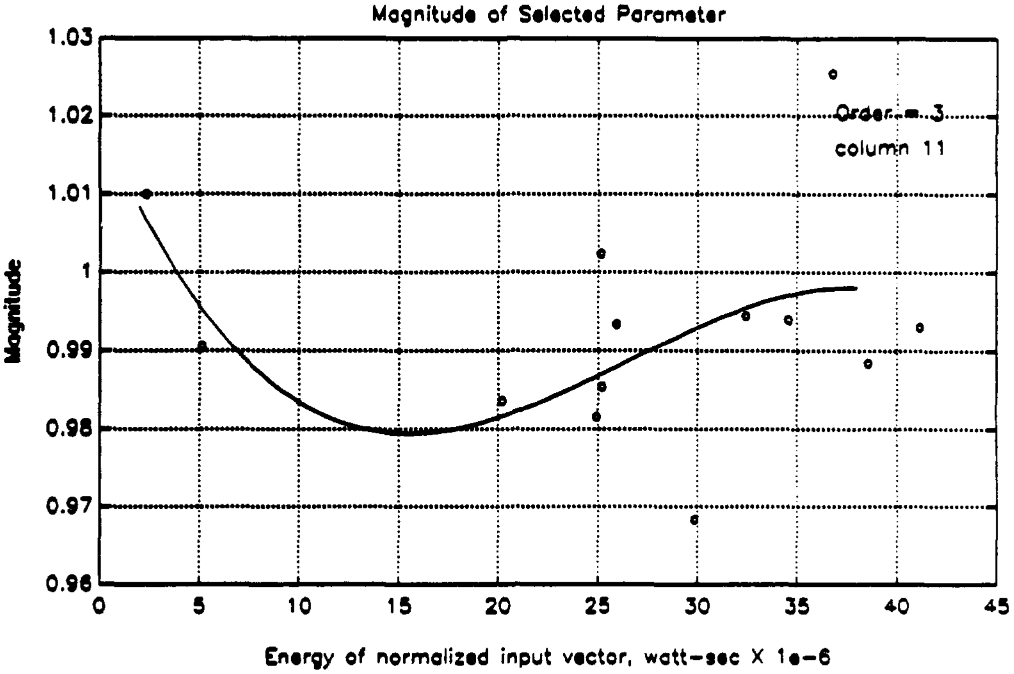

CPLX POLE PAIR 1, '44A (D, N=1)

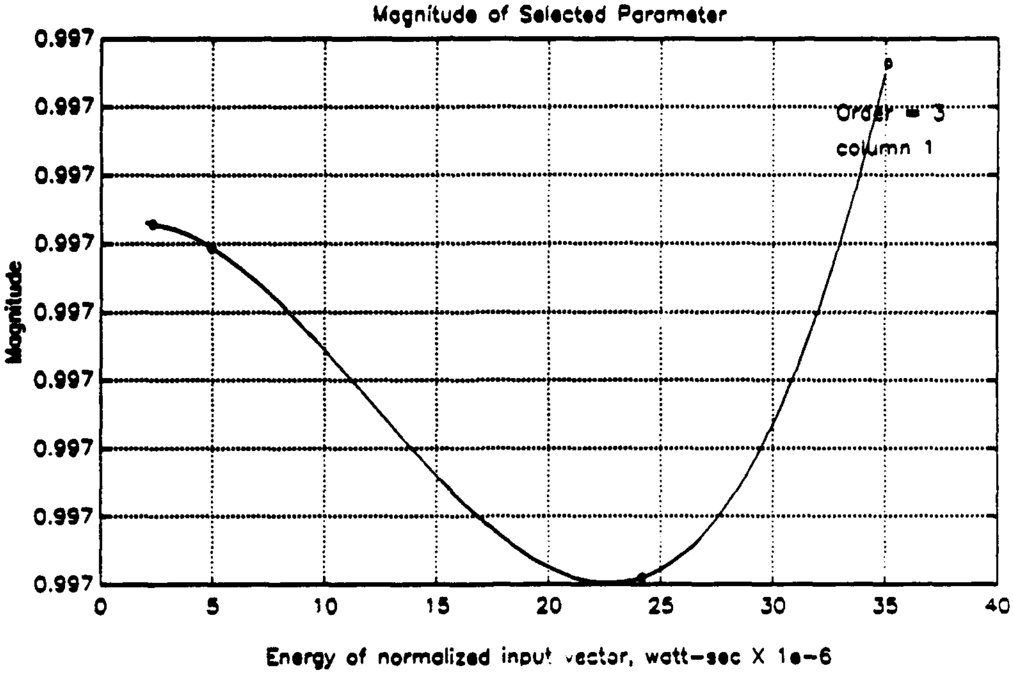

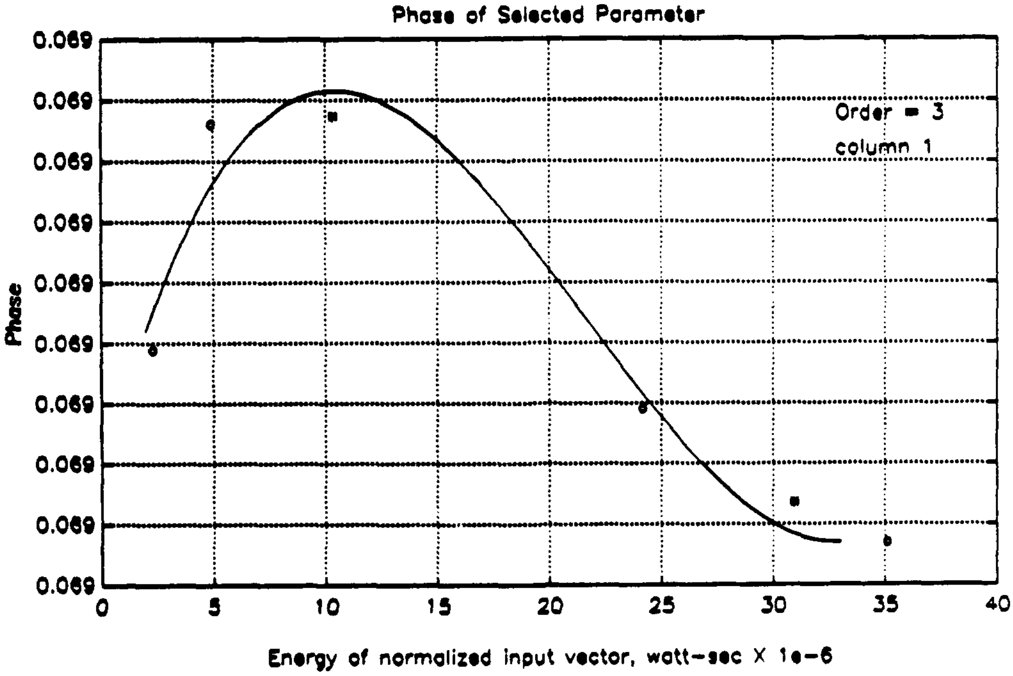

CPLX POLE PAIR 2, '44A (D, N=1)

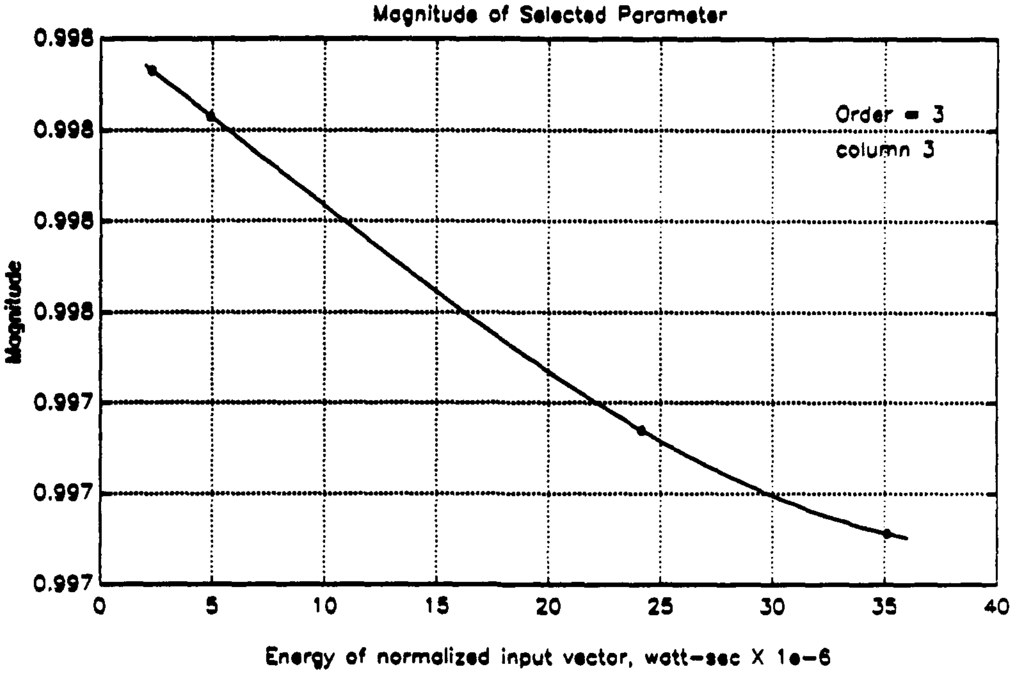

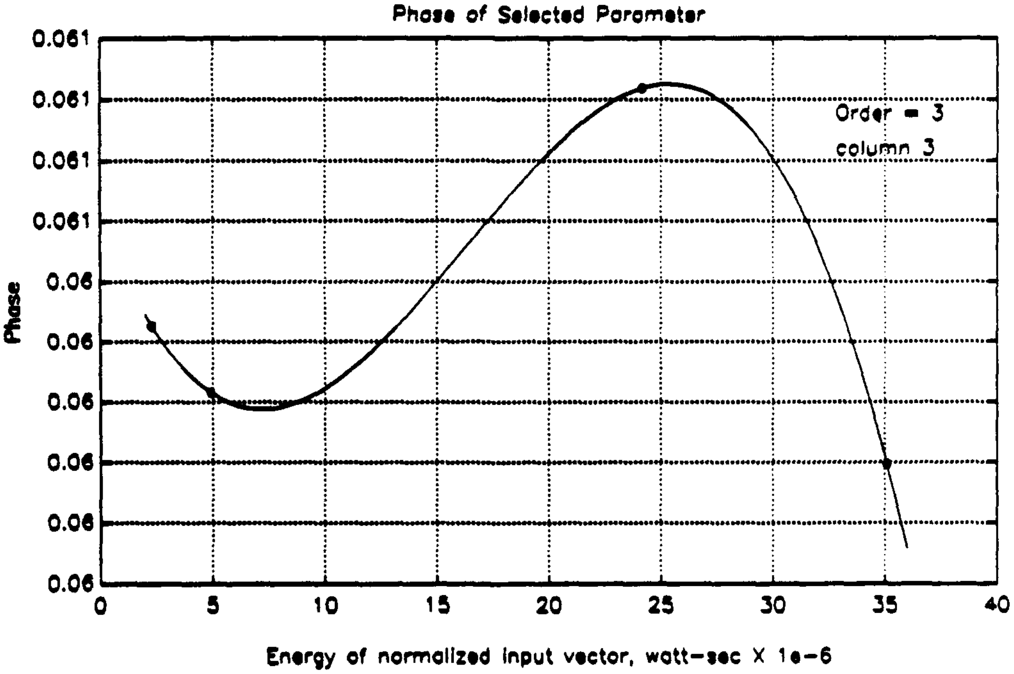

CPLX ZERO PAIR 1, '44A (D, N=1)

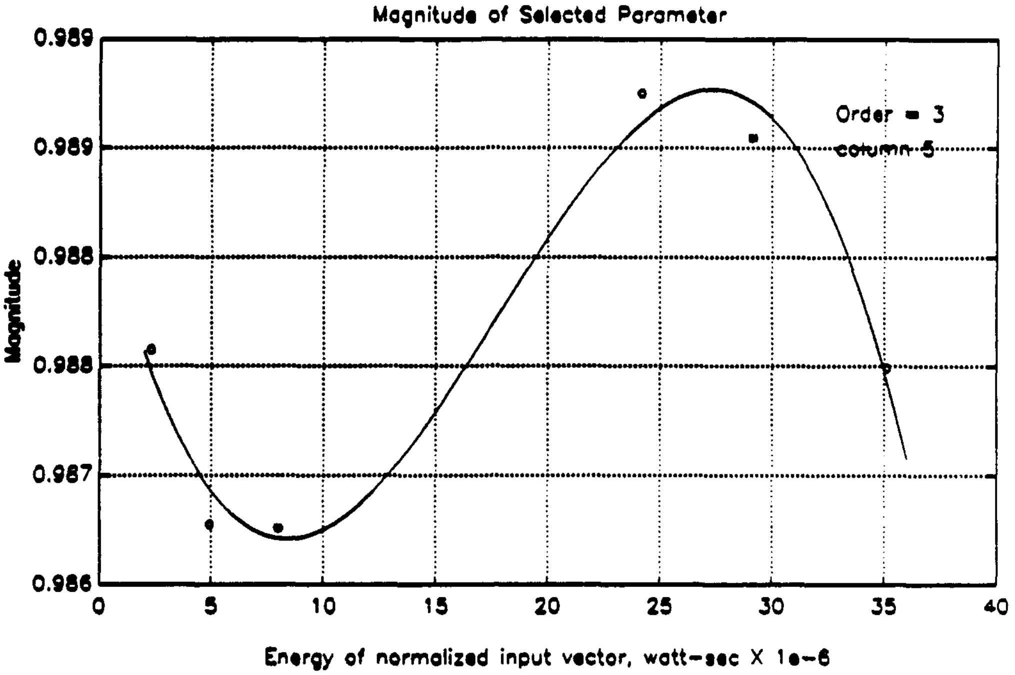

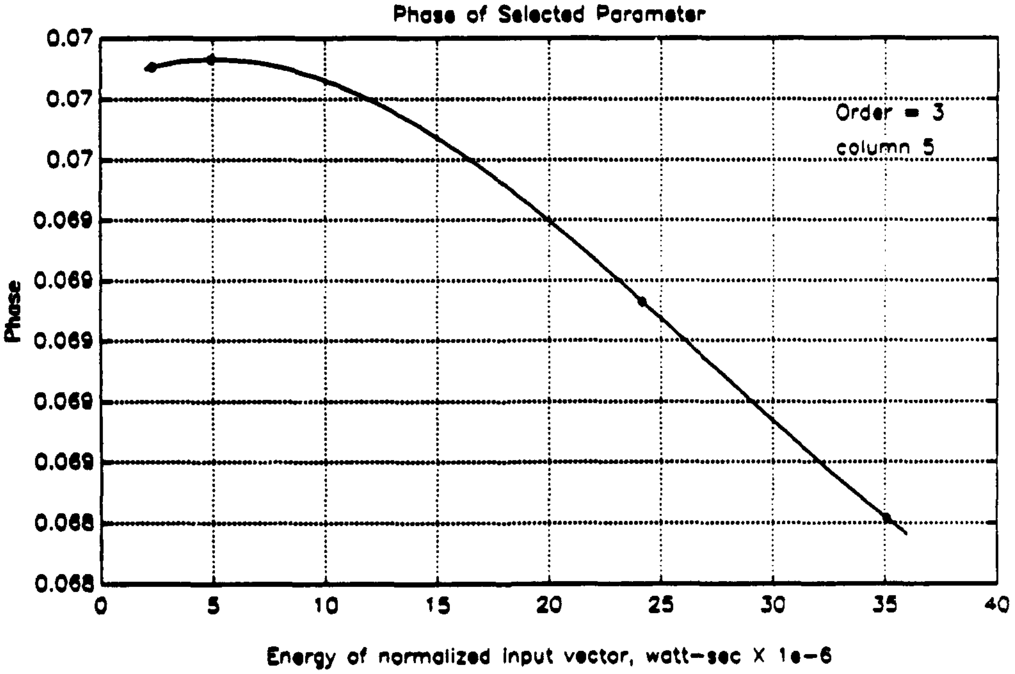

REAL ZERO, '44A (D, N=1)

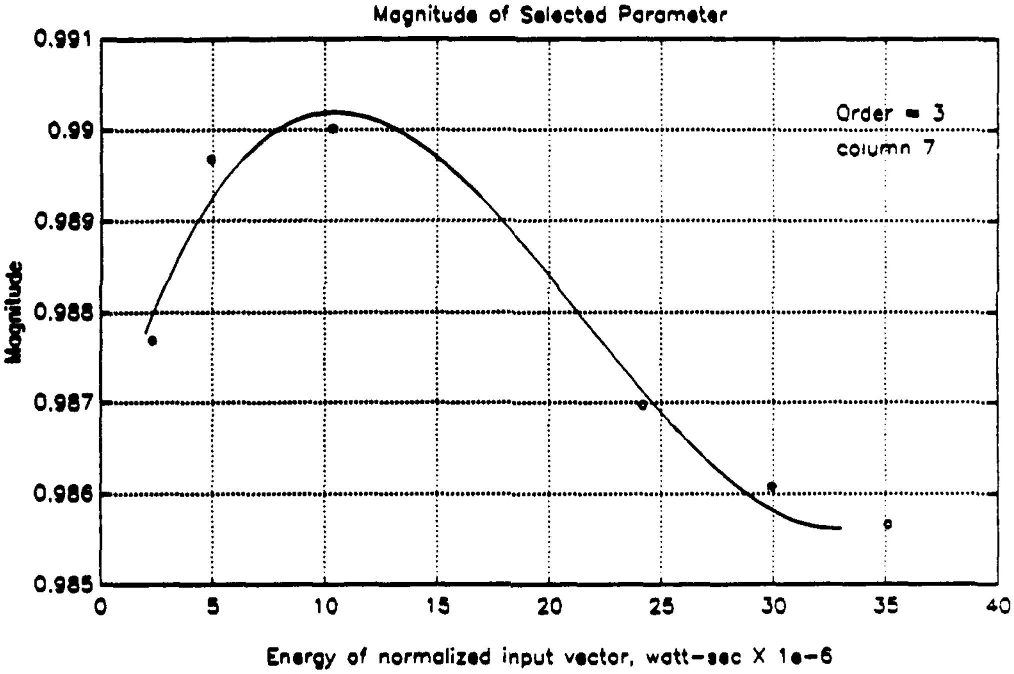

CPLX POLE PAIR 1, '42 (A, N=1, 5 PAIRS)

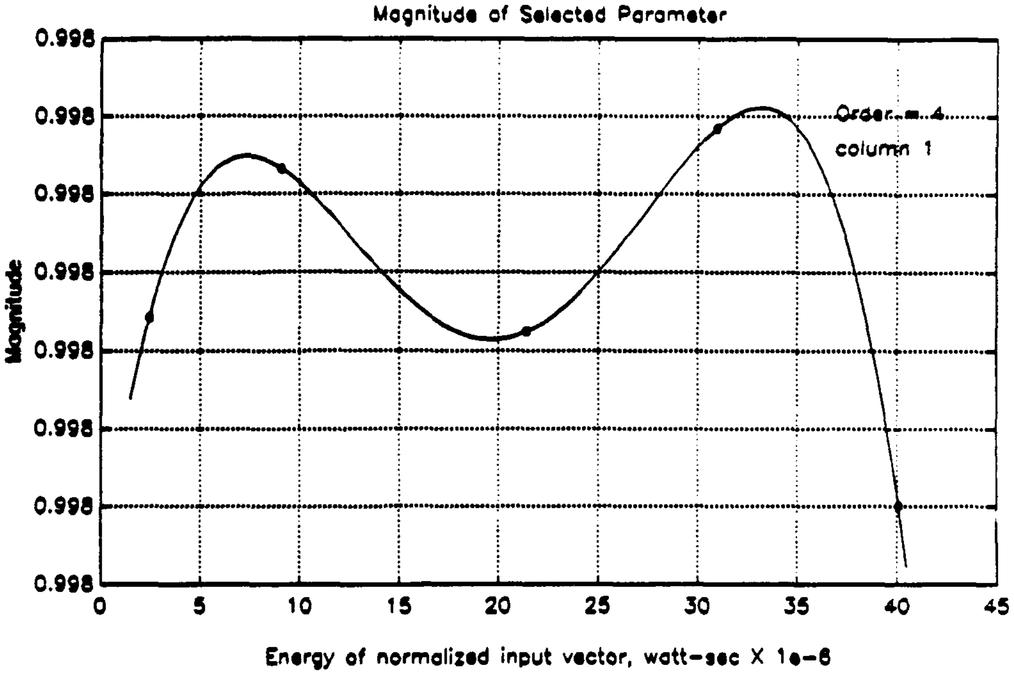

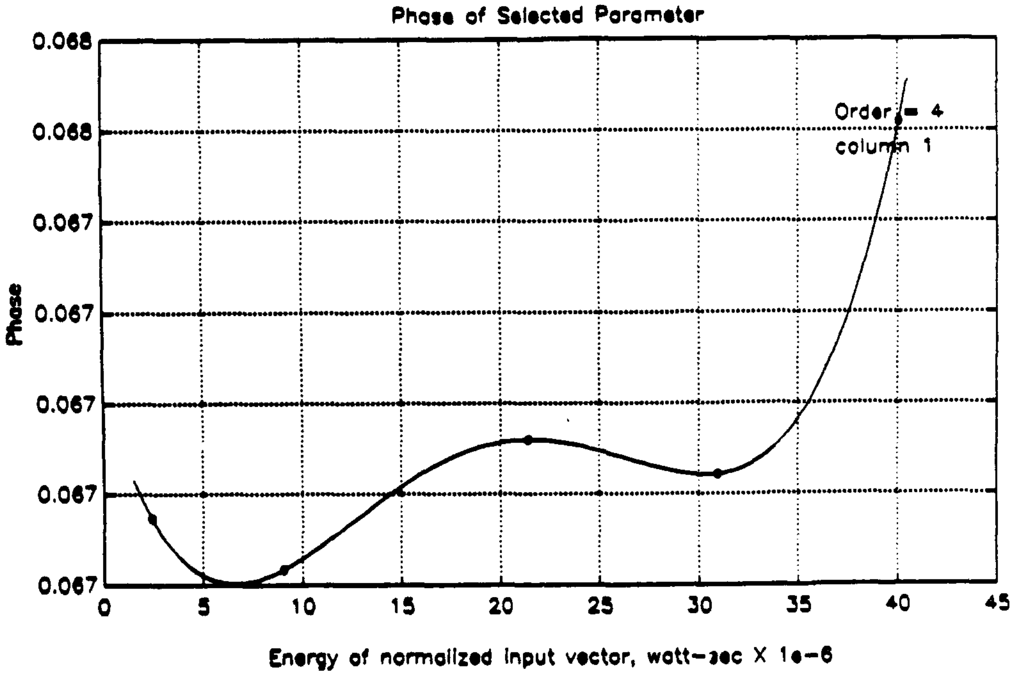

CPLX POLE PAIR 2, '42 (A, N=1, 5 PAIRS)

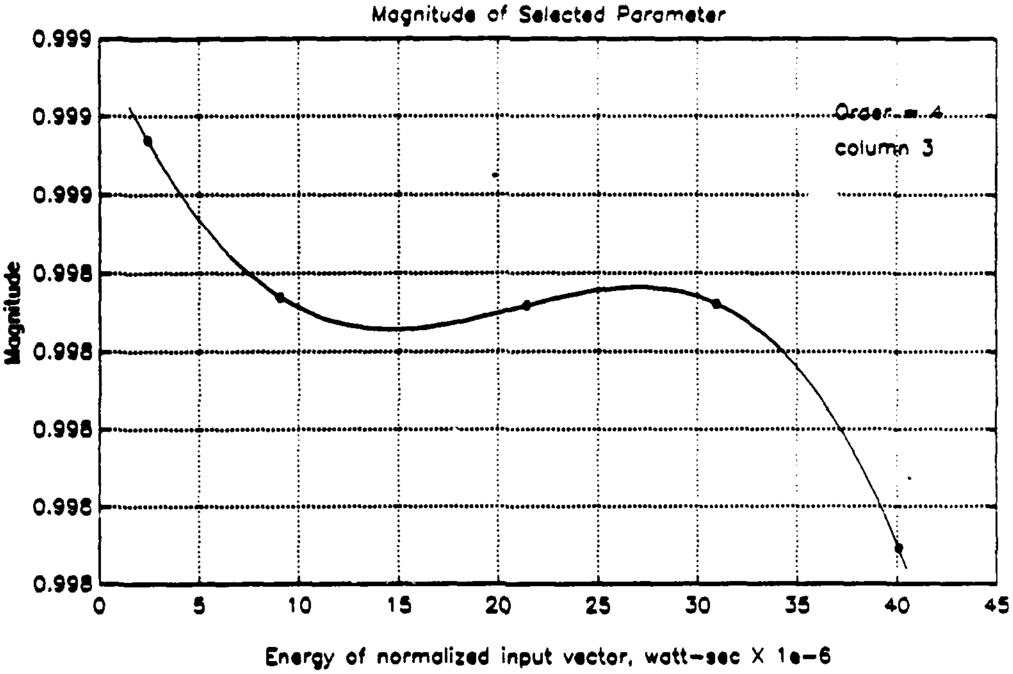

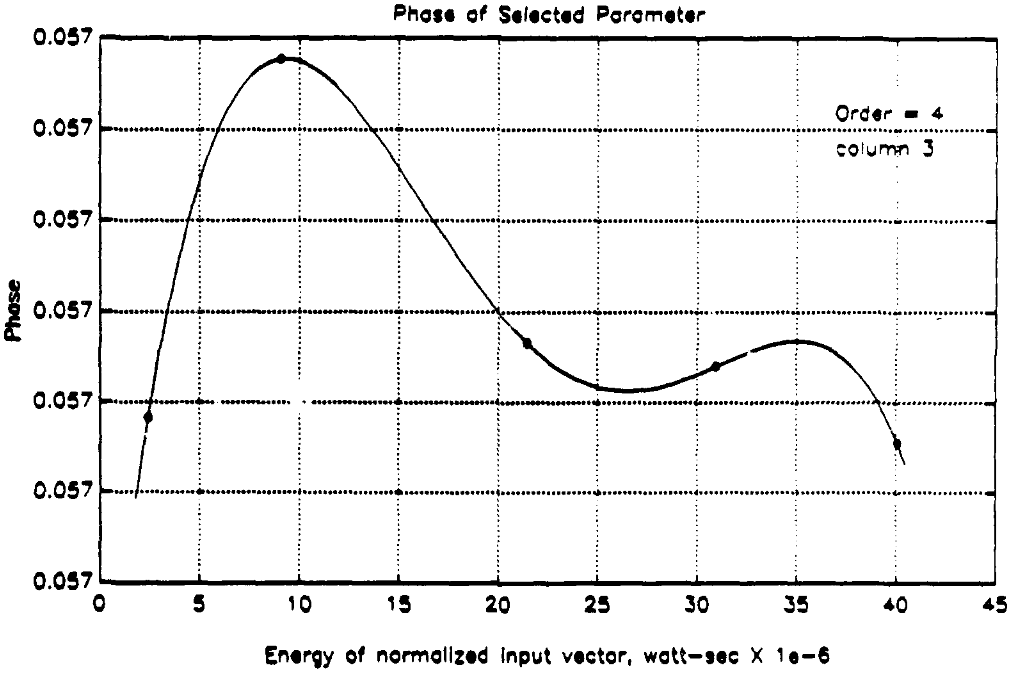

CPLX ZERO PAIR, '42 (A, N=1, 5 PAIRS)

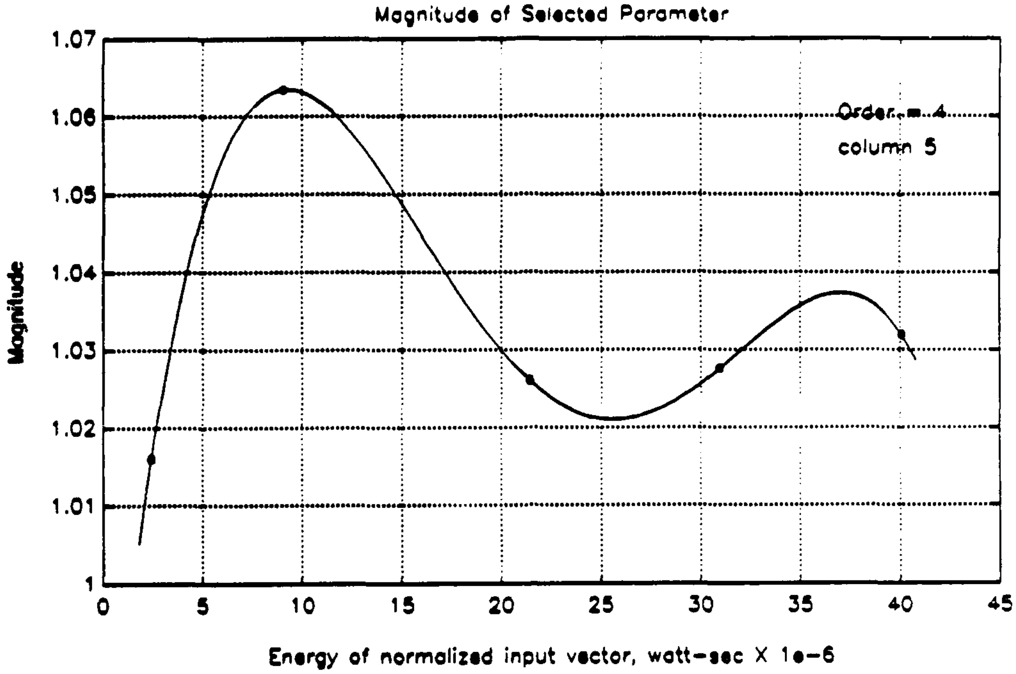

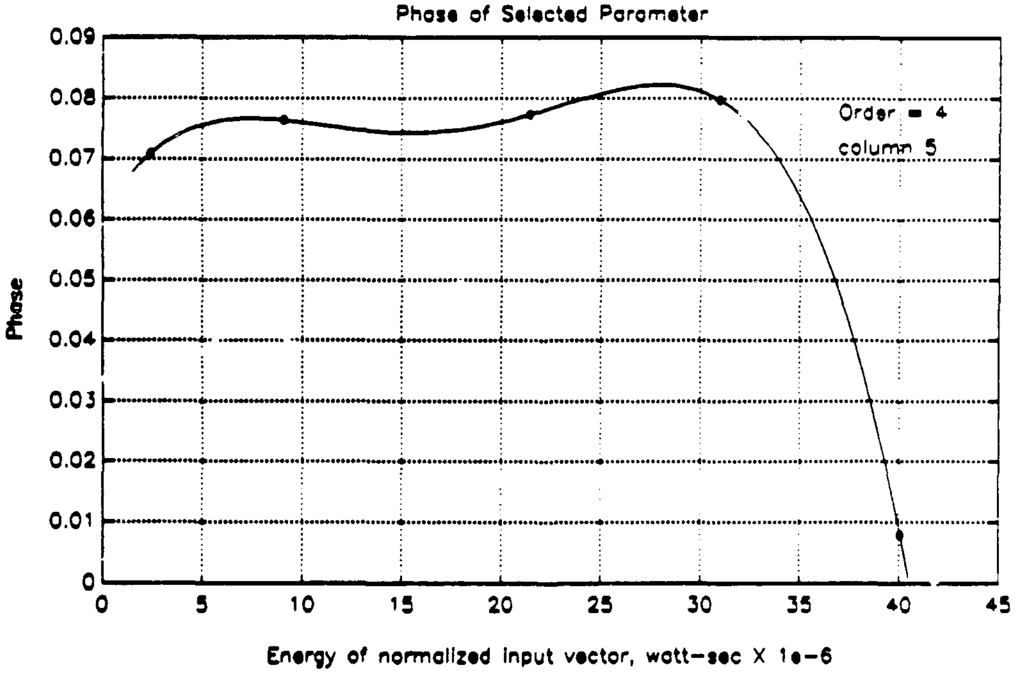

REAL ZERO, '42 (A, N=1, 5 PAIRS)

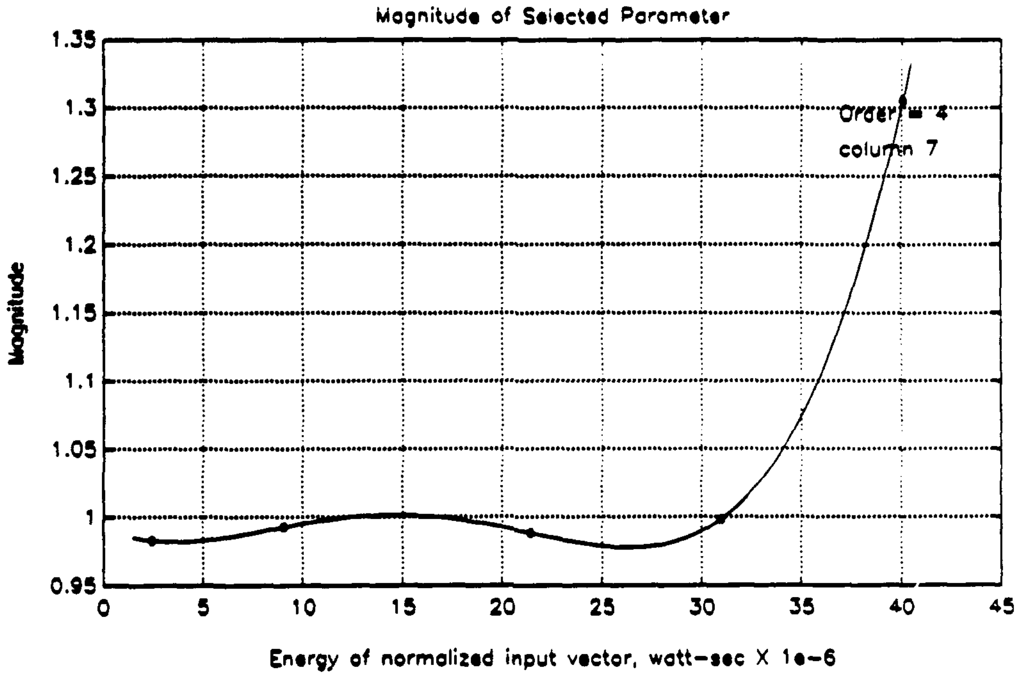

[THIS PAGE INTENTIONALLY LEFT BLANK]

APPENDIX D

SELECTED MATLAB PROGRAM LISTING

The following MATLAB M-files are part of the simulation program. The main file is SIMZ, which calls more than fifty functions in the course of a simulation run. Space does not permit a full listing here. The last function listed, MODEL_YW, was used for modeling and is not directly part of the simulation program.

```
% SIMZ:  Simulates controlling the AN/FPN-42 and 44A Loran-C
%   transmitters in the z domain.
% Calls SETUP, AR2, XMTR, INTERP, ERRORS, PULS_INI, MAINMENU,
%       FIND_PSV, ENVEL, DISPZ
%   and the function defined in 'fcall' (see SETUP).
%   Also calls file named in row string matrix ALG_SWP (See SETUP)

% Dean C. Bruckner, 4/22/92, rev. 9/12/92

% ***************** Initialize program **********************

clear
setup                                  % Declare vars & intialize
first_run='y';
done_simz='n';
mainmenu                               % First menu (see end of loop
                                       %   for other occurrence)
while done_simz=='n'

% **************** Enter control loop ************************

for p=1:length(control);

  if p==1;num_iter=num_iter1;else num_iter=num_iter2;end
  % If drift will be used, start with nonzero random drift vector
  %   if first run.
  if drift_iter~=0 & first_run=='y';
    [drift,drift_stor]=ar2(drift_stor,step);
  end

  PSTR=['Pulse ',num2str(control(p))];
  PC=phasecode(control(p));
  tdw=tdw_pci(:,p);                    % Select one input pulse
  puls_ini                             % Initialize pulse convergence
                                       %   plot and misc error matrices
                                       %   for this loop only.
  done_pulse='n';m=1;md=1;ms=1;
  t0=clock;
  while done_pulse=='n'
    if m>1;times(m)=etime(clock,t0);end
    t0=clock;
    M=num2str(m);M1=num2str(m-1);

    % ************ Find rest1 for GRI of subject pulse ***************

    rest1=rests(rest_indx);            % Rest time for pulse 1 of GRI

    blank=blanks(rest_indx);           % 1=rate blanked in this iter.
                                       % 0=rate not blanked.
    rest_indx=rest_indx+T_dso/rate1;   % Find rest_indx for next time.
    while rest_indx>length(rests)-1    % Wrap index around
      rest_indx=rest_indx-length(rests)+2;
    end;

    if m<5 & err_disp==1;plot(tdw);pause;end

    if blank==1;
  if err_disp==1;                   % Skip blanked GRI
    disp([' Rate 1 blanked between m = ',M1,' and m = ',M])
  end
  blanksav=[blanksav m];

else

  % ********** Get ps_volt for subject pulse in GRI **************

  ps_volt=find_psv(rest1)*psv_sim(control(p)); % Find rest time
                                    %   for beginning of new GRI
                                    %   & estimate ps_volt for
                                    %   p-th pulse

  % ********** Generate & capture rf ******************************

  if step_iter~=0 & ms>step_iter & p==1;  % If time has arrived,
    step=1;m_step=[m_step m];       %   switch transmitters & record
    ms=1;
    if err_disp==2;                 % Inform user
      text(m,4.3e-4,'x');text(m,4.37e-4,'^');
    else
      disp(['Switched transmitters at iteration ',M])
    end
  else
    step=0;
    ms=ms+1;
  end

  if drift_iter ~= 0 & (md>=drift_iter|step==1)
    [drift,drift_stor]=ar2(drift_stor,step);
    md=1;
  else
    md=md+1;
  end

  rf=xmtr(tdw,PC,drift,ps_volt);
  if m<5 & err_disp==1;plot(rf),pause;end
  if m==1 | skip_flag==1;y=envel(rf,tdw,PC);end

  % ********** Calculate, display & record errors ****************

    if m==1
      err_sav(m,:)=errors(y,y0,PC,m,err_disp);
    else
      err_sav(m,:)=errors(y,y0,PC,m,err_disp,err_sav(m-1,:));
    end
  if any(err_sav(m,2:4)>[.01 .03 .1])==1
    OOT(m)=1;                       % Record out of toler. iterations
  end

  if err_disp==2;                   % Flash if out of tolerance
    semilogy(num_iter/9,1.3e-4,'w*'),hold on
    if OOT(m)==1 & round(m/2)==m/2
      semilogy(num_iter/9,1.3e-4,'i*'),hold on
    end                             % Note: 'round' used to ident.
  end                               %   every other iteration.

  ps_sav(m,:)=[rest1 ps_volt];
  drift_sav(:,m)=drift;
  y_sav(:,m)=y;
```

```
    %snr_tdw(m)=snr(tdw);             % record SNRs for averaging
    %snr_rf(m)=snr(rf);               % Note: change DISPZ also

    % ********** Produce new tdw *************************************

    eval(f_call)

    % ********** Fill AFG buffer with new inputs *******************

    for pp=p:length(control)          % (pth & following pulses)

      % If in GRI A, boost each following tdw in GRI A so when it is
      %   controlled, convergence will be faster.  Undo the phasecode
      %   of each pulse & then reapply it as appropriate.  Variable
      %   "boost" is set in ****_INI, not in XMTR_CFG (since knowledge
      %   of needed boosts should be experimentally obtained).
      %   To boost the tdws in GRI B when controlling a pulse in GRI A,
      %   scale back to pulse 1 in GRI A and then skip to GRI B, scaling
      %   up from the first pulse in GRI B.
      % If in GRI B, do the same.

      if control(pp)<=len_p/2;        % both in GRI A
        tdw_pci(:,pp)=boost^(control(pp)-control(p))*...
           (tdw*(-1)^PC)*(-1)^phasecode(control(pp));
      elseif control(p)<=len_p/2      % in different GRIs
        tdw_pci(:,pp)=boost^(1-control(p))*...
                      boost^(control(pp)-len_p/2-1)*...
                      (tdw*(-1)^PC)*(-1)^phasecode(control(pp));
      else                            % both in GRI B
        tdw_pci(:,pp)=boost^(control(pp)-control(p))*...
           (tdw*(-1)^PC)*(-1)^phasecode(control(pp));
      end

    end

    % ********** Swap XMTR loads if error below threshold **********

    if xmtr_load=='Dummy Load' & all(err_sav(m,2:4)<[.006 .015 .05])==1
      m_swp=m;
      xmtr_load = 'Antenna   ';           % Change to antenna
      eval(alg_swp(alg,:))                % Reset part of algorithm
      if err_disp==2;                     % Inform user
        text(m,4.3e-4,'a');text(m,4.37e-4,'^');
      else
        disp(['Switched to antenna after iteration ',M])
      end
      skip_flag=1;
    end

    m=m+1;

  end                                 % end 1 iteration

  if m>=num_iter+1;done_pulse='y';end

end                                   % end 1 pulse

% *************** Save rf and display results for pth pulse *********

rf_pci(:,p)=rf;
if err_disp==2
```

```
    text(.47,.2,'Press <Enter> to continue','sc'),pause
    hold off
  else
    disp('Press <Enter> to continue'),pause
  end

  if any(control(p)==analyze)==1;dispz;end
end                                     % end 1 simulation run (all puls)
first_run='n';
mainmenu                                % get new parameters for more runs
end                                     % end all runs & leave SIMZ
```

```
% SETUP:  Sets up workspace for Loran-C simulation file SIMZ.
%   Declares global variables and assigns values to them.  Sets up
%   workspace format and declares default settings such as the type
%   of random number distribution, etc.  When user selects a control
%   method a script file is used to initialize only those control
%   variables for the selected algorithm, including the control
%   function call in a text string.  Note that when a default setting
%   is changed here, it should also be changed in MAINMENU.  If
%   an algorithm is added, review MAINMENU carefully to ensure
%   parallel changes are made properly.
% Calls PGEN, FLIPLR, ENVEL, and files named in string matrix ALG_INI
%       ... COEFFSAV.MAT (created by MOD1FMT1), H_SCRPT, EOUT_EIN.MAT,
% Declares all global variables used in this simulation.

% For complete list of variables see INDEX.

% Dean C. Bruckner, 4/22/92, rev. 9/2/92

format compact
format short
rand('normal')
clc;disp('Initializing ...')

% **************** INITIALIZE TRANSMITTER MODEL **********************

% **************** Declare global variables

global phasecode rate1 rate2 sta_id
global coeff bound root_indx ps_id cp cn cc cr
global drift_sdev drift_ref ar2_var ar2_a ztoler ztimes
global eout_ein ps_tau ps_prev ps_imp ps_indx N fs fs_adjust
global xmtr_id xmtr_load bits imbalance sig_noise y0D y0A tdw_noise

% **************** Set up dual rate parameters

load restvars                           % Load variables for dual-rate
                                        %   simulation (rests, sta_id,
                                        %   rate1, rate2)
T_dso=4;                                % Interval at which rf pulses
                                        %   are sampled by the digital
                                        %   storing oscilloscope (secs)
rs=rand('dist');rand('uniform')         %
rest_indx=round(rand*.9*length(rests)); % Start rest times index randomly.
rand(rs)
```

```
% **************** Set up Pulse measurement parameters

ztimes=(-25:5:30)'*1e3;                 % Zero crossing times (ns)
ztoler=[ 2000 1500 1000 500 250    0   100 100 100 100 100 100
        1000 100 75 50 50   0   50 50 50 50 50 50]';
% These correspond to the category 2 & 1 xmtrs in the Loran signal spec.
% The '42 is a cat. 2 xmtr; the '44A is cat1 (Note that xmtr_id is
% opposite from this:  xmtr_id=1 is for the '42; xmtr_id=2 is the '44A)


% **************** Configure transmitter

xmtr_id=1;                              % 1 = 42, 2 = 44A
xmtr_load='Dummv Load';                 % Starting load of xmtr,
                                        %   'Antenna    '  or
                                        %   'Dummy Load' (note: string
                                        %   lengths must be equal!!)
if sta_id(1)=='S';                      % Phasecode: 0=pos, 1=neg
  phasecode=[0 0 0 0  0 1 1 0        0 1 0 1  0 0 1 1'];
else
  phasecode=[0 0 1 1  0 1 0 1  0     0 1 1 0  0 0 0 0  1'];
end
len_p=length(phasecode);
imbalance=0;                            % [0-100]; pct. by which the ampl.
                                        %   of neg. phase coded pulses is
                                        %   decreased.

% **************** Load curves of xmtr model

N=1;                                    % Default decimation factor
xmtr_cfg                                % Configure transmitter

% **************** Set up parameters for simulation

skip_flag=0;                            % Used in switching automatically
                                        %   from dummy load from antenna
control=1;                              % Pulses to control
analyze=1;                              % Pulses to analyze (after
                                        %   convergence)
tau=0;                                  % Assigned local ECD
ETA=0;                                  % Early timing adjust in
                                        %   microsecs (used in PGEN)
bits=8;                                 % Function generator resolution
                                        %   ('0' selects best floating
                                        %   point resol. of the computer)
num_iter1=100;                          % Iterations of 1st selected pulse
num_iter2=20;                           % Iterations of following pulses
step_iter=0;                            % Interval between xmtr steps
                                        %   (switches)
err_disp=2;                             % Method of displaying errors
                                        %   during convergence
                                        % 0=none,1=text,2=plot

% ****************** INITIALIZE CONTROL ALGORITHM ********************

alg=1;                                  % Default algorithm to start

% The following 5 string matrices are used to handle the current
%   algorithm without listing the names of the algorithms or their
%   associated files anywhere else in the program than here.  The first
%   string matrix holds the names of the algorithms; the following 4
%   matrices hold names of files associated with each algorithm which
%   are called at different points in the program.  Lines 2 and following
%   of each matrix should be the same length as line 1 and should follow
%   suit.
%   Example:
% alg_name=['Steepest Descent ';
%           'Neural Network   ';
%           'Recursive LS     '];
% The Steepest Descent Algorithm uses 6 modular M-files:
% DESC          The function
% DESC_INI      Initializes the algorithm
% DESCMENU      Lets the user change parameters easily
% DESCHEAD      Menu header for DESCMENU
% DESC_SWP      Resets part of the algorithm when xmtr load is swapped
% DESCDISP      Displays alg params for most recent run in DISPZ
% Other algorithms should use the same file structure.  Details of the
%   minimum requirements for each of the above files are listed in the
%   text of each file.

alg_name=['Steepest Descent '];         % Algorithm names
alg_menu=['descmenu'];                  % M-file names
alg_swp =['desc_swp'];                  %  "       "
alg_ini =['desc_ini'];                  %  "       "
alg_disp=['descdisp'];                  %  "       "

eval(alg_ini(alg,:))                    % Initialize algorithm
```

```
function rf=xmtr(tdw,PC,drift,ps_volt)

% Function rf=XMTR(tdw,PC,drift,ps_volt):  Simulates the AN/FPN-42
%   or AN/FPN-44A Loran C transmitter.  To account for nonlinearities,
%   the poles & zeros of the xmtr's transfer function are modeled
%   as a function of the normalized power supply voltage and the
%   energy of the normalized input waveform.
% Uses global variables:  bits, imbalance, sig_noise, xmtr_load
% Calls:  ENERGY, FIND_AB, FIND_PSV

% Local variables:
%       A               Amplitude of output vector (volts)
%       a,b             Denominator & numerator polynomials of model
%       cr              Number of rows in 'coeff'
%       drift           Parameter vector modeling xmtr drift
%       energy_in       Energy of input vector (watt-sec); R=1.
%       energy_no       Energy of normalized input vector (watt-sec); R=1.
%       h               Transmitter impulse response sequence
%       lc              Slope & intercept of energy in/out of xmtr
%       ps_volt         Estimated normalized power supply voltage: (0,1]
%       rest1           Power supply recovery time since last pulse
%       tdw             Transmitter drive waveform
%       xmtr_load       String:  Defines load connected to xmtr:
%                         'A'=antenna, 'D'=dummy load
%       rf              (Radio freq) output pulse

% Dean C. Bruckner, 7/17/92, rev. 9/7/92

% **************** Obtain xmtr transfer function ********************
```

```
if nargin<4;ps_volt=1;end                   % Default: fully recovered
if nargin<3;drift=zeros(cr,1);end           % Default: no drift
if nargin<2;PC=0;end                        % Default: pos phase code

len_tdw=length(tdw);                        % Length of input vector
[energy_in,energy_no]=energy(tdw);          % Energy of input vector
                                            %   (regular & normalized)

[a,b]=find_ab1(energy_no,ps_volt,drift); % Denom & num polynomials

% **************** Produce output ***********************************

rf=filter(b',a',tdw);

% **************** Adjust output ************************************

if xmtr_load=='Dummy Load';                 % Apply input energy vs output
  lc=eout_ein(2,:);                         %   energy to find output
else                                        %   amplitude.
  lc=eout_ein(1,:);
end
energy_out=lc(1)*energy_in + lc(2);
rf=rf/max(rf);                              % Normalize output sequence &
A=sqrt(energy_out/((rf'*rf)*N*100e-9)); %   calculate final normalization
                                            %   power (power norm. to R=1)
rf=A*rf*ps_volt;                            % Assign estimated output energy
                                            %   to output sequence, including
                                            %   power supply droop.
rf=rf-mean(rf);                             % Remove DC bias

% Note on tube xmtr imbalance:
% Initially the xmtr imbalance (between the 2 banks of tubes which
%   amplify the positive & negative parts of the pulse, respectively)
%   was modeled in detail, as shown below, by adding up to one percent
%   distortion to the positive samples.
%rf(find(rf>0))=(1-.01*imbalance) * rf(find(rf>0));  % xmtr imbalance
% Apparently this is an accurate representation of the distortion.
%   However, I could not find real documentation on the phase code
%   balance adjustment that described exactly how this was remedied,
%   just that the imbalance caused negatively phase coded pulses to
%   be smaller in amplitude (both pos & negative parts equally), as
%   described in LCDR Taggart's EERP & VXIbus reports.  According to
%   him, the phase code balance adjustment simply increases the amplitudes
%   of the TDWs for the negatively phase coded pulses, not adding any
%   DC bias level, etc.  Therefore, the imbalance is now modeled
%   as a percentage decrease in the amplitude of rf.  This will
%   be compensated for automatically just like droop, since each pulse
%   of the PCI is controlled independently.

if PC==1;                                   % For negatively phase coded
  rf=rf*(1-.01*imbalance);                  %   pulses, decrease amplitude
end                                         %   by a percentage.

if sig_noise~=0                             % Misc white noise in output
  rs=rand('dist');rand('normal')            %   (std dev expressed as
                                            %   percentage of peak ampl.)
  rf=rf + .01*sig_noise*max(rf)*rand(length(rf),1);
  rand(rs);
end

if bits ~=0;                                % Amplitude resolution in DSO
```

```
  max_rf=max(rf);
  rf=round(rf/max_rf*(2^bits)/2) / (2^bits)*2*max_rf;
end
```

```
function tdw=pgen(x,PC,ETA);

% Function tdw=PGEN(x,PC,ETA):  Simulates analog pulse generator,
%   given a 16-element vector of peak voltage values (pos & neg
%   or all pos).  Pulse is triggered 10 us after beginning of
%   data vector.  Due to the problems of dealing with fractional
%   values of samples per period, tdw is formed at 5.0 MHz and
%   decimated down to the desired sampling frequency.
% Calls global variables:  bits, xmtr_id, fs

% Variables:
%       ETA     Early timing adjust, in microsecs.  Changes phase
%                 of tdw within window (pulse still begins exactly
%                 at the trigger--ref. discussion w/ LCDR G. Kmiecik
%                 on 5/22/92).  The effect of the ETA shows up in
%                 the Envelope-to-Cycle-Difference (ECD) of the output.
%       fs_pg   Sampling frequency used to build tdw
%       len_pg  Number of samples in tdw at fs_pg
%       PC      TDW phase code (0=pos, 1=neg)
%       s_eta   Number of samples in ETA
%       spp     Samples per period (period = 10 us)
%       tdw     Transmitter drive waveform
%       x       16-element input vector of pk voltage values
%                 (pos & neg or all pos)

% Dean C. Bruckner, 2/21/92, rev. 9/7/92

% ******************* Verify inputs *********************************

if N>=2
  fs_pg=5e6;len_pg=2048;                    % 5 MHz has a whole number of
                                            %   samples in each half-cycle.
else
  fs_pg=fs;len_pg=4096;
end

if nargin<3;ETA=0;end
if nargin<2;PC=0;                          % Check phase code
elseif PC~=0 & PC~=1;error('Phase code must equal 0 or 1');
end
if nargin<1;x=ones(16,1);                  % Default: all 1/2 cycles equal
elseif size(x)==[1,16];x=x';               % Reorient if necessary
end

if size(x)~=[16,1];error('Size of x incorrect');end
x=abs(x);

% ************ Generate PGEN input vector *************************

s_eta=round(ETA*1e-6*fs_pg);
spp=10e-6*fs_pg;
k=(1:8*spp)';
```

```
m=ones(spp/2,1)*x';                     % Extend vector x to each "bin"
m=reshape(m,round(8*spp),1);            %   which is mult. by tdw

tdw(1:spp,1)=zeros(spp,1);              % Trigger pulse at 10 us point
temp1=sin(2*pi*k/spp - pi*PC).*m;       % Generate sine pulse
temp1(length(temp1)-s_eta+1:length(temp1))=[];  % Apply ETA
temp2=-flipud(temp1(1:s_eta));
tdw(spp+1:9*spp)=[temp2;temp1];         % Recombine
if xmtr_id==2
  nn=1:len_pg-9*spp;                    % Tail drive circuit
  tdw(9*spp+1:len_pg)=x(16)*...
             (exp((-(1e6*nn/fs_pg)/22)).*sin(.2*pi*1e6*nn/fs_pg-pi*PC))';
else
  tdw(9*spp+1:len_pg)=zeros(len_pg-9*spp,1);
end

if N>2
  tdw=tdw(1:round(fs_pg/fs):len_pg);    % Decimate (ignore aliasing)
end

if bits ~=0;                            % Amplitude resolution in AFG
  max_tdw=max(tdw);
  tdw=round(tdw/max_tdw*(2^bits)/2) / (2^bits)*2*max_tdw;
end

if sig_noise~=0                         % Misc white noise in input
  rs=rand('dist');rand('normal')        %   (std dev expressed as a
                                        %   percentage of peak amplitude)
  tdw=tdw + .01*tdw_noise*sig_noise*max(tdw)*rand(length(tdw),1);
  rand(rs);
end
```

```
function ps_volt=find_psv(rest1)

% Function ps_volt=FIND_PSV(rest1):  Given the time the xmtr power
%   supply has had to recover from the last pulse of the preceding
%   GRI, this function estimates the new power supply voltage
%   (normalized and in the range (0,1]) for pulse 1 in the new GRI.
% Uses global vars:  ps_tau ps_prev ps_imp
% Calls:

% Variables:
%       ps_volt         Estimated normalized power supply voltage: (0,1]
%       rest1           Power supply recovery time since last pulse

% Dean C. Bruckner, 7/20/92, rev. 9/7/92

if rest1<.001;error('rest1 must be >= .001 sec.');end
t=-ps_tau*log(1-(ps_prev-ps_imp));      % Point on the curve where
                                        %   recovery starts at end of
                                        %   last GRI  (note:  "log" is
                                        %   the natural logarithm)
ps_volt=1-exp(-(t+rest1)/ps_tau);       % ps_volt after resting "rest1"
                                        %   seconds
```

```
function [a,b,h_yw]=model_yw(h,p,q)

% Function [a,b,h_yw]=MODEL_YW(h,p,q):  Solves Yule-Walker equations to
%   find pole-zero model of Loran-C data vector.

% Dean C. Bruckner, 4/7/92.  Adapted from algorithms written by
%   Tom Johnson of the Naval Postgraduate School.
%   Ref:  C. W. Therrien, Discrete Signal Proc. & Statistical Signal
%   Processing, Prentice-Hall, 1992.

len_h=length(h);
Rx=lorcorr(h);                          % Autocorrelation vector by ffts
R=toeplitz(Rx(1:len_h),Rx(1:p+1));      % ACF mtx
Re=R(q+2:len_h,:);                      % Extended corr mtx (Ther. 9-168)

[re,ce]=size(Re);
a=[1;-Re(:,2:ce)\Re(:,1)];              %   using extended Y-W method
                                        %   Note:  Matrix pinv calculated
                                        %   by gaussian elimination.


ha=filter(1,a,[1;zeros(len_h-1,1)]);    % Use Shank's method to
Ha=toeplitz(ha,[ha(1),zeros(1,q)]);     %   find "b" parameters.
b=inv(Ha'*Ha)*ha'*h;                    %   (Therrien ch. 9)

h_yw=filter(b,a,[1;zeros(len_h-1,1)]);     % ARMA model impulse resp.

disp('Poles:  ');
[abs(roots(a)) angle(roots(a))]
disp('Zeros:  ');
[abs(roots(b)) angle(roots(b))]
disp('Press <Enter> to show plots');pause

clg
if q>0;rts_b=roots(b); rts_b=rts_b(find( abs(rts_b)<2 ));
polar(angle(rts_b),abs(rts_b),'go');hold on;end;
polar(angle(roots(a)),abs(roots(a)),'rx');
grid;title('Pole/zero plot of the Yule-Walker estimate');
pause
hold off


clg;plot(1:length(h),h,'-',1:length(h_yw),h_yw,'--')
grid;title('Original & modeled sequence')
xlabel('Sample number');ylabel('Magnitude')
text(.5,.15,['MSE = ',num2str(mse(h,h_yw)*1e6),'e-6'],'sc')
pause
```

[THIS PAGE INTENTIONALLY LEFT BLANK]

REFERENCES

1. *Specification of the Transmitted Loran-C Signal*, USCG Commandant Instruction M16562.4, July, 1981.

2. Malcolm F. Willoughby, "The Story of LORAN," Chapter 10 of *The U.S. Coast Guard in World War II*, 1989.

3. Loran-C Engineering Course Manual, USCG Academy.

4. Bonnie Dahl, *The Loran-C User's Guide*, Richardsons' Marine Publishing Inc., Steamwood, IL, 1986.

5. Gordon West, "The Electronic Radionavigation Plan," *Trailer Boats*, January 1988.

6. *Federal Radionavigation Plan*, 1988.

7. Doug Taggart and Ben Stewart, "Electronics Equipment Replacement Project (EERP)," Technical Report, USCG Electronics Engineering Center, 1989.

8. Loran-C Engineering Course Reference Manual, USCG Academy, 1988.

9. Benjamin Peterson, Thomas Thomson, and Jonathan Riffe, "Measurement of Loran-C Envelope to Cycle Difference in the Far Field," Technical Report, USCG Academy.

10. Doug Taggart and Jon Turban, "VXIbus Based Loran-C Transmitter Monitor and Control System," Technical Report, USCG Electronics Engineering Center, 1991.

11. Project W1180, "Timing and Control Equipment (TDE) Redesign," USCG EECEN Project Planning Document, 1992.

12. Robert Strum and Donald Kirk, *Discrete Systems and Digital Signal Processing*, Addison Wesley Publishing Co., Menlo Park, CA, 1989.

13. Benjamin Peterson, personal communication, August 1991.

14. Charles Therrien, personal communication, August 1991.

15. Gary L. May, "Pole-Zero Modeling of Transient Waveforms: A Comparison of Methods With Application to Acoustic Signals," M.S. Thesis, Naval Postgraduate School, 1991.

16. Charles W. Therrien, *Discrete Random Signals and Statistical Signal Processing*, Prentice Hall, Inc., Englewood Cliffs, NJ, 1992.

17. Lawrence Rabiner and Ronald Schafer, *Digital Processing of Speech Signals*, Prentice Hall, Inc., Englewood Cliffs, NJ, 1978.

18. Gene Golub and Charles Van Loan, *Matrix Computations*, The Johns Hopkins University Press, Baltimore, MD, 1983.

19. Simon Haykin, *Adaptive Filter Theory*, Prentice Hall, Inc., Englewood Cliffs, NJ, 1991.

20. Benjamin Peterson, "Closed Loop Control of Loran-C Pulse Shape for Tube Type Transmitters," Derivation, USCG Academy, 1988.

21. Rodrigo Steinvorth, "An Adaptive, Digital Loran-C Pulse Generator," Project Report, USCG Academy, 1989.

22. Huibert Kwakernaak and Raphael Sivan, *Linear Optimal Control Systems*, John Wiley and Sons, Inc., New York, 1972.

23. Lennart Ljung, *System Identification: Theory for the User*, Prentice Hall, Inc., Englewood Cliffs, NJ, 1987.

24. Lennart Ljung, *User's Guide to the System Identification Toolbox for MATLAB*, published by The Math Works, 1991.

25. Bernard Widrow and others, "Adaptive Noise Cancelling: Principles and Applications," *Proc. IEEE*, Vol. 63, No. 12, December 1975.

26. *Loran-C Data Acquisition (LORDAC) Set User's Guide*, USCG Electronics Engineering Center.

27. *Loran-C User Handbook*, USCG Commandant Instruction M16562.3, May 1980.

28. Benjamin Peterson and Kevin Dewalt, "Loran and the Effects of Terrestrial Propagation", Technical Report, USCG Academy, 1992.

29. Richard Hartnett and Ronald Hewitt, "The U.S. Coast Guard's Loran-C Remote Operating System," Technical Report, USCG Electronics Engineering Center.

30. Benjamin Peterson and Richard Hartnett, "Measurement Techniques for Narrowband Interference to Loran," Technical Report, USCG Academy.

31. Benjamin Peterson and Richard Hartnett, "Loran-C Interference Study," Technical Report, USCG Academy.

32. Doug Taggart and D. C. Slagle, "Loran-C Signal Stability Study: West Coast," Technical Report, USCG Research and Development Center, 1986.

33. Doug Taggart and D. C. Slagle, "Tangible Effects of Loran-C Phase Modulation," Technical Report, USCG Research and Development Center, 1984.

34. Benjamin Peterson, "Bounded Error Adaptive Identification and Control," M.S. Thesis, Yale University, 1983.

35. *Aids to Navigation Manual, Radionavigation Manual*, USCG Commandant Instruction M16500.13, 1989.

36. L. E. Sartin, "A Quarter Century of Loran-C," Analytical Systems Engineering Corp., Burlington, MA.

37. *Tactical Loran C/D Ground Chain*, USAF Electronic Systems Division, Program Management Plan 450A/404L, 1975.

38. "St. Mary's River Loran-C Mini-Chain", USCG Office of Research and Development, July 1981.

39. *386-MATLAB User's Guide*, published by The Math Works, 1991.

40. *Loran-C Transmitting Sets AN/FPN-44A, AN/FPN-44 and AN/FPN-45*, Supplement to Technical Manual, USCG.

[THIS PAGE INTENTIONALLY LEFT BLANK]

INITIAL DISTRIBUTION LIST

No. Copies

1. Defense Technical Information Center 2
Cameron Station
Alexandria, VA 22314-6145

2. Library, Code 52 2
Naval Postgraduate School
Monterey, CA 93943-5100

3. Chairman, Code EC 1
Department of Electrical and Computer Engineering
Naval Postgraduate School
Monterey, CA 93943-5000

4. Professor Murali Tummala, Code EC/Tu 2
Department of Electrical and Computer Engineering
Naval Postgraduate School
Monterey, CA 93943-5000

5. Professor Roberto Cristi, Code EC/Cx 1
Department of Electrical and Computer Engineering
Naval Postgraduate School
Monterey, CA 93943-5000

6. Professor C. W. Therrien, Code EC/Ti 1
Department of Electrical and Computer Engineering
Naval Postgraduate School
Monterey, CA 93943-5000

7. CAPT B. B. Peterson 1
Chief, Electrical Engineering Section
Department of Engineering
U.S. Coast Guard Academy
New London, CT 06320

8. Commandant (G-NRN-1) 1
U.S. Coast Guard
2100 W. 2nd Street S.W.
Washington, D.C. 20593-0001
Attn: CDR Doug Taggart

9. Commandant (G-PIM-2/O) 1
U.S. Coast Guard
2100 2nd Street, S.W.
Washington, D.C. 20593-0001

10. Commandant (G-TPR-2) 1
U.S. Coast Guard
2100 2nd Street, S.W.
Washington, D.C. 20593-0001

11. Commanding Officer (nlx) 1
U.S. Coast Guard Electronics Engineering Center
P.O. Box 60
Wildwood, NJ 08260-0060
Attn: LT Dean C. Bruckner

12. Commanding Officer (nlx) 1
U.S. Coast Guard Electronics Engineering Center
P.O. Box 60
Wildwood, NJ 08260-0060
Attn: LCDR G. Kmiecik